Characterization of the Diet-Microbiota-Gut-Brain Axis and its Role in Neuroinflammation

by

Stephanie Makdissi

Submitted in partial fulfilment of the requirements
for the degree of Master of Science

at

Dalhousie University
Halifax, Nova Scotia
August 2022

Dalhousie University is located in Mi'kma'ki,
the ancestral and unceded territory of the Mi'kmaq.
We are all Treaty people.

DEDICATION PAGE

I would like to dedicate this thesis to my grandparent whom I lost too early, due to Alzheimer disease.

TABLE OF CONTENTS

LIST OF TABLES

LIST OF FIGURES

Abstract

Neurodegenerative Diseases (NDs) are the leading causes of disability/death globally. The Diet-Microbiota-Gut-Brain (DMGB) axis is a promising area of research for NDs, investigating how intercommunication between diet, intestinal microbiota, and the intestinal epithelium distally effect the brain. NDs also co-appear with perturbed metabolic and oxidative regulators in the gut, such as peroxisome organelles, that control tissue integrity and commensal populations. Therefore, I hypothesized that peroxisomes in the gut are important modulators of the DMGB axis. Recruiting the *Drosophila melanogaster* (fruit fly) as my model, I depleted peroxisome function in the animal's intestinal epithelium (midgut), which effected climbing behaviour, accompanied by redox stress, inflammation and cellular death throughout the brain over aging. I also screened these midguts for peroxisome-dependent transcription factors that control DMGB axis communication, and identified Myo-inhibitory peptide (*Mip)* expression corresponded to the climbing deficit that was observed. Therefore, *Mip* in the DMGB axis of *Drosophila* requires further investigation.

LIST OF ABBREVIATIONS USED

AD	Alzheimer Disease
AMP	Antimicrobial Peptide
APP	Amyloid Precursor Protein
Att	*Attacin*
AV	Annexin V
AX	Axenic
BACE	Beta-secretase (gene)
BBB	Blood Brain Barrier
BDNF(s)	Brain Derived Neurotropic Factor(s)
BDSC	Bloomington *Drosophila* Stock Center
cDNA	Complimentary DNA
CM	Cornmeal
CNS	Central Nervous System
Commensals	Gut microbiota
CTCF	Corrected Total Cell Fluorescence
DA	Dopaminergic
DHE	Dihydroethidium
DMGB	Diet-Microbiota-Gut-Brain
Do	Days old
ECs	Enterocytes
EE	Enteroendocrine cells
ENS	Enteric Nervous System

FAs	Fatty Acids
GBD	Global Burden of Disease
gDNA	Genomic DNA
Gut	Intestinal epithelium
HFD	High Fat Diet
IBD	Inflammatory Bowel Disease
ICs	Inflammatory Cytokines
IF	Immunofluorescence
ISCs	Intestinal Stem Cells
KD	Knock Down
KDRC	Korean *Drosophila* Resource Center
LCFAs	Long Chain Fatty Acids
LI	Learning Index
Midgut	*Drosophila* intestinal epithelium (small-intestine)
Mip	Myo-Inhibitory Peptide (Gene)
Mip	Myo-Inhibitory Peptide
ND	Normal Diet
NDs	Neurodegenerative Diseases
NFTs	Neurofibrillary Tangles (Tau)
NGCA	Negative Geotaxis Climbing Ability
NGS	Normal Goat Serum
NPRs	Neuropeptide Receptors
NPs	Neuropeptides

PAM	Protocerebral Anterior Medial
PBD(s)	Peroxisome Biogenesis Disorder(s)
PCR	Polymerase Chain Reaction
PD	Parkinson Disease
PEX3	Peroxin 3 (Gene)
PEX3	Peroxin 3 (Protein)
PEX5	Peroxin 5 (Gene)
PEX5	Peroxin 5 (Protein)
PI	Propidium Iodide (Necrosis marker)
PNS	Peripheral Nervous System
PPL1	Protocerebral Posterior Lateral 1
qPCR	Quantitative Polymerase Chain Reaction
ROS	Reactive Oxygen Species
SCFAs	Short Chain Fatty Acids
SN	Substantia Nigra
SNCA	Alpha-Synuclein (Gene)
TAGs	Triacyl Glycerols
TEM	Transmission-Electron Microscopy
TH	Tyrosine Hydroxylase
TUNEL	Terminal deoxynucleotidyl transferase dUTP Nick End Labeling
UMI	Unique Molecular Index
Upd3	*Unpaired-3*
VDRC	Vienna Drosophila Resource Center

VLCFAs	Very Long Chain Fatty Acids
α-Synuclein	Alpha-Synuclein (Protein)
β- Secretase	Beta-Secretase (Protein)

ACKNOWLEDGEMENTS

The first person I would like to thank is God, for getting me this far into my career, and I am blessed every day of my life that He has lead me to meet and work with amazing people such as the second most important person I would like to thank, my mentor Dr. Di Cara. I would like to thank her most of all for all her patience and efforts to provide me with the best graduate experience and learning opportunities, in order for me to grow into a more well-rounded individual in academia. So thank you Dr. Di Cara for always pushing me to be the best version of myself, and encouraging me to keep going. I would also like to acknowledge and thank my co-supervisor Dr. Andrew Makrigiannis and supervisory committee members Dr. Jamie Kramer and Dr. Jean Marshall for their endless and invaluable support, advice, and critiques which helped to enrich my learning experience and guide me on the path to success. Furthermore, I would like to thank our collaborators Dr. Denis Top and Dr. Hua Bai for helping us understand whether our phenotypes were truly neuronal, and all the time and effort put into those assays.

Next I would like to thank our lab team, especially Lauren DeWolfe, for contributing her time and efforts to the project. Lauren helped validate many transcriptomic screen hits via qPCR, which would have taken much longer to complete without her help.

Finally, I would like to acknowledge my parents for all of their love and support in no matter what I take on in life, and my closest friends for sending me cat memes and encouraging pep-talks to keep my spirits high throughout the whole process.

CHAPTER 1: INTRODUCTION

1.1 Introduction to neurodegenerative disease

The brain is the body's primary information, coordination, and communication hub (Thau et al., 2022; Y, Wang et al., 2020). Part of the Central Nervous System (CNS), the brain connects to distal parts of the body via the Peripheral Nervous System (PNS); modulating interorgan communication and moderating tissue homeostasis (McHugh & Gil, 2018; Peters, 2006). However, aging of the peripheral organs can effect these communication and coordination processes, such as hormonal, or mechanical abnormalities of the aging body (Ali et al., 2018, Venkat et al., 2015). The brain may become stressed from trying to correct dysregulated inter-organ communication throughout the body, thus making the brain more susceptible to injury (Peters, 2006). Injury is especially concerning with declining organ-reserve as the brain ages, jeopardizing cellular survival throughout the brain (Atamna et al., 2018). Diseases of exacerbated and progressive and brain-wide neuronal death are classified as neurodegenerative diseases (NDs), such as Alzheimer (AD) and Parkinson (PD) diseases (Muddapu et al., 2020).

NDs are one of the leading causes of disability and death world-wide by metrics of Global Burden of Disease (GBD) studies (Aarli et al., 2006; Feigin et al., 2019, 2020; Health, 2022). Accompanied by severe and progressive cognitive and motor disturbances, (Jahn, 2019; Loučanová et al., 2015; Muddapu et al., 2020), the consequences of NDs are debilitating, and effected individuals often require in-home/hospital-care from family/medical staff (Family Resource, 2021). These medical expenses are financially unforgiving for both the individual and family (Aarli et al., 2006; Feigin et al., 2019, 2020), and the strain on global health care systems plus the global economic burden are heavy

(Ou et al., 2021; Vossius et al., 2011; Weintraub & Horn, 2008; Wong, 2020, W.Yang et al., 2020). As the exponentially growing global population ages, and life span is prolonged due to medical advancements, the incidence of NDs will rise (Durães et al., 2018). According to the World Health Organization in 2022, the current global incidence of NDs like dementias (i.e. AD) is roughly 55 million, and expected to reach 139 million by 2050 (World Health Organization, 2022). Additionally, the global incidence of PD is around 6.1 million (Ou et al., 2021), and expected to reach 12 million by 2040 (Dorsey et al., 2018). Despite best efforts to find a cure, and alleviate the GBD of NDs, the aetiologies remain elusive and research on pathogenesis is still speculative (Durães et al., 2018).

NDs are categorized into two groups; sporadic, contributing to over 90% of cases, and genetic (Bekris et al., 2021; Pang et al., 2017). Sporadic NDs are the most difficult to study because, pathogenesis is driven by both spatial and temporal interactions of environmental and genetic factors, which are still largely unknown (Hampel et al., 2021; Lu & Vogel, 2009; Muddapu et al., 2020; Pang et al., 2017). Genetic cases are much easier to study, allowing scientists to investigate the pathogenic nature of mutant-alleles, which are linked to and may be the causative agents of neurodegeneration (Bekris et al., 2021). Advancements in genomic sequencing (Next-Generation Illumina sequencing) have also provided new vantage points to unraveling the origins of genetic and sporadic NDs (Pang et al., 2017; Zheng & Chen, 2022). However, carrying mutant-genes linked to NDs does not guarantee onset of these diseases, and thus there are environmental components that contribute to onset (Hampel et al., 2021; Pang et al., 2017). Therefore, by studying genetic-linked NDs, the environmental factors that may contribute to sporadic NDs are also considered.

Recently, the repurposing of antimicrobial drugs to treat NDs, has added an additional layer of complexity to the study, suggesting peripheral origin of these diseases (Durães et al., 2018). For example, the intestinal epithelium (gut) and its vast metabolic function and gut microbiota (commensal) populations, heavily influenced by dietary lifestyles, have been implicated to have neuroprotective effects on the brain and even seed NDs in the gut when perturbed (Brudek, 2019; Castelli et al., 2021; Challis et al., 2020; Q Chen et al., 2019; Mertsalmi et al., 2020). Therefore, the pathogenesis of NDs may not be confined to the brain, but originate from interorgan-communication networks (axes), especially the Diet-Microbiota-Gut-Brain (DMGB) axis. Finally, since the gut may be a source of pathogenesis for NDs, finding alternative treatment options such as dietary changes, would help to prevent less side effects than current psychotherapeutics (Winiarska-Mieczan et al., 2020). Ultimately, providing accessible and inexpensive treatment options for all, to reduce global prevalence.

1.1.1 Alzheimer disease: pathophysiology, pathology, and pathogenesis

Dementias, such as AD, are the most common types of NDs and twice as prevalent in females than males (Mielke, 2018; Podcasy & Epperson, 2016; Y. Wang et al., 2020). The hallmark pathologies of AD have been identified in both sexes to negatively effect cognition such as long and short-term memory, and locomotor behaviour (Clancy, 2013; Da Costa et al., 2013; Ju et al., 2013; Levenson, et al., 2014; Podcasy & Epperson, 2016; Raskin et al., 2015). These hallmarks include misfolded protein oligomers (that aggregate) such as extracellular β-amyloid plaques and intracellular neurofibrillary tangles (NFTs, made of tau microtubule associated protein) (Hampel et al., 2021; Kou et al., 2011;

Mohandas et al., 2009; Tracy et al., 2022) (Figure 1). Moreover, neurons that possess these aggregates within or in proximity of the cell have compromised survival, and additionally promote the same fate to surrounding neurons (prion-like effects) (Guest, 2019; Morley et al., 2018; Raskin et al., 2015; Sarantseva et al., 2009; Shadfar et al., 2015). Damages to the cell as a result include oxidative stress, mitochondrial damage, and ultimately cellular death which triggers local to wide-spread inflammation in the brain and atrophy (Figure 1) (Ashraf et al., 2014).

In particular, β-amyloid plaques have also been proposed to occur outside of the CNS, in the Enteric Nervous System (ENS) of the gut (Kowalski et al., 2019). This is because Amyloid Precursor Protein (APP) and β and γ secretases (which cleave APP into β-amyloid monomers) are regularly expressed in the enteric neurons (Kowalski et al., 2019; Sarantseva et al., 2009). Furthermore, preliminary studies in transgenic APP *Mus musculus* (mice) have identified that accumulation of β-amyloid in enteric neurons leaves mice more vulnerable to local inflammation of the gut (Chalazonitis & Rao, 2018; Kowalski et al., 2009). Although the study of β-amyloids and AD in the gut is still in its infancy, there are many propositions as to how β-amyloids promote NDs in the brain from the gut (Chalazonitis & Rao, 2018). For example, a popular hypothesis is that β-amyloids are cross-seeded within the gut to the brain via an unknown mechanism of gut-brain communication (Braak et al., 2003; Kowalski et al., 2019).

Recent evidence has demonstrated that soluble β-amyloid monomers play important roles in the regulation of synaptic neurotransmission, and have antimicrobial/antioxidant properties (helping prevent inflammatory injury) (Y. Li et a., 2012; Mohandas et al., 2009). These monomers are therefore involved in facilitating

communication between neurons, injury prevention and recovery of brain tissue and even maintenance of Blood Brain Barrier (BBB) integrity that protects the immune-privileged brain (Mohandas et al., 2009). Since the ENS is just as vast in neuronal networks as the CNS, and neurodegenerative brain pathologies can also occur in the ENS (Braak et al., 2003; Kowalski et al., 2019), then APP is likely neuroprotective in enteric neurons too. Thus, maintaining the integrity of the intestinal-epithelial-barrier of the gut, analogous to the BBB of the brain (Chalazonitis & Rao, 2018). The antimicrobial/antioxidant role of APP in the CNS is thus justified in the ENS because, the gut epithelium is frequently self-renewing to prevent injury and infection (Rath & Haller, 2022). The gut also has a diverse and protective microbiome which can be perturbed due to pathogenic infection/antibiotic use and/or local inflammation (Hakansson & Molin, 2011; Rinninella et al., 2019).

The existence of β-amyloids are then possible in the ENS. However what triggers these pathologies to arise is unknown. It has been proposed that some bacterial species in the gut, such as *Escherichia coli,* can produce bacterial amyloids (Kowalski et al., 2019), which may also act like prions that could promote β-amyloid oligomerization and aggregation in the gut (Hetz & Saxena, 2017; Simon, 2018), or promote cleavage of APP into its Aβ42 β-amyloid isoform which is more prone to oligomerization (Bekris et al., 2021; N. Li et al., 2019; Sarantseva et al., 2009; Simon, 2018). Aggregates therefore form, hindering ENS signaling, which then translates what is happening in the gut to the brain. The nature of this gut-brain communication has been hypothesized by Dr. Heiko Braak (Braak et al., 2003), that pathologies of NDs are likely to start in the gut and then, through an unknown mechanism of gut-brain communication, appear in the brain shortly after.

Tauopathies are an example of Braak's hypothesis; similar to β-amyloid pathogenesis of NDs in the brain, tau monomers oligomerize and form aggregates known as NFTs and neuritic plaques, which can cause inclusions (inflammation due to intra/extra-cellular damage) in and around neurons (Anwal, 2021; Bălaşa et al., 2020; Guest, 2019). In-fact, tauopathies have been found to occur decades before any clinical symptoms are present, and proposed to promote and intensify β-amyloid pathology (Kametani & Hasegawa, 2018). Moreover, both β-amyloid and also tau tangles/plaques both promote local intestinal inflammation and weakening of the gut epithelial barrier (Kowalski et al., 2019). This weakened barrier can cause metaflammation (low-grade chronic systemic inflammation) linked to NDs (Komleva et al., 2021; Rydbom et al., 2021), thus gut-brain communication along the ENS may not be the sole contributor to NDs. The roles of tau and β-amyloid peptides are therefore likely to be amplifying neurodegenerative disease pathologies, like positive feedback. Therefore, the environment of the gut (the diet and commensals) may be distally seeding NDs in the brain in more ways than one (Berding et al., 2021); this is an example of communication within the DMGB axis (Figure 1).

Although studies involving neurodegenerative disease-linked genes and peptides are very limited in DMGB axis research, the mechanisms of pathogenesis for both β-amyloids and tau can be hypothesized using the rapidly expanding research on another neurodegenerative disease-linked gene for PD, known as α-Synuclein. Peptide α-Synuclein, which also oligomerizes, creates extracellular lesion and has prion-like effects in the tissue it occupies, as does tau and β-amyloid (Bendor et al., 2013; Ruiz-Riquelme et al., 2018). Therefore, α-Synuclein is another potential candidate of pathogenesis of NDs.

1.1.2 Parkinson disease: pathophysiology, pathology, and pathogenesis

Parkinson disease is another common neurodegenerative disease, defined primarily by progressive loss of motor-coordination, initiation and bradykinesia due to death of dopaminergic neurons in the Substantia Nigra (SN) (Figure 1) (Dorsey et al., 2018; Faustini et al., 2017). According to sources such as (Dorsey et al., 2018), PD is one of the most rapidly growing NDs in the world, and males are more likely to develop these particular NDs than females (Feigin et al., 2019; Moisan et al., 2016; Podcasy & Epperson, 2016). Patients with PD may also develop AD later during the course of PD (high comorbidity). This is thought to be due to cross-related mechanisms of pathogenesis between the two NDs (Xie et al., 2014).

Anatomically, PD begins with atrophy in the brain stem at the SN, an essential brain region that produces and projects dopamine to the limbic system, and then into higher cortical areas (Figure 1) (Mayfeild, 2010). These projections are known as the nigrostriatal pathways, and reach certain cortical areas which are known for initiating and coordinating movement (Figure 1), i.e. the basal ganglia (Faustini et al., 2017; Sonne, et al., 2022).
Hallmark pathologies of PD include intracellular misfolded protein aggregates of α-Synuclein oligomers (synucleinopathies) that form plaques called Lewy bodies in the SN (Figure 1) (Y. Huang et al., 2015; Shahmoradian et al., 2019; G. Wang et al., 2016). These intracellular inclusions are suspected to cause aberrant neurotransmission because, α-Synuclein is a SNAP-associated protein in neurons (CNS/PNS/ENS) that tethers and primes pre-synaptic vesicles for exocytosis (Killinger et al., 2019). Similar to β-amyloids, α-Synuclein has been found in preliminary studies to appear in the gut/ENS (Devos et al.,

2013), therefore, the peptide is not confined to driving neurodegenerative pathology in the brain only, just as Braak hypothesized (Braak et al., 2003).

In fact, α-Synuclein aggregates have been identified in the gut epithelium of humans years before clinical onset of PD, presenting non-motor symptoms in the forms of constipation, and Inflammatory Bowel Disease (IBD) (Barbut et al., 2019; Brudek, 2019; Q. Chen et al., 2019). IBD is influenced by the gut commensals (Custers et al., 2022; Dinan & Cryan, 2017; Hakansson & Molin, 2011; Moloney et al., 2016; Zeng et al., 2017), and therefore commensals are suspected to play a role in the formation of α-Synuclein Lewy bodies (Mertsalmi et al., 2020; Rinninella et al., 2019). IBD has also been linked to mitochondrial abnormalities in the gut (Jackson & Theiss, 2020), and PD (Brudek, 2019). Protein α-Synuclein aggregates have been found to cause mitochondrial damage by interacting with complex-I of the electron-transport-chain, and slowing down mitochondrial metabolism (Faustini et al., 2017; Kamp et al., 2010). This type of mitochondrial stress increases the redox state of intestinal epithelial cells and can create inflammation (Console et al., 2020; Friedman & Nunnari, 2014). Therefore, α-Synuclein may act just like β-amyloids and tau in AD, as a facilitator and amplifier of PD by seeding pathology in the gut to ultimately affect the brain (Braak et al., 2003; Kitani-Morii et al., 2021).

Recent evidence in mice has found that α-Synuclein may literally be seeded in the gut and then migrate to the brain via an unknown method of gut-brain communication. For example, fluorescently tagged-α-Synuclein was inoculated into the intestines of the mice and then tracked (Challis et al., 2020). What the researchers found was that the tagged-α-Synuclein translocated from the gut to the brain of the mice, and created human Parkinson-

like behaviours. In addition, what was also observed after inoculation was abnormalities in GI function as well as inflammation, which is also characteristic of pre-clinical human PD patients described in the previous paragraph (i.e. constipation and inflammatory bowel disease) (Challis et al., 2020; Dinan & Cryan, 2017). Moreover, this study in particular suggested that α-Synuclein are metaphorically like seeds, and that the one who sows the α-Synuclein is the gut-epithelium. Therefore, the metabolic status of the gut and commensals within the DMGB axis ultimately effect/promote prion-like protein aggregation. All that's left to understand now is how this axis is perturbed (aetiologies of disease)

Overall, PD and AD are two common NDs which have been studied on their own within the brain. However, as more evidence emerges on the pathogenesis of the canonical genes that characterize these diseases, it is becoming clear that the body is not only controlled and coordinated by the brain but, the body can communicate back and effect the brain.

1.1.3 A holistic approach to studying neurodegeneration

For decades the study of genetic-based NDs have generated several theories on sporadic disease pathogenesis (Garden & Spada, 2012), based on how the disease pathologically presents in the brain; including aberrant neurotransmission, mitochondrial dysfunction, and oxidative stress. However, emerging evidence has proven that cells are not autonomous between tissue types, as pathologies that were previously characterized in brains affected by NDs have also been found in distal parts of the body, such as the gut/ENS. An example would be α-Synuclein Lewy bodies found in enteric neurons (Barbut et al., 2019; Challis et al., 2020). Moreover, these findings highlight how NDs are not

confined to the brain as previously believed, and instead aid in bidirectional communication with the rest of the body for in inter-organ communication/coordination and the maintenance of tissue homeostasis (McHugh & Gil, 2018; Peters, 2006). Especially communications within the DMGB axis briefly described below.

One reason why NDs should be studied using a holistic approach is because of the role of peptide hormones as neurotransmitters (Hoffmann et al., 2021). Typically, the brain is known to secrete endocrine hormones (from the pituitary glad most of the time) to communicate and activate/deactivate physiological mechanisms in distal tissue/glands, to maintain energy balance throughout the body (Hoffmann et al., 2021, Sadiq & Tadi, 2022). Likewise, in vertebrates and invertebrates, distal organs such as the gut are also known to participate in endocrine (peptide hormone) signaling back with the brain, to balance energy expenditure, regulate growth, immunity, and stress of the gut, by coordinating metabolism and feeding behaviour (Hentze et al., 2015; Sadiqu & Tadi, 2022). The mechanism of action for regulating this energy homeostasis is still unclear. However, certain peptide hormones (neuropeptides, NPs) are suspected to be secreted by the gut, then bind and signal through neurons of the ENS to the CNS. For example, galanin in mammals is considered to be one of these NPs, which also has an orthologue in other animals such as *Drosophila melanogaster* (Hentze et al., 2015; Hoffmann et al., 2021; Min et al., 2016). Furthermore, NPs of the gut have also been implicated in AD and PD, because disturbances in gut metabolism/commensals can alter secretion of neuroprotective NPs like galanin (Wraith et al., 2009).

Other ways of perturbing gut metabolism and gut-brain communication is through metabolic organelle stress/damage of peroxisomes and mitochondria (Rath & Haller, 2022;

Schrader et al., 2015). Both peroxisomes and mitochondria have been linked to neurodegeneration, and even share roles in Reactive Oxygen Species (ROS) homeostasis, which can cause inflammation and damage in the gut (Petkovic et al., 2021; Yakunin et al., 2010; Yan et al., 2021). As introduced in section 1.1.1, inflammation of the gut epithelium in inflammatory/IBD have been identified in PD patients. This gut inflammation can be triggered by fatty diets, and changes of gut-commensal populations, triggering mitochondrial dysfunction; possibly peroxisomes too, since both organelles share similar metabolic roles (Console et al., 2020; Moloney et al., 2016) (to be discussed later). Inflammation of the gut can then weaken the intestinal epithelium, and allow opportunistic pathogens or inflammatory mediators in the gut to enter the systemic circulation, causing metaflammation, or exhausting the immune system enough to warrant immunosenescence (loss of proliferative ability by immune cells) (Komleva et al., 2021), leaving the individual more susceptible to infection and disease (especially NDs).

Conclusively, approaching the study of NDs from a holistic point of view will help to uncover the aetiologies of disease, because environmental factors such as diet are highly considered in holistic general health. As of recently, the study of NDs and aetiologies of these diseases have been confined and focused on pathogenesis in the brain. However, emerging evidence is slowly proving that pathogenesis may be on a larger scale which includes, and may begin in other organs (such as the gut) (H. Chen et al., 2022; Q. Chen et al., 2019). Based on what has been introduced this far about AD, PD and holistic research of NDs, the best highly intertwined network of communication that can drive NDs when disrupted is the DMGB axis.

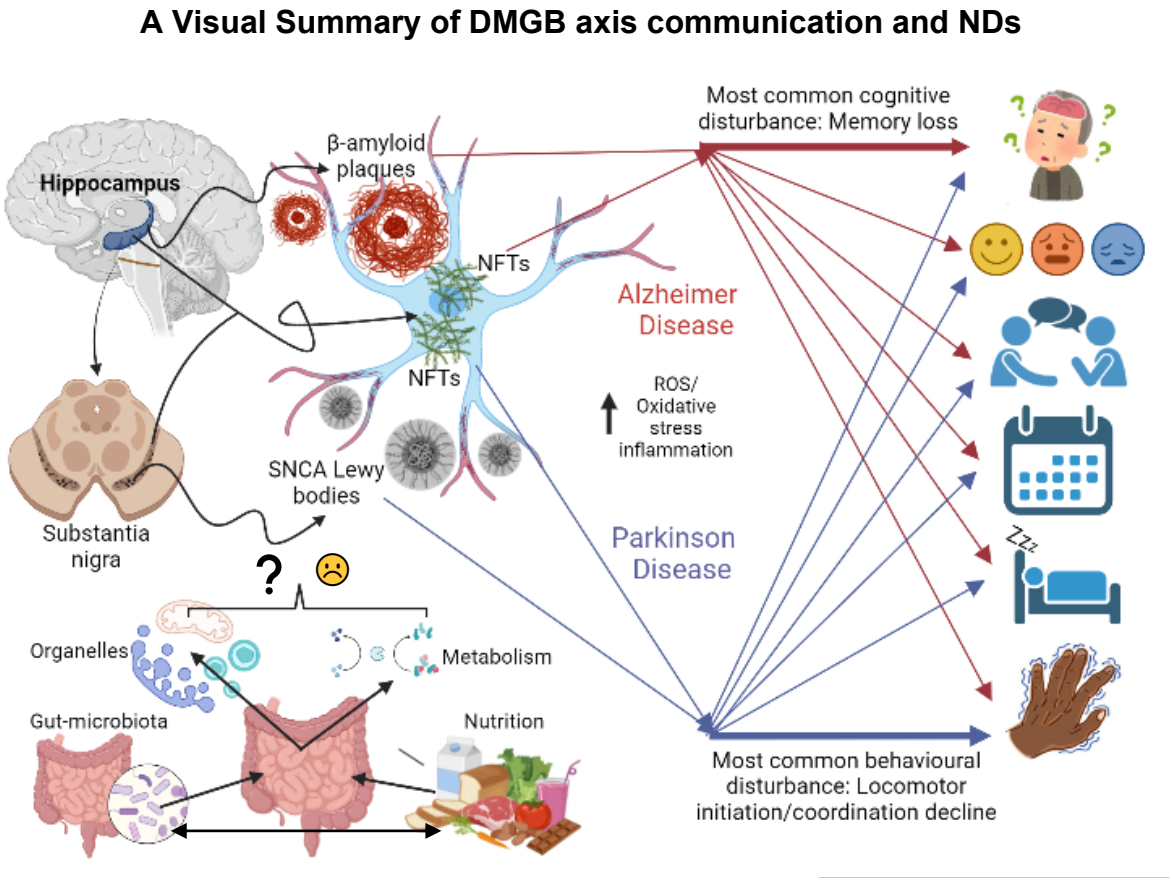

Figure 1. A visual summary of the physical and behavioural pathologies of Alzheimer and Parkinson diseases as a result of perturbing diet-microbiota-gut-brain axis communication. The gut (particularly the small intestine) forms a triad of communication and coordination with the gut microbiota and diet (nutrition). As depicted in the bottom left of the diagram, this cross talk within the triad effects organelle function and metabolism of the gut-epithelial cells, and by mechanisms that are still unclear, these messages are then relayed to the brain. As a consequence of perturbed gut-brain communication (sad face to the bottom left), protein aggregate pathologies have been implicated to arise (β-amyloid plaques, α-Synuclein Lewy bodies, and NFTs) of tau microtubule associated protein). Finally, by following the arrows rightward, these pathologies correspond to elevated ROS/oxidative stress and inflammation in the AD and PD brain, along with debilitating behavioural changes (on the right-most side of the diagram from top to bottom: Memory loss, dramatic shifts in mood, trouble communicating, trouble with organization (executive function), sleep and locomotor disturbances).

Diagram constructed via https://app.biorender.com/.

1.2 Studying neurodegeneration in *Drosophila melanogaster*

To study NDs in the brain is difficult, however to study highly-intertwined inter-organ communication between the gut-epithelium, gut-commensals, and brain is even more challenging in a complex mammalian system. Therefore, by using the *Drosophila melanogaster* (fruit fly), a simpler invertebrate model which carries out similar gross organ function and inter-organ communication compared to a mammalian system, one can begin to study, hypothesize, and unravel NDs in a better controlled system (Cassim et al., 2018; Jeibmann & Paulus, 2009; Perrimon et al., 2016). Moreover, due to gene and metabolic homologies between both the fly, transgenic AD and PD models, that present similar behavioural/cellular pathologies to human NDs, have been successfully constructed expressing canonical human-linked alleles of NDs such as α-Synuclein and β-secretase (Cassim et al., 2018; Jahromi et al., 2020; Prüßing et al., 2013). Therefore, making human disease easier to study in a less complex organism.

The humble fruit fly is an amenable model organism, considered one of the pioneers of genetic and inter-organ communication research (Bodine et al., 2021; Cassim et al., 2018). For many reasons, the *Drosophila* remains the best model for fundamental research; the first reason being the simplicity of its four chromosome genome (Cassim et al., 2018). Next, the fly also has a low genetic redundancy and high homology/orthology to human disease-associated genes. For example, about 75% of disease genes in humans have a functional ortholog in *Drosophila* (Cassim et al., 2018). This allows the ability to create transgenic fly models, to easily study the function of specific mammalian/human-linked genes that may function in the same biochemical pathways in flies. Moreover, the *Drosophila* also has a large arsenal of genetic tools, which helps to manipulate the

expression of human-linked disease genes in a spatial and temporal manner in the fly (Cassim et al., 2018; Brand & Perrimon, 1993). One of the most powerful systems in the fly is known as the *Gal4-UAS* system which enables knock-in/out/down genetic manipulation (Figure 2) (Cassim et al., 2018). In particular, for this thesis the *Gal4-UAS* binary genetic system was used to create model flies for NDs.

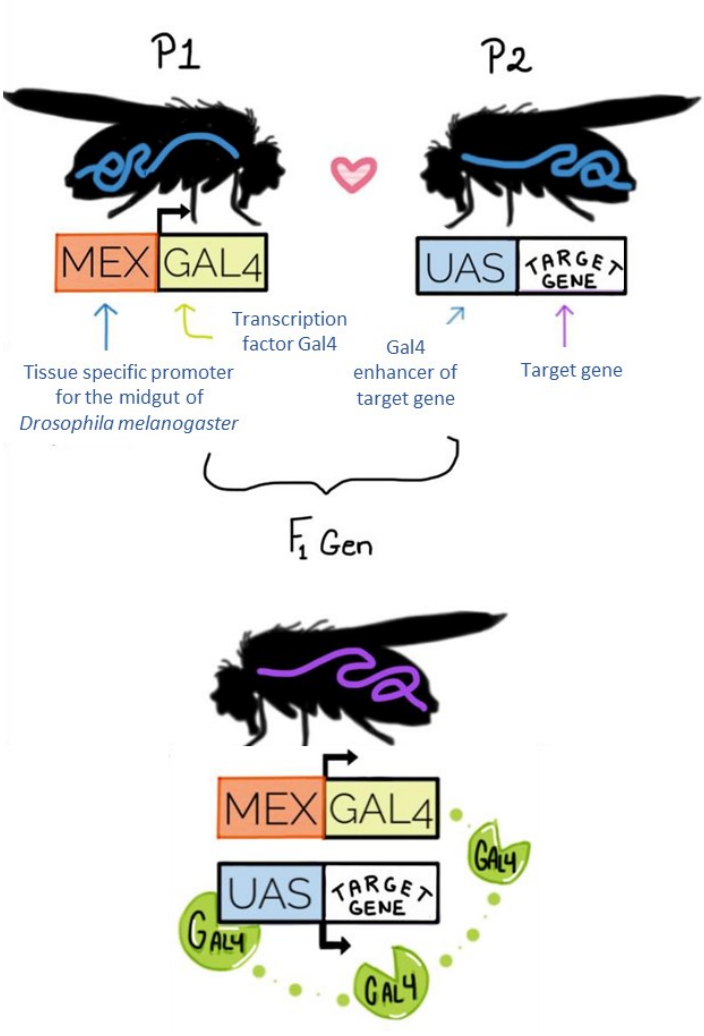

Figure 2. A simplified schematic of how the *Gal4-UAS* system works to drive gene expression in *Drosophila melanogaster*. A fly expressing *Gal4* transcription factor exclusively in the midgut under a tissue specific promoter *Mex* (P1 or parent 1), is crossed to a fly line expressing under the enhancer *UAS*, a target gene sequence or inverted repeat of a target gene sequence for RNAi (P2 or parent 2). The filial generation (F1 Gen) will then express more or less of the target gene.

Many types of metabolic pathways in *Drosophila* have been identified as conserved with humans. This includes signalling pathways, such as immuno-inflammatory pathways Toll, JAK/STAT and immunodeficiency (Imd) in *Drosophila*, and equivalent TLR-4, JAK/STAT and NF-kB pathways in humans (Myllymäki et al., 2014; Hoffman, 2003; Hoffmann & Reichhart, 2002). In-fact, the Toll-pathway was first discovered in *Drosophila* by Dr. Jules Hoffmann before being translated into humans (Hoffmann & Reichhart, 2002; Lye & Chtarbanova, 2018). Additionally, about 80% of functional proteins that are orthologous to mammals have a conserved functional domain with mammals (Cassim et al., 2018). Therefore, metabolic discoveries in *Drosophila* have great potential to be translated into humans.

Another important piece of information to remember is that *Drosophila* only have an innate and lack an adaptive immune system (Lye & Chtarbanova, 2018). These innate immune-inflammatory pathways, whether in humans or *Drosophila,* respond to infection and aging/injury by promoting expression of inflammatory Antimicrobial Peptides (AMPs) (Myllymäki et al., 2014). For human NDs, chronic systemic inflammation caused by the innate immune system (AMPs and inflammatory cytokines) can lead to inflammation of the brain (Arora & Ligoxygakis, 2020; Lye & Chtarbanova, 2018). Typically, AMPs during infection are neuroprotective, but when constantly present in the brain with aging, AMPs elicit neurotoxic effects leading to neurodegeneration (Cao et al., 2013; Kounatidis et al., 2017; Lye & Chtarbanova, 2018). For example, in the fly intestinal epithelium (midgut), when Relish (an Imd downstream transcription factor) was supressed and expression of AMPs was dampened, the outcome of age-dependant neurodegeneration improved (Cao et al., 2013; Lye & Chtarbanova, 2018). Therefore, studying NDs in the

Drosophila in the context of inflammation is ideal, because the fly shares three similar innate immune-inflammatory pathways with humans, and lacks the added complexities of an adaptive immune response to consider when unraveling pathogenesis of NDs.

Chronic sterile inflammation has also been hypothesized to influence sporadic NDs, but still unclear how (Arora & Ligoxygakis, 2020; Katzenberger et al., 2013; Lye & Chtarbanova, 2018). The *Drosophila* Toll-pathway, which is linked to the over expression of pathogenic amyloid-beta 42 (Aβ42) in a transgenic AD model of *Drosophila* (Lye & Chtarbanova, 2018; Tan et al., 2008), and the Imd pathway have both been implicated in sterile inflammation of the brain during (Katzenberger et al., 2013). However, what about in the peripheral organs such as the midgut of the fly?

The *Drosophila* gastrointestinal tract has been researched over decades in regards to interorgan communication (Capo et al., 2019; Hung et al., 2020). The midgut in particular is compared to the mammalian small intestine, and has very similar organization of epithelial cells (Capo et al., 2019), especially where the enterocytes of the fly also have bristle brush boarders, like humans, to help with food absorption/metabolism (Held, 2017). Additionally there are other important cells found in the gut such as enteroendocrine cells for hormone release and suspected to secrete important neuroprotective neurotrophic factors (Capo et al., 2019; Di Cara et al., 2018; Ma et al., 2019). Moreover, like humans, the *Drosophila* has a gut commensal community which is involved in metabolism and survival of the gut epithelium (Capo et al., 2019). Not only influencing disease in the fly when perturbed (as seen in transgenic neurodegenerative disease models of the fly, similar to humans (Mertsalmi et al., 2020; Rydbom et al., 2021), but also effecting the longevity

of the animal (Kitani-Morii et al., 2021; Neophytou & Pitsouli, 2022; Schretter, 2020; von Frieling et al., 2020).

Drosophila also share other similarities in body organ function and interorgan communication to mammals, despite different anatomy (https://droso4schools.wordpress.com/organs/). For example, the nervous system of the fly has similar essential functional brain regions as mammals, such as the mushroom body for learning and memory, analogous to the mammalian hippocampus, and central complex for movement, comparable to the basal-ganglia and precentral gyrus in humans (Barnstedt et al., 2016; Gomez-Marin et al., 2016). Moreover, the nervous system of the fly and mammals share similar mechanisms of neurotransmission; for example, dopamine in dopaminergic neurons of the central complex facilitate locomotion, as the basal ganglia does in mammals (Martin & Krantz, 2014). Therefore, the findings of neurodegenerative disease research in the fly could be translated into humans, considering similar physiology on the cellular level.

Finally, working with *Drosophila* is also easier when considering maintenance of the animal. The fly has an average generational time-span of approximately 10 days, and does not need much to survive; where small amounts of food changed regularly will suffice (Cassim et al., 2018; Fernández-Moreno et al., 2007). This generational time is faster than most mammalian models; for example, rats and mice which only produce a small litter of offspring every 3 weeks, compared to about one-hundred per-day for the fly (Cassim et al., 2018). Therefore, *Drosophila* are perfect models for obtaining multiple biological replicates to confirm findings during experimentation, increasing statistical power (in other words, increasing the confidence that what is observed during experimentation is true or

false), and is overall a powerful model organism. It is an indispensable tool for basic research in, genetic, developmental biology, aging, and behaviour (Marra et al., 2021). Considering all that was mentioned above, the *Drosophila* is one of the most versatile model organisms to study mechanisms of disease, especially as complex as NDs and interorgan communication (Figure 3).

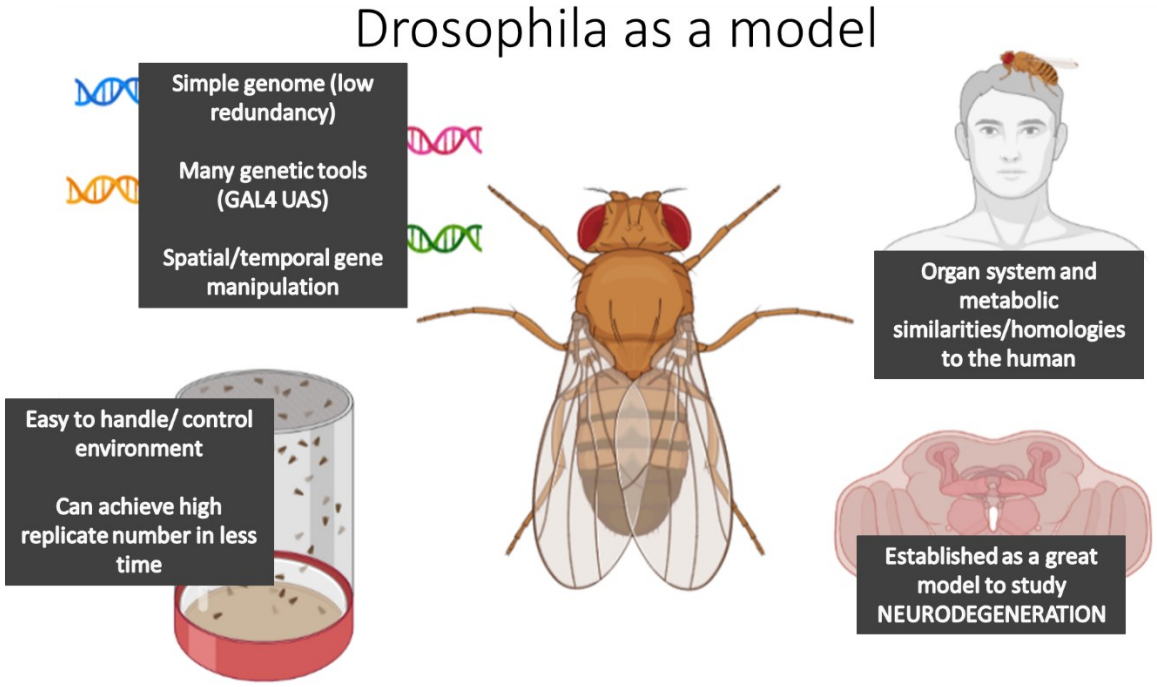

Figure 3. A visual summary of the many benefits of using *Drosophila melanogaster* as a model organism. Diagram constructed via https://app.biorender.com/.

1.3 Introduction to the diet-microbiota-gut-brain axis.

The diet-microbiota-gut-brain axis is a rapidly expanding area of research, suggesting that distal interorgan communication of the gut, gut-commensals and environment through food has an overall impact on the entire body, especially the brain

(Carabotti et al., 2015; de Wouters d'Oplinter et al., 2021; Kitani-Morii et al., 2021). Dysfunction of this axis has been linked to NDs, such as AD and PD (Berding et al., 2021). In the following section, each component of the DMGB axis is summarized, giving examples of vast multiple interactome of this axis, and how NDs have been linked to axis dysfunction.

1.3.1 The diet

Food is essential for replenishing energy expenditure however, the type of diets that are consumed can also dictate an individuals protection against or increase the risk for developing disease, especially NDs (Cena & Calder, 2020). For example, certain types of diets, such as the Mediterranean diet have been proven to have anti-inflammatory benefits, because this diet is rich with Short Chain Fatty Acids (SCFAs) that are considered to be neuroprotective (Cena & Calder, 2020; Joseph, 2017; McEvoy et al., 2017; Virmani et al., 2013). In NDs such as AD, the alteration of cellular membrane lipids in the brain as well as lipid-based signaling moieties known as lipid-rafts, which can be influenced by dietary fat intake, have been found to impinge on the brains ability to resist/recover from incidences of oxidative/inflammatory stress (Denisova et al., 1998; Shen et al., 2004; Joseph et al., 2009). Certain lipid accumulation in the gut (like saturated fatty acids), can trigger systemic metaflammation and release of inflammatory mediators into the peripheral circulation, which can reach and enter the brain to promote vulnerability to inflammation/oxidative stress, by weakening the BBB, making neurons more accessible to these circulating inflammatory mediators (Joseph et al., 2017; Komleva et al., 2021)

Dietary lipids such as fatty acids (FAs) and their derivatives play multiple roles in cellular homeostasis throughout the body. The homeostatic functions of lipids include cellular membrane dynamics such as structure of cells and fluidity (i.e. Phospholipids and cholesterols), signaling (i.e. Phosphatidylinositol's), and energy storage via high-energy bonds (Alberts et al., 2002; Hebbar et al., 2019). These processes are especially important in the brain, to maintain neuronal integrity, facilitate signal transduction between/within neurons via lipid-rafts and neurotransmission, and finally provide the brain with a backup source of energy (Mattson, 2005; Yaqoob & Shaikh, 2010). In-fact, in many NDs, essential lipids directly or metabolically derived from the diet, such as omega-3 FAs, plasmalogens, sphingolipids (like phospholipids) and ceramides (mediate lipid-rafts), are either accumulated in excess or lacking; this lipid imbalance has been identified in countless cases of NDs (Dinicolantonio & Keefe, 2020; Senanayake & Goodenowe, 2019; Swanson et al., 2012; Yaqoob & Shaikh, 2010). Moreover, in the *Drosophila* models of NDs, similar lipid metabolic disturbances are observed (J. Lee et al., 2011; Sellin et al., 2018: Van Veldhoven & Baes, 2013). This ultimately suggests that lipid-metabolism is highly involved in the pathogenesis of NDs (Yadav & Tiwari, 2014)

SCFAs in particular, the metabolic end-products of gut-commensal fermentation of fibrous food, not only have implicated neuroprotective roles, but also can influence neuroinflammation and neurodegeneration (Baxter et al., 2019; Custers et al., 2022; Dinan & Cryan, 2017; Onyango et al., 2015). SCFAs have also been linked to the maintenance of gut and immune homeostasis in mammalian systems, with a neuro-immunoendocrine regulatory role in the gut-brain axis (H. Chen et al., 2022; Silva et al., 2020). For example, dietary butyrate which participates in anti-inflammatory innate-immune system regulation

not only in the gut (i.e. IBD) (Baxter et al., 2019), but also in the brain by influencing BBB permeability (H. Chen et al., 2022). Concurrently, in *Drosophila* models of PD, the administration of sodium-butyrate was shown to reduce degeneration of dopaminergic neurons and improve the locomotor deficits, in a pan-neuronal transgenic fly model for mutant-human-linked α-Synuclein (St Laurent et al., 2013). SCFAs also protect intestinal barrier function, where a high-fat-diet has been found to increase intestinal permeability, which may allow access of opportunistic microbes/local inflammatory mediators to the blood-stream, and therefore creating metaflammation (Custers et al., 2022; Neophytou & Pitsouli, 2022). Therefore, dietary SCFAs can be neuroprotective or neurotoxic, depending on which SCFAs are in abundance (H. Chen et al., 2022).

SCFAs are not the only FAs that can be neuroprotective and neurotoxic in relation to abundance. Very long chain fatty acids (VLCFAs, normally oxidized by peroxisomes), dietarily derived from vegetable oils, nuts and seeds (Letters, 2013), can be lipotoxic to any tissue when accumulated, and have been found in AD along with abnormal peroxisome function in the brain (Kou et al., 2011). On the other hand, VLCFAs are also component of sphingolipids and glycerophospholipids, which are extremely important for cellular structure and signalling in the CNS, PNS, and implicated in the ENS (Kurek et al., 2013; Sassa & Kihara, 2014). For example Docosahexaenoic Acid (DHA, 22:6n-3, a product of peroxisome metabolism), has been extensively studied in animals and humans for their neuroprotective roles in the body and brain, and for alleviating neurodegenerative disease symptoms (Custers et al., 2022; Dinicolantonio & Keefe, 2020; Swanson et al., 2012). In-fact, in *Drosophila,* it has already been identified in a study by (Di Cara et al., 2018), that peroxisomal dysfunction produces dysplasia of intestinal stem cells and elevated redox

status (inflammation) in the fly midgut. As well as aberrant lipid metabolism due to an accumulation of non-esterified fatty acids (as discussed above) in the guts of these *Drosophila.* In addition, Long Chain Fatty Acids (LCFAs) (oxidized by mitochondria) have roles in reducing immune function, overwhelming mitochondria when accumulated, and inducing oxidative stress (Custers et al., 2022; Swanson et al., 2012). Therefore, dysfunctional mitochondria in the gut due to LCFA accumulation may cause abnormalities in neurotransmission of the ENS, by compromising gut integrity and ultimately creating an unstable inflammatory local environment in the gut (IBD), linked to NDs (Q. Chen et al., 2019).

In humans and *Drosophila*, diet has an impact on inflammation locally (i.e. IBD) and systemically (i.e. metaflammation), but specific mechanisms of action are still unknown; the field of research pertaining to the diet-microbiota-gut-brain axis in the context of NDs is still in its infancy (Diop et al., 2017; Kitani-Morii et al., 2021). However, diets high in fats, and sugars can induce metabolic syndromes (insulin resistance), which can lead to decreased longevity, sleep abnormalities, locomotor defects, and mitochondrial dysfunction/inflammation in the gut and systemically in both the fly and mammals (Komleva et al., 2021; Murashov et al., 2021).

Other nutrients such as vitamins also play an important role in both the human and *Drosophila* for maintaining gut and brain health; such as antioxidant in fruits (i.e. blueberries), to counteract other foods, like fats, which are known to create free radicals that need to be detoxified in the gut (Hung et al., 2020; Komleva et al., 2021; Qi et al., 2019). For the brain in particular, dietary vitamin group B, such as B3 (niacin), B9 (folic acid), and vitamin B12 (cobalamin) are known to effect learning, memory, and overall

cognition in both mammal studies (Staff & Windebank, 2014; Virmani et al., 2013). However, an excess of vitamins, B12 can be toxic to the body (Staff & Windebank, 2014). In both human and *Drosophila,* emerging evidence suggests that vitamin B3 (niacin) improves locomotor deficits of human PD patients and PD model flies (Jia et al., 2008; Wakade et al., 2021). The gut microbiota is also a source of such metabolites, especially of B-group vitamins (Morowitz et al., 2011; Virmani et al., 2013). Therefore, dietary metabolites that are not lipids may act in neuroprotective ways within the DMGB axis of humans and *Drosophila* to prevent the onset of NDs.

In conclusion, the diet plays a large role in influencing brain health directly and indirectly. Despite a lack of clarity as to how certain dietary derived metabolites may mediate their neuroprotective or neuroinflammatory roles on the brain (of both humans and *Drosophila*), the effects of diet on gut-metabolism is limited without commensals to help break down and digest ingested nutrients. Thus gut microbiota dictate how dietary nutrients are digested.

1.3.2 The gut microbiota

In its abundance, the human microbiome is composed of around 10x more cells than cells of the human body (>200 taxa) (J. Yang et al., 2020), acting as a major organ system vital for human survival. In-fact, dysbiosis of gut commensal populations leads to metabolic and inflammatory diseases of the gut, as diversity has been positively correlated with protection against NDs (Dinan & Cryan, 2017). With emerging evidence on host-commensal interactions, it is now recognized that neurological diseases, such as NDs are co-morbid with gastrointestinal disturbances (Sampson & Sarkis, 2015; Vandvik et al.,

2004). Likewise, in human PD-linked mutant-gene models of *Drosophila*, the appearance of protein aggregates in the brain have been observed in concurrence with commensal dysbiosis in the gut (Kitani-Morii et al., 2021; Rydbom et al., 2021). In *Drosophil*a, gut commensal diversity is not as magnificent (<30 taxa) (Newell & Douglas, 2014) however, there are many phylogenetically common species shared with humans, which makes this animal an amenable model to study fundamental gut-commensal interactions (Douglas, 2018; Newell & Douglas, 2014; Trinder et al., 2017).

In humans and *Drosophila*, the phyla Firmicutes dominates the gut, where the Firmicutes is composed of many *Lactobacillus* species, (Douglas, 2018; Newell & Douglas, 2014; Trinder et al., 2017). These Lactobacillus species have been found to influence host metabolism and behavioural pathologies of NDs in various gut-commensal studies in humans/mammals and the *Drosophila* (Newell & Douglas, 2014). *Lactobacillus plantarum* in mammals has also been found to influence gut-lipid metabolism, increasing butyrate (SCFAs) which is known to be anti-inflammatory (Storelli et al., 2011). In *Drosophila L.plantarum* also alters gut metabolism, such as the TOR insulin signalling pathway, implicated in pathogenesis of NDs in both the fly and humans (Komleva et al., 2021; Newell & Douglas, 2014; Spinelli et al., 2019; Storelli et al., 2011). Moreover, *L.plantarum* has also been found to influence AD effected behaviours (such as memory) of humans/mammals. For example, the abundance of *L.plantarum* ameliorates age-dependant memory impairment in *Mus musculus* (mouse) models of PD (Castelli et al., 2021). This species also ameliorates mating-preference memory of *Drosophila,* which is effected in fly models of NDs (Schretter, 2020; Schretter et al., 2018). Furthermore, a species that effects locomotion, which is the hallmark negative symptom (a behaviour that

is reduced from what is considered normal behaviour) of PD, in humans is unknown, however in *Drosophila* that species is considered to be *Lactobacillus brevis* (Schretter et al., 2018). Therefore, *Lactobacillus* species may be the culprits behind PD pathogenesis in the gut. So, by studying the fundamentally microbiota of the fly in the DMGB axis, species that influence NDs and the aetiologies which effect those species may be unraveled in humans.

It is now known that the gut microbiota affect host signaling, nutrition/metabolism, intestinal barrier function, and co-adapted with the immune system to counteract infection (Hakansson & Molin, 2011; Newell & Douglas, 2014; Rinninella et al., 2019). Moreover, the commensals are heavily involved with the immune system in the context of inflammation. As previously discussed, the gut microbiota can bring on metaflammation by elevating the redox status of the gut, thus weakening the gut epithelium, all events linked to NDs (Kowalski et al., 2019). In-fact it has been demonstrated that the species that colonize the gut pre and postnatally may increase the risk of metaflammation and of developing neurological disorders later on in adulthood (Grochowska et al., 2019; Ma et al., 2019; Silva et al., 2020). However, it has also been proposed that commensal or pathogenic bacterial secretions, of prion-like peptides, may trigger other proteins in the gut that are sensitive to misfolding and oligomerization to aggregate, such as α-Synuclein (S, Chen et al., 2016; Q, Chen et al., 2019). Then, these misfolded proteins will somehow trigger protein aggregation of NDs peptides in the brain via the vagus nerve (Braak et al., 2003). This hypothesis was confirmed with preliminary data of *Rattus norvegicus* (lab rat) fed with bacteria that produce prion-like curli, where brain neuronal α-syn deposition is increased in the gut and brain (S. Chen et al, 2016)

In conclusion, the communication of the gut-commensals with the CNS is becoming increasingly recognized in the context of NDs, as gut commensals have been discovered to influence the secretion and production of important neuroprotective metabolites, and promote or prevent inflammation in parallel innate immunity. However, the microbes cannot carry out all of these communicative functions without interacting first with the host through the intestinal epithelium.

1.3.3 The intestinal epithelium

The intestine literally has a mind of its own, hosting an ENS with a neuron density much greater than that of the CNS. The gut is also proposed to secrete important neuroprotective neurotrophic factors, which promote neuron survival and plasticity. For example, Brain Derived Neurotrophic Factors (BDNFs) that are produced by gut epithelium are suggested to affect the development and survival of vagal nerve afferents. The vagus nerve is the major route of sensory information of the gut to the brain, and one proposed route of DMGB axis communication (Braak et al., 2003; Biddinger & Fox, 2014). Damage to the vagal afferents is expected to perturb feeding, and therefore the overall metabolism of an organism, directly and indirectly effecting the brain (Biddinger & Fox, 2014). Moreover, the gut also integrates information from the environment, and resident immune system (the gut microbiota), in order to relay to other organs, including the brain, to protect against oxidative stress and cell death.

As mentioned above, digested and processed metabolites in the gut after a meal may communicate to the brain via two ways, the systemic circulation, or the vagal nerve through the ENS. In particular, some of these secretions have been identified as

neuroprotective trophic factors (Liu, 2018), in the ENS, but also CNS and PNS; this is true for humans, and proposed for *Drosophila* gut communication (Di Cara et al., 2018). Therefore, the disruption of gut metabolism due to dramatic changes in diet and commensal populations, may disrupt these neuroprotective trophic factors, causing the brain to become more vulnerable to infection and disease, especially NDs. For example, a BDNF in humans, orthologous to *Drosophila* Neurotropin 1 (DNT1), is neuroprotective in the brain. However, when released from the gut, is also known to protect the death of enteric glial cells which are vulnerable to local inflammation, therefore protecting the support cells of enteric neurons, and in-turn the enteric neurons and vagal afferents (Steinkamp et al., 2012). In fact, in a study conducted by (Vidal-Martínez et al., 2016), it was suggested that gut-derived BDNF may protect enteric neurons against damage caused by misfolding α-Synuclein.

To recapitulate what was previously introduced, emerging evidence has linked commensal dysbiosis to local and systemic inflammation, promoting NDs and corresponding pathologies (Q. Chen et al., 2019; Campos-Acuña et al., 2019). Moreover, it has been speculated that signals of inflammation from the gut may be relayed to the brain by the enteric nervous system, via the vagus nerve (a telephone wire-like, major axonal highway to the brain) (Breit et al., 2018). Thus the gut acts more like the relay center in the DMGB axis, receiving, processing and distributing information to the brain from the diet and gut commensals. However, just like a game of 'telephone', if the person (the gut) receiving the messages cannot hear properly (abnormal metabolic/physiologic function), then the message will not be relayed correctly which may be disastrous (NDs). One

organelle in particular, known as the peroxisome, is the 'deafening' factor to consider within DMGB axis communication.

1.4 Introduction to the peroxisome

The peroxisome is a highly metabolic cellular organelle, present in virtually every cell of the body and conserved across eukaryotes, from yeast to humans (Baron et al., 2016, Smith & Aitchison, 2013). This busy organelle participates in a broad range of conserved cellular-metabolic processes, most notably β-oxidation of VLCFAs, the anabolism and catabolism of complex lipids such as ether phospholipids (like plasmalogens), and synthesis and turnover of Reactive Oxygen and Reactive Nitrogen Species (ROS/RNS). These metabolites are essential for supporting cellular energetic processes, limiting redox stress, maintaining cell structure, signalling, and mitigating inflammation (Di Cara, 2020; Smith & Aitchison, 2013). Moreover, peroxisomes tightly coordinate these processes with other organelles such as mitochondria (Schrader et al., 2015), especially for oxidative homeostasis of the cell to prevent apoptosis. However, the extent to which peroxisomes interact, and may regulate the function of other organelles such as mitochondria, is still unclear (Tanaka et al., 2019).

All operations that make and keep the peroxisome functional are mediated by peroxisomal proteins known as peroxins (PEX). The loss of peroxisome function, as a consequence of *PEX* mutations, causes Peroxisome Biogenesis Disorders (PBDs). This autosomal recessive spectrum disorder in humans can be mimicked and has been studied in animal models such as *Mus musculus*, and *Drosophila melanogaster* with the same *PEX*

mutations (Hiebler et al., 2014; Klouwer et al., 2015; Mast et al., 2011; Yakunin et al., 2010). Of the roughly 30 known peroxins (Smith & Aitchison, 2009), 14 are known in humans to cause PBD if mutated (Klouwer et al., 2015). The most common peroxin to cause PBDs is PEX1 (Hiebler et al., 2014; Smith & Aitchison, 2013), which is involved in the ubiquitination step required to recycle PEX5 and PEX7, that act as receptors to bind and transport essential peroxisomal enzymes to the peroxisome (Smith & Aitchison, 2013). PBDs manifest as aberrant multi-organ developmental diseases. Clinically, children born with PBDs presents with facial malformations, neurodevelopmental delays, learning disabilities, and general behavioural changes (Klouwer et al., 2015). However, the consequences of peroxisome dysfunction are not limited to development, but also have been implicated in the onset and progression of other disease pathologies, such as NDs later on in life.

1.4.1 Peroxisomes as modulators of the DMGB axis

In many NDs, such as AD and PD, increased peroxisome numbers and metabolic disturbances linked to the organelle within neurons of the brain have been identified (Cipolla & Lodhi, 2017; Kou et al., 2011). In particular, lipid profile changes in the brain are a characteristic of NDs. This is demonstrated in lipid composition analysis of post-mortem brains of AD patients in which an accumulation of VLCFAs, substrates of peroxisome β-oxidation, were found (Kou et al., 2011). There is also a parallel decrease in ether-phospholipids, products of peroxisomal metabolism, (Kou et al., 2011), which have antioxidant properties necessary for reducing ROS-mediated oxidative stress and preventing cellular death/tissue inflammation respectively. These ether-phospholipids

include plasmalogens (Kuczynski & Reo, 2006), which can be found in both white and grey matter of the brain and are known to be neuroprotective (Estes et al., 2021; Liu & Zhang, 2014; Su et al., 2019). VLCFAs, or their precursors, are primarily derived from diet even though both can also be endogenously synthesized by peroxisomes. This suggests that abnormal peroxisomal metabolism regardless of breakdown or synthesis of VLCFAs, can lead to inflammation. Although evidence of peroxisome dysfunctions in the development of NDs in the brain has received substantial attention, there is a paucity of research into the contribution that gut peroxisomes play via the DMGB axis.

Lipids are very important for cellular structure, cytoskeletal dynamics, and intra- and inter-cellular signalling, and neuron survival (Custers et al., 2022). Interestingly, in AD, peroxisomes are absent from the dendritic/bouton projections of the neurons and instead cluster at the soma (Kou et al., 2011). In addition, in areas of low peroxisomal localization, AD pathologies such as protein aggregate pathologies are apparent (Kou et al., 2011). This suggests that peroxisome dysfunction is affecting cytoskeletal dynamics such as cellular trafficking, and therefore their own ability to localize to other areas of the cell where needed, such as the plasma membrane for signalling purposes. Cytoskeletal remodelling defects are common in pathophysiology's of NDs, especially synucleinopathies of PD which exhibit dysfunctional vesicle trafficking and exocytosis of neurotransmitters. Given the crucial role peroxisomes play in the remodelling of the cytoskeleton (Di Cara et al., 2017), it is plausible that peroxisome dysfunctions could also underlie intestinal synucleinopathies observed in the ENS of humans and mice. For example, in PBD mouse models, peroxisome dysfunction is associated with α-Synuclein oligomerization and deposition (Yakunin et al., 2010). Additionally, recent work shows

that *Drosophila* peroxisome dysfunction in macrophage-like cells (hemocytes), alters the cells lipid-profile and in-turn impedes cytoskeletal remodelling (for phagocytosis) (Nath et al., 2022). This suggests that the association between intestinal peroxisomes and α-Synuclein promote pathologies of NDs in the gut epithelium and/or ENS.

As mentioned previously, α-Synuclein plaques have been identified in the gut and enteric neurons of PD patients prior to the onset of disease, as well as in cases of inflammatory diseases that compromise the gut epithelial barrier (Challis et al., 2020; Derkinderen et al., 2021; Hawkes et al., 2010). Likewise, peroxisome dysfunction has been found to compromise the integrity of the gut, by activating Tor kinase dependant autophagy and promoting dysplasia of the gut epithelium, as reported in *Drosophila* gut-specific peroxisome KD models by (Di Cara et al., 2018). In this way, peroxisomes were also found to modulate the gut microbiota (Di Cara et al., 2018), further suggesting that perturbation of gut-commensals promotes local and systemic inflammation and altered lipid metabolic profiles corresponding to onset of NDs.

There remains a lot that is still unknown or unclear about how peroxisomes of the gut may contribute to the pathogenesis of NDs, since this organelle is overlooked even as a potential metabolic regulator within the gut, let alone in the DMGB axis. However, peroxisomes may also influence the secretion of BDNF, promoting the survival of neurons in the CNS and PNS of both humans and *Drosophila* (Braverman et al., 2013; Di Cara, 2020). This evidence supports a potential role for peroxisomes in the secretion of neuroprotective neurotrophic factors from the gut to the brain. Therefore, I hypothesize that peroxisomes in the gut are important modulators of the DMGB axis, and when perturbed can lead to the development of NDs (Figure 4).

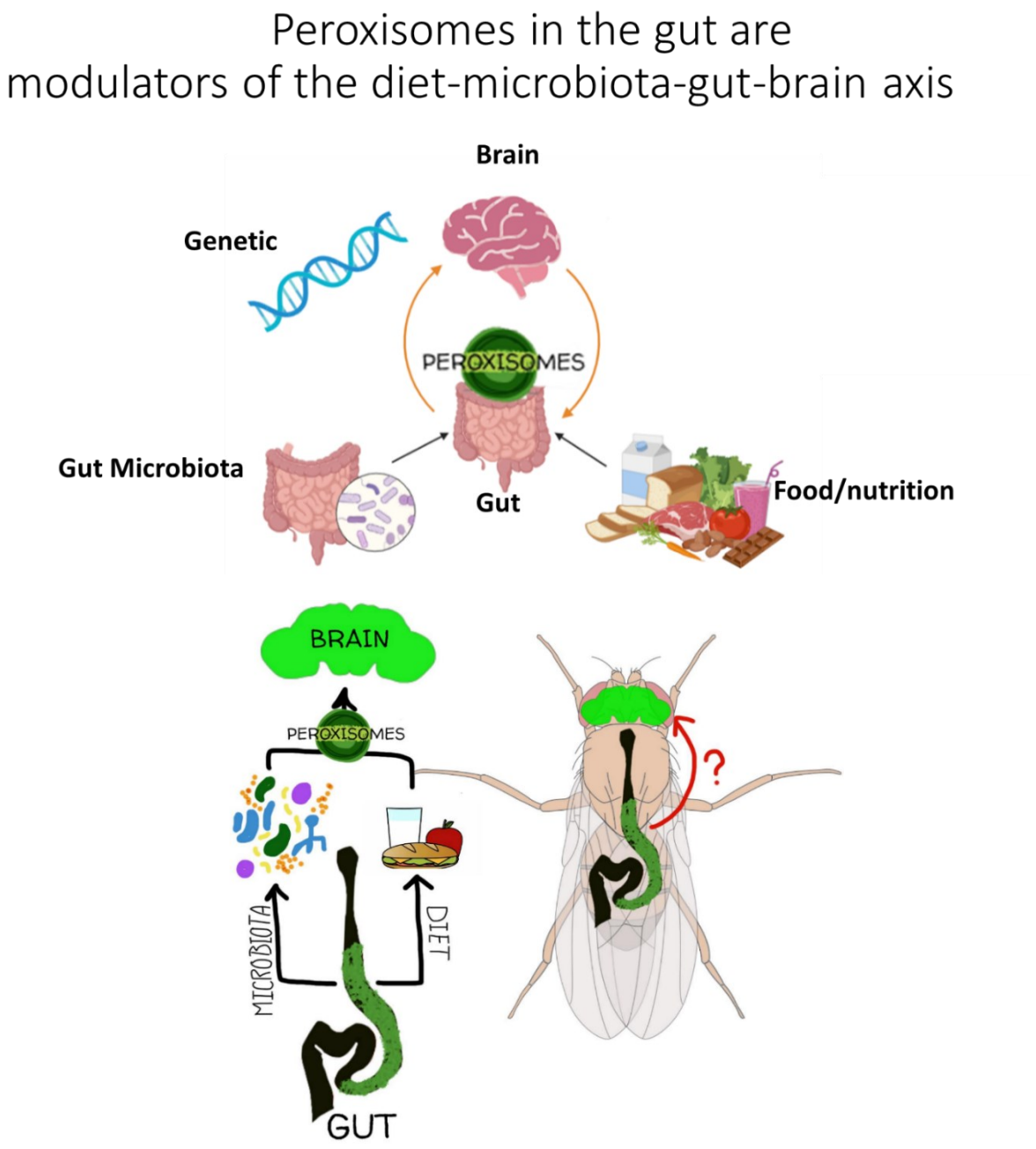

Figure 4. The hypothesis as a visual summary: peroxisomes are important modulators of the diet-microbiota-gut-brain axis in *Drosophila melanogaster*. Peroxisomes are proposed to integrate signals from the gut microbiota and environment such as the diet in order to communicate with the brain in a neuroprotective way. If peroxisomes are thus rendered dysfunctional in the gut, neurodegenerative diseases may develop in the fly. Diagram partially constructed via https://app.biorender.com/.

1.5 Thesis hypothesis: perturbed peroxisomes in the intestinal epithelium modulate neurodegeneration through the DMGB axis

I hypothesized that peroxisomes in the gut are important modulators of the DMGB axis, and when perturbed can lead to NDs. To test this hypothesis in the simpler *Drosophila melanogaster* model, I knocked down *Peroxin 5* (*PEX5*) in the midgut of the fly. PEX5 is an essential transporter of peroxisome-targeted matrix enzymes, and a depletion of PEX5 would mean a depletion of peroxisome metabolic capacity, thus compromising metabolism in the gut (Smith & Aitchison, 2013). I constructed this genotype by crossing a fly expressing the Gal4 transcription factor exclusively in the midgut under a tissue specific promoter (*Mex-Gal4*) (P1 in Figure 2), to a fly line expressing an inverted repeat of *PEX5* (*Mex>Pex5*-i) under the enhancer *UAS* (P2 in Figure 2); yielding a knockdown of *PEX5* in the midgut of these animals (F1 in Figure 2). Additionally, I used the *Gal4-UAS* system to overexpress canonical human-linked mutant-alleles of NDs; α-Synuclein (*Mex>SNCA*) and β-secretase (*Mex>BACE*), as gut-specific reference models for NDs. These models aimed to not only compare the consequences of peroxisomal dysfunction to well known mutant alleles of NDs, but also look at what disturbing mitochondria, therefore metabolism in the midgut, would have on the fly brain. This is because, mitochondria and peroxisomes share close metabolic interactions within the cell, such as fatty acid β-oxidation.

To begin testing the hypothesis, I first wanted to confirm through behavioural assays that the brain was effected as a result of altering transcriptional expression of *PEX5* in the gut (Figure 5). Therefore I primarily used negative geotaxis climbing assays to test locomotor ability of my genotypes for both sexes as a common measure of NDs in *Drosophila* (Madabattula et al., 2015). For *Mex>Pex5*-i, the sex where I observed a deficit

in Negative Geotaxis Climbing Ability (NGCB) were primarily the males on normal Cornmeal conditions (CM); all other genotypes were effected by their overexpression of canonical human-linked neurodegenerative disease-genes in the gut. I then conducted these climbing assays again on different dietary conditions, such as high fat (HFD), and antibiotic treated/axenic (AX) conditions, to test the effects of dramatically altering diet and gut microbiota populations.

After observing climbing deficits of the males on normal conditions, I then wanted to confirm whether any behavioural phenotype in *Mex>Pex5*-i, *Mex>BACE and Mex>SNCA* references were neurobehavioral and not due to feeding nor developmental defects of the heart. Thus, in collaboration with Dr. Deniz Top, we carried out feeding assays on the *Mex>Pex5*-i and *Mex>SNCA* male flies, and respective driver controls *Mex>w*^{1118} and *Mex>GFP*. To test the heart of the aforementioned genotypes, we collaborated with Dr. Hua Bai at Iowa State University. Moreover, as another mean of assessing behaviour of NDs in the flies, I also looked at memory of the flies in collaboration with Dr. Jamie Kramer at Dalhousie University, to stress the effect of peroxisome metabolic dysfunction in the gut, on memory. Additionally, to try and counteract any neurobehavioral phenotypes I observed, and in order to begin unraveling a mechanism of action, I treated *Mex>Pex5*-i and *Mex>SNCA* male flies where a decline of climbing phenotype was observed, compared to respective driver controls, with niacin (vitamin B3). Then I assessed these treated and non treated flies for improvements of climbing behaviour in parallel with ROS (H_2O_2) quantification in the brains of treated and un-treated flies as well. I did this because, niacin is reported to improve locomotion deficits in flies, which may be involved in a peroxisome-linked gut-brain communication pathway. These findings

were further confirmed using fluorescent ROS maker dihydroethidium (DHE) to visualize ROS accumulation in the CM *Mex>Pex5*-i and *Mex>SNCA* male brains.

After confirming a behavioural phenotype in the males, I looked at inflammation and structural/functional abnormalities in the brain in *Mex>Pex5*-i and control *Mex>w*^{1118}, and *Mex>SNCA* and control *Mex>GFP* (Figure 5). To do this I looked at redox accumulation according to expression of AMPs in the brains of the aforementioned male models, via insect AMP *Attacin* (*Att*) and *Drosomycin*, and inflammatory cytokine *Unpaired-3* (*Upd3*), associated with sterile inflammation (Kenmoku et al., 2017). Next, since ROS accumulation was confirmed in these male brains, and accumulation has been linked to mitochondrial abnormalities, using Transmission Electron Microscopy (TEM), I looked for mitochondrial abnormalities in the brains, such as mitophagy or abnormal cristae patterns. These results were then confirmed using MitoSOX®, a stain for superoxide accumulation in mitochondria which indicates mitochondrial stress.

Additionally, to look at structural/functional abnormalities in the brain as a result of any inflammation identified, I specifically looked at the Dopaminergic (DA) neurons using the antibody Tyrosine Hydroxylase (TH), since death of these neurons in humans and *Drosophila* with PD/PD-like pathologies have been identified along with locomotor disturbances. I focused on two clusters known as Protocerebral Anterior Medial (PAM) and Protocerebral Posterior Lateral 1 (PPL1) DA neurons.

Finally, after looking at the behavioural changes of the flies, to further investigate a mechanism of action for any neurobehavioral phenotype observed, I performed -omic screens on the *Mex>Pex5*-i midguts. For this thesis, I focused primarily on the transcriptomic screens of the gut (Figure 5), to try and identify a peroxisome mediated

DMGB axis communication pathway. The transcriptomic analyses were carried out on the guts of *Mex>Pex5*-i and respective driver controls *Mex>w*^{1118} on different food conditions. I then used QIAGEN™ open access analysis bioinformatic tool GeneGlobe™ to run an enrichment analysis of the transcriptomic screens, and identified genes that encode for neuropeptides and their receptors as potential hits; which are common signaling molecules/receptors from the gut to brain. These NPs/NPRs were then validated, and tested in the two sexes and conditions High Fat Diet, and Axenic (AX, antibiotic cocktail) separately over aging, in order to identify hits that were comparable to the behavioural assays. Additionally, I completed genetic manipulation of our strongest gene hit Myo-inhibitory peptide (*Mip*), to see how behaviour is effected with overexpression of *Mip* in the midgut. This was done to begin identifying the first block of a potential mechanism by which *Mip* and the other potential transcriptomic hits cause brain inflammation, neuronal death, and abnormal behaviour through the DMGB axis.

Conclusively, my project is a novel study in the rapidly expanding field of ND research pertaining to the DMGB axis because, the peroxisome is an overlooked organelle when it comes to studying diseases other than PBDs in the brain, let alone in the gut. With this thesis, I hope to bring to light that the peroxisome is as important to disease pathogenesis anywhere in the body as other organelles such as mitochondria. Additionally, I aim to contribute to the urgent and ever expanding field of NDs research in hopes of finding a cure or better treatment options to alleviate global disease burden.

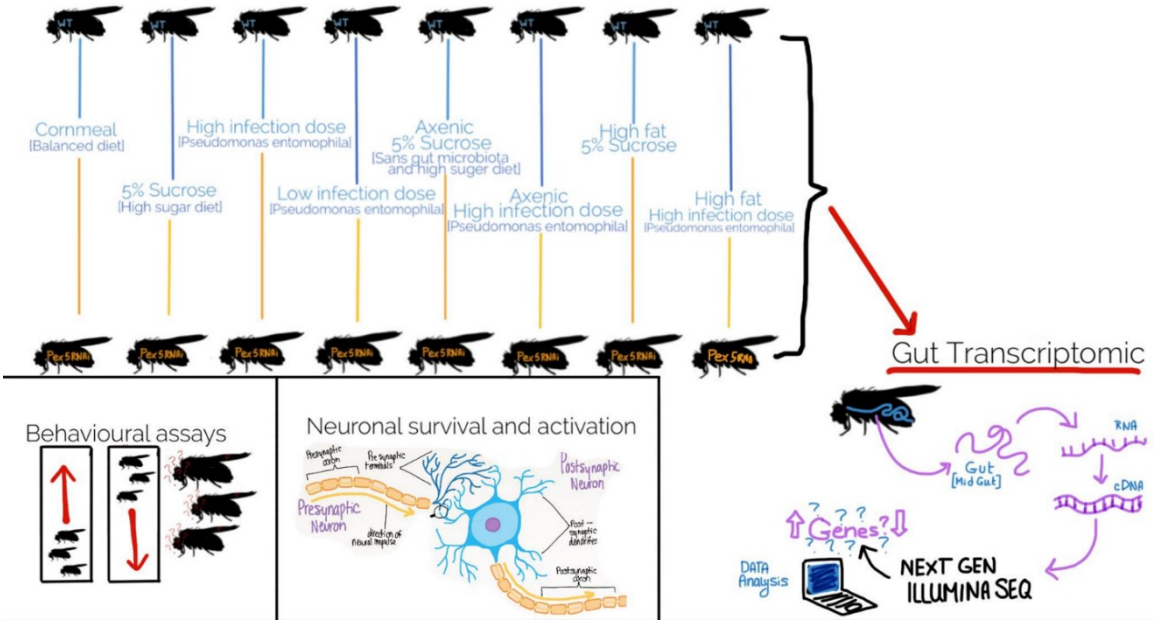

Figure 5. A visual summary of the three main objectives employed to test the hypothesis. Hypothesis: perturbed peroxisomes in the intestinal epithelium modulate neurodegeneration through the DMGB axis. After knocking down peroxisome function in the midgut of the fly (*MexPex5*-i), three main objectives were carried out as outlined. 1) negative geotaxis climbing assays and courtship short-term memory assays to investigate locomotor and memory deficits that arise from neurodegeneration, 2) to look at neuron survival and activation in the brain by assessing brain inflammation/oxidative status/cell death and the abundance of active metabolic factors (such as TH in DA), and 3) carry out -omic screens of the midgut, transcriptomic is priority, to further investigate a peroxisome-linked DMGB axis mechanism of communication.

CHAPTER 2: MATERIALS AND METHODS

2.1 Behavioural studies

2.1.1 Ethics statement

There are no ethical issues surrounding invertebrate models, such a the *Drosophila melanogaster* (fruit fly), for experimentation.

2.1.2 *Drosophila* stocks and husbandry

All active *Drosophila melanogaster* fly strains/crosses were maintained at 25°C in an incubator set at 60% humidity with a 12hr light:dark cycle. Multiple 46 mL polypropylene *Drosophila* food vials (AS507, ThermoFischer Scientific™) of necessary crosses were set up for each experiment, to ensure enough female and male flies in the filial progeny (F1) eclose. The virgin females (driver strains) used to make each cross were primarily of a transgenic strain that carries a P element expressing the midgut-specific driver *Mex-Gal4*, integrated into the *Drosophila* genome on the X-chromosome (Bloomington *Drosophila* Stock Center, BDSC:91367, *P{w[+mC]=mex1-GAL4.2.1}9-1, y[1] w[1118]*). Collected virgins were separated from males until sexual maturity (normally aged to 2-4 days old (do) for optimal mating). Mature virgin females were then crossed with males of w^{1118} (BDSC:5905, *w[1118]*), *UAS-Pex5* RNA-i (Vienna *Drosophila* Resource Center, VDRC:42332, *w[1118]; P{GD14972}v42332*), *UAS-GFP* (BDSC:5137, *w[1118]; P{w[+mC]=UAS-mCD8::GFP.L}LL5, P{UAS-mCD8::GFP.L}2*), *UAS-SNCA* (BDSC:51375, *w[1118]; P{w[+mC]=UAS-SNCA.J}1/CyO*), *UAS-BACE* (BDSC:29877, *w[1118]; P{w[+mC]=UAS-BACE1.L}2*), and *UAS-Mip* (Korean *Drosophila* Resource Center, KDRC:10027, *w[1118](I); P(UAS-*

Mip) vie72a (II)). Additionally, another enterocyte driver used in the midgut was *Myo1A^{ts}-GAL4; Tub-GAL80^{ts}, UAS-GFP* (Jiang et al., 2009) (A kind gift from Dr. Edan Foley, University of Alberta). This driver was crossed to *UAS-Cas9* (BDSC:54595, *w[1118]; P{y[+t7.7] w[+mC]=UAS-Cas9.C}attP2*) and *sgRNA Pex3* (A strain made in the Di Cara Lab) separately. Finally, a brain driver used to express *UAS-BACE* as a brain-only positive control was *Elav-Gal4* (BDSC:458, *P{w[+mW.hs]=GawB}elav[C155]*). Moreover, crosses of interest were always set in parallel with controls for same day eclosure of F1 adults (Table 1), to ensure aged-matched mutants and controls on the day of assay.

Table 1. Table of relevant crosses. *Drosophila* follow Mendelian genetic inheritance. The following table highlights this method of inheritance with a list of all the crosses constructed for this thesis project. *Drosophila* have four chromosomes; the 1st (X/Y), and 2nd and 3rd (autosomal) only are used for genetic manipulation.

Crosses F0	**F1 ♂**	**F1 ♀**
(Mex GAL4 ☿) x (w^{1118} ♂) $\frac{Mex\ GAL4}{Mex\ GAL4};\frac{+}{+};\frac{+}{+}\ x\ \frac{X}{Y};\frac{+}{+};\frac{+}{+}$	$\frac{Mex\ Gal4}{Y};\frac{+}{+};\frac{+}{+}$	$\frac{Mex\ Gal4}{X};\frac{+}{+};\frac{+}{+}$
(Mex GAL4 ☿) x (UAS PEX5 RNAi ♂) $\frac{Mex\ GAL4}{Mex\ GAL4};\frac{+}{+};\frac{+}{+}\ x\ \frac{X}{Y};\frac{UAS\ PEX5\ RNAi}{UAS\ PEX5\ RNAi};\frac{+}{+}$	$\frac{Mex\ Gal4}{Y};\frac{UAS\ PEX5\ RNAi}{+};\frac{+}{+}$	$\frac{Mex\ Gal4}{X};\frac{UAS\ PEX5\ RNAi}{+};\frac{+}{+}$
(Mex Gal4 ☿) x (UAS GFP/Cyo♂) $\frac{Mex\ Gal4}{Mex\ Gal4};\frac{+}{+};\frac{+}{+}\ x\ \frac{X}{Y};\frac{UAS\ GFP}{Cyo};\frac{+}{+}$	$\frac{Mex\ Gal4}{Y};\frac{UAS\ GFP}{+};\frac{+}{+}$	$\frac{Mex\ Gal4}{X};\frac{UAS\ GFP}{+};\frac{+}{+}$
(Mex Gal4 ☿) x (UAS SNCA/Cyo♂) $\frac{Mex\ GAL4}{Mex\ GAL4};\frac{+}{+};\frac{+}{+}\ x\ \frac{X}{Y};\frac{UAS\ SNCA}{Cyo};\frac{+}{+}$	$\frac{Mex\ Gal4}{Y};\frac{UAS\ SNCA}{+};\frac{+}{+}$	$\frac{Mex\ Gal4}{X};\frac{UAS\ SNCA}{+};\frac{+}{+}$
(Mex Gal4 ☿) x (UAS BACE♂) $\frac{Mex\ GAL4}{Mex\ GAL4};\frac{+}{+};\frac{+}{+}\ x\ \frac{X}{Y};\frac{UAS\ BACE}{UAS\ BACE};\frac{+}{+}$	$\frac{Mex\ Gal4}{Y};\frac{UAS\ BACE}{+};\frac{+}{+}$	$\frac{Mex\ Gal4}{X};\frac{UAS\ BACE}{+};\frac{+}{+}$
(Mex Gal4 ☿) x (UAS Mip♂) $\frac{Mex\ GAL4}{Mex\ GAL4};\frac{+}{+};\frac{+}{+}\ x\ \frac{X}{Y};\frac{UAS\ Mip}{UAS\ Mip};\frac{+}{+}$	$\frac{Mex\ Gal4}{Y};\frac{UAS\ Mip}{+};\frac{+}{+}$	$\frac{Mex\ Gal4}{X};\frac{UAS\ Mip}{+};\frac{+}{+}$

Table 1. continued. Table of relevant crosses

Crosses F0	F1 ♂	F1 ♀
(Myo1A^{ts}-Gal4 ☿) x (UAS Cas9 ♂) $\frac{X}{X};\frac{Myo1A[ts]-Gal4}{Cyo};\frac{\frac{Tub-Gal80[ts],}{UAS-GFP}}{Tm6\ B}$ $x\ \frac{X}{Y};\frac{+}{+};\frac{UAS\ Cas9}{UAS\ Cas9}$	$\frac{X}{Y};\frac{Myo1A[ts]-Gal4}{+};$ $\frac{Tub-Gal80[ts],}{\frac{UAS-GFP}{UAS-Cas9}}$	$\frac{X}{X};\frac{Myo1A[ts]-Gal4}{+};$ $\frac{Tub-Gal80[ts],}{\frac{UAS-GFP}{UAS-Cas9}}$
(Myo1A^{ts}-Gal4 ☿) x (sgRNA PEX3 ♂) $\frac{X}{X};\frac{Myo1A[ts]-Gal4}{Cyo};\frac{\frac{Tub-Gal80[ts],}{UAS-GFP}}{Tm6\ B}x$ $\frac{X}{Y};\frac{U6-sgRNA\ PEX3\ KO}{Cyo};$ $\frac{UAS\ Cas9}{Tm3\ sb}$	$\frac{X}{Y};\frac{Myo1A[ts]-Gal4}{U6-sgRNA\ PEX3\ KO};$ $\frac{UAS-Cas9}{\frac{Tub-Gal80[ts],}{UAS-GFP}}$	$\frac{X}{X};\frac{Myo1A[ts]-Gal4}{U6-sgRNA\ PEX3\ KO};$ $\frac{UAS-Cas9}{\frac{Tub-Gal80[ts],}{UAS-GFP}}$
(Elav Gal4☿) x (w^{1118}♂) $\frac{Elav\ Gal4}{Elav\ Gal4};\frac{+}{+};\frac{+}{+}\ x\ \frac{X}{Y};\frac{+}{+};\frac{+}{+}$	$\frac{Elav\ Gal4}{Y};\frac{+}{+};\frac{+}{+}$	$\frac{Elav\ Gal4}{X};\frac{+}{+};\frac{+}{+}$
(Elav Gal4☿) x (UAS BACE♂) $\frac{Elav\ Gal4}{Elav\ Gal4};\frac{+}{+};\frac{+}{+}\ x\ \frac{X}{Y};\frac{UAS\ BACE}{UAS\ BACE};\frac{+}{+}$	$\frac{Elav\ Gal4}{Y};\frac{UAS\ BACE}{+};\frac{+}{+}$	$\frac{Elav\ Gal4}{X};\frac{UAS\ BACE}{+};\frac{+}{+}$

The F1 progeny were collected and kept at 25°C, separated by genotype, sex, and date collected (to track aging). Collection of the flies involved the use of CO2 anesthesia, which would not be administered for more than 5 min at a time to prevent animal death. If F1 progeny were left to age, the fly food vials were changed every 3-5 days.

2.1.3 *Drosophila* food: cornmeal, high fat diet, axenic diet, niacin diet

Preparation of the cornmeal (CM) fly food followed the recipe of the Bloomington stock center https://bdsc.indiana.edu/information/recipes/bloomfood.html. Once the food

was finished cooking, a thermometer was placed to monitor the cooling down of the food as the stove-top is turned off. At 70-80°C anti-mold was added (per liter : 4 mL propionic acid (402907, Sigma-Alrich™), 1 mL phosphoric acid (P5811, Sigma-Aldrich™), and 3g of Methyl-Benzoate (JRD0440, Sigma-Aldrich™) in 100 mL 95% EtOH. Then the liquid food was poured into a DrosoFiller™ (Flystuff 59-168 Droso-filler, Narrow, Genesee Scientific) for mass dispensing into polypropylene 46 mL housing vials. Another option was to use Genesee scientific™ Nutrifly® mix (66-116, Genesee Scientific™) when consistency in the fly food was needed: per 100 mL of water 17.77g/100 mL of Nutrifly® mix was cooked following the same instructions as the CM food and addition of anti-mold described above.

High-fat food was made using a 4:1 ratio cornmeal food to fat. The fat mix was a 3:1 ratio of coconut oil (C1758, Sigma-Aldrich) to erucic acid (Broccoli-seed oil, E3385, Sigma-Aldrich™). The choice of the fats was made to obtain a mixture of Long Chain Fatty Acids (LCFAs) (coconut oil) and Very Long Chain Fatty Acids (VLCFAs) (erucic acid). Anti-mold was added.

The antibiotic cocktail/axenic (AX) food was prepared using Nutrifly® and a cocktail of antibiotics, weighed under a fume hood and dissolved in sterile water. Antibiotics were then added to obtain final concentrations of: 100 µg/mL Ampicillin (A1593, Sigma-Aldrich), 100 µg/mL Metronidazole (M3761, Sigma-Aldrich), 100 µg/mL Neomycin (N1876, Sigma-Aldrich), 250 µg/mL Tetracycline (0.8168, Sigma-Aldrich), and 50 µg/mL Vancomycin (1709007, Sigma-Aldrich). Anti-mold was added.

Finally, niacin (nicotinic acid) food was also prepared using Nutrifly® mix and 0.100g/100 mL of nicotinic acid (N4126, Sigma-Aldrich) to cooked Nutrifly® food, dissolved in water, for a final concentration of 100 mmol. Anti-mold was added.

2.1.4 Negative geotaxis climbing assays

Negative geotaxis climbing assays were carried out according to a protocol designed and optimized by (Madabattula et al., 2015), to assess upward-climbing locomotor behavior in the fly. To set up the assay area, a sturdy table was placed in a low humidity room (~40%), a Pyrex™ 250mL graduated cylinder (3066, Corning® by Sigma-Aldrich™) was placed in the middle of a foam mat on the table, and the bottom of the cylinder was traced onto the mat with a marker, to keep the positioning of the cylinder in the room consistent (Figure 6). The room was moderately lit, and an extra desk lamp was placed above the cylinder to add extra illumination for the camera (Figure 6). The lamp was placed where the light illuminated the area but not the cylinder directly, to avoid reflection of light within the cylinder which may affect the climbing of the flies.

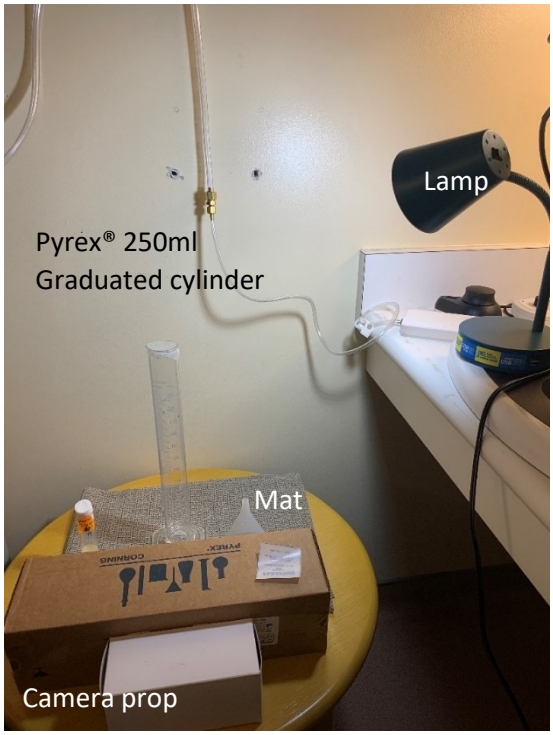

Figure 6. The general room setup of the negative geotaxis climbing assay arena.

Cohorts of 20 *Drosophila* per replicate were collected and then separated by genotype, day of collection, and sex. The flies were assayed at age 10, 15, 20, 30, 40, and 50 days old (do), in parallel with controls. To conduct each assay, replicates were tapped into a 250 mL glass cylinder gently using a funnel, and the record button was pressed on the video recording device (iPhone XR: A1984, Apple Inc.). As the recording began, the cylinder was lifted up and then tapped back down gently 10 times to bring all of the flies to the bottom of the cylinder, then tapped ten times again in an asynchronous manner with shaking in-between to startle and disorient the animals. The negative geotaxis climbing ability (NGCA) of the flies were recorded for 2 min.

To score the assays, the following spreadsheet was set up to track and calculate the percentage of flies that had climbed over the target height of 190 mL (considered a successful climb), in 10 sec intervals for 2 min (Figure 7). Only flies that climbed over the

target line, and not just reached the target line, were considered in the data collection (count). The identified ideal timeframe that was used, that showed the least variance within the same genotype was between 10-20 sec, was based on the optimized protocol by (Madabattula et al., 2015). These measurements were also considered in accordance to other previously published negative geotaxis climbing experiments, also using *Drosophila* models of PD and AD with locomotor deficits (Chakraborty et al., 2011; Feany & Bender, 2000). The mean percentage (M) and standard deviation (SD) of flies over the target line for all replicates within each genotype, age and sex were calculated on Microsoft® Excel® (v 2103 [16.0.13901.20400] 2021). The data was then plotted with statistical analysis carried out using simple two-tailed, unpaired Student's t-tests, assuming equal variance and an α=0.05, on GraphPad PRISM (v 9.4.0). Statistical tests were carried out in accordance to the original protocol reported by (Madabattula et al., 2015).

Sex: M	Age: 10	Time Interval:	00:10	00:20	00:30	00:40	00:50	01:00	01:10	01:20	01:30	01:40	01:50	02:00	Tot	%
Trial #:	1	Time:	00:31	00:41	00:51	01:01	01:11	01:21	01:31	01:41	01:51	02:01	02:11	02:21		Peak %:
start time:	00:21	Climbed up	0	9	6	0	1	1	1	0	0	0	0	0	18	85
Starting #:	20	Climbed down	0	0	1	0	0	0	0	0	0	0	0	0	1	Endpoint%
Dead at Bottom:	0	cumulative	0	9	14	14	15	16	17	17	17	17	17	17	17	85
Alive:	20	percentage	0	45	70	70	75	80	85	85	85	85	85	85		

Calc	Endpoint Peak	
average	83.16667	85.5
std	7.595076	7.245688
ste	2.401774	2.291288

Figure 7. A sample of the spread sheet used to calculate the climbing success for each replicate of the negative geotaxis climbing assays. The spread sheet also calculates the endpoint indicating how many flies were above 190 mL at the end of each assay according to (Madabattula et al., 2015). Time is in 10 sec intervals, 'climbed up/down' refers to how many flies between two consecutive intervals have successfully climbed over or below 190mL, 'cumulative' indicates how many flies have successfully climbed over the 190mL accounting for the ones that also climbed down, and percentage is total number of successful flies over total flies in each cohort at each selected time interval.

2.1.5 Courtship memory assays

Courtship in *Drosophila* is an easy way to test for memory deficits, since male courtship/mating behavioral patterns are simple to identify. What courting assays measure, is the ability of virgin males to reduce courting/mating behavior as a result of rejection,

after being trained to learn and remember what rejection looks like by a non-receptive pre-mated-female. Therefore, short-term courtship memory in male *Drosophila* was carried out in collaboration with Dr. Jamie Kramer at Dalhousie University in accordance with an optimized protocol published by Koemans et al., in 2017.

Drosophila Cantron-R strains were used to obtain mated-females were prepared according to (Koemans et al., 2017), in parallel with target crosses for the genotypes of interest, *Mex>Pex5*-i, *Mex>w*^{1118}, *Mex>SNCA*, and *Mex>GFP*; set in narrow polypropylene food/housing vials 46 mL. One day before collecting virgin males of the interested phenotype to be tested (day 0), Canton R males and females were collected and placed together to mate for 4 days (until day 3). Then on day 1, virgin males eclosed from the crosses set to obtain the genotypes of interest and were collected every 30-60 min throughout the day, using an aspirator to gently place each male into individual wells of a housing block (96 deep well plates filled with cornmeal food). Each genotype was divided into two groups, trained and non-trained (See below). To obtain enough replicates for statistical power, and in the interest of time, fly collection and assay/data collection spanned over three consecutive days, where the Canton-R flies were always one day older than the virgin males.

On the day of the assay, from 10am to 11am, pre-mated Canton-R females were anesthetized and separated from the males (1hr before training). At 11am, the pre-mated females were anesthetized again and individually placed into single wells of a new housing block. Then, without anesthetization and using an aspirator as described by Koemans et al., 2017, the virgin males to be trained were placed into each well with an individual pre-mated female. From 11am to 12pm (1hr) the virgin males were left in each well to learn

and identify rejection from the non-receptive female. Afterwards, the groups of trained males were moved once again into a vacant housing plate without the females and left to rest in solitude from 12pm to 1pm (1hr) in the arena incubator before assaying. At 1pm the trained males were gently moved into assay wells with a new pre-mated female, and courtship was recorded for ten min.

Each assay was scored for 5/10 min using a stopwatch to record the total time a male fly was courting/coupling to a pre-mated female; starting and stopping the same timer as the male starts and stops courting/coupling. Courtship behavior can be identified by males orienting towards, following, and touching a female, and extending one wing outwards and vibrating it while following the female (courtship song). When all assays were scored, the average percentage of time spent courting over 5 min was calculated (courting index) for each genotype and from there the learning index was calculated (LI = [CI naive – CI trained] / CI naive), both according to Koemans et al., 2017; indicating how well (in %) a male has learned and remembered how to court and be rejected. The data was then plotted with statistical analyses using using a multiple unpaired t-test, assuming equal variance and an $\alpha = 0.05$, on GraphPad PRISM (v 9.4.0). The simple t-test was deemed fitting for comparing between genotypes and not conditions, which was the main interest of this thesis.

2.1.6 Feeding assays

In collaboration with Dr. Deniz Top at Dalhousie University, feeding assays conducted on CM *Mex>Pex5*-i or *Mex>SNCA* males in comparison to CM controls

Mex>w^{1118} or *Mex>GFP* males were composed of four replicates of 15 male flies (n=60); this assay was adapted from (Botero et al., 2021).

3D printed acrylic feeding chambers were used to house flies during the assay, where each well of the chamber contained 1% agar as a source of hydration, and 5µl borosilicate glass capillaries filled with liquid fly food and tracking dye. The microcapillaries were then connected and sealed off to the feeding chambers (Figure 8). Three days before the assay, the flies were kept in original food vials within the assay incubator, set a 25 °C 12 hr light-dark cycle, to habituate. Then on day one of the assay, each individual assay chamber was occupied by one fly (Figure 8), and from days one to three a camera in the incubator recorded how much food was being consumed over a period of 36 hrs (during the active 12 hr light-cycle of the fly) (Figure 8). After three days, the data was collected and trimmed down and the same steps were repeated for each of the remaining replicates; at the end the data was pooled with approximately 60 flies per genotype after eliminating flies that had died during the assay. Then GraphPad Prism (v 9.2.0) was used to visualize the data and run statistical analyses, using two-tailed, unpaired Student's t-tests, assuming equal variance and an α=0.05, as calculated by our collaborato

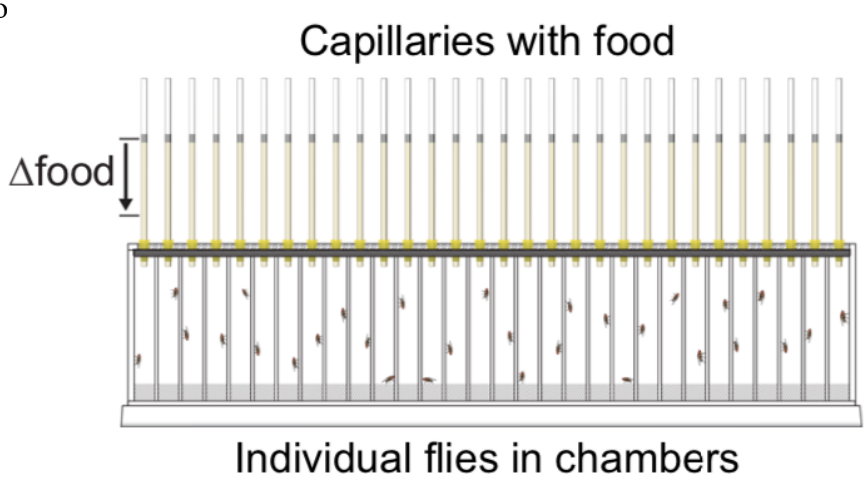

Figure 8. Apparatus of the feeding assays. As depicted, male *Drosophila* occupy a single chamber with a microcapillary filled with food, where 15 chambers were designated to the genotypes of interest, and the remaining 15 chambers to controls. Image source: MacKayla Williams, BSc Hon. Neuroscience, working in the lab of Dr. Deniz Top.

2.1.7 Heart assessments

In collaboration with Dr. Hua Bai at Iowa state university, the hearts of approximately 30 male and female flies per genotype were assessed for abnormalities of heart rate, heart pressure, arrythmia, diastole, and systole using a protocol developed by (Fink et al., 2009) according to (K. Huang et al., 2020). Moreover, statistical analyses consisted of one-way ANOVAs in accordance with (K. Huang et al., 2020).

2.2 BRAIN PATHOLOGY

2.2.1 Quantitative polymerase chain reaction of antimicrobial peptides and inflammatory cytokines in *Drosophila* heads

The easiest way to begin looking at inflammation in the brain of *Drosophila* is by quantifying antimicrobial peptides (AMPs) or inflammatory cytokines (ICs) expression in the whole-head of the fly. Individual replicates of approximately n=13 heads were carefully cut at the neck of the fly, using Dumont straight micro-dissection scissors and #5 micro-dissection forceps (15040-11 and 11251-10, Fine Science Tools™), making sure to avoid piercing the head and inducing inflammation through injury. Then, the heads were preserved in 250 µl of TRIzol™ reagent (15596026, ThermoFischer Scientific™) in a 1.5 mL Eppendorf ™ centrifuge tubes (022363204, Eppendorf™). Once three biological replicates were collected of each genotype, in addition to separating males and females,

the samples were kept on ice during collection and processed by RNA extraction, or frozen at -80 °C for later RNA extraction.

To proceed with RNA extraction, the samples were homogenized on ice; first manually, to make sure the soft brain tissue was exposed to the TRIzol™ reagent, and then using an electric-motorized pestle to further homogenize the lysate (pestles 47747-358, cordless motor 47747-370, VWR®). The samples were immediately centrifuged at 4°C (centrifugation speed: 13,000 g-force) for 3 min, placed on ice again, and then the supernatant was carefully separated into another 1.5 mL microcentrifuge tube; avoiding the debris from the fly head cuticle at the bottom of the tube, which clogs the RNA extraction column in the following steps. An equivalent volume of 95% ethanol was added to the collected supernatant, to precipitate the RNA, and mixed gently but thoroughly by pipetting up and down until there was no phase separation observed. The mixture was immediately pipetted into a column-tube of the ZYMO™ Research, Direct-zol® RNA Microprep kit (R2061, ZYMO™), and then further processed as instructed by the kit. Once the RNA was isolated, samples were either immediately quantified on QUBIT™ fluorometer (Q33238, ThermoFischer Scientific™), Nanodrop™ spectrophotometer (ND-ONEC-W, ThermoFischer Scientific™), or preserved at -80°C.

After quantification, 1µg of RNA was prepared into complimentary DNA (cDNA) using Applied Biosystems™ High Capacity cDNA Reverse Transcription kit (4387406, Thermo Fischer Scientific™), following the manufacturing instructions for the cDNA reaction mix, and using an Eppendorf 6331 Nexus Gradient Flexlid Thermal Cycler for an approximately 3hr PCR reaction; 10 min 25°C → 120 min 37°C → 5 min 85°C → 4°C hold. The cDNA was then stored at -25°C undiluted, or immediately diluted with nuclease

free water (1:5) to be used in a Quantitative Polymerase Chain Reaction PCR (qPCR) assay, following a PowerTrack SYBR Green Master Mix qPCR reaction kit (A46109, ThermoFischer Scientific™) protocol and using 10 nmol of target primers per reaction: *Attacin (Att* AMP: forward primer 5′AGTCACAACTGGCGGAC3', reverse primer 5′TGTTGAATAAATTGGCATGG3'), *Unpaired-3 (Upd3* IC: forward 5'AAAACGGCCAGAACCAGGAA3', reverse 5'CATGGCCAAGGCGAGTAAGA3'), and *Drosomycin (Drosomycin* AMP: forward 5′GACTTGTTCGCCCTCTTCG3', reverse 5′CTTGCACACAGACGACAG3'). All AMPs/ICs were tested against an internal control *Ribosomal protein L23 (RPL23)* also diluted to 10 nmol per reaction (forward 5′GACAACACCGGAGCCAAGAACC3', reverse 5′GTTTGCGCTGCCGAATAACCAC3'). The QuantStudio™ 6 Flex Real-Time PCR (qPCR) System was used to carry out the qPCR reaction, using quick-cycling techniques in accordance with the PowerTrack™ SYBR Green Master Mix manufacturing instructions; 2 min 95°C (x 1) → 5 sec 95°C + 30 sec 60°C (x 40) → 4°C hold.

Data was exported as a Microsoft Excel® file reporting raw cycle threshold values (CT), and a relative quantification of gene expression (Relative expression ratio) was calculated for each sample (formulas are reported below in Figure 9). These ratios were normalized using primer efficiencies for each oligonucleotide pair that indicate how well the primers bind and amplify the target template. Primer efficiencies were easily calculated using the slope of the a serial dilution curve constructed using target tissue cDNA and 10 nmol of forward and reverse primer per reaction (a serial dilution of 1:5) (As outlined in Figure 9). The relative expression ratios were then copied into PRISM GraphPad Prism (v 9.4.0) for graphing and statistical analyses using a two-tailed, unpaired Student's t-tests,

assuming equal variance and an α=0.05. This statistical test was deemed appropriate because only two groups were being compared.

Calculating Primer efficiency

RPL								
Dilution factor	TR1	TR2	TR3	Log	Average	slope	Primer Efficiency	E(amp)
1	12.186	12.267		0	12.2265	-2.97988	116.5626003	2.165626003
0.2	13.819	13.902		-0.69897	13.8605			
0.04	16.116	16.176		-1.39794	16.146			
0.008	18.367	18.448		-2.09691	18.4075			

Slope Prompt into excel: = SLOPE(Average dilution 1 to 0.008, Log 1 to 0.008)

Primer efficiency in % = (10(-1/slope)-1)*100

Amplification coefficient E_{amp} =10^(-1/slope)

Calculating Relative expression ratio for each replicate:

$$E_{AMP\ or\ IC} = (E_{RPL}{}^{CT\ RPL}) / (E_{AMP\ or\ IC}{}^{CT\ AMP\ or\ IC})$$

Figure 9. Calculations for primer efficiencies and relative expression ratios for general qPCR gene quantification. Most equations written out will work as Microsoft Excel® prompts, especially for slope. One thing to note is that E_{amp} is the amplification coefficient, while $E_{AMP\ or\ IC}$ indicates the amplification coefficient for a target antimicrobial peptide or inflammatory cytokine.

2.2.2 Oxidative stress assessment in the brain: DHE and H_2O_2

Another way to assess inflammation in the brain is to look at the redox state of the brain through Dihydroethidium (DHE) accumulation (30980035MG, ThermoFischer Scientific ™), as reported by (Di Cara et al., 2018). To do this, *Drosophila* brains were incubated with 33 µmol of DHE in SFM4 (*Drosophila* cell media: 89130-770, VWR™) immediately after dissection, using #5 microdissection forceps. All brains were left to incubate in the DHE solution for 2 min, rinsed once briefly with 1x PBS (Phosphate Buffered Saline, recipe reported in supplementary table 1), before washing 3 times for ~1 min in 1x PBS. After washing, the brains were immediately fixed for 7 min in 4%

formaldehyde (diluted 1:4, J19943.K2, Thermo Fischer Scientific™), received 3 more washes in 0.05% PBSTritonX (Phosphate Buffer Saline mixed with 0.05% Triton-X detergent: 9036-19-5, Sigma-Aldrich™), and then rinsed once more in 1x PBS before mounting onto glass microscope slides using ProLong™ Gold Antifade mounting media (P10144, ThermoFischer Scientific™).

To carry out H_2O_2 quantification, as reported by (Di Cara et al., 2018), *Drosophila* heads were dissected using Dumont straight micro-dissection scissors and #5 micro-dissection forceps, and then homogenized in a 1.5 mL Eppendorf™ microcentrifuge tube using 1x PBS, before centrifuging at (~13,000 g-force) until the debris of the head cuticle was situated at the bottom of the tube. H_2O_2 was then measured using Amplex™ Red Hydrogen Peroxide/Peroxidase Assay Kit (A22188, ThermoFischer Scientific™) following the protocol of the kit, and then the results of each sample were normalized against protein concentrations quantifies using a Qubit™ Protein BR Assay Kit (A50669, ThermoFischer Scientific) on a Qubit™ fluorometer. The data collected was then copied and graphed in GraphPad PRISM (v 9.4.0), and statistical analyses were carried out using a two-way ANOVA as reported by (Di Cara et al., 2018).

2.2.3 Mitochondrial damage in the brain: Transmission electron microscopy

Structural abnormalities of mitochondria in the brain neuropil of *Drosophila* have been identified in ND models (V. Costa et al., 2010; Risiglione et al., 2021). Therefore age-matched 30do *Mex>Pex5*-i and control *Mex>w*^{1118} males and females brains were prepared, cut and imaged using transmission electron microscopy (TEM) to visualize and identify abnormalities of mitochondria as a result of knocking down *PEX5* in the midgut.

The following protocol has been provided and carried out by Mary Ann Trevor's at the EM Core Facility of Dalhousie University (excluding dissections). Seven to ten brains from each genotype and sex were immediately dissected using #5 micro-dissection forceps and kept in a cold fixative composed of 2.5% glutaraldehyde fixative diluted in 0.1M sodium cacodylate buffer. The brains were then washed three times for 10 min using 0.1M sodium cacodylate buffer, fixed and washed again before staining for 2hrs with 1% Osmium Tetroxide to add contrast and help visualize most intracellular components of the neurons. After 2hrs, the samples were briefly rinsed in distilled H_2O, and then submerged in 0.25% uranyl acetate for an overnight incubation at 4°C. The next day, the tissues were then gradually dehydrated with a series of acetone washes. This dehydration step readies the samples to be infiltrated and then embedded into an Epon Araldite Resin (EAR) in preparation for sectioning.

Before embedding the tissue in the resin, the tissue needs to be infiltrated with the resin over two days. Then the tissue is embedded into 100% EAR and cured for 48hours at 60°C. Once the tissue has been embedded into a cured resin a Reichert-Jung Ultracut E ultramicrotome was used to section the tissue (100 nm thick). Samples were placed on a pre-stained slot-shaped copper-mesh grid. Moreover, for each biological replicate (n=2) of each sex and genotype, transverse and coronal sections were cut with two to three technical replicates per biological replicate. Once ready, the samples were viewed using a JEOL JEM 1230 transmission electron microscope (80kV) using a Hamamatsu ORCA-HR digital camera; the fields of magnifications imaged were 1k, 30k, 50k, 60k and 100k. The area of primary focus was dorsal (transverse cut) and dorsal anterior (coronal cut) (Figure 11A,B).

2.2.4 MitoSOX® Staining

MitoSOX™ Red Mitochondrial Superoxide Indicator (M36008, ThermoFischer Scientific™) was used to evaluate internal mitochondrial stress via superoxide accumulation in the brains of age-matched 30do *Mex>Pex5*-i, control *Mex>w*^{1118}, *Mex>SNCA,* and control *Mex>GFP*. To do this, MitoSOX™ reagent stock solution was diluted to 5 mmol in 1x PBS (working solution). Brains were then placed in dissecting wells and submerged with the working solution and incubated 30 min at 25˚C in the dark on a shake-plate. The brains were then rinsed with 1x PBS three times and immediately mounted on microscope slides with ProLong™ Gold Antifade mounting media. Both the Zeiss AXIO-Observer fluorescence microscope and Zeiss LSM 880 confocal microscope were used to image the brains at magnifications of 10x and 40x with a numerical aperture of 1.4. All images were taken on Zeiss Zen-Blue, and edited to add scale bars on Zeiss Zen-blue-lite programs.
https://www.zeiss.com/microscopy/int/products/microscope-software/zen-lite.html?vaURL=www.zeiss.com/zen-lite.

2.2.5 Terminal deoxynucleotidyl transferase dUTP nick end labeling

In attempts to visualize brain-wide cellular death, Tali™ Apoptosis Kit - Annexin V (AV) Alexa Fluor™ 488 & Propidium Iodide (PI) (A10788, Thermo Fischer Scientific), and In Situ Cell Death Detection Kit, TMR red (TUNEL: 12156792910, Roche™ Sigma-Aldrich™) fluorescent markers were used to visualize apoptosis (AV and TUNEL), and necrosis (PI). For AV and PI, brains were dissected in 1x PBS, washed with 190µl of 1x Annexin Binding Buffer (ABB), and then submerged in 200µl of a working solution made

of 10µl of the annexin V in 190µl of 1x ABB. Then the brains were incubated in the dark at 25˚C room temperature for 10 min.

After incubation, the working solution was removed and the brains were rinsed in 190µl of ABB, before being resubmerged in a second working solution made of 10µl of propidium iodide counter stain in 190µl of ABB. The brains were incubated again for 10 min, and rinsed twice with 1x PBS. Then a fluorescent DNA binding stain 4′,6-diamidino-2-phenylindole (DAPI: ab228549, abcam™ Sigma-Aldrich™) was added at a 1:1000 dilution for 10-15 min, to help identify individual neurons during fluorescent imaging. The brains were then mounted on glass slides using ProLong™ Gold Antifade mounting media for fluorescent imaging, anterior side up (the part where the brain is the most bulbous and not flat).

The TUNEL stain for apoptosis followed a similar protocol. 20 brains were submerged in 50µl of working solution make of 45µl Label solution and 5µl Enzyme solution. The brains were then incubated at 25°C room temperature for 30 min. After incubation, the samples were briefly rinsed in 1x PBS, before mounting on glass microscope-slides using ProLong™ Gold Antifade mounting media. Both the Zeiss AXIO-Observer fluorescence microscope and Zeiss LSM 880 confocal microscope were used to image the brains at magnifications of 10x, 20x, and 40x with a numerical aperture of 1.4. All images were taken on Zeiss Zen-Black, and edited to add scale bars on Zeiss Zen-blue-lite programs https://www.zeiss.com/microscopy/int/products/microscope-software/zen-lite.html?vaURL=www.zeiss.com/zen-lite.

While collecting the images, brains were observed to be much smaller in size for the male *Mex>Pex5*-i and *Mex>SNCA* compared to controls. To calculate brain size in

image editing software FIJI ImageJ https://imagej.net/software/fiji/, the measuring tool as outlined in (Figure 10) was selected, the scale bar was measured, and the length of the scale bar was set to 200 μm by going to Analyze > Set Scale > Known distance (To 200 μm in Figure 10) > Ok. After ruler calibration, the measuring tool is used again to measure the brain from end to end in two ways, distal to distal (eyelobe to eyelobe) or dorsal to ventral (top to bottom). After measuring the brain, Analyze> Measure, and a pop-out window appeared displaying length (Figure 10). From there, measurements for both controls and mutants were collected using both measuring techniques aforementioned, and then copied in to GraphPad PRISM (v 9.4.0) for graphing and statistical analyses using two-tailed, unpaired Student's t-tests, assuming equal variance and an $\alpha=0.05$. This statistical test was deemed appropriate because only two groups were being compared at a time.

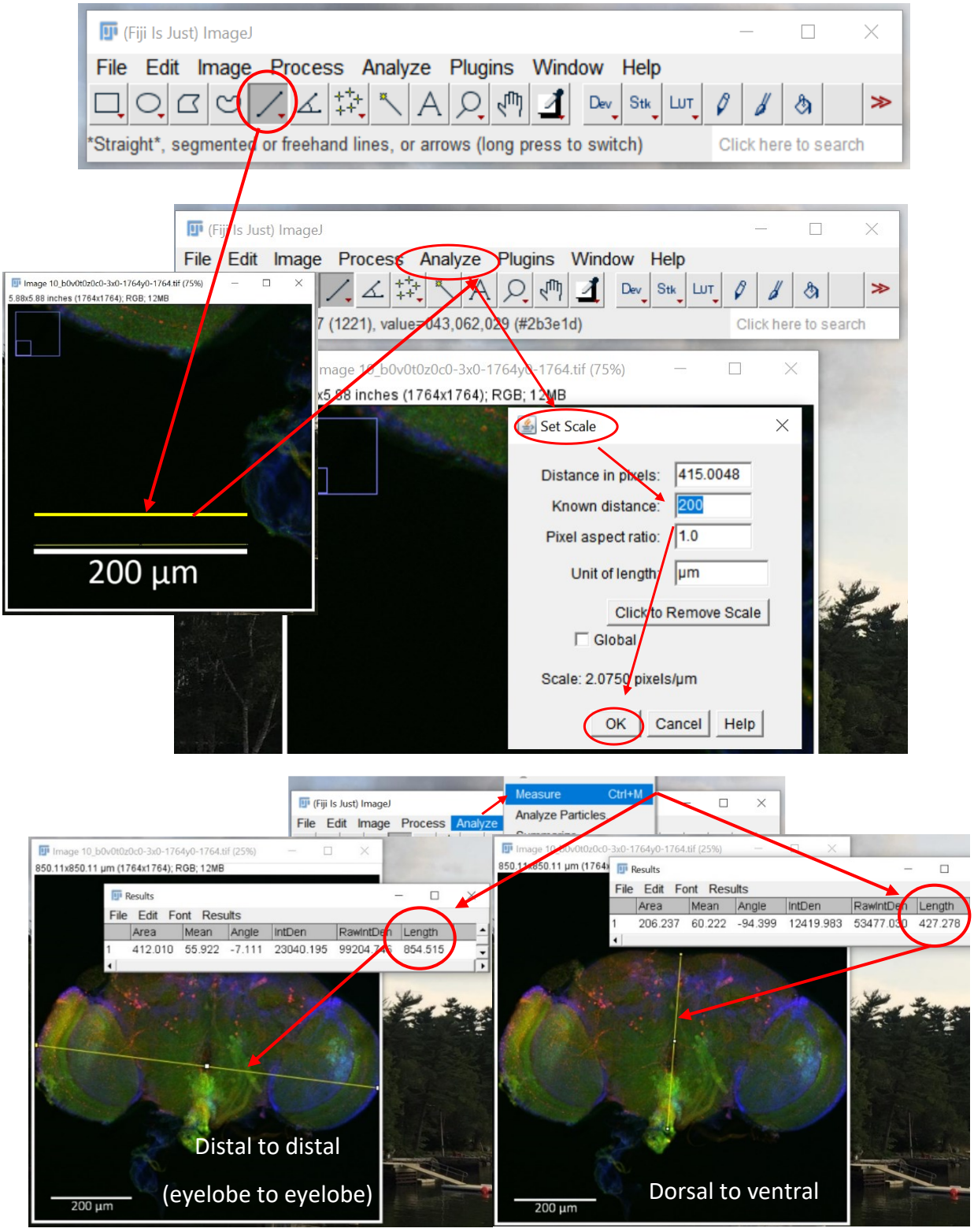

Figure 10: A visual aid to measuring and calculating the size of *Drosophila melanogaster* brains using FIJI ImageJ https://imagej.net/software/fiji/.

2.2.6 Tyrosine hydroxylase immunofluorescence: assessing dopaminergic neuron death and activity

For immunofluorescence of the *Drosophila* intestine, midguts were dissected and fixed in 4% paraformaldehyde in 1x PBS (diluted 1:4, J19943.K2, ThermoFischer Scientific™) for 30min, washed three times in 0.3% PBST (0.3% Triton-X detergent: 9036-19-5, Sigma-Aldrich™ in 1x PBS), and blocked (to prevent non-specific antibody binding) for 1hr at 25°C room temperature in 5% Normal Goat Serum (NGS) (NGS: 31872, ThermoFischer Scientific™, in 0.3% PBST). After incubation, the primary antibody Armadillo β-catenin (N2 7A1, Developmental Studies Hybridoma Bank™, 1:100 dilution) in 5% NGS was added for an over night incubation at 4°C. The next day the guts were washed five times in 0.3% PBST, before the addition of secondary antibody donkey-α mouse Alexa Fluorophore 555 (Red: A-21202, ThermoFischer Scientific™) in 5% NGS and 4′,6-diamidino-2-phenylindole (DAPI: ab228549, abcam™ Sigma-Aldrich™) both diluted 1:1000 and incubation at 25°C room temperature for 2hrs. Excess secondary was then washed off with 4 washes in PBSTw (0.2% Tween-20: 003005, ThermoFischer Scientific™, diluted in 1x PBS) before mounting in Prolong™ Gold Antifade (P10144, ThermoFischer Scientific) on glass microscope slides. Both the Zeiss AXIO-Observer fluorescence microscope and Zeiss LSM 880 confocal microscope were used to image the midguts at magnifications of 10x, 20x, and 40x with a numerical aperture of 1.4. All images were taken on Zeiss Zen-Blue/Black, and edited to add scale bars on Zeiss Zen-blue-lite programs https://www.zeiss.com/microscopy/int/products/microscope-software/zen-lite.html?vaURL=www.zeiss.com/zen-lite.

To investigate effected neuronal clusters, specifically dopaminergic (DA) that are locomotor neurons, Tyrosine Hydroxylase (TH) (Rate-limiting-step enzyme for intracellular dopamine production according to (Daubner et al., in 2011) was used to visualize DA neurons. The *Drosophila* brains were dissected in cold 1x PBS and immediately placed in a 1.5 mL Eppendorf™ microcentrifuge tube (022363204, Eppendorf™) containing 200 µL of 4% formaldehyde fixative (diluted 1:4, J19943.K2, ThermoFischer Scientific™) on ice. Once all of the brains were dissected, the samples were left to fix well for an additional 30-40 min on a mechanical shake-plate at 25°C room temperature. The fixative was then removed, the brains were quickly rinsed with 0.5% PBSTw, and permeabilized with 6 x 5 min washes of 0.5% PBSTw. The brains were then submerged in a blocking solution of 5% NGS in 0.5% PBSTw solution overnight at 4°C on a mechanical shake-plate. The blocking solution was removed the next day and replaced with the primary antibody (Rabbit anti-TH: AB152 , abcam™ Sigma-Aldrich™, at a 1:200 dilution) in 5% NGS 0.5% PBSTw solution. The brains were left in primary overnight at 4°C on a mechanical shake-plate. Then, the next day, the primary antibody was removed, and the brains were thoroughly washed 6 x 10 min using 0.5% PBSTw. The brains were then submerged in secondary antibody donkey-α rabbit Alexa fluorophore A555 (Red), or donkey-α rabbit A488 (Green: A-21206, ThermoFischer Scientific™) if co-stained with TUNEL (Red), at a 1:500 dilution, and DAPI (Blue) at 1:1000 dilution in 0.5% PBSTw, and left to incubate on a mechanical shake-plate at 25°C room temperature for 2hrs, or at 4°C overnight. After incubation in secondary antibody, the brains were kept out of direct light (or under aluminum foil) and washed thoroughly 3 x 5 min in 0.5% PBSTween before mounting on glass microscope-slides, with round cover slips, and using ProLong™ Gold

Antifade mounting media. The brains were oriented to flatter posterior side facing the glass slide and anterior side facing the coverslip, in order to visualize the neurons of interest located mostly anterior (Figure 11A) .

Using a Zeiss LSM 880 confocal microscope and program Zeiss Zen-Black to image the brains (at 10x and 20x, numerical aperture of 1.4), a Z-stack of the brain was imaged, in order to visualize both anterior and posterior neurons of interest (Figure 11A,B). Protocerebral Anterior Medial dopaminergic (PAM) and Protocerebral Posterior Lateral 1 dopaminergic (PPL1) neurons were the clusters of interest because these clusters project into the mushroom body for memory and motor function as depicted in (Figure 11C) (Siju et al., 2021). Furthermore, data analysis consisted of quantifying the count and fluorescent intensity of both the PAM and PPL1 neurons. Fluorescent intensity was collected and calculated according to https://theolb.readthedocs.io/en/latest/imaging/measuring-cell-fluorescence-using-imagej.html using FIJI ImageJ. The pipeline for quantifying fluorescent intensity is visually outlined in (Figure 12): Open FIJI ImageJ → Open file of interest in TIFF format → Image → Colour → Split channels. Once the TH channel was selected (Green or Red depending on the antibody), the image was left in grey-scale before setting the measurements of data collection: Measure → Set Measurements (Area, Min and max gray value, Integrated density and Mean gray-value. After setting the measurements, free-form was selected → target neurons were highlighted, and then Analyzed → and measured (Figure 12 at the #1), as well as areas of the brain with no fluorescence to correct for autofluorescence (Figure 12 at the #2). For each neuron the corrected total cell fluorescence (CTCF) was calculated according to the following equation: CTCF = Integrated Density – (Area of selected cell * Mean background fluorescence). The CTCF

values were then copied in to GraphPad PRISM (v 9.4.0) for graphing and statistical analysis using two-tailed, unpaired Student's t-tests, assuming equal variance and an $\alpha=0.05$. This statistical test was deemed appropriate because only two groups were being compared at a time.

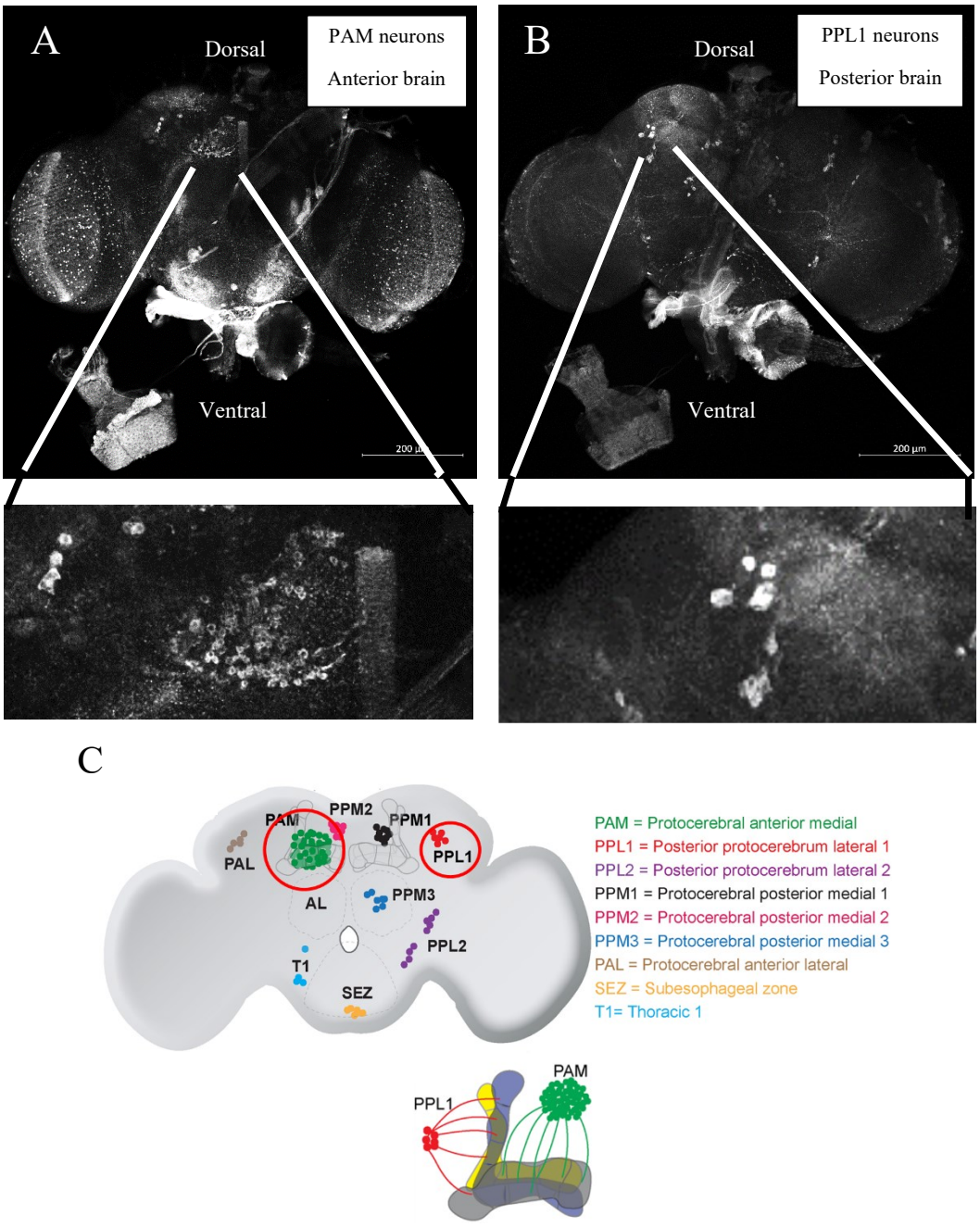

Figure 11. Orientation of the *Drosophila melanogaster* brain and location of dopaminergic neurons on the anterior and posterior sides. Location of A) PAM and B) PPL1 neurons according to C) a visual map of all DA neuron clusters in the anterior and posterior brains depicted in one image illustrated by and according to (Siju et al., 2021)**,** and also depicting how PPL1 and PAM connect to the mushroom body of the fly (analogous to the mammalian hippocampus, and both important for memory).

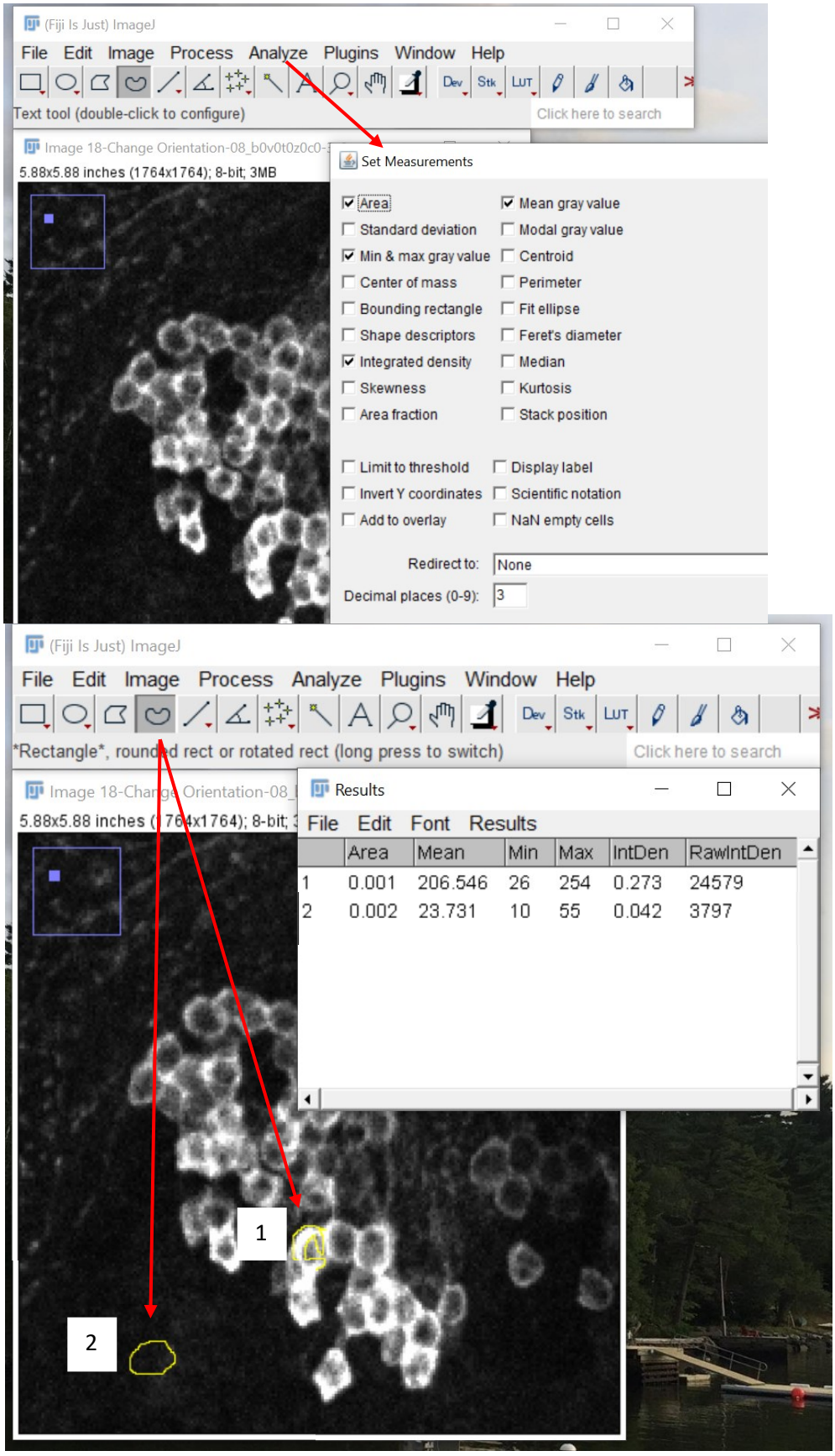
(Fiji Is Just) ImageJ
File Edit Image Process Analyze Plugins Window Help
Text tool (double-click to configure)
Click here to search
Image 18-Change Orientation-08_b0v0t0z0c0-1
5.88x5.88 inches (1764x1764); 8-bit; 3MB
Set Measurements
Area
Mean gray value
Standard deviation
Modal gray value
Min & max gray value
Centroid
Center of mass
Perimeter
Bounding rectangle
Fit ellipse
Shape descriptors
Feret's diameter
Integrated density
Median
Skewness
Kurtosis
Area fraction
Stack position
Limit to threshold
Display label
Invert Y coordinates
Scientific notation
Add to overlay
NaN empty cells
Redirect to:
None
Decimal places (0-9):
3
(Fiji Is Just) ImageJ
File Edit Image Process Analyze Plugins Window Help
Rectangle, rounded rect or rotated rect (long press to switch)
Click here to search
Results
File Edit Font Results
Area Mean Min Max IntDen RawIntDen
1 0.001 206.546 26 254 0.273 24579
2 0.002 23.731 10 55 0.042 3797
1
2

Figure 12. Visual aid on how to use FIJI ImageJ to calculate fluorescent intensity of neurons in the brains if *Drosophila* according to:

https://theolb.readthedocs.io/en/latest/imaging/measuring-cell-fluorescence-using-imagej.html.

2.3 Transcriptomic screens and gene hit validation

2.3.1 Experimental conditions

Each RNA library was prepared in biological duplicates for *Mex>Pex5*-i and control *Mex>*^{w1118}. Libraries for 8 different conditions were prepared. The conditions were a regular cornmeal, a sucrose diet, an infection (high and low doses of *Pseudomonas entomophila*), a high fat with and without an infection, and an axenic diet with and without and infection. The control condition was the regular CM food. The flies used were a mix of males and females (1:1), and were aged to 7 days at 29C before dissecting the midguts. The main conditions included a sucrose treatment which lasted 16hrs, where the flies were placed in a vials of sugar-water soaked filter paper. For the infection treatment of *Pseudomonas entomophila,* a *Drosophila* specific pathogen, the flies were placed in vials with a dry vial-plug and filter paper at the bottom which was soaked in pre-grown (16-24hrs the day before) *Pseudomonas entomophila* in Luria-Bertani broth. Finally, the high-fat and axenic diets included a 16hr period of feeding on HFD and AX food as described previously in section 2.1.3.

2.3.2 Dissections, RNA extraction, DNase treatment, and quality control

After being subject to one of the 8 different treatments, on the day of dissection, the flies were anesthetized using CO2, and dissected 20 at a time (20 guts= 1 replicate, 10

males and 10 females). Since only the midgut was of interest, during the dissection process, either micro-dissection scissors or #5 micro-dissection forceps were used to sever the hind and foregut regions (Capo et al., 2019). Each midgut was dissected, and immediately placed in 250µl of TRIzol® reagent on ice in a 1.5 mL Eppendorf™ microcentrifuge tube to immediately be processed for RNA extraction, or frozen at -80 for later processing.

After 2 biological replicates of each genotype within each condition were collected (a total of 32 samples), the QIAGEN™ RNeasy Mini kit was used to extract the RNA from the samples (74104, QIAGEN™) according to the manufacturers protocol. RNA extraction procedures were carried out with high-precaution on a bench sterilized with 70% ethanol and RNaseZap™ (83930, Sigma-Aldrich™) to eliminate surface RNases. The samples were taken out of the -80C, 4 were processed at a time, and left to thaw on ice before homogenizing for approximately 10 sec with a VWR™ motorized pestle, and let sit at 5 min at 25°C room temperature. Then 250µl of additional TRIzol® was added (topping the homogenate up to 500µl) before the addition of 100µl of chloroform (366927, Sigma-Aldrich™) for a TRIzol®/Chloroform phase separation. Once the chloroform was added, the samples were shaken vigorously by hand for 15-20 sec, and left to sit on the bench for 3 min before centrifugation for 15 min at 4°C (~13,000 g-force). After centrifugation, the upper aqueous layer, containing the RNA, was collected carefully not to draw-up any of the TRIzol® at the interface. After separating the upper phase to a new 1.5 mL microcentrifuge tube, one volume of 70% ethanol was added, mixed thoroughly by pipetting up and down until there was no sign of phase separation, and then immediately pipetted into a 2 mL RNeasy spin column and proceeded as instructed by the QIAGEN™ RNeasy Mini kit (74004, QIAGEN™). The concentrations and integrity of the RNA were

then quantified using a Qubit™ Broad Range RNA quantification assay kit (Q10210, Thermo Fischer Scientific™), and the Qubit™ RNA IQ assay kit (Q33221, Thermo Fischer Scientific™), on a Qubit™ fluorometer.

These samples were also contaminated with genomic DNA (gDNA), as confirmed by an Agilent Technologies 2100 Bioanalyzer and RNA Pico Chip (5067-1513, Agilent™). Therefore, each sample was treated with QIAGEN RNase-Free DNase set (79254, QIAGEN™) and Invitrogen™ Deoxyribonuclease1 (DNase1:18047019, Thermo Fischer Scientific™) according to the manufacturers protocols. After DNase treatment the RNA samples were immediately placed on ice for quantification on Qubit™ fluorometer before library prep.

2.3.3 Transcriptomic library preparation and quality control

Once all of the samples were collected, and treated with DNase to eliminate gDNA contamination, the QIGEN QIAseq™ UPX 3' Transcriptome Kit (333088, QIAGEN™) was used to make one transcriptomic library per condition. This library kit uniquely tags individual samples with a unique molecular index or cell-ID (UMI) which allows pooling of samples under one library index. Indices 1-8 were used from the QIAseq UPX 3' Trans. 12-index (48) index set (333074, QIAGEN), with one index per condition. Therefore, a total of eight libraries were constructed of four samples (biological duplicates of *Mex>Pex5*-i and control *Mex>w*^{1118}), according to the QIAGEN™ QIAseq™ UPX 3' Transcriptome Kit manual below: https://www.qiagen.com/us/resources/resourcedetail?id=28512222-986f-4027-bb45-2c7e65d3fd2b.

Before quantifying each library, quality control was approached in two different ways; 1) using gel-electrophoresis to check the library size (ideally between 400-600 bp) and 2) using the Agilent™ Bioanalyzer and Bioanalyzer High Sensitivity DNA Analysis (5067-4626, Agilent™) to check the library size in bp and the presence of remaining gDNA contamination. Additionally, the average library size was required for the QIAGEN QIAseq™ Library Quant Assay Kit (333314, QIAGEN™), in order to accurately quantify library concentration before sequencing. Libraries were considered the optimal size for sequencing (Supplementary Figure 3), and therefore the libraries proceeded to Next Generation Illumina Sequencing at Gémone-Québec Canada.

2.3.4 Demultiplexing/alignment/mapping and enrichment analyses

Once sequencing was complete, the QIAGEN CLC Genomic Workbench https://digitalinsights.qiagen.com/products-overview/discovery-insights-portfolio/analysis-and-visualization/qiagen-clc-genomics-workbench/ was used to demultiplex and convert each library into FASTQ files. Once the libraries were converted into FASTQ, QIAGEN open source Bioinformatics tool GeneGlobe was used to further demultiplex individual UMIs and to run an enrichment analysis https://go.qiagen.com/GeneGlobeResearchCycle?cmpid=CM_PCR_GG_GGAwareness_0621_SM_TwitterOrg. Additionally, the enrichment analysis (secondary analysis) on GeneGlobe provided a list of hits ranked by p-values that indicated which genes were the most to least likely, truly differentially expressed. These p-values were then ranked from smallest to largest (most likely to be truly differentially expressed to least). Then, using DAVID Bioinformatics Database https://david.ncifcrf.gov/, another open source

bioinformatics tool, the genes were further investigated in order to identify the best fits for the study, based on enrichment of the hits in biological processes. Ultimately, neuropeptides and neuropeptide receptors emerged as gene hits of interest.

2.3.5 Gene hit validation and analytics

Once target genes were identified, the first step was to validate the expression of these genes (using calculations from Figure 9), and to try and understand expression directionality in each genotype and sex. Similar samples to the transcriptomic screen were prepared on CM, HFD, and AX conditions, the midguts were dissected, 1µg of RNA was extracted using ZYMO® Research: Direct-zol RNA Microprep kit, and quantified on a NanoDrop® spectrophotometer for concentration (ng/µl), and quality. Quality was assessed by checking the absorbance ratios of each concentration: 230/280 and 260/280 (ratios of nucleic acid purity). Samples that did not meet the 260/280 ratio of ~1.8-2.0 or 260/230 ratio of ~2.0-2.2 were discarded. The RNA was then reverse transcribed into cDNA using High Capacity RNA-to-cDNA™ Kit. Then using PowerTrack SYBR™ Green PCR Master Mix (using 10 nmol of each primer) and QuantStudio™ 6 Flex Real-Time PCR machine, the following gene hits identified from the transcriptomic screens were tested. Amn (FBgn0086782), AstA (FBgn0015591), AstA-R1 (FBgn0015591), Bursicon (FBgn0038901), CCAP (FBgn0039007), CCAP-R (FBgn0039396), CCHa2 (FBgn0038147), CCHa2 (FBgn0033058), Dsk (FBgn0000500), FMRFa (FBgn0000715), Mip (FBgn0036713), Ms-R2 (FBgn0264002), NPF (FBgn0027109), PDF-R (FBgn0260753), sNPF (FBgn0032840), Tk (FBgn0037976). All genes can be found on FlyBase for reference https://flybase.org/. Primers used are listed in Table 2 below.

Table 2. Sequences of neuropeptide and neuropeptide receptor primers

Gene of interest	Oligonucleotide sequences (written 5'-3')
AMN-F	5'ATT CCG CGC CCG AAT TTT TC3'
AMN-R	5'CGT TTC GCT GTC GTT GCA TA3'
AstA-F	5'CGC CTG CCG GTC TAT AAC TT3'
AstA-R	5'CTT GTT CTG TCG GCC AGG TC3'
AstA-R1-F	5'CCC GTA TTC TTT GGC ATT ATC GG3'
AstA-R1-R	5'GGC CAG GTT GAT TAT CAG CAG A3'
CCAP-F	5'GTC ATC GTT CTG GGC AAT TCA3'
CCAP-F	5'TCG CTG GAA AGG GAG AAC A3'
CCAP-R	5'GAT GTC GGT GAG GAC GTT GA3'
CCAP-R	5'TCG TCC ACA GCC TGT AAA TGC3'
CCHa2-F	5'CGC CAA ATG AAC AGG TGC C3'
CCHa2-R	5'GTC GGC GAG GTC GGT TAA3'
CCHa2-R -F	5'GAC GGC GGA ATA GTA CCG TAT3'
CCHa2-R -R	5'CGG TGG CGA AAG AAG ATG ATG3'
DSK-F	5'TCG GCG ACT ACA GGA ATT GGA3'
DSK-R	5'TCC CCG AAT AGA GAG AAT GAT GG3'
FMRFa-F	5'TCT GTG ATT GGC ATC GAC TAC T3'
FMRFa-R	5'CTC TTG CCG AAG TGC ATG AAG3'
MIP-F	5'CGA GGA GAT ATA TAG TCA GCT ATG G'
MIP-R	5'TCG CTC TCG CTA AGT TGG TC3'
MsR2-F	5'AAG TTT CAC TCG GTA TTT CCC C3'

Gene of interest	Oligonucleotide sequences (written 5'-3')
MsR2-R	5'CGA TTC CTT TGC GGA TAG CTT AC3'
NPF-F	5'TCC GCG AAA GAA CGA TGT CA3'
NPF-R	5'CTC CTC ATT AAA ACC GCG AGC3'
Nplp1-F	5'ATG CTG CTC AAT GCC GCT ATT3'
Nplp1-R	5'ACT GGG GCT CAT CAG TTG ATT TA3'
Pdf-F	5'TCG CTA CAC GTA CCT TGT CG3'
Pdf-R	5'GAT AGC GAC AGA GAG TGG CC3'
Pdfr-F	5'CCC TGG AAT CTA ACG CTT GC3'
Pdfr-R	5'TCC TGT TTG TGG TAG GGTGTA AT3'
Rpl23-F	5′GACAACACCGGAGCCAAGAACC3'
Rpl23-R	5'GTTT GCG CTG CCG AAT AAC CAC3'
sNPF-F	5'GTG TTC CTC AGT TCG AGG CAA3'
sNPF-R	5'AGT TCA AAA GCG AGT TGT ACC A3'
Tk-F	5'CAA TTC CTT TGT GGG GAT GCG3'
Tk-R	5'CTG CTG TTT TCC TCT CAA GTC AT3'

CHAPTER 3: EFFECTS OF GUT-SPECIFIC *PEX5* DEPLETION AND *SNCA/ BACE* OVEREXPRESSION ON BEHAVIOUR AND THE BRAIN

3.1 A genotypic & condition dependant decline of NGCA

3.1.1 A decline of NGCA in male *Mex>Pex5*-i on CM conditions

As previously published, a Knock Down (KD) of *Peroxin 5* (*PEX5*) in the *Drosophila* intestinal epithelium (midgut) resulted in dysplasia of Enterocytes (ECs) (Di Cara et al., 2018). Thus, compromising metabolism in the midgut (Smith & Aitchison, 2013). Moreover, the conjecture of compromising the gut epithelium in humans is the increased vulnerability and likeliness of developing Neurodegenerative Diseases (NDs). Furthermore, sharing physiological affinity to the human small intestine (Capo et al., 2019), the *Drosophila* midgut may also have an important role in neuroprotective signaling, thus intestinal instability may have a negative outcome on the brain. For this reason, *PEX5* was depleted (*Mex>Pex5*-i) in the midguts of male and female flies, and then stained with an anti-Armadillo antibody (armadillo protein in *Drosophila* is the homolog of mammalian β-catenin) to visualize dysplasia of ECs and intestinal stem cells (ISCs) in the model. In order to identify and connect any phenotypes observed in and of the brain to midgut alterations.

In parallel, the effects of overexpressing canonical human-linked mutant-alleles of NDs in the midgut was also considered; in order to probe the distal effects of these common disease genes on the brain in comparison to a *PEX5* midgut-KD fly. For example, a mutant allele of α-Synuclein (*SNCA*), linked to Parkinson Disease (PD), and encodes a protein that damages mitochondrial activity and leads to neuronal death (Faustini et al., 2017), was overexpressed in the midgut of the animal. Both peroxisomes and mitochondria organelles

share similar metabolic activity in the gut, and since *SNCA* in the gut is linked to NDs in the brain (Yan et al., 2021), then *Mex>SNCA* acts as a great reference model for studying the contributions of peroxisome metabolism in the Diet-Microbiota-Gut-Brain (DMGB) axis of NDs.

Both *Mex>Pex5*-i and the *Mex>SCNA* males displayed midgut dysplasia in the form of elevated ISC proliferation, clumping into larger clusters of cells (Figure 13A), when compared to age matched controls at 20 days old (do) (Figure 13A). These findings were recapitulated in male midgut-specific Crispr Cas9-specific Knock Out (KO) model of *PEX3* at 20do (Figure 13B); PEX3 is another essential peroxin involved in peroxisomal de-novo biogenesis (Smith & Aitchison, 2013). Ultimately indicating that the phenotype was not caused by the *Mex-Gal4* tissue-specific driver, nor exclusively caused by depletion of *PEX5* rather than general peroxisomal function. Additionally, *PEX3* CRISPR KO male midguts underwent Terminal deoxynucleotidyl transferase dUTP Nick-End Labeling (TUNEL) to detect apoptosis. Results indicated that the proliferating and clumping ISCs were also dying, while there were no visible apoptotic cells in the control midguts; confirming gut-epithelial dysplasia (Figure 13B). The female *Mex>Pex5*-i did not show the same ISC proliferation and clumping as the males, the ISCs of the females were instead sporadic and individually scattered (Figure 13C). On the other hand, the *Mex>SNCA* females did display increased ISC proliferation but, no clumping (Figure 13C).

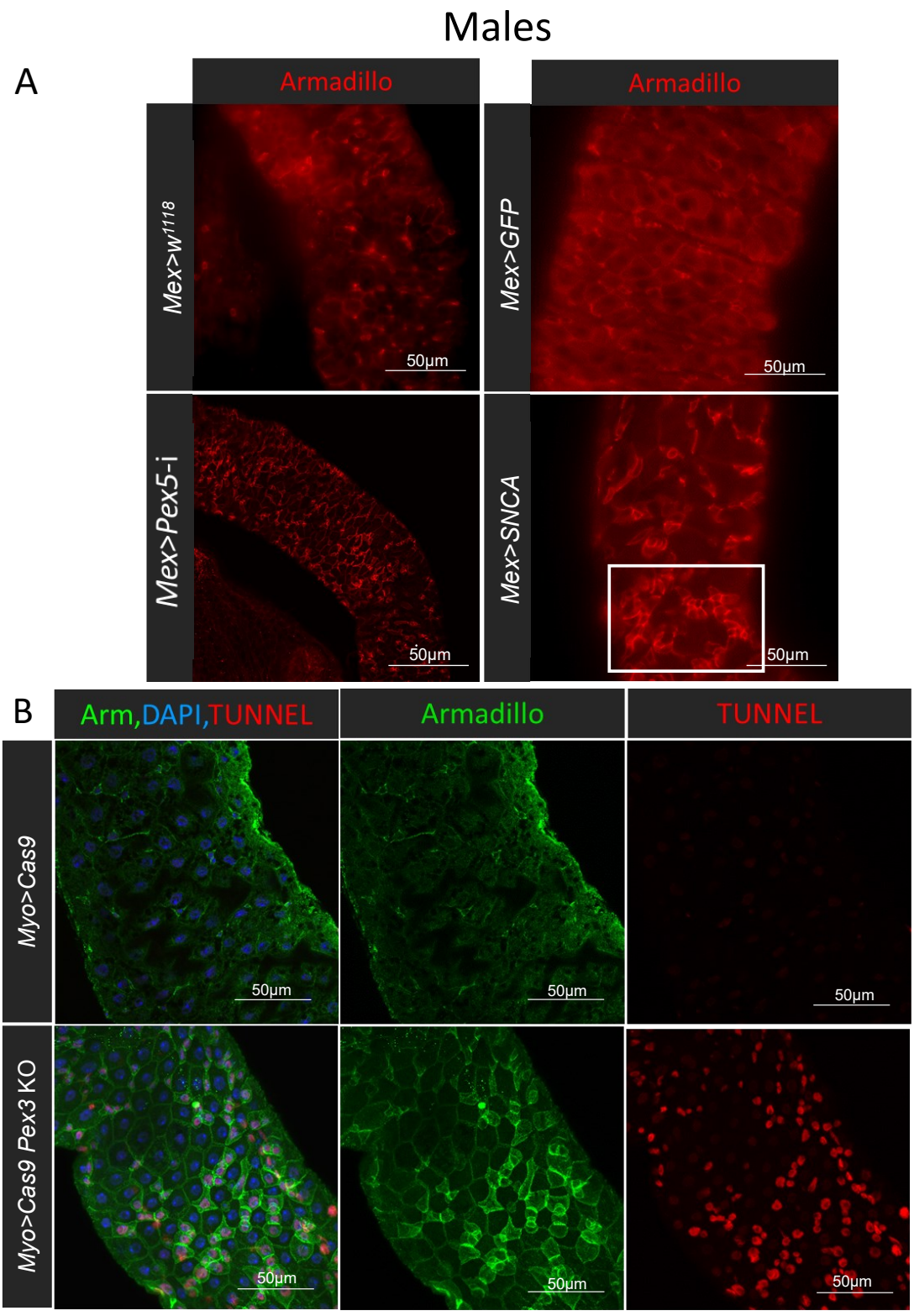
Males
A
Armadillo
Armadillo
Mex>w1118
Mex>GFP
Mex>Pex5-i
Mex>SNCA
50µm
50µm
50µm
50µm
B
Arm,DAPI,TUNNEL
Armadillo
TUNNEL
Myo>Cas9
Myo>Cas9 Pex3 KO
50µm
50µm
50µm
50µm
50µm
50µm

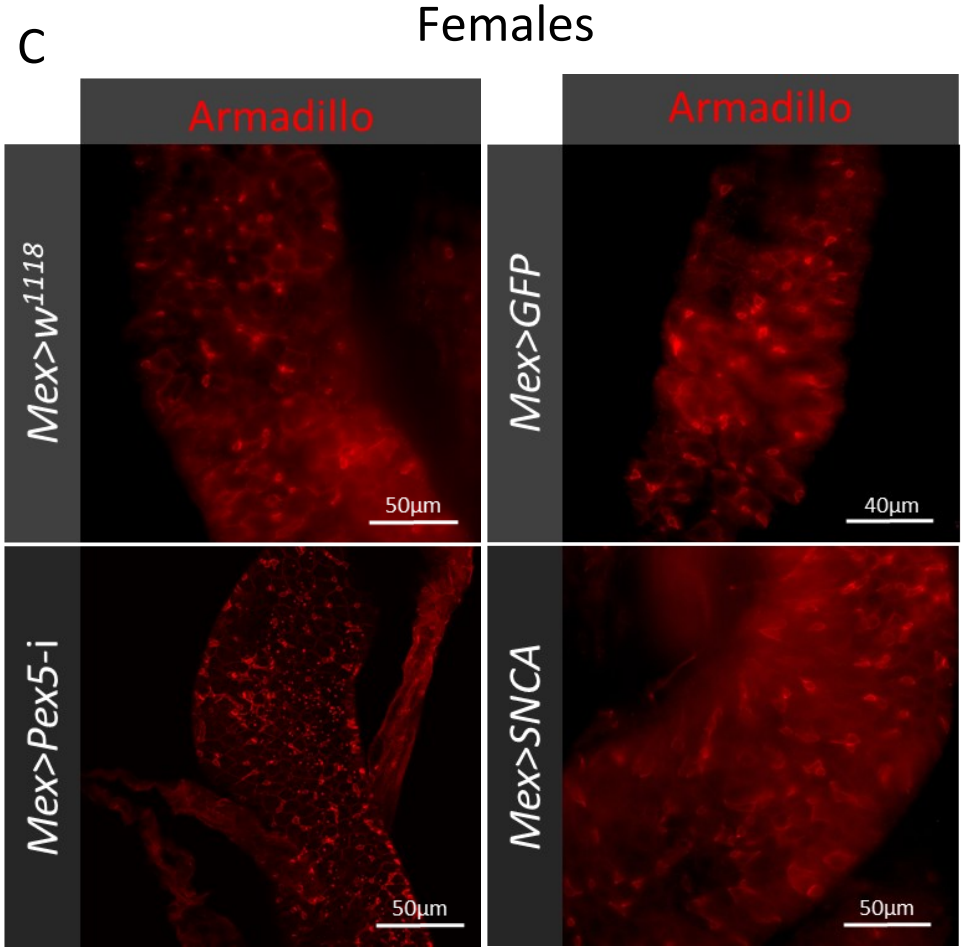

Figure 13. Dysplasia in the midguts of *Mex>Pex5*-i males and *Mex>SNCA* males and females. Representative images of the Intestinal stem cell (ISC) staining of male and female midguts all aged matched at ~20do, using N2 7A1 Armadillo β-catenin antibody, and secondary antibody Alexa Fluorophore 555 (Red) or 488 (Green). A) Dysplasia can be observed by the actively proliferating and clumpy enterocyte progenitors in both *Mex>Pex5*-i males (bottom left panel) and *Mex>SNCA* males (bottom right panel, with the white box) in red, compared to controls in the upper panels. All midguts were imaged on Zeiss Axio Observer fluorescent microscope at 40x magnification except *Mex>Pex5*-i males imaged using a Zeiss LSM 880 confocal microscope at 40x magnification. All scale bars read 50µm. B) Armadillo staining (Green) of *Myo1A>Pex3* Cas9 KO midguts. Dysplasia can be observed in the form of actively proliferating enterocyte progenitors (Green), and cellular death stained by TUNEL (Red), compared to the control in the upper panel. All midguts were imaged on a Zeiss LSM 880 confocal microscope at 40x, and all scale bars read 50µm. C) *Mex>Pex5*-i and control females are comparable with no dysplasia. *Mex>SNCA* females (bottom right panel) compared to controls in the upper panels, however there is little to no clumping of progenitor cells. All midguts were imaged on Zeiss Axio Observer fluorescent microscope at 40x magnification except *Mex>Pex5*-i females imaged using a Zeiss LSM 880 confocal microscope at 40x magnification, and all scale bars read 50µm, except for the female *Mex>GFP* reading 40µm.

After observing dysplasia in the midgut, behavioural assays were used to assess whether damage to the intestinal epithelial structure and physiology effects the brain in a neurodegenerative manner, especially over aging of the animal. Therefore, negative geotaxis climbing assays (locomotor assays) were used to assess the Negative Geotaxis Climbing Ability (NGCA) of *Mex>Pex5*-i that successfully climbed up over the target height (190 mL on a 250 mL graduated cylinder) than the respective, age-matched controls (*Mex>w*^{1118}). Flies were tested in cohorts of 20 on a regular Cornmeal (CM) diet first, at time points 10, 15, 20, 30, 40 and 50do.

I observed that there was a lower average percentage of *Mex>Pex5*-i male flies showing a decline of NGCA as early as 20do and as late as 30do. All statistics were calculated using two-tailed, unpaired Student's t-tests, assuming equal variance and α=0.05. The number of flies assayed ranged from n=60-160 flies per genotype. At 20do, the *Mex>Pex5*-i males displayed a ~17% lower success rate in climbing (NGCA) (M=26.00%, SD=3.000) compared to the controls (M=42.60%, SD=3.228); t(6)=7.206, ***p=0.0004 (Figure 14A). At 30do, *Mex>Pex5*-i (M=26.67%, SD=12.58) displayed a ~48% decline of NGCA compared to the control (M=75.63%, SD=12.60); t(4)=4.665, **p=0.0096 (Figure 14A). However, female *Mex>Pex5*-i were comparable to controls on a CM diet over all time points of aging (Figure 14B).

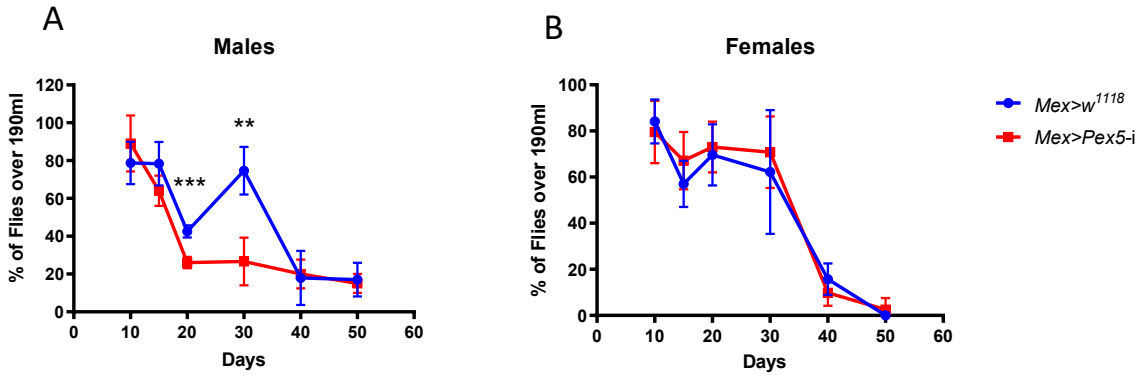

Figure 14. *Drosophila* negative geotaxis climbing assays of *Mex>Pex5*-i and respective controls *Mex>w^{1118}*, reared at 25°C on a CM diet (comparing between genotypes). The x-axis is reporting days aged, and the y-axis is reporting NGCA as the mean % of flies that have successfully climbed up over a target height. All statistical analyses were carried out using two-tailed, unpaired Student's t-tests, assuming equal variance and an α=0.05. The number of flies assayed ranged from n=60-160 per genotype. A) Male *Mex>Pex5*-i were assayed in comparison to *Mex> w^{1118}* controls, at time points 10do (t(9)=1.261, p=0.2390), 15do (t(4)=1.783, p=0.1492), 20do (t(6)=7.206, ***p=0.0004), 30do (t(4)=4.665, **p=0.0096), 40do (t(6)=0.2561, p=0.8064), and 50do (t(6)=0.4075, p=0.6978). B) Female *Mex>Pex5*-i were assayed in comparison to *Mex> w^{1118}* controls, at time points 10do (t(5)=05251, p=0.6220), 15do (t(4)=0.9827, p=0.3814), 20do (t(6)=0.3876, p=0.7117), 30do (t(6)=0.5549), p=0.5990), 40do (t(6)=1.3350, p=0.2302), and 50do (t(6)=1.000, p=0.3559)

These climbing assays were then repeated with animals of the same genotypes, but reared at 29°C instead, because the *Gal4-UAS* system used to perform the *PEX5* KD is stronger at 29°C. The reason for testing flies reared at 29°C, was to ensure that the flies used for the transcriptomic screen (aged 7do, raised at 29°C) were comparable in climbing deficit to the ones raised at 25°C over aging, at 10, 20 or 30do. Indeed, what was concluded from these assays was that male *Drosophila* reared at 29°C, aged approximately 10 days faster than at 25°C. All statistical analyses were carried out using two-tailed, unpaired Student's t-tests, assuming equal variance and α=0.05. The number of animals assayed ranged from n=100-200 flies per genotype. At 10do, there is a significant ~45% decline of NGCA displayed by the *Mex>Pex5*-i males (M=12.50%, SD= 11.33) compared to the

respective controls *Mex>w*^{1118} (M=56.75%, SD= 14.37); t(14)=7.258, ****p= <0.0001 (Figure 15A). Additionally, the female *Mex>Pex5*-i and controls *Mex>w*^{1118} were comparable over aging at time points 10, 20 and 30do (Figure 15B).

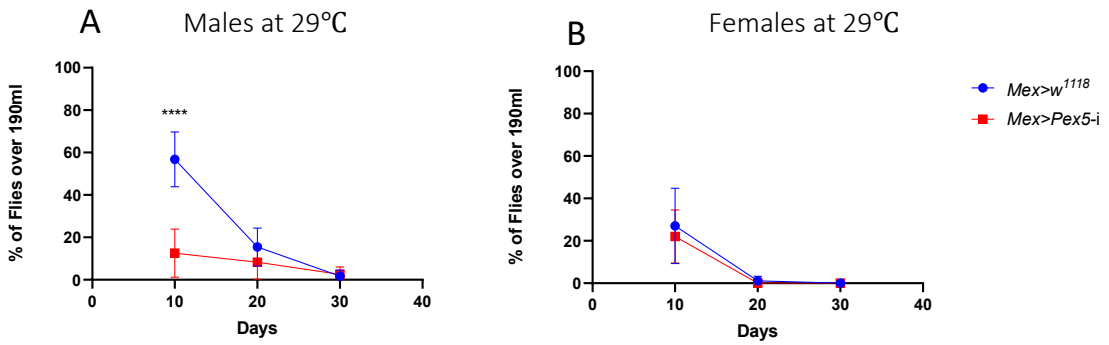

Figure 15. *Drosophila* negative geotaxis climbing assays of *Mex>Pex5*-i and respective controls *Mex>w*^{1118}, reared at 29°C on a CM diet (comparing between genotypes). The x-axis is reporting days aged, and the y-axis is reporting NGCA as the mean % of flies that have successfully climbed up over a target height. All statistical analyses were carried out using two-tailed, unpaired Student's t-tests, assuming equal variance and an α=0.05. The number of flies assayed ranged from n=100-200 flies per genotype. A) Male *Mex>Pex5*-i were assayed in comparison to *Mex> w*^{1118} controls, at time points 10do (t(14)=7.258, ****p= <0.0001), 20do (t(14)=1.675, p=0.1161), and 30do (t(3)=0.2928, p=0.7888). B) Female *Mex>Pex5*-i were assayed in comparison to *Mex> w*^{1118} controls, at time points 10do (t(18)=0.7259, p=0.4772), 20do (t(16)=1.512, p=0.1500), and 30do (t(8)=0.0000, p>0.9999).

3.1.2 A HFD and AX conditions exacerbates a decline of NGCA in male and female *Mex>Pex5*-i

A *PEX5* KD perturbs midgut metabolism on a regular CM diet, corresponding to a decline of NGCA in male *Drosophila*. Other ways of disrupting gut metabolism is by changing the diet, such as feeding a high fat diet (HFD), or treating the animals with antibiotics (axenic or AX) to eliminate the gut microbiota (commensals). Since peroxisomes modulate dietary and commensal gut metabolism, I hypothesized that by

disturbing midgut metabolism of *Drosophila* by feeding control flies (*Mex>w*^{1118}) with a HFD, or an antibiotic cocktail (AX), a deficit of NGCA will arise and mimic the phenotype of the *PEX5* KD. For ease of data collection, only the 10do, 20do and 30do time points were measured for these conditions. Additionally, instead of 20 flies per cohort (biological replicate) 25 flies were used to avoid a dramatically shrinking population (n) size with aging since HDF and AX conditions can impact survival. All statistics were calculated using two-tailed, unpaired Student's t-tests, assuming equal variance and an α=0.05. The number of flies assayed ranged from n=60-160 flies per genotype.

After the HFD treatment and recovery, the NGCA of male controls mimicked that of *Mex>Pex5*-i at 30do ($t(6)=0.6057$, $p= 0.5669$) (Figure 16A). This decline of NGCA in the HFD male controls was recapitulated when comparing against CM conditions. The control males were dramatically effected by the HFD at 30do, where there is a significant ~35% decline of NGCA between the HFD (M=39.00%, SD=16.00) and CM (M=75.63%, SD=12.60); $t(9)=3.438$, **$p=0.0074$ (Figure 17A). Moreover, *Mex>Pex5*-i males on HFD versus CM were comparable over aging, at 10, 20 and 30do (Figure 17A), and therefore the HDF did not effect the *Mex>Pex5*-i males to a greater extent than the *PEX5* gut KD.

On AX conditions, the NGCA of male controls was effected so much that it mimicked that of *Mex>Pex5*-i males at 10do ($t(6)=1.465$, $p=0.1934$), 20do ($t(6)=0.7160$, $p=0.7089$), and 30do ($t(6)=0.6679$, $p=0.5290$), where results are comparable (Figure 16B). These results were recapitulated within the same genotype at 30do, where there was a significant 45% drop of NGCA in the control AX males (M=15.00%, SD=16.00) compared to the control CM males (M=60.00%, SD=13.00); $t(5)=3.962$, *$p=0.0107$ (Figure 17B). Moreover, the AX diet did not greatly nor significantly effect the NGCA of *Mex>Pex5*-i

males to CM males, with comparable results at 10do (t(6)=1.465, p=0.1934), 20do (t(6)=0.3916, p=0.7089), and 30do (t(6)=0.6679, p=0.5291) (Figure17B).

The HFD effected the females greatly. For The females, there was no difference when comparing between the two genotypes, *Mex>Pex5*-i and *Mex>w*^{1118} controls, on the HFD at 10do (t(6)=0.4736, p= 0.6525), 20do (t(6)=1.477, p= 0.1901), nor 30do (t(5)=0.08227, p= 0.9376) (Figure 16A). However, when comparing within the same genotypes between HFD and CM conditions, it was evident that there was a great decline of NGCA within the each female genotype, observed at all time points over aging. At 10do control females on a HFD (M= 56.00%, SD= 26.00) exhibited a ~28% decline of NGCA compared to female controls on CM, although it was not statistically significant (M=84.09%, SD=9.549); t(7)=2.030, p=0.0819 (Figure 17C). At 20do, there was a statistically significant ~55% decline of NGCA exhibited by HFD controls (M=17.00%, SD=14.00) compared to the CM controls (M=72.00%, SD=18.00); t(7)=5.249, **p=0.0012 (Figure 17C). Finally, at 30do there was a significant ~50% decline of NGCA in the control HFD group (M= 62.22%, SD= 26.86) compared to CM controls (M= 14.00%, SD= 19.80), t(7)=3.294, *p=0.0132 (Figure 17C). Within the *Mex>Pex5*-i females, flies on HFD were comparable to the CM at 10 and 20do. However, at 30do the NGCA of HFD females significantly declined by ~56% when *Mex>Pex5*-i HFD (M=15.18%, SD=16.38) was compared to *Mex>Pex5*-i CM (M= 70.83%, SD= 15.55); t(7)=5.176, **p= 0.0013 (Figure 17C).

The AX effected the females greatly, like the HFD. There was no difference when comparing between the two genotypes, *Mex>Pex5*-i and *Mex>w*^{1118} controls, on the AX at 10do (t(6)=0.4736, p= 0.6525), 20do (t(6)=1.477, p= 0.1901), nor 30do (t(5)=0.08227,

p= 0.9376) (Figure 16B). Females on AX conditions displayed a significant decline of NGCA within *Mex>Pex5*-i between AX and CM at all time points of aging. At 10do, NGCA of *Mex>Pex5*-i AX (M=63.00%, SD=4.000) declined by ~17% compared to *Mex> Pex5*-i CM (M= 79.56%, SD= 13.50); t(6)=02.684, *p= 0.0363 (Figure 16B). At 20do, NGCA of *Mex>Pex5*-i AX (M=34.00%, SD=10.00) significantly declined by 39% compared to *Mex>Pex5*-i CM (M= 73.00%, SD= 11.00); t(7)=5.569, ***p= 0.0008 (Figure 16B). Finally, at 30do NGCA of *Mex>Pex5*-i AX (M=28.00%, SD=16.00) significantly declined by ~49% versus Mex> *Pex5*-i CM (M= 70.83%, SD= 15.55); t(7)=4.040, **p= 0.0049 (Figure 16B).

When comparing within the same genotype, NGCA of AX *Mex>w^{1118}* control females, greatly declined compared to CM *Mex>w^{1118}* control females at 10do, 20do, and 30do (Figure 17D). At 10do, AX controls (M= 59.00%, SD= 12.00) displayed a significant ~25% decline of NGCA compared to CM controls (M=84.09%, SD=9.549); t(5)=3.100, *p=0.0269 (Figure 17D). At 20do, there was a non-significant ~31% decline of NGCA in AX controls (M=41.00%, SD=28.00) compared to the CM *Mex>w^{1118}* (M=72.00%, SD=18.00); t(5)=1.829, p=0.1269 (Figure 17D). Finally, at 30do there was a significant ~58% decline of NGCA by the AX controls (M= 62.22%, SD= 26.86) compared to the CM controls (M= 4.000%, SD= 7.000), t(7)=3.711, *p=0.0138 (Figure 17D). Indicating that for both *Mex>Pex5*-i and controls, the elimination of gut microbiota severely impacts the NGCA of females regardless of genotype.

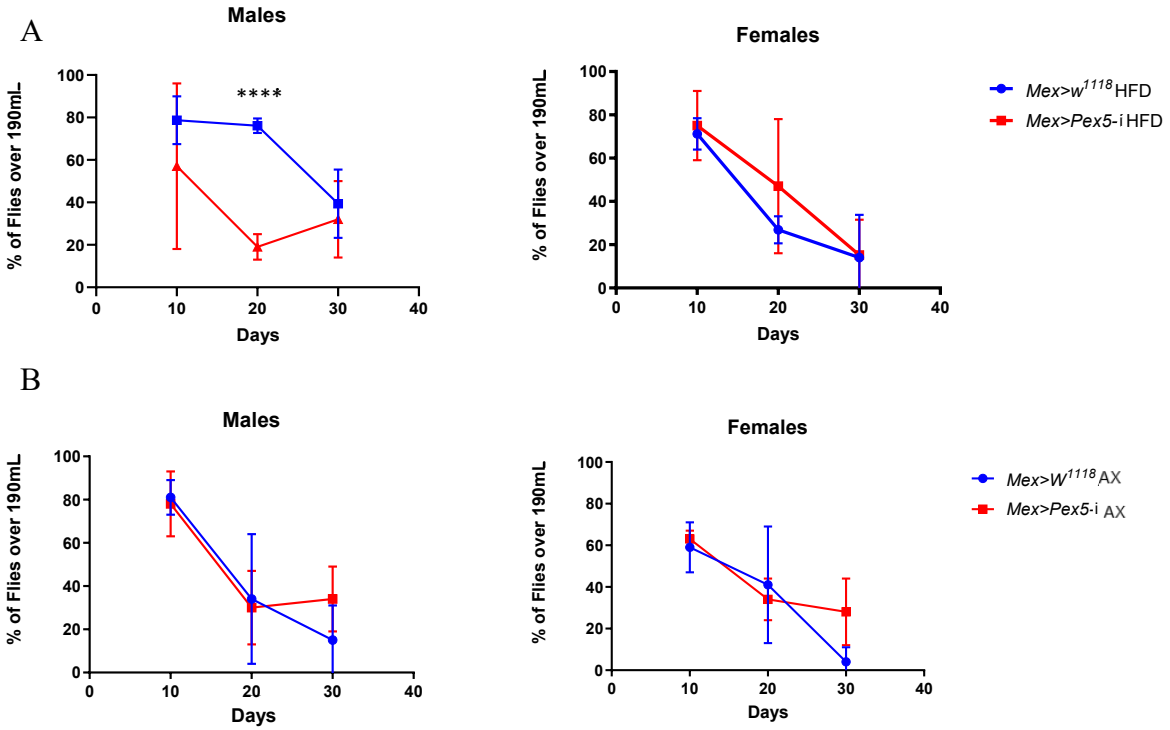

Figure 16. *Drosophila* negative geotaxis climbing assays of *Mex>Pex5*-i and respective controls *Mex>w^{1118}*, reared at 25°C on a HFD and AX diet (comparing between genotypes). The x-axis is reporting days aged, and the y-axis is reporting NGCA as the mean % of flies that have successfully climbed up over a target height. All statistical analyses were carried out using two-tailed, unpaired Student's t-tests, assuming equal variance and an α=0.05. The number of flies assayed ranged from n=60-160 per genotype. A) HFD Male *Mex>Pex5*-i were assayed in comparison to respective *Mex> w^{1118}* controls, at time points 10do (t(9)=1.536, p=0.1589), 20do (t(7)=18.64, ****p= <0.0001), 30do (t(6)=0.6057, p= 0.5669). HFD Female *Mex>Pex5*-i were assayed in comparison to respective *Mex> w^{1118}* controls, at time points 10do (t(6)=0.4736, p= 0.6525), 20do (t(6)=1.477, p= 0.1901), and 30do (t(5)=0.08227, p= 0.9376). B) AX Male *Mex>Pex5*-i were assayed in comparison to respective *Mex> w^{1118}* controls, at time points 10do (t(6)=1.465, p=0.1934), 20do (t(6)=0.7160, p=0.7089), and 30do (t(6)=0.6679, p=0.5290). AX Female *Mex>Pex5*-i were assayed in comparison to respective *Mex> w^{1118}* controls, at time points 10do (t(6)=02.684, *p= 0.0363), 20do (t(7)=5.569, ***p= 0.0008), and 30do (t(7)=4.040, **p= 0.0049).

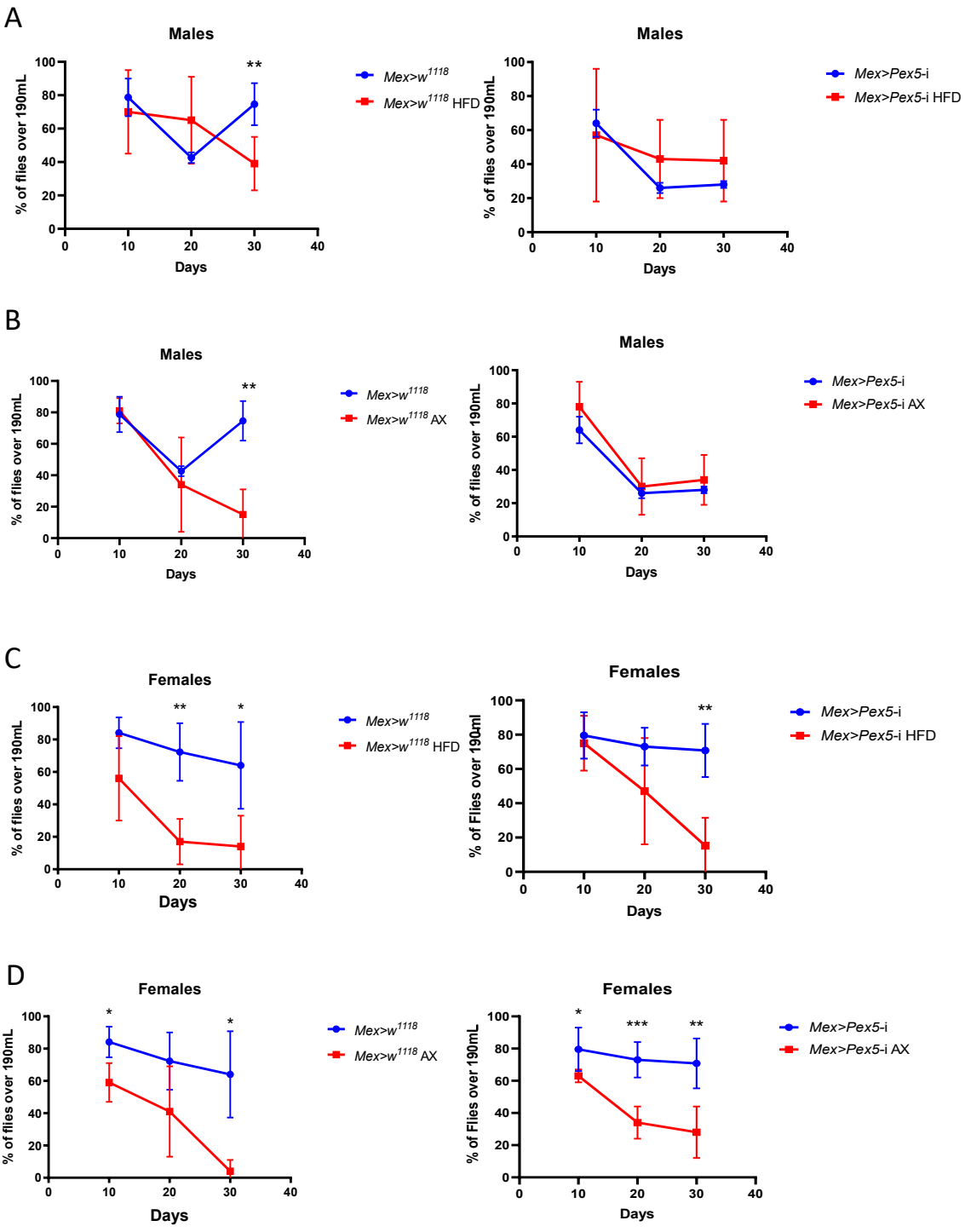

Figure 17. *Drosophila* negative geotaxis climbing assays of *Mex>Pex5*-i and respective controls *Mex>w^{1118}* reared at 25°C on a HFD and AX diet (comparing within genotypes). The x-axis is reporting days aged, and the y-axis is reporting NGCA as the mean % of flies that have successfully climbed up over a target height. All statistical analyses were carried out using two-tailed, unpaired Student's t-tests, assuming equal

variance and an α=0.05. The number of flies assayed ranged from n=60-160 per genotype. A) HFD male *Mex>Pex5*-i were assayed in comparison to CM male *Mex>Pex5*-i, at time points 10do (t(4)=0.3045, p=0.7759), 20do (t(4)=1.269, p=0.2731), and 30do (t(4)=1.007, p=0.3710). HFD male *Mex> w^{1118}* controls were assayed in comparison to CM male *Mex> w^{1118}* controls, at time points 10do (t(9)=1.536, p=0.1589), 20do (t(9)=3.438, **p=0.0074), and 30do (t(6)=0.6057, p= 0.5669). B) AX male *Mex>Pex5*-i were assayed in comparison to CM male *Mex>Pex5*-i, at time points 10do (t(6)=1.465, p=0.1934), 20do (t(6)=0.3916, p=0.7089), and 30do (t(6)=0.6679, p=0.5291). AX male *Mex> w^{1118}* controls were assayed in comparison to CM male *Mex> w^{1118}* controls, at time points 10do (t(5)=0.4216, p=0.6908), 20do (t(5)=0.5616, p=0.5986), and 30do (t(5)=3.962, *p=0.0107). C) HFD female *Mex>Pex5*-i were assayed in comparison to CM female *Mex>Pex5*-i, at time points 10do (t(4)=0.3774, p=0.7250), 20do (t(5)=1.592, p=0.1722), and 30do (t(7)=5.176, **p= 0.0013). HFD female *Mex> w^{1118}* controls were assayed in comparison to CM female *Mex> w^{1118}* controls, at time points 10do (t(7)=2.030, p=0.0819), 20do (t(7)=5.249, **p=0.0012), and 30do (t(7)=3.294, *p=0.0132). D) AX female *Mex>Pex5*-i were assayed in comparison to CM female *Mex>Pex5*-i, at time points 10do (t(6)=02.684, *p= 0.0363), 20do (t(7)=5.569, ***p= 0.0008), and 30do (t(7)=4.040, **p= 0.0049). AX female *Mex> w^{1118}* controls were assayed in comparison to CM female *Mex> w^{1118}* controls, at time points 10do (t(5)=3.100, *p=0.0269), 20do (t(5)=1.829, p=0.1269), and 30do (t(7)=3.711, *p=0.0138).

3.1.3 Niacin treatment improves NGCA of aged *Mex>Pex5*-i males

After observing a locomotor decline in the males, the next step was to figure out how this phenotype could be rescued. In previous literature, vitamin B3 or niacin has been found to improve locomotion in PD humans and flies (Jia et al., 2008; Wakade et al., 2021). Therefore, *Mex>Pex5*-i and *Mex>w^{1118}* control flies were fed a CM diet mixed with 10 mmol of niacin for 30 days after eclosure (n=60 flies per genotype and condition), and then assayed for NGCA. All statistics were calculated using two-tailed, unpaired Student's t-tests, assuming equal variance and an α=0.05. The number of flies assayed were n=60 flies per genotype. At 30do, there was a small but statistically insignificant ~22% improvement of NGCA in response to niacin treatment for *Mex>Pex5*-i males compared to non-treated animals; t(4)=0.7584, p=0.4904 (Figure 18). Additionally *Mex>w^{1118}* controls (M= 64.47%, SD=4.235) also showed a small but statistically significant ~21%

improvement when treated with niacin compared to untreated (M= 43.52%, SD=10.72); t(4)=3.149, *p=0.0345 (Figure 18).

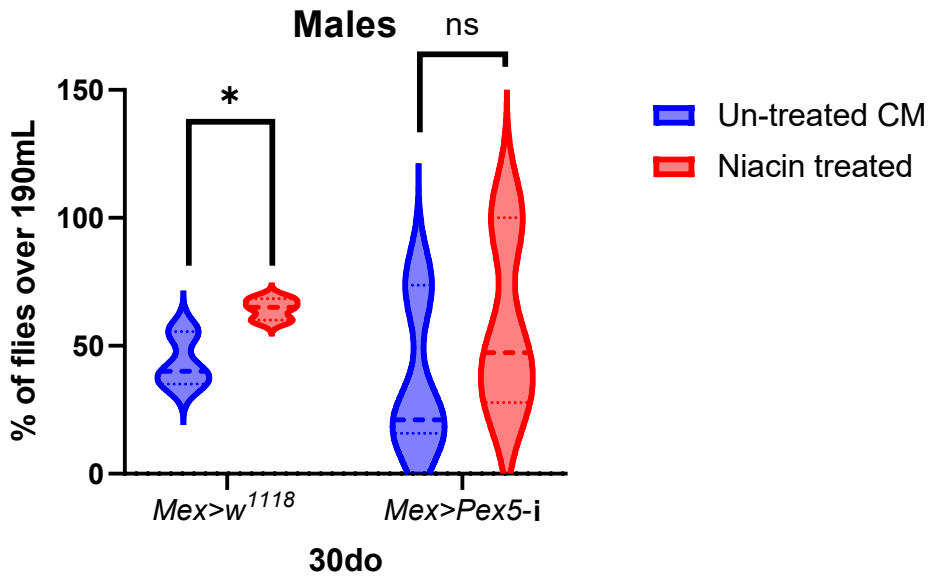

Figure 18. *Mex>Pex5*-i and *Mex>w^{1118}* males treated with niacin for 30 days show an improvement of locomotor ability compared to flies on CM conditions. For each genotype n=60 flies, and statistical analyses were carried out using two-tailed, unpaired Student's t-tests, assuming equal variance and an α=0.05. There was only a significant improvement of NGCA on niacin versus no niacin treatments exhibited by *Mex>w^{1118}* males (*p=0.0345).

3.1.4 *Mex>SNCA* and *Mex>BACE* males exhibit deficits of NGCA on CM conditions

By overexpressing canonical human-linked mutant-alleles of NDs that encode for α-Synuclein (*SCNA*), or β-secretase (*BACE*) in the brains of *Drosophila,* a neurodegenrtive phenotype/ pathologies arise (Greeve et al., 2004; Jahromi et al., 2020; Prüßing et al., 2013). However, what about in the midgut? To understand whether the expression of these mutant proteins in the intestinal tract can seed and trigger AD and PD phenotypes in the brain from the gut, as hypothesized in few mammalian studies (Braak et al., 2003; Challis

et al., 2020), these models were assayed for climbing deficits. These models were also used as a midgut metabolism perturbation positive control for the *Mex>Pex5*-i.

On CM conditions, *Mex>BACE* males displayed a decline of NGCA at 15do and 20do however, there was a high mortality in both sexes between 20 and 30 days compared to the respective *Mex>GFP* strain used as controls. At 15do, there was a significant ~55% decline of NGCA exhibited by *Mex>BACE* (M= 12.63%, SD= 2.743) compared to control (M=67.59%, SD= 5.814); t(6)=17.10, ****p<0.0001 (Figure 19A). Likewise, at 20do there was a significant ~41% decline of NGCA exhibited by *Mex>BACE* (M= 12.16%, SD= 4.616) compared to the control (M=53.10%, SD= 18.42); t(8)= 4.820, **p=0.0013 (Figure 19A). On the contrary at 15do, female *Mex>BACE* on CM conditions (M=64.06%, SD= 8.469) displayed no decline of NGCA compared to the female CM *Mex>GFP* control (M=71.30%, SD= 14.15); t(11)=1.092, p=0.2981 (Figure 19A). At 20 days the *Mex>BACE* females were climbing significantly better by ~26% (M=75.07%, SD= 18.21) compared to the controls (M=49.47%, SD= 19.77); t(10)=2.282, *p=0.0457 (Figure 19A). However, the standard deviations were very large, and the significance is very close to the alpha value of 0.05, so there may not be a difference at all. Thus, it was concluded that on CM conditions, only male *Mex>BACE* display a deficit of NGCA.

On regular CM conditions, the NGCA of *Mex>SNCA* males declined significantly compared to male CM *Mex>GFP* controls at both 10do and 20do. As early as 10do, the NGCA of *Mex>SNCA* (M=32.00%, SD=13.00) declined by ~54% compared to the controls (M=86.20%, SD=7.050); t(7)=8.046, ****p< 0.0001 (Figure 19B). At late as 20do before controls began to decline to the same degree, NGCA of *Mex>SNCA* (M=12.00%, SD=12.00) significantly decreased by ~41% compared to controls (M=53.00%,

SD=16.48); t(6)= 3.719, **p= 0.0099 (Figure 19B). The female CM *Mex>SNCA* also displayed a decline of NGCA compared to the female CM *Mex>GFP* control at 10do and 20do, but not 30do and 40do (Figure 19B). Additionally, unlike the males, the mortality of the females was high around 50do (absence of 50do time point). At 10do, *Mex>SNCA* (M=43.00%, SD=7.000) flies displayed significantly reduced NGCA by ~33% compared to controls (M=76.16%, SD=13.92); t(11)= 3.893, **p=0.0025 (Figure 19B). At 20do, *Mex>SNCA* (M=55.00%, SD=8.000) displayed a significant ~22% decline of NGCA compared to controls (M=74.85%, SD=11.60); t(7)= 2.625, *p= 0.0342 (Figure 19B).

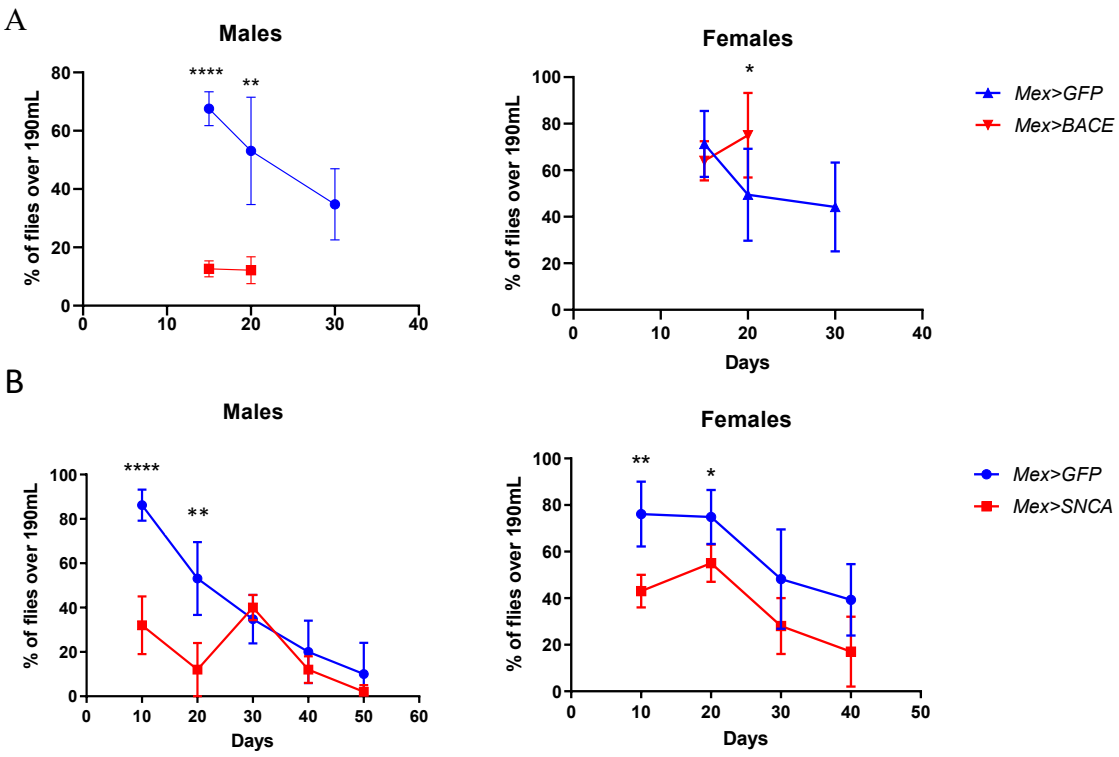

Figure 19. *Drosophila* negative geotaxis climbing assays of *Mex>BACE*, *Mex>SNCA* and respective controls *Mex>GFP*, reared at 25°C on a CM diet (comparing between genotypes). The x-axis is reporting days aged, and the y-axis is reporting NGCA as the mean % of flies that have successfully climbed up over a target height. All statistical analyses were carried out using two-tailed, unpaired Student's t-tests, assuming equal variance and an α=0.05. The number of flies assayed ranged from n=60-160 per genotype. A) CM male *Mex>BACE* were assayed in comparison to respective control CM male *Mex>GFP,* at time points 15do (t(6)=17.10, ****p<0.0001), and 20do (t(8)=

4.820, **p=0.0013). CM female *Mex>BACE* were assayed in comparison to respective CM female *Mex>GFP* controls, at time points 15do (t(11)=1.092, p=0.2981), and 20do (t(10)=2.282, *p=0.0457). B) CM male *Mex>SNCA* were assayed in comparison to respective CM male *Mex>GFP* controls, at time points 10do (t(7)=8.046, ****p< 0.0001), 20do (t(6)= 3.719, **p= 0.0099), 30do (t(7)= 0.8568, p= 0.4199), 40do (t(3)= 5.035, p= 0.4253), and 50do (t(3)= 1.028, p= 0.3796). CM female *Mex>SNCA* were assayed in comparison to CM female *Mex>GFP* controls, at time points 10do (t(11)= 3.893, **p=0.0025), 20do (t(7)= 2.625, *p= 0.0342), 30do (t(8)=1.700 p= 0.1275) and 40do (t(8) 2.272 p= 0.0527).

3.1.5 HFD and AX conditions exacerbate the decline of NGCA in male and female *Mex>BACE* and *Mex>SNCA*

Similarly to the *PEX5* gut-KD models, *Mex>BACE* or *Mex>SNCA* and control *Mex>GFP* were subjected to a HFD and AX diet. However, the results of *Mex>BACE* males and females were confusing, and did not correspond to what was observed with the *Mex>Pex5*-i males nor females for some of the same conditions.

On HFD condtions, *Mex>BACE* male fly sruvival had improved on the HFD condition and enough flies survived to assay at 30do (Figure 20A). However, at 30do *Mex>BACE* males (M=12.00%, SD=12.00) exhibited a significant 38% decline of NGCA compared to the HFD *Mex>GFP* male controls (M=50.00%, SD=2.000); t(4)=4.20281, *p=0.0136 (Figure 20A). On the contrary to the males, HFD *Mex>BACE* females (M=3.000%, SD=3.000) hardly climbed up the cylinder at all, with a 3% total climbing success rate over the 190 mL mark, compared to the respective HFD *Mex>GFP* female controls (M=53.04%, SD=24.21); t(5)=3.476, *p=0.0177 (Figure 20A). At 20do the *Mex>GFP* females dropped to the same climbing success rate as the *Mex>BACE* females, thus both genotypes were comprarable and effected greatly after consumption of a fat rich

diet; t(6)=0.5336%, p=0.6128 (Figure 20A). Unlike the males, the females still did not live as long as 30do on the HFD nor AX diet.

Only at 30do, AX *Mex>BACE* male flies displayed a significant ~41% decline of NGCA (M=15.00%, SD=12.00) compared to male AX Mex>GFP controls (M=56.00%, SD=23.00); t(7)=3.477, *p=0.0103 (Figure 20B). Interestingly, the trend of NGCA over aging for the female AX *Mex>BACE* flies were similar to the males on AX conditons at 10, 20 and 30do (Figure 20B). At 10do, both AX *Mex>BACE* females and control AX *Mex>GFP* females were comparable; t(8)=0.6519, p=0.5328. At 20do, there was an unusual significant ~32% improvement of *Mex>BACE* NGCA (M=67.00%, SD=12.00) than the control (M=34.69%, SD=14.00), t(8)=3.366, **p=0.0098 (Figure 20B). Finally, at 30do, there was a ~29% significant NGCA decline exhibited by *Mex>BACE* (M=15.00%, SD=12.00) compared to the control (M=43.75%, SD=11.31); t(8)=3.898, **p=0.0046 (Figure 20B).

A

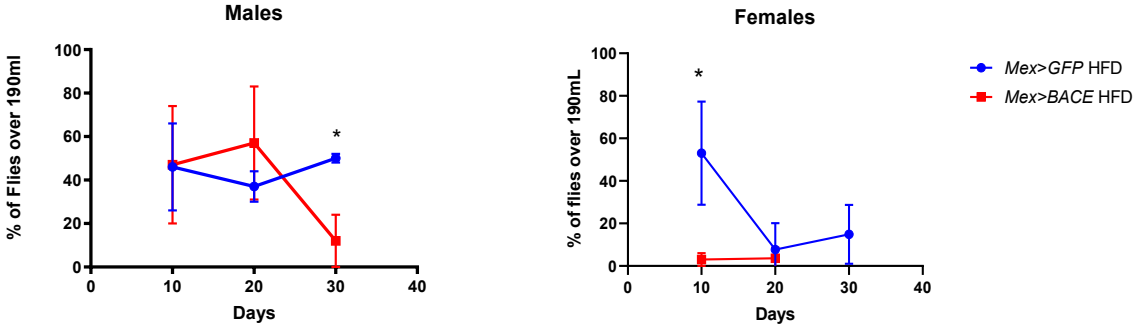

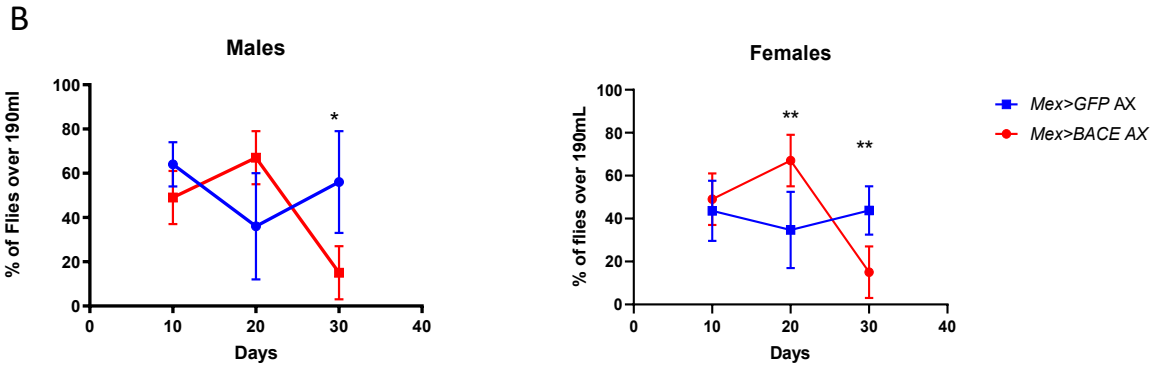

Figure 20. *Drosophila* negative geotaxis climbing assays of *Mex>BACE* and respective controls *Mex>GFP,* reared at 25ºC on a HFD and AX diet (comparing between genotypes). The x-axis is reporting days aged, and the y-axis is reporting NGCA as the mean % of flies that have successfully climbed up over a target height. All statistical analyses were carried out using two-tailed, unpaired Student's t-tests, assuming equal variance and an α=0.05. The number of flies assayed ranged from n=60-160 per genotype. A) HFD male *Mex>BACE* were assayed in comparison to respective HFD male *Mex>GFP* controls, at time points 10do (t(8)= 0.0570, p=0.9560), and 20do (t(8)= 1.272, p=0.2391), and 30do (t(4)=4.20281, *p=0.0136). HFD female *Mex>BACE* were assayed in comparison to respective HFD female *Mex>GFP* controls, at time points 10do (t(5)= 3.476, *p=0.0177), and 20do (t(6)=0.5336%, p=0.6128). B) AX male *Mex>BACE* were assayed in comparison to respective AX male *Mex>GFP* controls, at time points 10do (t(7)=2.051, p=0.0794), 20do (t(6)=2.311, p=0.0602), and 30do (t(7)=3.477, *p=0.0103). AX female *Mex>BACE* were assayed in comparison to AX female *Mex>GFP* controls, at time points 10do (t(8)= 0.6519, p=0.5328), 20do (t(8)=3.366, **p=0.0098), and 30do (t(8)=3.898, **p=0.0046).

Males and females on a HFD and AX diet exhibited no difference of NGCA between the *Mex>SNCA* and respective HFD *Mex>GFP* controls, at 10do, 20do nor 30do (Figure 21). However, only at 10do, there was a ~24% decline of NGCA in the control *Mex>GFP* AX males (M=33.09%, SD= 13.53) compared to *Mex>SNCA* AX males (M=57.20%, SD= 6.606); t(8)=3.581, **p=0.0072 (Figure 21). These phenotypes were similar to what was observed for the male and female *Mex>Pex5*-i flies, when challanegd with a HFD and AX treatment to remove gut commensals.

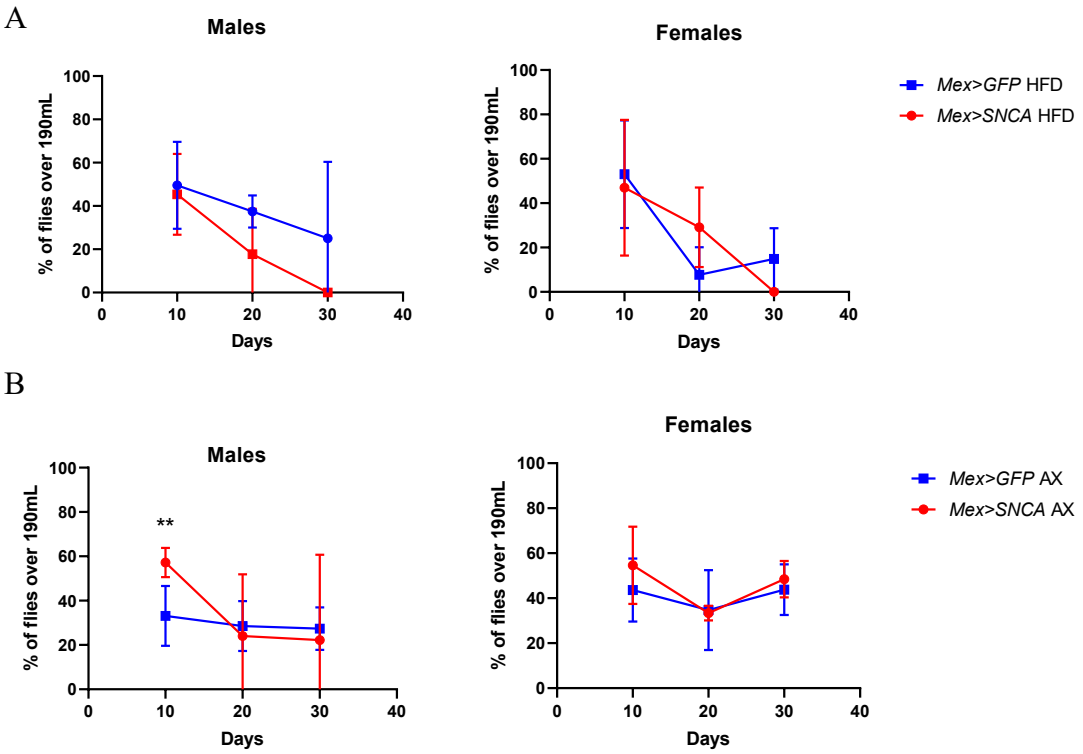

Figure 21. *Drosophila* negative geotaxis climbing assays of *Mex>SNCA* and respective controls *Mex>GFP,* reared at 25°C on a HFD and AX diet (comparing between genotypes). The x-axis is reporting days aged, and the y-axis is reporting NGCA as the mean % of flies that have successfully climbed up over a target height. All statistical analyses were carried out using two-tailed, unpaired Student's t-tests, assuming equal variance and an α=0.05. The number of flies assayed ranged from n=60-160 per genotype. A) HFD male *Mex>SNCA* were assayed in comparison to respective HFD male *Mex>GFP* controls, at time points 10do (t(8)=0.3405, p=0.7423), 20do (t(6)=1.772, p=0.1268), and 30 (t(2)=1.000, p=0.4227). HFD female *Mex>SNCA* were assayed in comparison to respective HFD female *Mex>GFP* controls, at time points 10do (t(7)= 0.3217, p=0.7571), 20do (t(8)=2.194, p=0.0596), 30do (t(6)=2.145, p=0.0757). B) AX male *Mex>SNCA* were assayed in comparison to respective AX male *Mex>GFP* controls, at time points 10do (t(8)=3.581, **p=0.0072), 20do (t(6)=0.3024, p=0.7726), 30do (t(4)=0.2248, p=0.8332). AX female *Mex>SNCA* were assayed in comparison to AX female *Mex>GFP* controls, at time points 10do (t(8)=1.109, p=0.2296), 20do (t(7)=0.1417, p=0.8913), and 30do (t(6)=0.6232, p=0.5561).

When comparing within genotypes, the NGCA of male *Mex>GFP* on HFD appeared to be impacted by the HFD significantly by ~37% at 10do (M=46.32%, SD=12.00) compared to *Mex>GFP* CM males (M=83.00%, SD=10); t(7)= 4.141,

**p=0.0043 (Figure 22A). Likewise, there was a significant ~23% drop of NGCA at 10do by the AX *Mex>GFP* males (M=60.32%, SD=10.83) compared to male CM *Mex>GFP* (M=85.00%, SD=8.446); t(9)= 3.533, **p=0.0064 (Figure 22A). Therfore, both the HFD and AX diets effected the *Mex>GFP* controls' climbing behaviour from a very young age.

The *Mex>GFP* HFD females were also severely effected by the HFD, at all time points instead of just the earliest time point at 10do. Diplaying a significant ~23%, ~41% and ~24% decline of NGCA at 10do (M=53.04, SD=24.21), 20do (M=7.714%, SD=12.44) and 30do (M=14.86%, SD=13.86) compared to the *Mex>GFP* CM females at 10do (M=76.16%, SD=13.92), 20do (M=48.19%, SD=21.34) and at 30do (M=39.30%, SD 15.33); 10do t(12)=2.288, *p=0.0411, 20do t(9)=3.727, **p=0.0047, and 30do t(8)=2.559, *p=0.0337 (Figure 22B). However, similar to the *Mex>GFP* AX males, the AX *Mex>GFP* females only exhibited a decline of NGCA at 10do (M=43.62%, SD=14.00) compared to their respective controls, the *Mex>GFP* CM females (M=76.16%, SD=13.92); t(13)= 4.260, ***p=0.0009 (Figure 22B).

When comparing within the *Mex>BACE* genotype, HFD and AX conditions appear to rescue the almost null climbing success rate that was exhibited by the *Mex>BACE* males on a CM diet. At 20do on HFD, there was a significant ~45% improvement of NGCA of the *Mex>BACE* males (M=57.00%, SD= 26.00) compared to *Mex>BACE* CM males (M=12.16%, SD= 4.616); t(10)=3.763, **p=0.0037 (Figure 22C). Likewise, at 20do there was a significant ~55% improvement of NGCA of AX males (M=67.00%, SD= 12.00) compared to CM males (M=12.16%, SD= 4.616); t(7)=9.511, ****p< 0.0001 (Figure 22C). On the contrary, instead of an improvement of NGCA, *Mex>BACE* HFD females exhibited a dramatic decline of NGCA, where the female flies hardly moved at the bottom

of the cylinder, compared to *Mex>BACE* CM. At 20do there was an ~72% decline of NGCA by the *Mex>BACE* HFD females (M=3.600%, SD= 5.000) compared to *Mex>BACE* CM females (M=75.07%, SD=18.22); t(6)=6.446, ***p=0.0007 (Figure 22D). Finally, on AX conditions there was no differnece in climbing at 20do between AX *Mex>BACE* females and CM *Mex>BACE* females; t(8)=0.8273, p=0.4321 (Figure 22D).

When comparing within the *Mex>SNCA* genotype, the HFD appears to have no further effects on the *Mex>SNCA* males compared to the *Mex>SNCA* CM males at 10do (t(7)=1.212, p=0.2647) and 20do (t(5)=0.4186, p=0.6929) (Figure 22E); similar to what was observed with *Mex>Pex5*-i on CM versus HFD. However, at 30do, *Mex>SNCA* HFD males decline to a 0% climbing success rate (M=0.000%, SD= 0.000), a 40% difference compared to the *Mex>SNCA* CM (M=40.00%, SD=6.000); t(4)=9.357, ***p=0.0007 (Figure 22E). When comparing between CM and AX *Mex>SNCA* males, over aging both conditional effects were comprabel, howver AX *Mex>SNCA* males (M=57.20%, SD= 6.606) climbed up the cylinder significantly better than the *Mex>SNCA* CM males (M=32.00%, SD=13.00) at and early age of 10do; t(7)=3.807, **p=0.0067 (Figure 22E).

Mex>SNCA HDF females only exhibited a significant 28% decline of NGCA at 30do (M=0.000%, SD=0.000), compared to *Mex>SNCA* CM females (M=28.00%, SD=12.000); t(6)=4.667, **p=0.0034 (Figure 22F). On AX conditions, there were no striking diffrences between the *Mex>SNCA* AX and *Mex>SNCA* CM females over aging (Figure 22F). However, at 20do, the *Mex>SNCA* AX females (M=33.39%, SD=3.303) displayed a ~21% drop of NGCA compared to *Mex>SNCA* CM females (M= 55.00%, SD=8.000); t(5)=4.989, **p=0.0041 (Figure 22F).

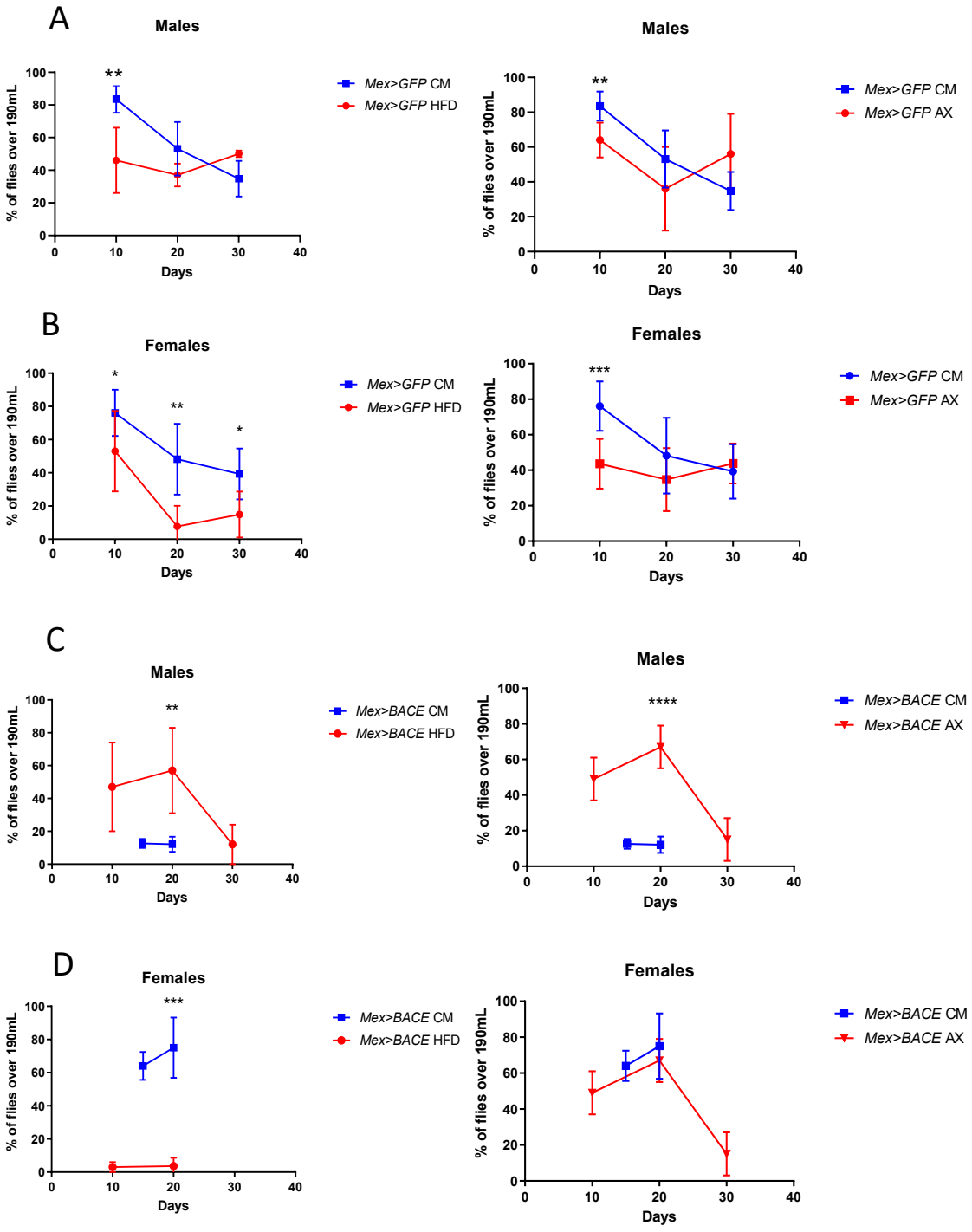
A
Males
**
% of flies over 190mL
Days
Mex>GFP CM
Mex>GFP HFD
Males
**
% of flies over 190mL
Days
Mex>GFP CM
Mex>GFP AX
B
Females
*
**
*
% of flies over 190mL
Days
Mex>GFP CM
Mex>GFP HFD
Females
***
% of flies over 190mL
Days
Mex>GFP CM
Mex>GFP AX
C
Males
**
% of flies over 190mL
Days
Mex>BACE CM
Mex>BACE HFD
Males
****
% of flies over 190mL
Days
Mex>BACE CM
Mex>BACE AX
D
Females
***
% of flies over 190mL
Days
Mex>BACE CM
Mex>BACE HFD
Females
% of flies over 190mL
Days
Mex>BACE CM
Mex>BACE AX

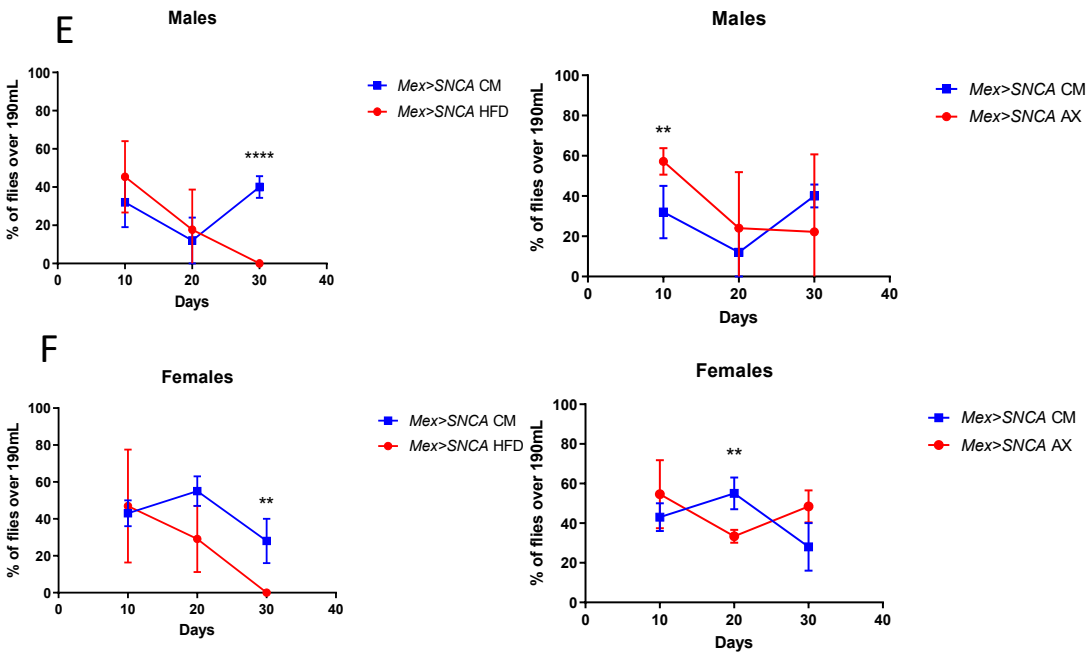

Figure 22. *Drosophila* negative geotaxis climbing assays of *Mex>BACE and* Mex *SNCA* and respective controls *Mex>GFP,* reared at 25°C on a CM, HFD and AX diet (comparing within genotypes). The x-axis is reporting days aged, and the y-axis is reporting NGCA as the mean % of flies that have successfully climbed up over a target height. All statistical analyses were carried out using two-tailed, unpaired Student's t-tests, assuming equal variance and an α=0.05. The number of flies assayed ranged from n=60-160 per genotype. A) CM male *Mex>GFP* controls were assayed in comparison to respective HFD male *Mex>GFP* controls, at time points 10do (t(7)= 4.141, **p=0.0043), 20do (t(6)=1.569, p=0.1677), and 30do (t(5)=1.852, p=0.1233). CM male *Mex>GFP* controls were assayed in comparison to respective AX male *Mex>GFP* controls, at time points 10do (t(9)= 3.533, **p=0.0064), 20do (t(7)=1,271, p=0.2443), and 30do (t(7)=1.841, p=0.1082). B) CM female *Mex>GFP* controls were assayed in comparison to respective HFD female *Mex>GFP* controls, at time points 10do (t(12)=2.288, *p=0.0411), 20do (t(9)=3.727, **p=0.0047), and 30do (t(8)=2.559, *p=0.0337). CM female *Mex>GFP* controls were assayed in comparison to respective AX female *Mex>GFP* controls, at time points 10do (t(13)= 4.260, ***p=0.0009), 20do (t(9)=1.124, p=0.2902), and 30do (t(9)=0.5366, p=0.6046). C) CM male *Mex>BACE* were assayed in comparison to HFD male *Mex>BACE,* at time point 20do (t(10)=3.763, **p=0.0037). CM male *Mex>BACE* were assayed in comparison to AX male *Mex>BACE*, at time point 20do (t(7)=9.511, ****p< 0.0001). D) CM female *Mex>BACE* were assayed in comparison to HFD female *Mex>BACE,* at time point 20do (t(6)=6.446, ***p=0.0007). CM female *Mex>BACE* were assayed in comparison to AX female *Mex>BACE*, at time point 20do (t(8)=0.8273, p=0.4321). E) CM male *Mex>SNCA* were assayed in comparison to HFD male *Mex>SNCA,* at time points 10do (t(7)=1.212, p=0.2647), 20do (t(5)=0.4186, p=0.6929), and 30do (t(4)=9.357, ***p=0.0007). CM male *Mex>SNCA*

were assayed in comparison to AX male *Mex>SNCA*, at time points 10do (t(7)=3.807, **p=0.0067), 20do (t(5)=0.6903, p=0.5207), and 30do (t(5)=0.9408, p=0.3810). F) CM female *Mex>SNCA* were assayed in comparison to HFD female *Mex>SNCA,* at time points 10do (t(6)=0.2154, p=0.836620do (t(6)=2.305, p=0.0606), and 30do (t(6)=4.667, **p=0.0034). CM female *Mex>SNCA* were assayed in comparison to AX female *Mex>SNCA*, at time points 10do (t(6)=1.089, p=0.3179), 20do (t(5)=4.989, **p=0.0041), and 30do (t(5)=2.526, p=0.0528).

3.1.6 *Mex>SNCA* males exhibit poor courtship memory

The second type of behavioural assay used measure neurodegeneration in the *Drosophila* brain was a short-term memory assay (courtship memory) designed for male flies (Koemans et al., 2017). Since the males had displayed the strongest phenotype, this assay was another way to assess neurodegeneration in the brain. Short term memory assays were carried out on *Mex>Pex5*-i, and control *Mex>w^{1118},* in addition to the reference model of *Mex>SNCA,* and respective control *Mex>GFP*. Furthermore, statistical analyses were carried out using multiple, unpaired t-tests assuming equal variance with an α=0.05, n=11-12 flies.

There was no courtship memory deficit displayed by the *Mex>Pex5*-i CM males because *Mex>Pex5*-i CM males (M=0.000%, SD=0.000) and *Mex>w^{1118}* CM males (M=6.444%, SD=11.42) were comparable after training; t(22)=1.955, p=0.0634 (Figure 23A). Moreover, both trained *Mex>Pex5*-i CM males, and trained *Mex>w^{1118}* CM males displayed significantly reduced courtship behaviour (by ~84-88%), compared to the naïve *Mex>Pex5*-i CM males (M=83.52%, SD=23.53) and naïve *Mex>w^{1118}* CM males (M=88.31%, SD=8.684) positive controls; t(21)=19.21, ****p<0.0001, and t(21)=12.32, ****p<0.0001 (Figure 23A). These results are recapitulated by the LI (learning index), which indicated how well the flies have successfully learned and remembered how to

identify rejection from a pre-mated female compared to the positive control. *Mex>w*^{1118} CM males have an LI of 93.13%, and *Mex>Pex5*-i CM males have an LI of 100%, both high values indicate that the male flies have effectively reduced their courtship behaviour in response to a pre-mated females, after training, just like the controls. Of note, these assays were only performed on flies younger than 20do, thus it will be important to test *Mex>Pex5*-i again at an older age.

The trained *Mex>SNCA* CM males did not reduce their courtship behaviour towards mated-females (M=68.9%3, SD= 34.66), but the trained *Mex>GFP* CM control males did (M=0.000%, SD=0.000); there were no signs of courtship identified, t(20)=6.597, ****p<0.0001 (Figure 23B). The trained *Mex>SNCA* CM males did not display the same degree of courtship to their naïve counterparts either, there was still a ~30% decline in courtship of the trained males (M=68.93%, SD=34.66) versus the naïve males (M=99.39%, SD=1.052); t(20)=2.913, **p=0.0086 (Figure 23B). However, this decline of courtship behaviour by the trained *Mex>SNCA* CM males compared to their naïve counterparts was not similar to the decline observed in the trained versus naïve control *Mex>GFP,* trained males (M=0.000%, SD=0.000) versus naïve males (M=68.93%, SD=34.66) ; t(20)=166.3, ****p<0.0001 (Figure 23B). Furthermore, the LI of *Mex>SNCA* CM males was LI= 30.64%, and *Mex>GFP* CM males LI= 100%, indicating that *Mex>SNCA* CM males were ~ 69% less effective at identifying the rejection of a pre-mated females than the *Mex>GFP* CM male controls (Figure 23B). Of note, these assays were also carried out on younger flies (~5do), therefore, the *Mex >SNCA* have a decline in learning memory already as young adults.

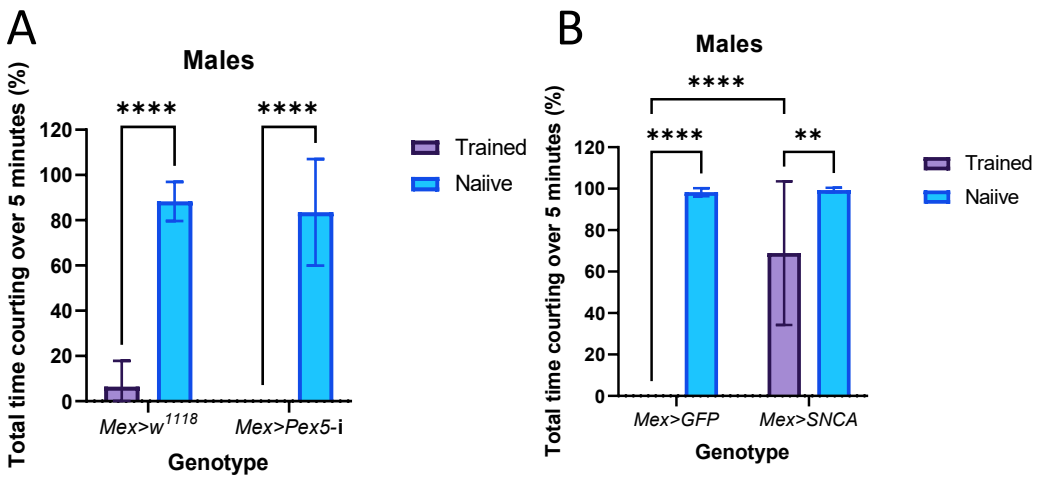

Figure 23. Short-term memory assays (courtship assays) of *Mex>Pex5*-i and control *Mex>w^{1118}* CM males, and *Mex>SNCA* and control *Mex>GFP* CM males. A) The LIs of *Mex>Pex5*-i and control *Mex>w^{1118}* CM males are 100.0% and 93.13% respectively which is concurrent with comparable average courting time after training between both genotypes. B) The LIs of *Mex>SNCA* and control *Mex>GFP* CM males are 30.64% and 100% respectively, concurrent with the ~69% increase of memory deficit in trained *Mex>SNCA* males compared to trained *Mex>GFP* controls (****p<0.0001). Statistical analyses were carried out using multiple, unpaired t-tests, assuming equal variance and an α=0.05.

3.1.7 *Mex>Pex5-i* and *Mex>SNCA* males and females do not have feeding nor heart abnormalities

To rule out feeding behaviour abnormalities as a confounding variable for the locomotor deficit observed in the male flies, in collaboration with Dr. Deniz Top, feeding assays were carried out to test male *Mex>Pex5*-i, *Mex>w^{1118}*, *Mex>SNCA,* and *Mex>GFP*. The conclusion was that the flies of each genotype do not show a feeding difference compared to controls (Figure 24.1). Dr. Top also provided data regarding when and how much food is consumed by the flies hourly, by average, over a 30hr time course. From the

spike graphs during the 12hr dark cycle the *Mex>Pex5*-i CM males appear to be more active and eating at more frequent time intervals than the control *Mex>w*^{1118}. The *Mex>w*^{1118} controls are in a rest state for the majority of the cycle, this is normal sleep behaviour for *Drosophila*, while the *Mex>Pex5*-i appear to be more active suggesting disturbances in sleep circadian at night (Figure 24.2). However, this observation will be discussed further with the collaborators to understand whether the changes observed are legitimate or negligible.

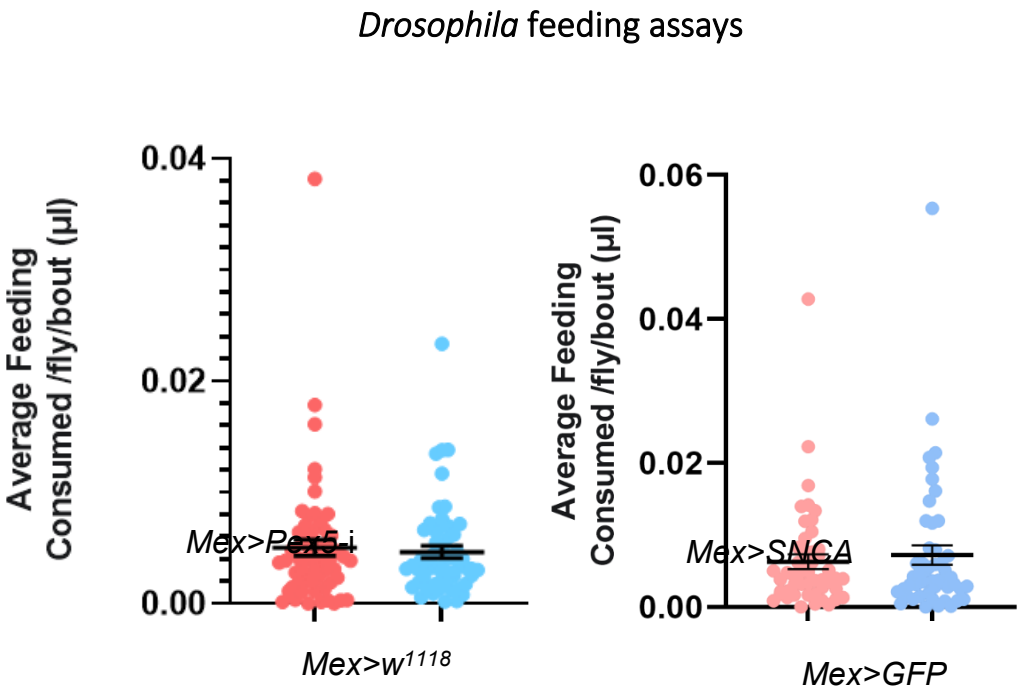

Figure 24.1. Feeding assays. The average amount of food consumed over three days, in µl versus genotypes *Mex>Pex5*-i control *Mex>w*^{1118}, *Mex>SNCA*, and control *Mex>GFP* males; n= 60 flies. No significant difference across genotypes was indicated by statistical analysis using a two-tailed unpaired t-test, assuming equal variance.

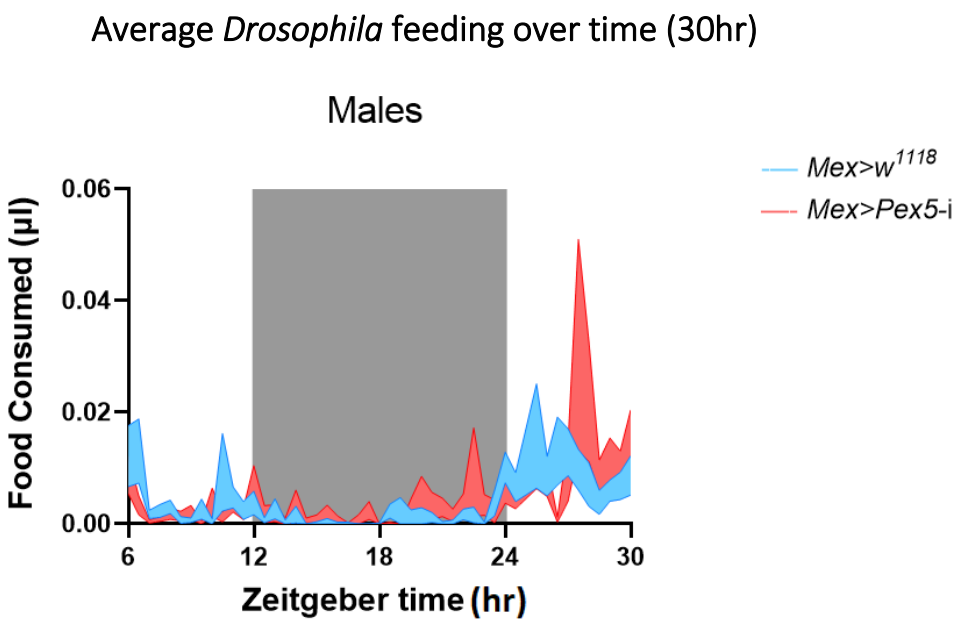

Figure 24.2. Feeding assays: in 1hr intervals over 30hrs.The white areas represents data being collected within the 12hr light cycle, while the medium gray areas indicate data collection during the dark 12hr light cycle.

Another potential confounder for the observed locomotor deficit could be a development defect in the heart, as a consequence of the *Pex5* gut-KD during development. Therefore, in collaboration with Dr. Hua Bai at Iowa State University, the hearts of both genotypes *Mex>Pex5*-i and *Mex>SNCA* males and females plus respective controls *Mex>w*^{1118} and *Mex>GFP,* were assessed on a CM (Normal Diet, ND) and HFD (Figure 25).

The five parameters measured were heart rate (HR), heart pressure (HP), arrhythmia (AI), diastole (DI) and systole (SI). HR and HP primarily measured whether the hearts were beating normally, not slower or faster against pressure in the systemic circulation, and that there are no mechanical defects of the heart. AI was used to identify abnormalities of the hearts pacemaker, and to rule out any physiological defects of the

heart. Finally, diastole and systole were used to measure contractility of the heart, to further rule out any mechanical or physiological defects.

Overall, there were no striking differences between *Mex>Pex5-i* and *Mex>w^{1118}* (Figure 25A,B) in both sexes. However, the HR of the female *Mex>Pex5*-i both on ND and HFD was faster in comparison to *Mex>w^{1118}* females on a ND, ***p=0.0003 and *p=0.0156 respectively. However, the HP of the *Mex>Pex5*-i females was longer (heart takes longer to fill and contract) than the controls on ND (*p=0.0335). The HP is recapitulated by the systole (the contractility of the heart to pump blood through the body) which was significantly increased (the heart is contracting more vigorously) in *Mex>Pex5*-i females compared to controls on both ND (*p=0.0215), and especially HFD (****p<0.0001).

Mex>SNCA and controls *Mex>GFP* females and males presented no differences in most parameters analyzed (Figure 25C, D). However, the HR of the female *Mex>SNCA* fed a HFD was faster than controls fed a HFD (*p=0.0085), and *Mex>SNCA* females fed a ND (*p=0.0384). This was also true for the SI of the fly, where output of the heart was decreased in *Mex>SNCA* females on a HFD compared to controls on a HFD (*p=0.0227), and *Mex>SNCA* on a ND (*p=0.0216).

Dr. Bai predicted that these changes in HR may not be enough to induce a locomotor phenotype in the flies, especially when considering the spread of the data. This is true for the *Mex>Pex5*-i, because females do not show the decline in negative geotaxis but the males do, and the males do not have any heart abnormalities. Conclusively, the heart is not a confounding variable, otherwise abnormalities in the heart would correspond to the locomotor deficits observed. This is also true for *Mex>SNCA* males but, *Mex>SNCA*

do exhibit a reduction of NGCA. However, the heart is not a confounding variable for *Mex>SNCA* either.

A

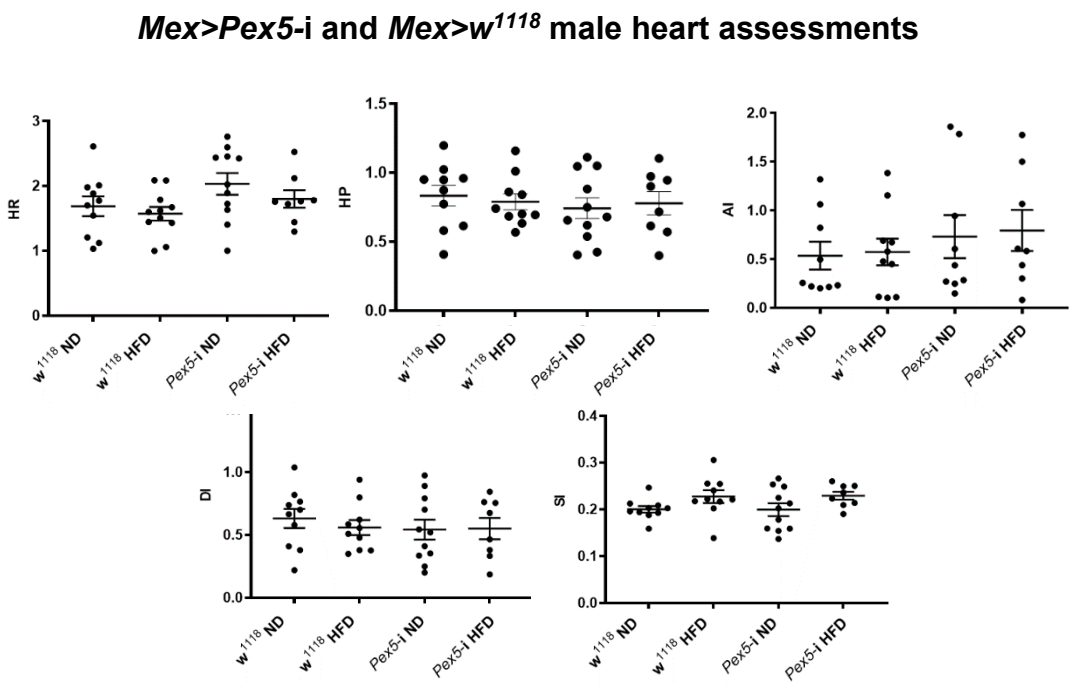

B

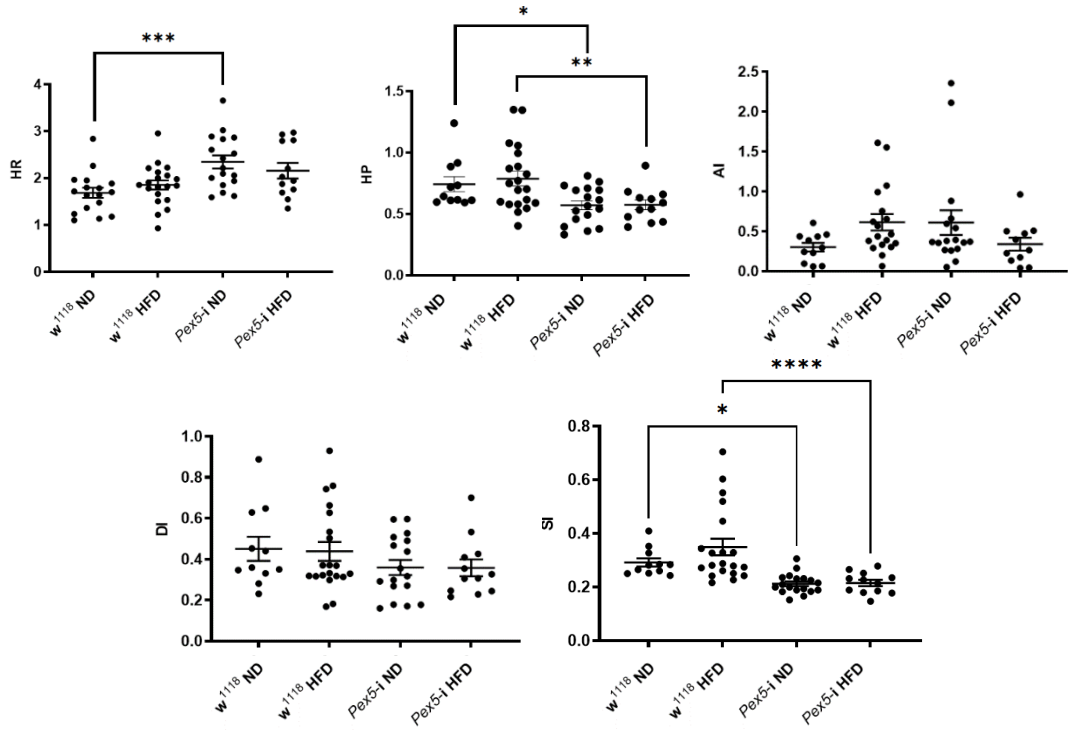

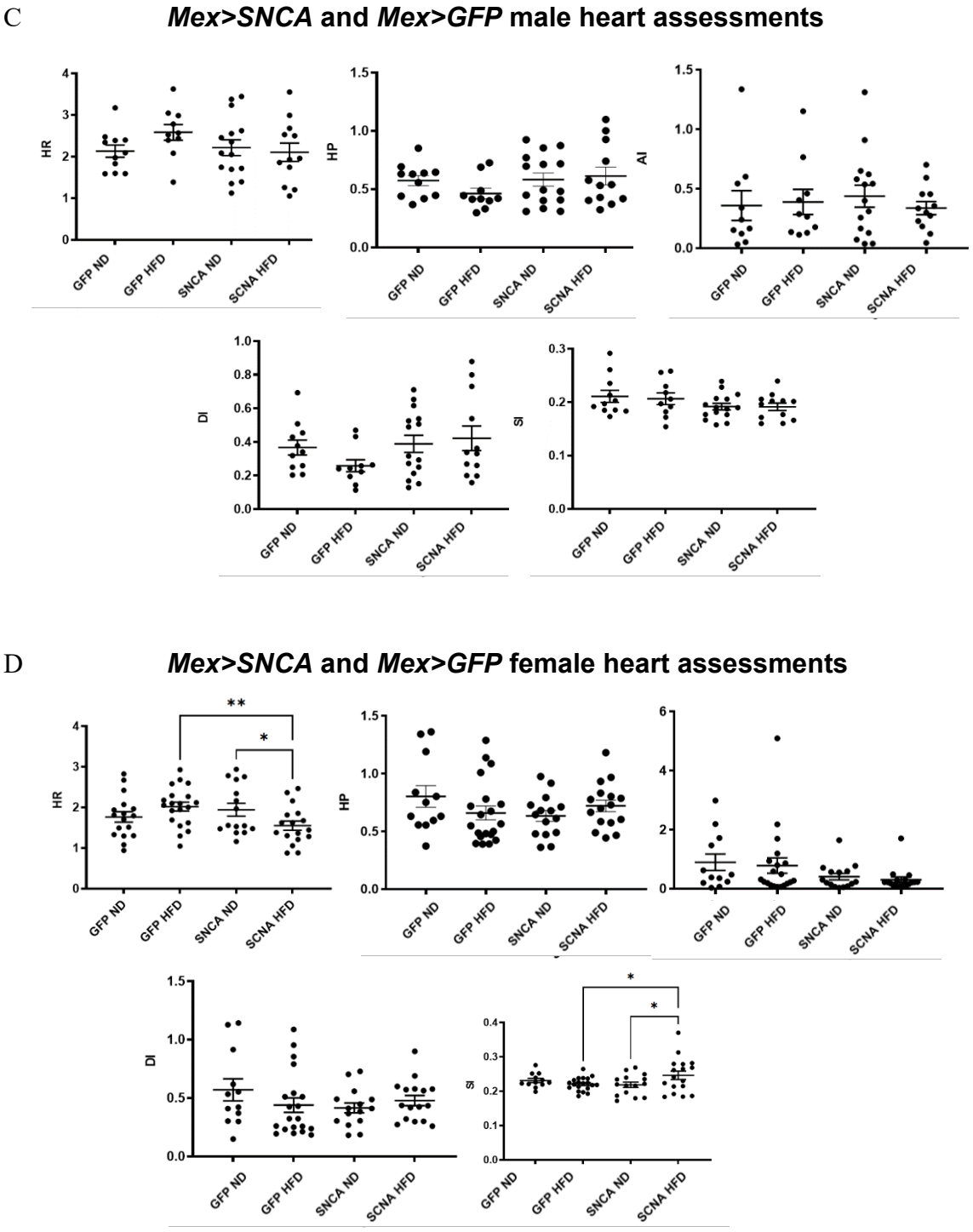

Figure 25. Heart assessments of *Mex>Pex5*-i and controls *Mex>w*^{1118} males and females, and *Mex>SNCA* and controls *Mex>GFP* males and females, aged to 20do. Five paramenters were tested: HR, HP, AI, DI and SI. A) *Mex>Pex5*-i and controls *Mex>w*^{1118} males B) *Mex>Pex5*-i and controls *Mex>w*^{1118} females. C) *Mex>SNCA* and controls *Mex>GFP* males. D) *Mex>SNCA* and controls *Mex>GFP* females. All Statistical analysis

was carried out using a one-way ANOVA, and no significant differences were observed between each genotype and respective control. Only *Mex>Pex5*-i and *Mex>SNCA* females exhibited elevated heart rates and more forceful heart contractions on ND and HFD compared to controls (as described above). (n=15-20 flies per sex, genotype, and condition).

3.1.8 Sub-section summary

In summary, *PEX5* gut-KD, and therefore dysfunction of peroxisomal metabolism in the midgut of flies raised on solely a CM diet, causes defects in locomotor negative geotaxis climbing ability for males but not females. When a HFD and AX conditions are introduced, the *Mex>Pex5-i* male locomotor phenotype does not worsen, however the control males are effected by both HFD and AX conditions. Locomotor climbing ability is only effected in the females when reared on HFD or AX conditions, and similar effect of HFD or AX are observed in control female flies as the males. Therefore I concluded that a defect in peroxisomal metabolism has a locomotor effect on the organism over aging, known to accumulate free fatty acids in the intestinal cells, and phenocopies the effect that a HFD and/or antibiotic treatment (AX) has (leading to dysbiosis of the midgut). Similarly, *Mex>SCNA* males present climbing deficits, although to a larger extent than the deficits observed in *Mex>Pex5*-i males. *Mex>SNCA* males also present memory impairment. Feeding behaviour and heart dysfunction were ruled out as confounding variables that may effect locomotion in males of both analyzed genotypes compared to the relative control. These assays highlighted the importance of the DMGB axis to preserve locomotor activity in aging animals. Moreover, to determine whether the locomotion defects are caused by high inflammation (inflammatory cytokines/antimicrobial peptides expression and/or high oxidative stress) in the brain of aging *Mex>Pex5-i* and *Mex>SNCA*, I measured these parameters using various assays (see next section). As locomotor defects and brain

inflammation was mainly observed in males, the brains of these flies were assessed for inflammation (looking at antimicrobial peptides, AMPs), redox stress, and physical/physiological damage. These assays helped to investigate how the effects that defective peroxisomes (*Mex>Pex5-i*) or mitochondria (*Mex>SCNA*) exclusively in the intestine, might affect brain health, and therefore behaviour. The males were the main focus for the remainder of the study.

3.2 Pathologies of the *Drosophila* brain in aged *Mex>Pex5*-i and *Mex>SNCA* males

After observing locomotor deficits in the NGCA of aging male flies, to further investigate whether the locomotor decline in males was truly a neuronal-phenotype caused by neurodegeneration of the brain, three inflammatory pathways were investigated to detect inflammations in the brain of the genotypes of interest. The first pathway considered was the activation of the immunodeficiency (IMD) pathway, using the expression of the AMP *Attacin* (*Att*) as a read-out for activation (Badinloo et al., 2018; Hoffmann, 2003); Myllymäki et al., 2014). The next pathway probed was the JAK/STAT pathway, using the expression of its transcriptional target inflammatory cytokine (IC) *Upd3* as a read-out, orthologous to Interleukin-6 (IL-6) in mammals (Oldefest et al., 2018; Sciambra & Chtarbanova, 2021). Moreover, the last pathways checked was the activation of Toll, using AMP *drosomycin* as a read-out for activation (Badinloo et al., 2018; Hoffmann, 2003).

3.2.1 *Mex>Pex5-i* male brains express more *Attacin* than controls

Using Quantitative Polymerase Chain Reaction (qPCR), the expression of *Att* (Myllymäki et al., 2014), in the heads of *Mex>Pex5*-i and *Mex>w*^{1118} was assessed. Flies were tested at age 20do and 30do, at both 29°C and 25°C.

At 29°C, there was no significant difference in *Att* expression between 20do *Mex>Pex5*-i and M*ex>w*^{1118} females; t(10)=0.6391, p=0.5371 (Figure 26.1A). However, the 20do *Mex>Pex5*-i males (M=9.515*10^{-5}, SD= 3.401*10^{-5}) had higher *Att* expression compared to the *Mex>w*^{1118} male controls (M=1.784*10^{-5}, SD= 8.394*10^{-6}); t(6)=4.415, **p=0.0045 (Figure 26.1A). At 25°C, there was no significant difference between 20do *Mex>Pex5*-i and M*ex>w*^{1118} within both males and females; males t(4)=1.220, p=0.2983, females t(4)=1.914, p=0.1281 (Figure 26.1B). However, *Mex>Pex5*-i males express more *Att* than the control males, while the *Mex>Pex5*-i females have less expression of *Att* compared to the control females.

At 25°C on CM conditions, there was no significant difference between 30do *Mex>Pex5*-i and M*ex>w*^{1118} within each sex; males t(4)=1.065, p=0.3650, females t(4)=0.5798, p=0.5931 (Figure 26.2). *Mex>Pex5*-i males express more *Att* than control males, however one replicate of the male *Mex> w*^{1118} samples at 25°C and 30do was undetectable during the qPCR reaction, and the statistical test reported above is merely for reference and does not have enough statistical power to be conclusive.

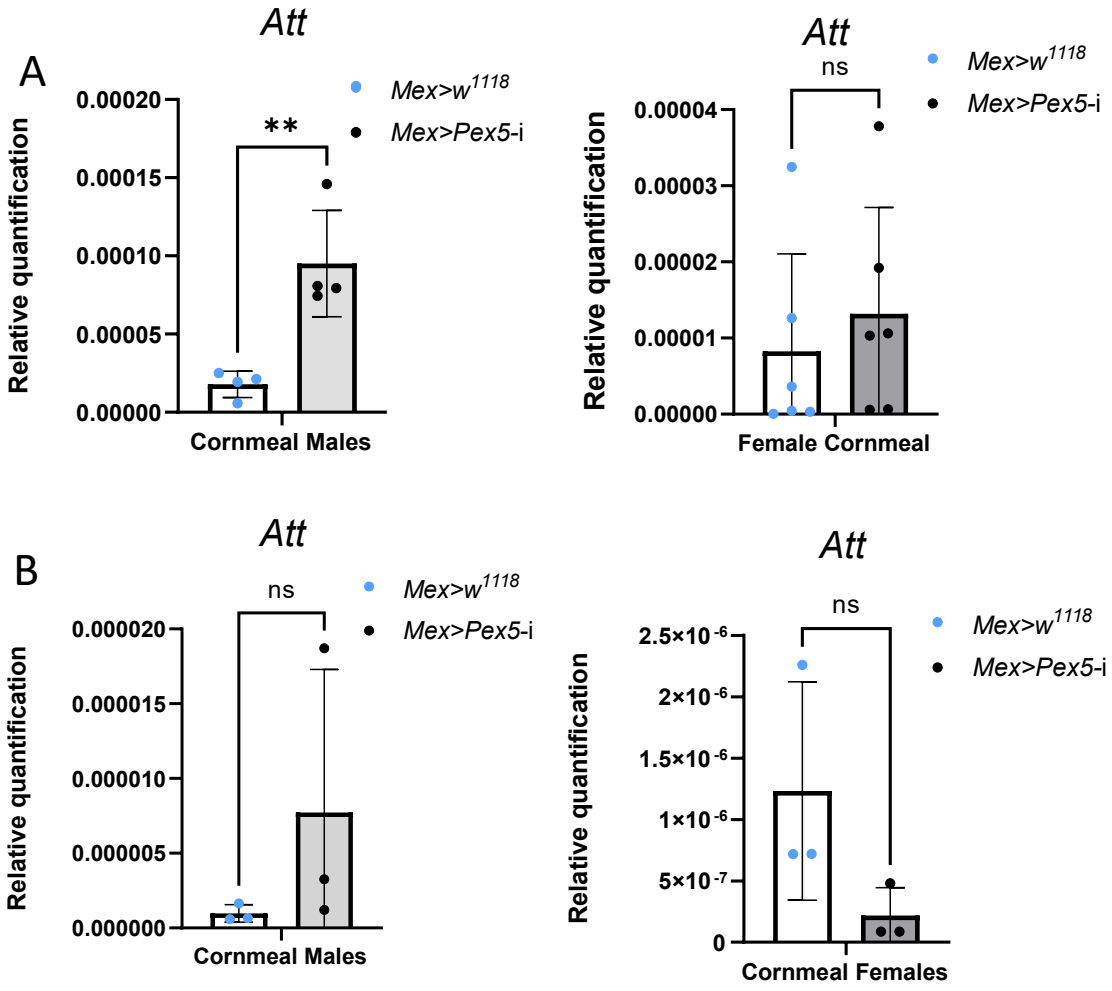

Figure 26.1. The relative quantification of *Attacin* in 20do *Drosophila* heads. The relative quantification of *Att:Rpl23* internal control in the heads of *Mex>Pex5*-i compared to *Mex>w*^{1118} age matched males and females aged to 20do. Each point on the graph represents one replicate of 14 fly heads. All statistical analysis was carried out using two-tailed, unpaired Student's t-tests, assuming equal variance and an α=0.05. A) CM male *Mex>Pex5-i* compared to male *Mex>w*^{1118} controls n=56 reared at 29°C. CM female *Mex>Pex5-i* compared to male *Mex>w*^{1118} controls n=84 reared at 29°C. B) CM male *Mex>Pex5-i* compared to male *Mex>w*^{1118} controls n=42 reared at 25°C. CM female *Mex>Pex5-i* compared to male *Mex>w*^{1118} controls n=42 reared at 25°C.

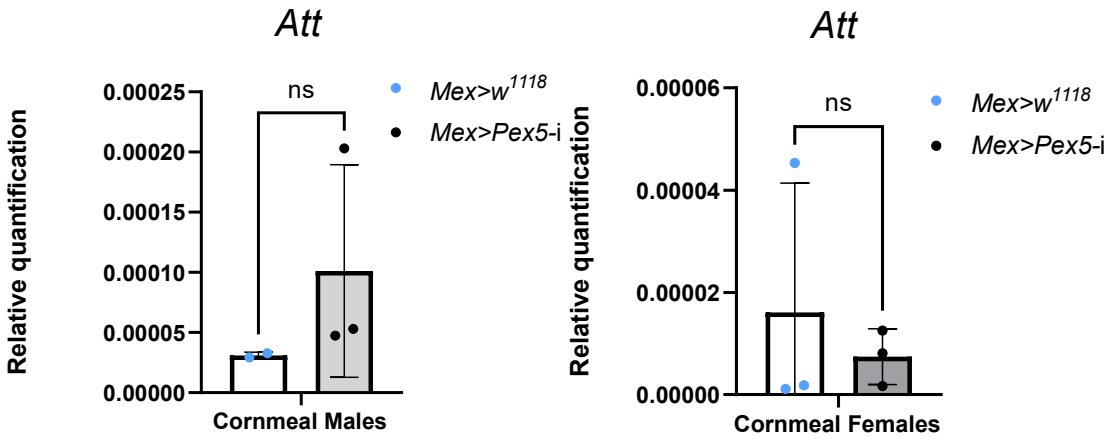

Figure 26.2. The relative quantification of *Att*acin in 30do *Drosophila* heads. The relative quantification of *Att:Rpl23* internal control in the heads of *Mex>Pex5*-i compared to *Mex>w*^{1118} age matched males and females raised at 25°C and aged to 30do. Each point on the graph represents one replicate of 14 fly heads. All statistical analysis was carried out using two-tailed, unpaired Student's t-tests, assuming equal variance and an α=0.05. A) CM male *Mex>Pex5-i* compared to male *Mex>w*^{1118} controls n=28-42. CM female *Mex>Pex5-i* compared to male *Mex>w*^{1118} controls.

Other inflammatory markers in the brain include *unpaired-3 (Upd3*) expression, an Inflammatory Cytokine (IC) which upregulates in the brain during aging in *Drosophila* (K. Huang et al., 2020; Rajan & Perrimon, 2012), and drosomycin, a downstream product of Toll-pathway activation, were tested. With six replicates for each genotype and sex, neither male nor female heads of *Mex>Pex5*-i nor *Mex>w*^{1118} showed any significant differences in *Upd3* expression between *Mex>Pex5*-i and *Mex> w*^{1118} (t(10)=0.7479, p=0.4717), nor the females (t(10)=0.7714, p=0.4583) (Figure 27), when the animals were aged to 20do and reared at 29°C

At 25°C on normal CM conditions, there was no significant difference in *drosomycin* expression between 30do *Mex>Pex5*-i and M*ex>w*^{1118} within both males and females; males t(3)=1.191, p=0.3192, females t(4)=0.9705, p=0.3867 (Figure 28). The

female *Mex> w*^{1118} show high variability in *drosomycin:Rpl23* ratio of relative expression, therefore the data is inconclusive and the more biological replicates are required per genotype to repeat the experiment (Figure 28). Similarly, one replicate of control *Mex> w*^{1118} male heads from animals aged to 30do reared at 25°C was undetectable during the qPCR reaction, and the statistical test reported above is merely for reference and does not have enough statistical power to be conclusive or non conclusive, therefore no conclusion can be made for the males.

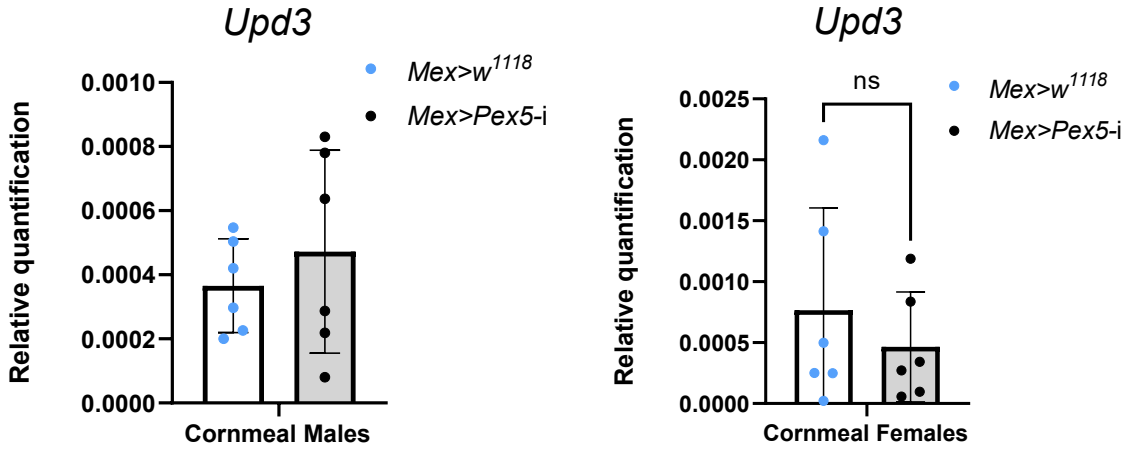

Figure 27. The relative quantification of *unpaired-3 (Upd3)* in 20do *Drosophila* heads. The relative quantification of *Upd3:Rpl23* internal control in the heads of *Mex>Pex5*-i compared to *Mex>w*^{1118} age matched males and females raised at 29°C and aged to 20do. Each point on the graph represents one replicate of 14 fly heads. All statistical analyses were carried out using two-tailed, unpaired Studen'ts t-tests. A) CM male *Mex>Pex5-i* compared to male *Mex>w*^{1118} controls, n=84. B) CM female *Mex>Pex5-i* compared to male *Mex>w*^{1118} controls, n=84.

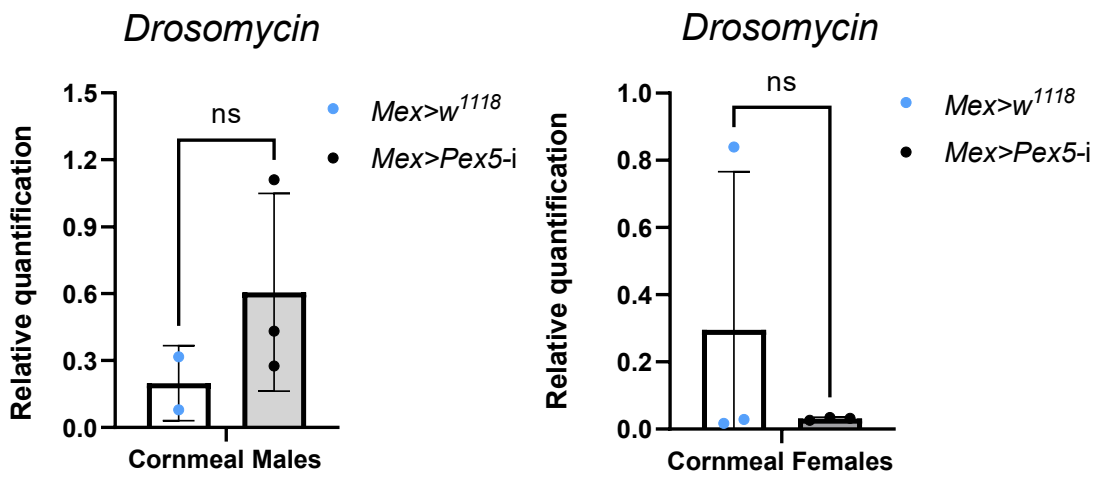

Figure 28: The relative quantification of *drosomycin* in 30do *Drosophila* heads. The relative quantification of drosmycin:RPL23 internal control in the heads of *Mex>Pex5*-i compared to *Mex>w*^{1118} age matched males and females raised at 25°C and aged to 30do. Each point on the graph represents one replicate of 14 fly heads. All statistical analysis was carried out using two-tailed, unpaired Student's t-tests, assuming equal variance and an α=0.05. A) CM male *Mex>Pex5-i* compared to male *Mex>w*^{1118} controls n=24-42. B) CM female *Mex>Pex5-i* compared to male *Mex>w*^{1118} controls, n=42.

In conclusion (Figure 29), there are no differences between *Mex>Pex5*-i and *Mex>w*^{1118} females in the expression of any of the AMPs/cytokines tested. There is a significant expression of *Att* in the heads of 20do males reared at 29°C (approximately 30do if reared at 25°C). This is also observed for males aged to 20do at 25°C, however the difference is not statistically significant. There is potential for elevated *Att* and *drosomycin* expression in 30do male flies aged at 25°C, however more replicates are needed to confirm this anecdotal observation. Therefore, the only conclusive evidence of accumulating inflammatory markers in the brain was obtained from the analyses of 20do male flies raised at 29°C.

Summary of *Att, Upd3*, and *drosomycin* expression in *Mex>Pex5*-i heads

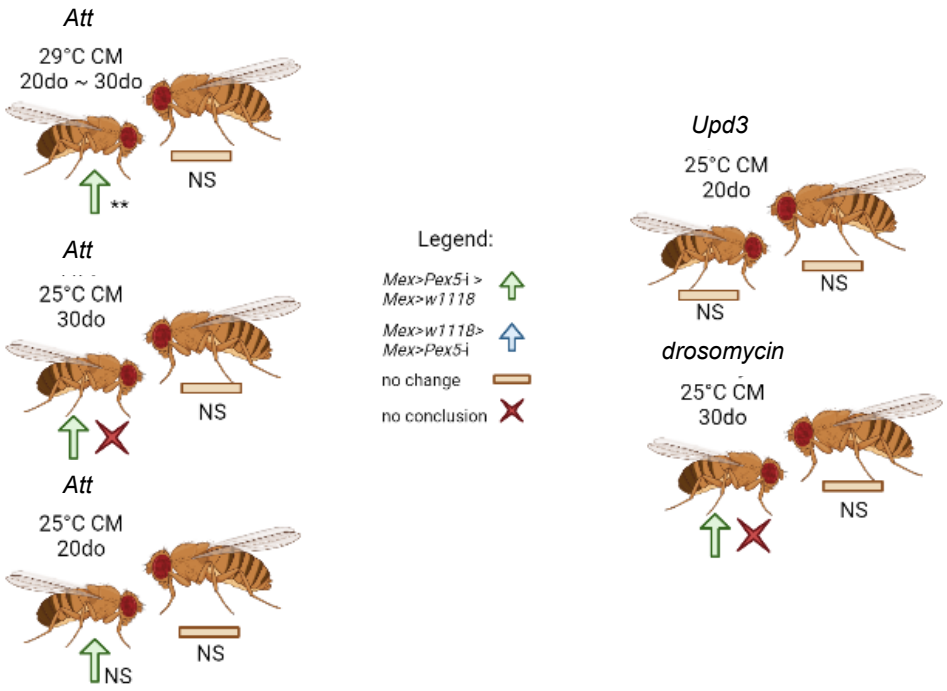

Figure 29: Summary of the results of neuroinflammatory markers *Att*, *Upd3* and *drosomycin*. Male flies are on the left of each fly pair, and females on the right. *Mex>Pex5*-i males express the inflammation marker *Att* and present decline in locomotor climbing activity on CM conditions at 20do and 30do. Furthermore, 30do males reared at 25°C are inconclusive due to insufficient replicates for statistical power, and neither *Att, Upd3,* nor *drosomycin* were expressed differently in the heads of *Mex>Pex5*-i females in comparison to *Mex>w*^{1118} females.

3.2.2 *Mex>Pex5-i and Mex>SNCA male brains accumulate ROS*

Quantifying AMPs/ICs in the heads of the flies proved to be challenging, therefore other methods of looking for inflammation in the brains of PEX5 gut-KD males were deployed, such as superoxide probe dihydroethidium (DHE) (Di Cara et al., 2018). When the brains of CM *Mex>Pex5*-i and control *Mex>w*^{1118} males at 30do at 25°C were stained with DHE, *Mex>Pex5*-i males exhibited a higher fluorescent intensity in the brain tissue than the controls; observed in patches of bright red fluorescence (Figure 30A). This indicated that there was an accumulation of Reactive Oxygen Species (ROS) in the brains

of male *Drosophila* with dysfunctional peroxisomes in the midgut. This ROS accumulation was also observed in the brains of male *Mex>SNCA* compared to age-matched controls *Mex>GFP* (Figure 30B).

A

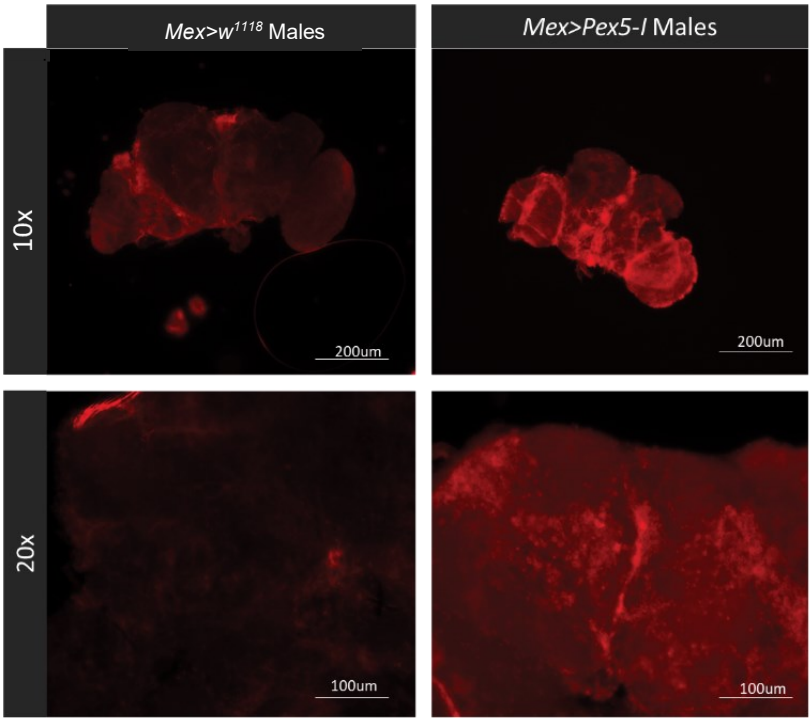

B

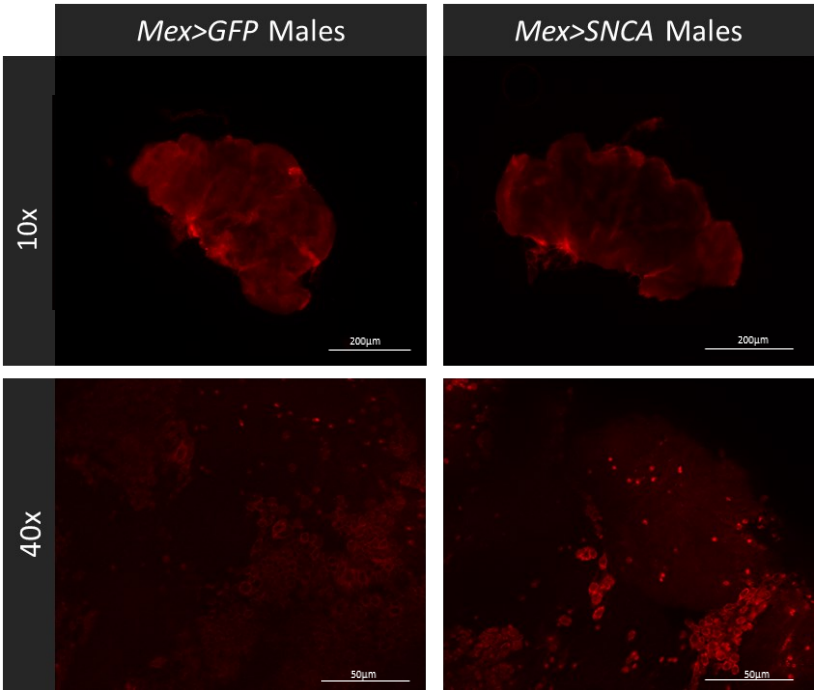

Figure 30: *Mex>Pex5*-i and *Mex>SNCA* males display reactive oxygen species accumulation (via dihydroethidium detection) of in the brains. A) 30do CM *Mex>Pex5*-i males (Right-most panels) show accumulation of ROS in the brain (Red fluorescence) compared to control *Mex>w*^{1118} males (Left-most panels). Scale bars read 200 μm at 5x magnification, and 100 μm at 20x magnification, imaged on a Zeiss AXIO Observer fluorescent microscope. B) 30do CM *Mex>SNCA* males (Right-most panels) show accumulation of DHE staining in the brain (Red fluorescence) compared to control *Mex>GFP* males (Left-most panels). Scale bars read 200 μm at 10x magnification, and 50 μm at 40x magnification, imaged on a Zeiss LSM 880 confocal microscope.

To validate what was observed with DHE, hydrogen peroxides (H_2O_2) was quantified in the brains of 30do *Mex>Pex5*-i male aged at 25°C. *Mex>Pex5*-i male brains have 350 pmol more H_2O_2 (M=402.7 pmol, SD= 50.66) than control *Mex>w*^{1118} (M=50.67 pmol, SD= 2.081); t(8)> 6.440, ****p<0.0001 (Figure 31). This phenotype, accumulation of H_2O_2 , was rescued by treating the flies with niacin. In Mex>*Pex5*-i male heads treated with niacin, the amount of H_2O_2 was significantly and dramatically reduced (M=19.00 pmol, SD= 5.292) in comparison to the untreated males (M=402.7 pmol, SD= 50.66); t(8)>6.440, ****p<0.0001 (Figure 31). The levels of H_2O_2 in the niacin treated *Mex>w*^{1118} appeared to be also slightly reduce compared to the untreated males, however there was no significance between both averages; t(8)>6.440, p=0.7436 (Figure 31).

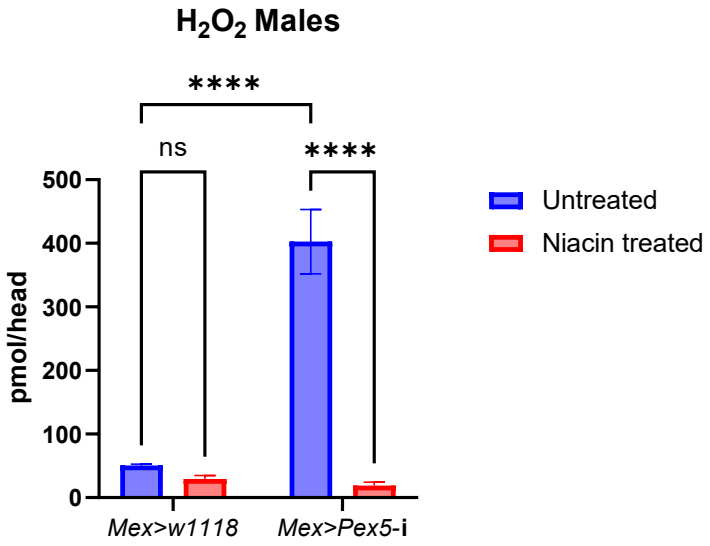

Figure 31. H_2O_2 accumulation in *Pex5*-i male brains is dramatically rescued with niacin. Age matched *Pex5*-i males on CM conditions revealed dramatic accumulation of ROS H_2O_2 in comparison to *Mex>w*^{1118} CM control males (****p<0.0001). When treated with niacin, H_2O_2 is significantly reduced to almost nothing (****p<0.0001). Statistical tests were carried out using a two-way ANOVA, n=60.

3.2.3 *Mex>Pex5*-i male brains display mitochondrial abnormalities

As mentioned in the introduction, oxidative stress can trigger mitochondrial damage. Therefore, using Transmission Electron Microscopy (TEM) to visualize ultrastructure's of the neurons, I observed a higher frequency of damaged mitochondria with abnormal cristae and/or mitophagy in the CM *Mex>Pex5*-i male brains versus control CM *Mex>w*^{1118}. Particularly, these observations were made in the anterior dorsal area of the brains, in proximity to the central complex and mushroom body important in locomotion and memory (Givon et al., 2017; Stark et al., 2020). In (Figure 32A) in the bottom left panel, there appears to be an autophagosome in the later stages of mitophagy (M), as well as one in the early stages of mitophagy formation at the very bottom of the panel (M). When magnified to 100x, the shape of the autophagosome becomes clear, appearing like a hollow horse-shoe structure in the bottom right panel (Figure 32A). In

Figure 32B, the cristae abnormalities observed in *Mex>Pex5*-i male brains are evident (AC). The mitochondria appear less organized, loose and with larger gaps between cristae in comparison to the organized and tightly packed cristae of control *Mex>w*^{1118} males (Figure 32B). Moreover, there was a higher frequency of abnormal/mitochondria in mitophagy compared to healthy mitochondria in the brain (Table 3). Therefore, the KD of PEX5 in the intestinal epithelial cells of *Drosophila* male reared on CM diet affects mitochondrial morphology and trigger mitophagy in the brain.

Mex>Pex5-i female brains did not present a higher frequency of mitochondria with abnormal cristae or mitophagy than controls in longitudinal brain sections, in comparison to the respective controls (Table 4). However, in transverse brain sections, *Mex>Pex5-i* females have more mitophagy and mitochondria with abnormal cristae. Therefore, the data is inconclusive for the females and requires more biological replicates to understand the phenotype that is more representative of the female population.

A

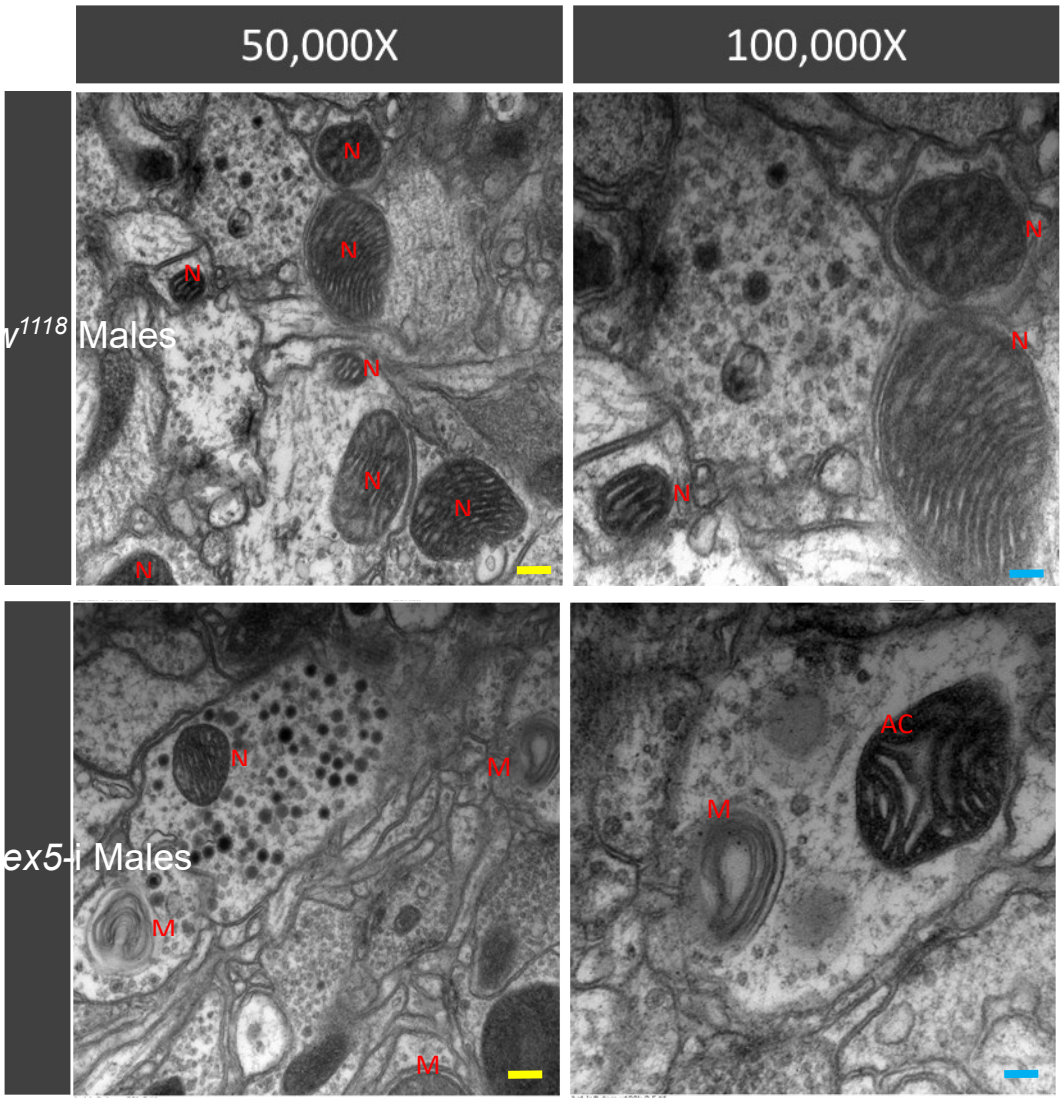

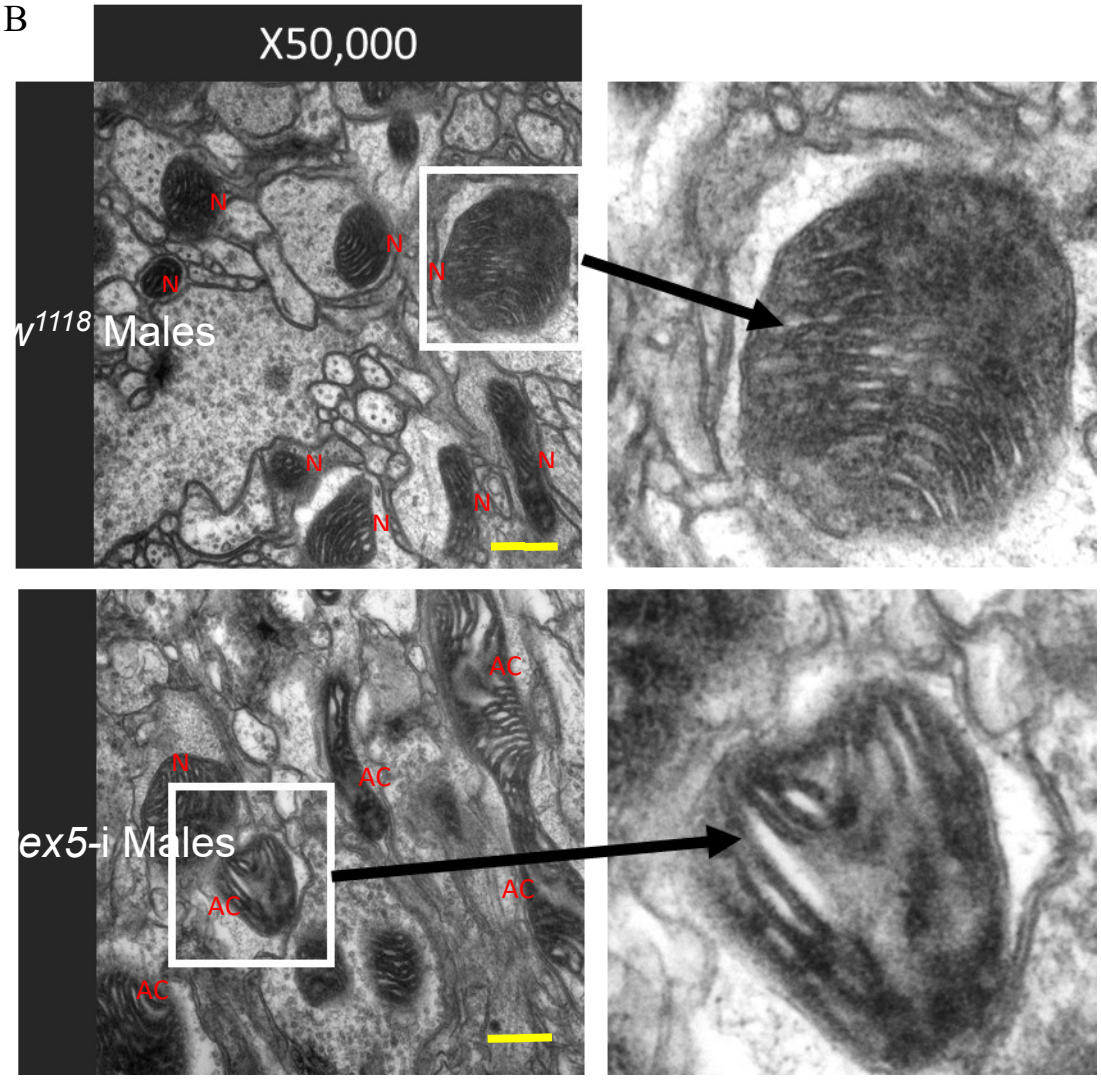

Figure 32: Transmission electron microscopy reveals mitochondrial abnormalities in the brains *Mex>Pex5*-i males. A) TEM of 30do CM *Mex>Pex5*-i and age-matched control *Mex>w*^{1118} male *Drosophila* brains where the brain section has been cut in a longitudinal manner. N: Normal mitochondria, M: Mitophagy, AC: Abnormal cristae (loose and disorganized). Scale bar 200 nm at x50k magnification (yellow scale bar) and 100 nm at x100k magnification (blue scale bar). B) TEM of *Mex>Pex5*-i and control *Mex>w*^{1118} male *Drosophila* brains. N: Normal mitochondria, M: Mitophagy, AC: Abnormal cristae (loose and disorganized). Looking at a transverse section of the fly brain. Scale bar 400 nm at a x50k magnification (yellow scale bar).

Table 3. *Mex>Pex5*-i male brain have more mitochondrial abnormalities than a control on CM conditions. The brains of both *Mex>Pex5*-i males and controls, age matched at 30do, were sliced in a transverse (the dorsal side of the brain), and longitudinal manner (the anterior side of the brain).When comparing the mitochondrial counts of transverse or longitudinal brains, with two pooled replicates (Br1, brain 1, and Br2, brain 2) from each genotype, there is a lower frequency of normal/healthy mitochondria, and a higher frequency of mitochondria in mitophagy and/or with abnormal cristae in the *Mex>Pex5*-i males (In dark purple) compared to controls (in light green).

Genotype (Males)	Normal (N)	%	Mitophagy (M)	%	Abnormal cristae (AC)	%	Total:
Mex>Pex5-i Trans Br1	32	50.79	3	4.762	28	44.44	63
Mex>Pex5-i Trans Br2	15	37.50	16	40.00	9	22.50	40
Total	47	45.63	19	18.45	37	35.92	103
Mex>Pex5-i Long Br1	32	60.38	18	33.96	3	5.660	53
Mex>Pex5-i Long Br2	22	44.00	12	24.00	16	32.00	50
Total	54	52.42	30	29.12	19	18.45	103
Mex>w^{1118} Trans Br1	21	55.26	4	10.52	13	34.21	38
Mex>w^{1118} Trans Br2	59	86.76	4	5.882	5	7.353	68
Total	80	75.47	8	7.547	18	16.98	106
Mex>w^{1118} Long Br1	32	55.17	9	15.52	17	29.31	58
Mex>w^{1118} Long Br2	37	80.43	2	4.348	7	15.22	46
Total	69	66.35	11	10.58	24	23.08	104

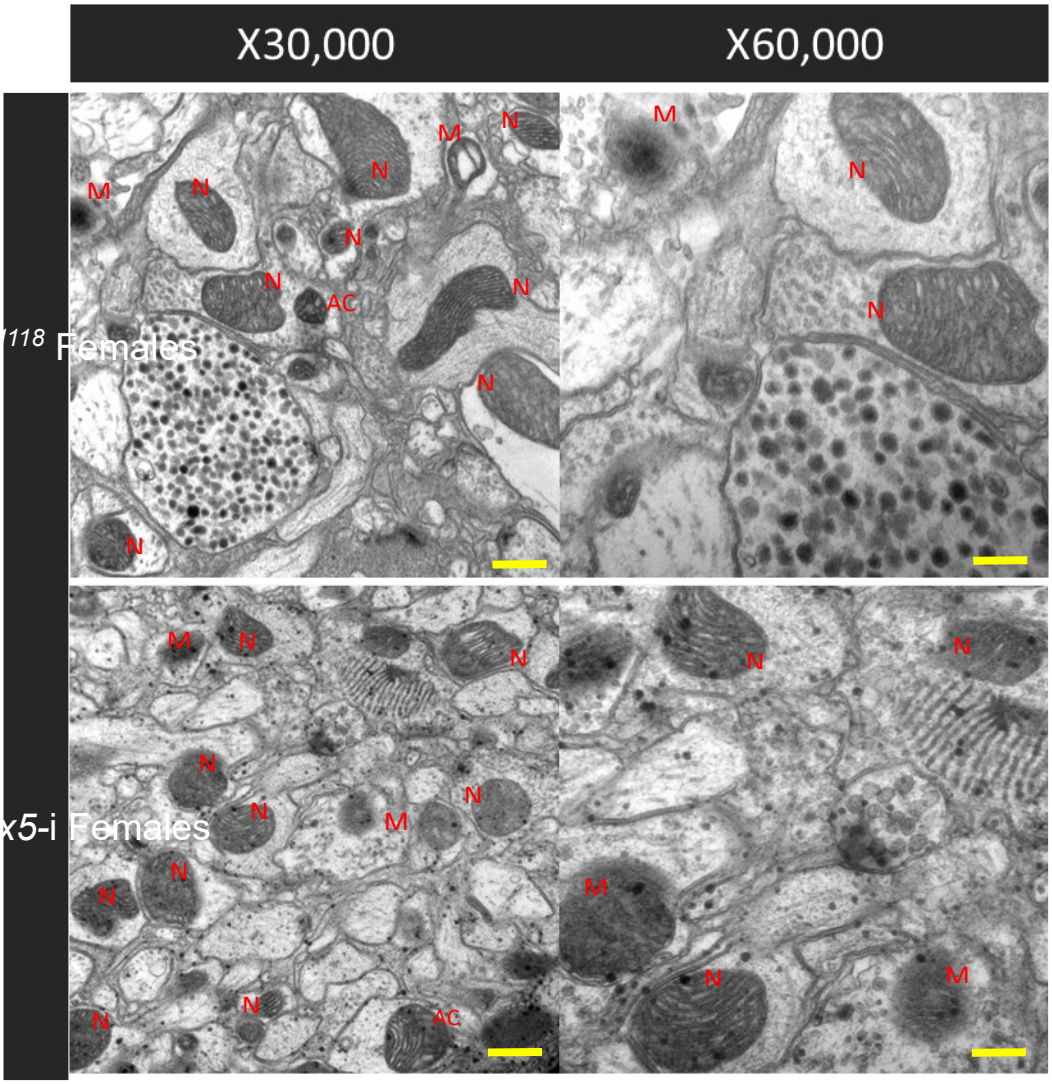

Figure 33. Transmission electron microscopy reveals little to no mitochondrial abnormalities in the brains of CM *Mex>Pex5*-i females. TEM of CM *Mex>Pex5*-i and age-matched control *Mex>w*^{1118} female *Drosophila* brains where the brain section was cut in a longitudinal manner. N: Normal mitochondria, M: Mitophagy, AC: Abnormal cristae (loose and disorganized). Scale bar 500 nm at x30k magnification (yellow scale bar) and 200 nm at x60k magnification (yellow scale bar as well).

Table 4: *Mex>Pex5*-i female brains have little to no mitochondrial abnormalities and are comparable to the control *Mex>w^{1118}*. The brains of both *Mex>Pex5*-i females and controls, age matched at 30do, were sliced in a transverse (the dorsal side of the brain) and longitudinal manner (the anterior side of the brain).When comparing the mitochondrial counts of longitudinal brains, with one replicate (Br1) from each genotype, there is no difference in frequency of normal/healthy mitochondria, or mitochondria in mitophagy and/or with abnormal cristae compared to controls. However in transverse brain sections, *Mex>Pex5*-i females appeared to have more mitophagy and mitochondria with abnormal cristae.

Genotype (Females)	Normal (N)	%	Mitophagy (M)	%	Abnormal cristae (AC)	%	Tot
Mex>Pex5-i Trans Br1	34	66.70	4	7.843	13	25.49	51
Mex>Pex5-i Long Br1	22	81.48	2	7.407	3	11.11	27
Mex>w^{1118} Trans Br1	33	100.0	0	0.000	0	0.000	33
Mex>w^{1118} Long Br1	26	86.67	2	6.670	2	6.670	30

To confirm that the mitochondria in the brain of *Mex>Pex5*-i males were indeed stressed and dying, as identified by TEM imaging, MitoSOX™ was used to stain for superoxide accumulation in mitochondria. *Mex>Pex5*-i male brains displayed more red fluorescence in the tissue at 10x magnification compared to the male *Mex>w^{1118}* control brains (Figure 34A). This observation was better recapitulated at a higher magnification of 40x, where the cell bodies for both genotypes are visible, but only the *Mex>Pex5*-i cell bodies fluoresce due to superoxide accumulation in mitochondria (Figure 34A). Similar results were observed in *Mex>SNCA* male brains using MitoSOX™ (Figure 34B).

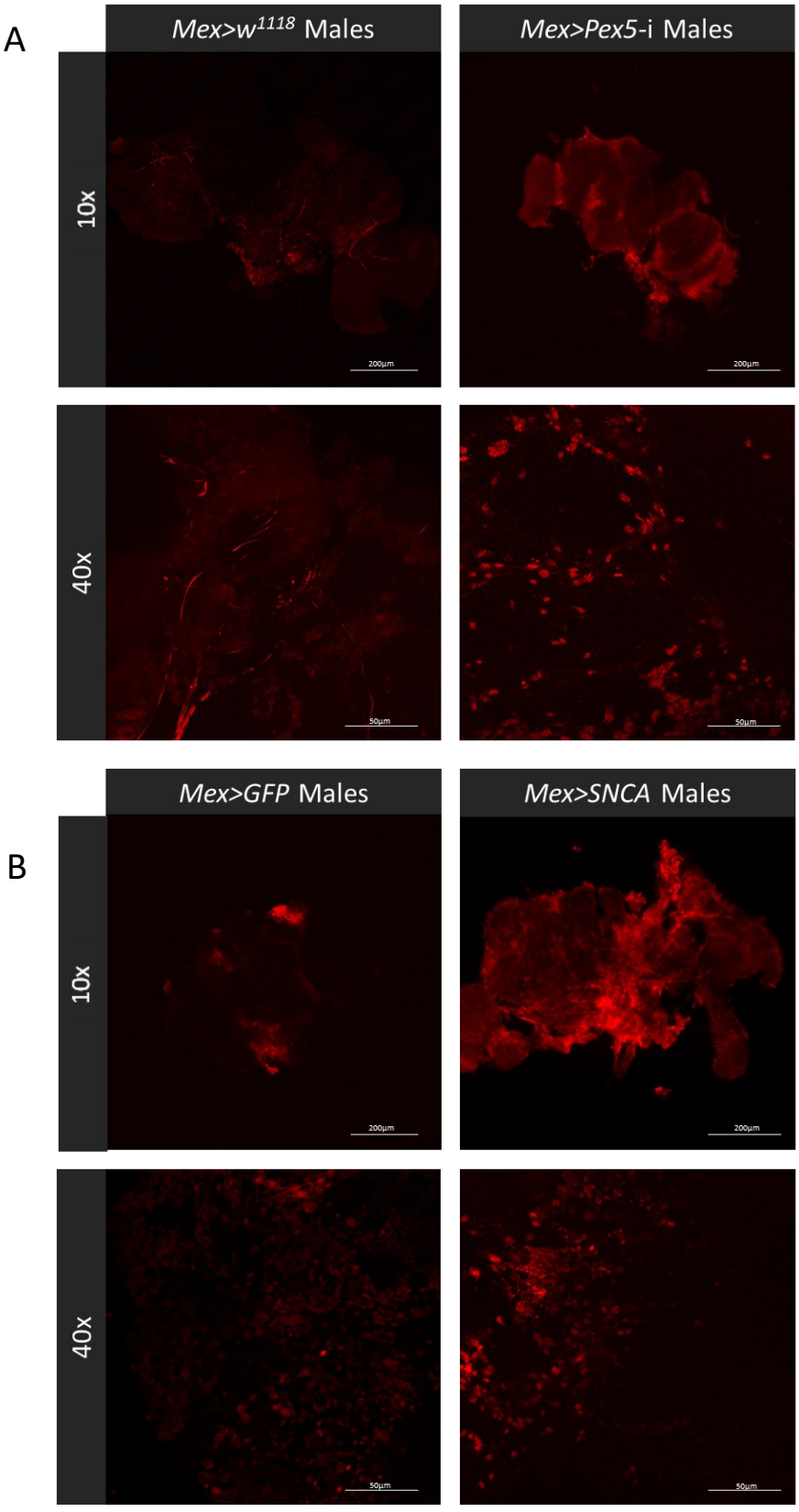
A
Mex>w1118 Males
Mex>Pex5-i Males
10x
40x
200µm
50µm
B
Mex>GFP Males
Mex>SNCA Males
10x
40x
200µm
50µm

Figure 34. MitoSOX® reveals that *Mex>Pex5*-i and *Mex>SNCA* male brains have more superoxide accumulation inside of mitochondria than controls *Mex>w^{1118}* and *Mex>GFP*. A) Staining with superoxide marker for mitochondria MitoSOX™ of 30do CM *Mex>Pex5*-i males (Right-most panels) shows accumulation of these ROS in mitochondria by lighting up entire neuron bodies in the brain (Red fluorescence) compared to control *Mex>w^{1118}* (Left-most panels) with little to no fluorescent neurons. Scale bars read 200μm at 19x magnification, and 50 μm at 40x magnification, imaged on a Zeiss LSM 880 confocal microscope. B) 30do CM *Mex>SNCA* males (Right-most panel) showing accumulation of ROS in the mitochondria of neurons (Red fluorescence of cell bodies) compared to control *Mex>GFP* (Left-most panels). Scale bars reading 200 μm at 10x magnification, and 50μm at 40x magnification, imaged on a Zeiss LSM 880 confocal microscope.

3.2.4 *Mex>Pex5-i* males display wide-spread neuronal death in the brain

After confirming that there is inflammation and redox stress in the brain of both CM *Mex>Pex5*-i and CM *Mex>SNCA* males, this indicates that neurons in the brain may be dying as a result. I began using annexin V (AV, marker for apoptosis), and Propidium Iodide (PI, marker for necrosis) to try and visualize cellular death in the brain. Despite countless attempts to optimize these protocols, efforts were unrequited (Supplementary Figure 1, and 2).

The final approach to visualizing widespread cellular death in the brain was to use Terminal deoxynucleotidyl transferase biotin-dUTP Nick End Labeling (TUNEL) to stain for apoptosis, that proved to be effective and consistent. CM *Mex>Pex5*-i males reared at 25 °C to the age of 30do, displayed more red fluorescent/dying cells across the entire brain than then age-matched male controls *Mex>w^{1118}* (Figure 35A). Additionally, these results were recapitulated in CM *Mex>SNCA* males and age-matched male *Mex>GFP* controls (Figure 35B). On the contrary to the males, and in agreement with the results from the CM climbing assays, age matched *Mex>Pex5*-i females and respective controls have no difference in red fluorescent intensity, indicating a lack of cellular death in both genotypes

(Figure 35C). However, there was an organized cluster of dying cells in the ventral regions of the brain, which at first was suspected to be an artifact, but was observed in multiple *Mex>Pex5*-i female brains; this phenotype prompts further investigation (Figure 35B). Conclusively, however, there is no sign of wide-spread cellular death for the *PEX5* gut-KD females versus controls (Figure 35C).

TUNEL Red death stain as an indicator of cellular apoptosis (Males)

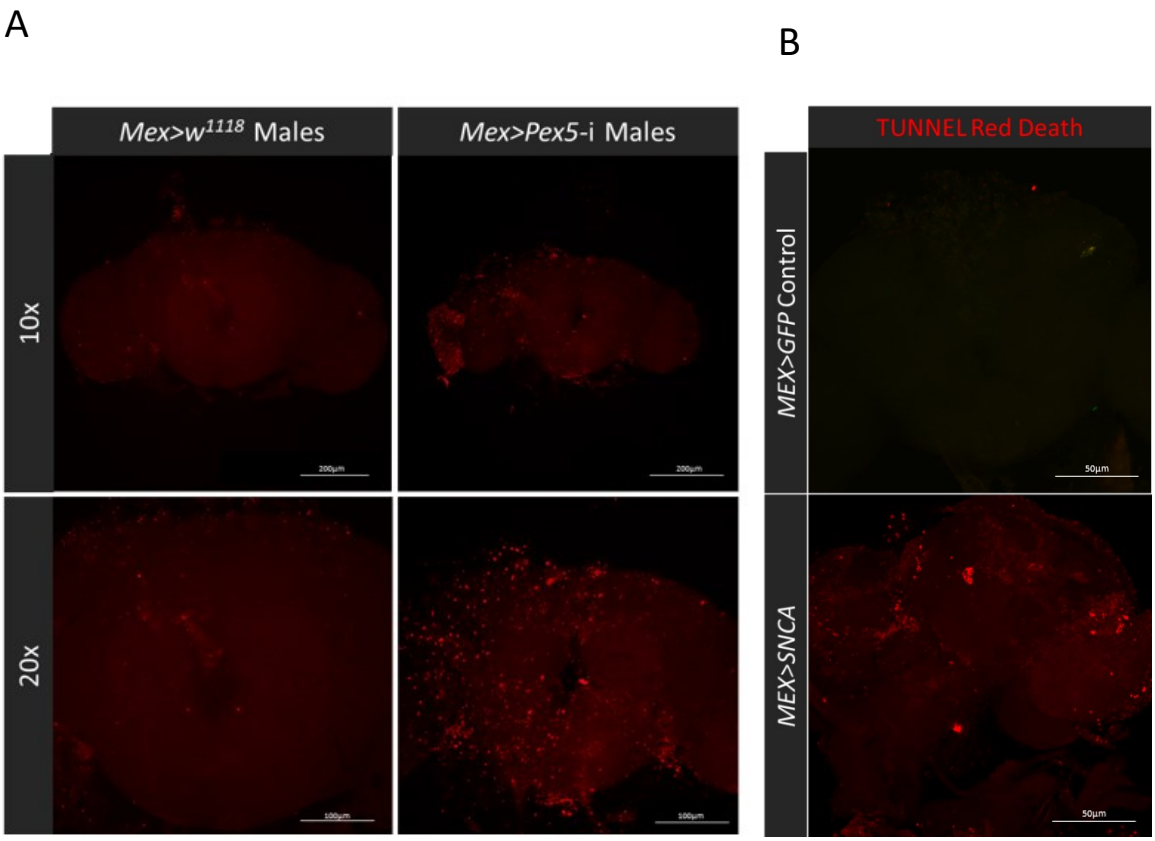

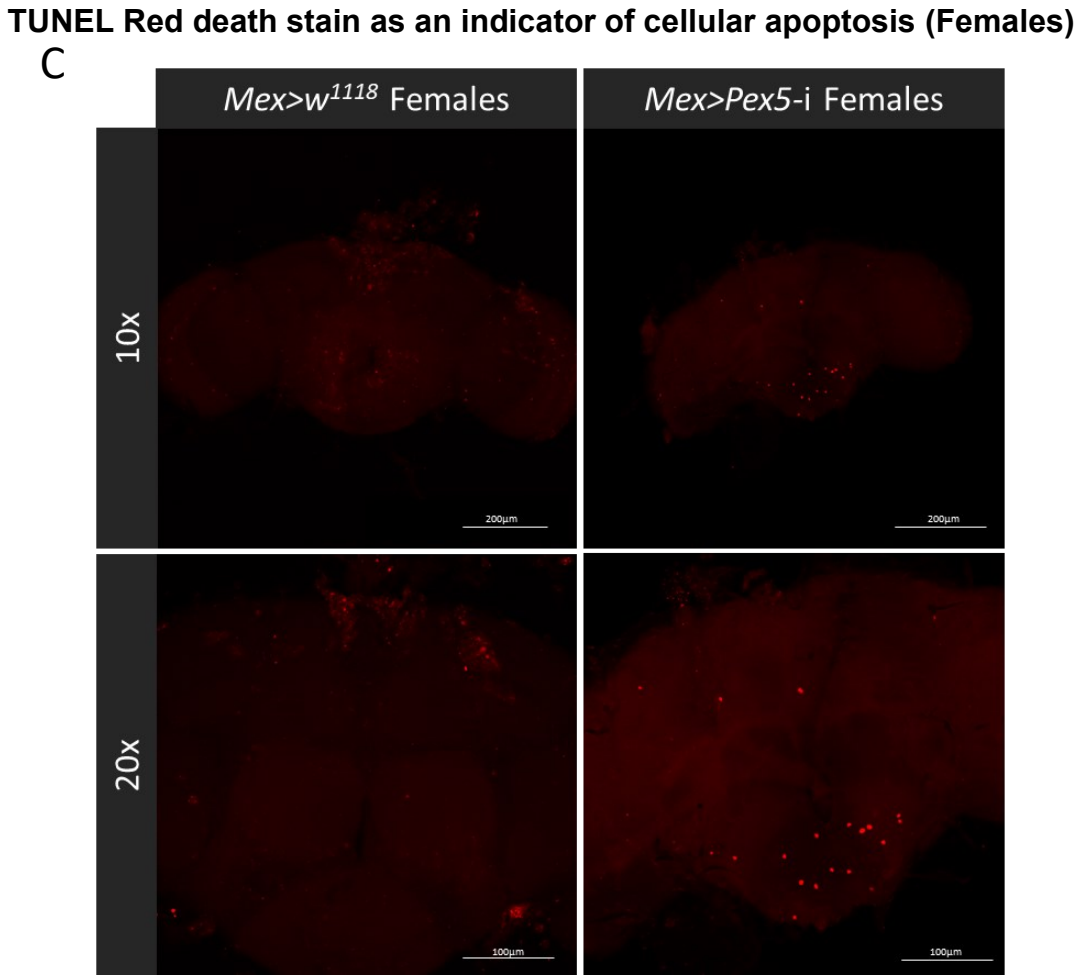

Figure 35. TUNEL stain for apoptosis reveals brain-wide cellular death in both *Mex>Pex5*-i and *Mex>SNCA* males in comparison to *Mex>w1118* and *Mex>GFP* controls. A) Staining with TUNEL marker for cellular apoptosis of 30do CM *Mex>Pex5*-i males (Right-most panels) shows death of neuron bodies in the brain (Red fluorescence) compared to control *Mex>w*^{1118} (Left-most panels) with little to no fluorescent neurons. Scale bars read 200 µm at 10x magnification, and 100 µm at 20x magnification, imaged on a Zeiss LSM 880 confocal microscope. B) 30do CM *Mex>SNCA* males (bottom panel) showing neuronal death (Red fluorescence of cell bodies) compared to control *Mex>GFP* (upper panel). Scale bars read 50 µm at 40x magnification, imaged on a Zeiss LSM 880 confocal microscope. C) 30do CM *Mex>Pex5*-i females do not show brain-wise neuronal cell death, and are comparable control *Mex>w*^{1118} females. Scale bars read 200 µm at 10x magnification, and 100 µm at 20x magnification, imaged on a Zeiss LSM 880 confocal microscope.

An additional observation while staining with tunnel was a smaller brain size in the male *PEX5* gut-KD flies compared to respective controls. A loss of brain mass is characteristic to NDs in humans and other animal models (Raskin et al., 2015), therefore the wide-spread cellular death seen in the *Mex>Pex5*-i brains at an older age may result in the brain shrinking over time. Two dimensions of brain size were measured, from one eyelobe to another (distal to distal), and from top of the brain to bottom (dorsal to ventral); confirming that the *Mex>Pex5*-i males reared at 25 °C and aged to 20do were indeed significantly smaller in size than the respective *Mex>w*^{1118} controls. Distal to distal, *Mex>Pex5-i* (M=647.4 µm, SD=46.91) versus *Mex>w*^{1118} (M=715.4 µm, SD=53.19); t(16)=2.878, *p=0.0109 (Figure 36A). Dorsal to ventral, *Mex>Pex5-i* (M=313.2 µm, SD=31.37) versus *Mex>w*^{1118} (M= 378.5 µm, SD=39.76); t(16)=3.864, **p=0.0014 (Figure 36A). Likewise, these results were recapitulated in *Mex>SNCA* males compared to control *Mex>GFP* males. Distal to distal, *Mex>SNCA* (M=325.9 µm, SD=40.66) versus control *Mex>GFP* (M=435.2 µm, SD=50.19); t(26)=6.334, ****p<0.0001 (Figure 36B). Dorsal to ventral, *Mex>SNCA* (M=158.6 µm, SD=22.31) versus control *Mex>GFP* (M=213.1 µm, SD=26.23); t(26)=5.919, ****p<0.0001 (Figure 36B).

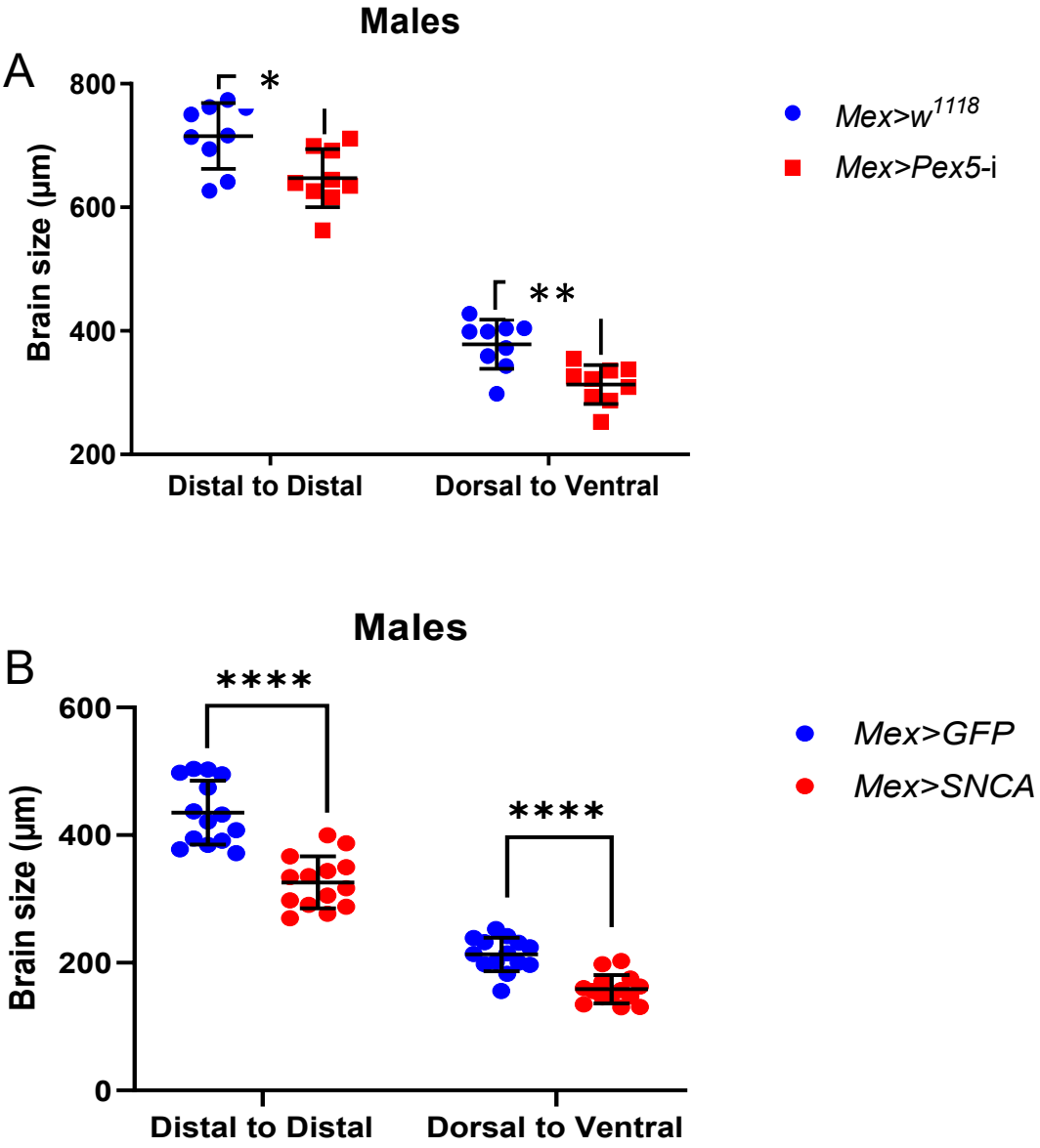

Figure 36. The brain size of CM *Mex>Pex5*-i males is significantly smaller than control males. Two different measurements of brain size (in µm) were considered, measuring from dorsal to ventral (top of brain to bottom) and from distal to distal (eye-lobe to eye-lobe). Statistical analyses was carried out using two-tailed, unpaired Student's t-tests, assuming equal variance and an α=0.05, with an n= 9 brains. A) *Mex>Pex5*-i males has a significantly smaller brain than *Mex>w*^{1118} control males. Measuring distal to distal (*p=0.0109) and dorsal to ventral (**p=0.0014). B) *Mex>SNCA* males had a significantly smaller brain size than control *Mex>GFP* males. Measuring distal to distal (****p<0.0001) and dorsal to ventral (****p<0.0001).

3.2.5 *Mex>Pex5*-i display PAM and PPL1 dopaminergic neuron death/dysfunction

After identifying widespread cellular death in the brains of the male *Mex>Pex5*-i in comparison to age matched *Mex>w*^{1118} males, further investigation of effected neurons specifically looked at Dopaminergic (DA) Protocerebral Anterior Medial (PAM) and Protocerebral posterior lateral 1 (PPL1) neuron clusters, which are part of the locomotor circuits, in the *Drosophila* brain. Using Tyrosine Hydroxylase (TH) to visualize and count PAM and PPL1 clusters, PAM but not PPL1 neurons were significantly less abundant in CM *Mex>Pex5*-i male brains (M=111.9, SD=24.49) than the respective control CM *Mex>w*^{1118} (M=134.6, SD=16.05); t(14)=2.210, *p=0.0443 (Figure 37A). There was no difference between *Mex>Pex5*-i and *Mex>w*^{1118} PPL1 neuron count (t(10)=2.019, p=0.0711 (Figure 37A), nor between *Mex>SNCA* and *Mex>GFP* male PAM (t(16)=0.7569, p=0.4601) or PPL1 (t(14)=0.2119, p=0.8352) (Figure 37B). However, there was a significant decline of TH fluorescent intensity in PPL neurons of *Mex>Pex5*-i males (M= 0.0058, SD=0.0039) compared to *Mex>w*^{1118} males (M=0.0151, SD=0.0051); t(6)=2.882, *p=0.0280 (Figure 38A). There was also a significant decreased fluorescent intensity of PAM neurons of *Mex>Pex5*-i males (M=0.0586, SD=0.0084) compared to *Mex>w*^{1118} males (M=0.1201, SD=0.0302); t(4)=3.396, *p=0.0274 (Figure 38B).

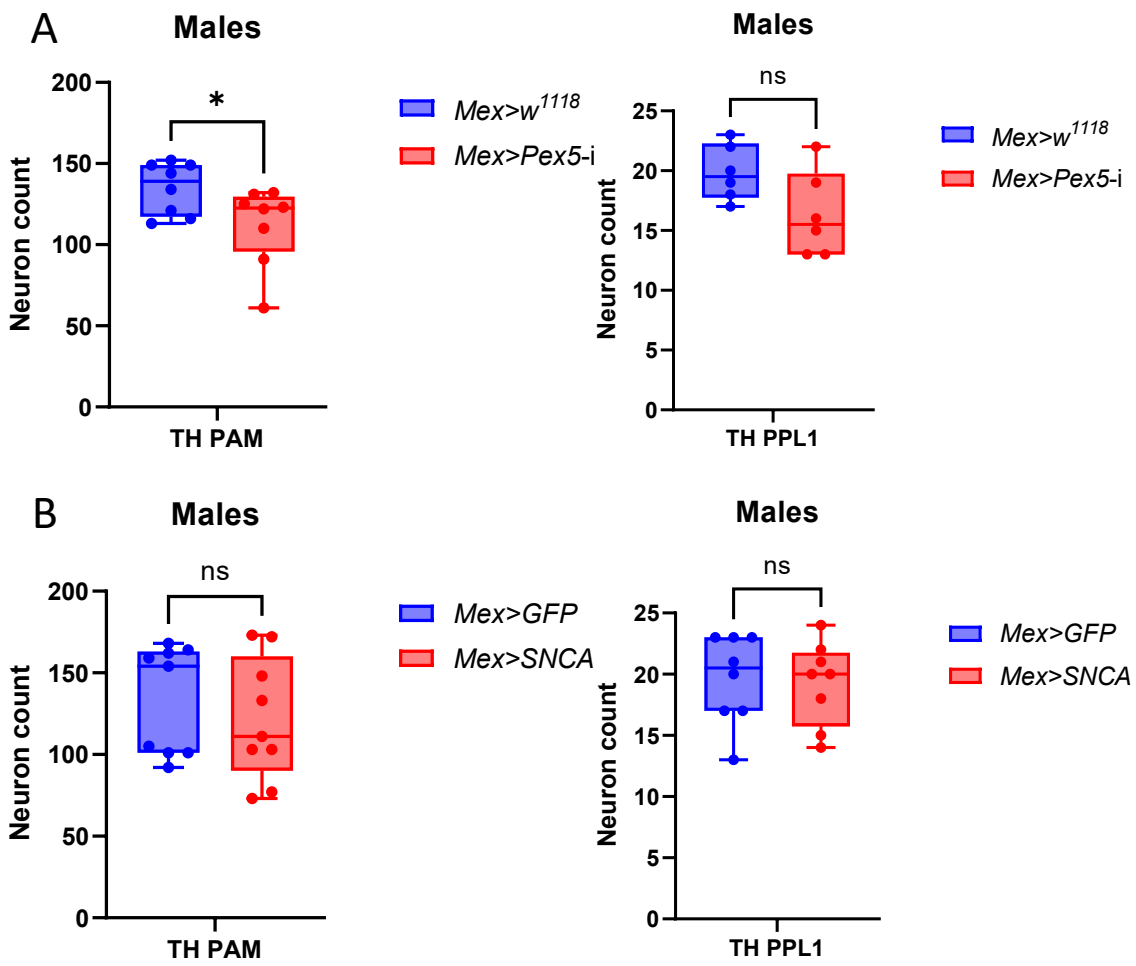

Figure 37. PAM DA neuron in the brains of 30do *Mex>Pex5*-i males are less abundant than in control *Mex>w^{1118}*. All brains were stained with TH to visualize and count of DA neurons (y-axis). A) The DA neuron counts of clusters PAM (n=9) and PPL1 (n=6) in *Mex>Pex5*-i male brains compared to control *Mex>w^{1118}*, were less abundant in the *Mex>Pex5*-i males. PAM neuron count was significantly less in mutants than controls (*p=0.0443), but PPL1 count in *Mex>Pex5*-i males compared to controls, although less abundant too, was not statistically significant. B) The DA neuron counts of clusters PAM (n=9) and PPL1 (n=8) in *Mex>SCNA* males were comparable to control *Mex>GFP*. All statistical analyses were carried out using a two-tailed, unpaired Student's t-test, α=0.05, assuming equal variance and an α=0.05.

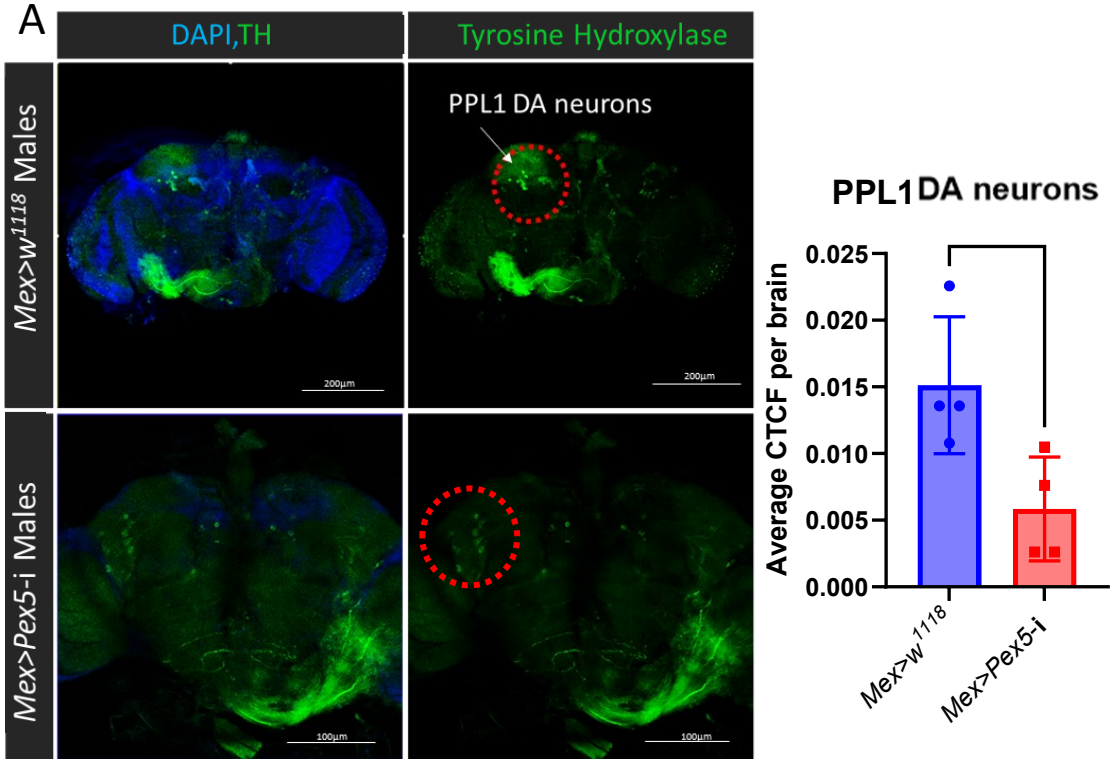
A
DAPI,TH
Tyrosine Hydroxylase
Mex>w1118 Males
Mex>Pex5-i Males
PPL1 DA neurons
200µm
100µm
PPL1 DA neurons
Average CTCF per brain
0.025
0.020
0.015
0.010
0.005
0.000
Mex>w1118
Mex>Pex5-i

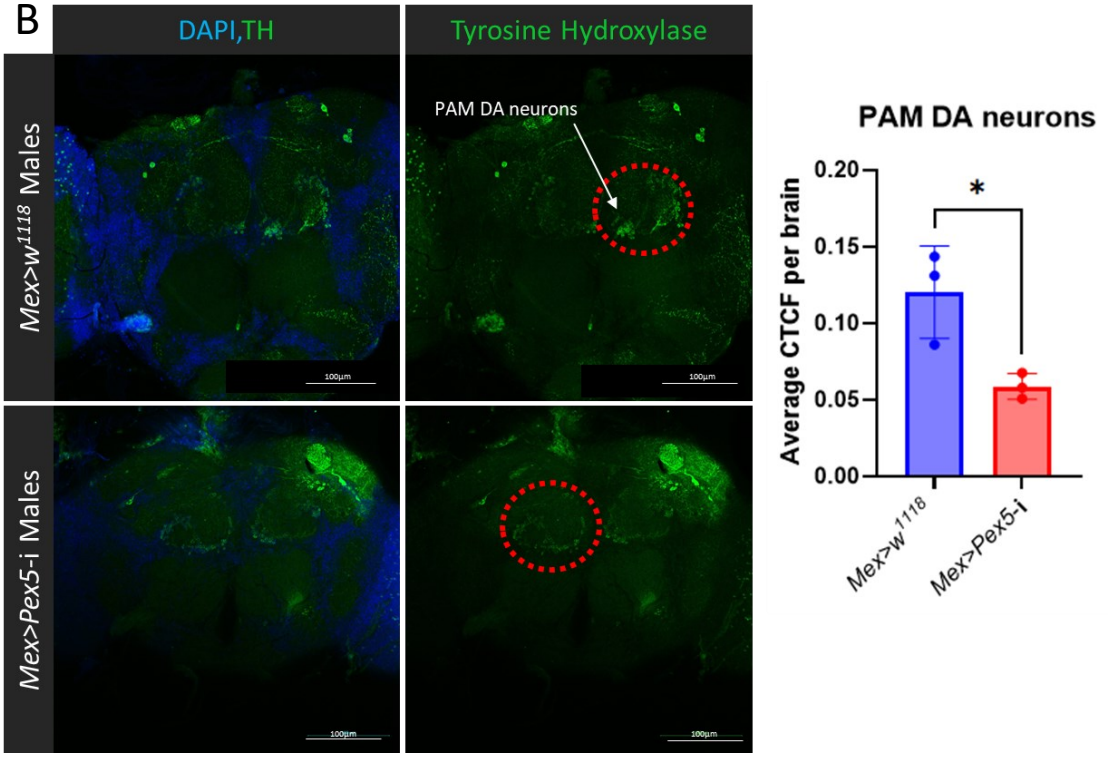
B
DAPI,TH
Tyrosine Hydroxylase
Mex>w1118 Males
Mex>Pex5-i Males
PAM DA neurons
100µm
PAM DA neurons
Average CTCF per brain
0.20
0.15
0.10
0.05
0.00
*
Mex>w1118
Mex>Pex5-i

Figure 38. PAM and PPL1 DA neuron fluorescence in the brains of 30do *Mex>Pex5*-i males is reduced compared to *Mex>w^{1118}* controls. Primary antibody used was anti-TH and secondary antibody Alexa Fluorophore 488 (Green). All images were imaged on a Zeiss LSM 880 confocal microscope at a magnification of 20x with a scale bar of 100 μm, except PPL1 *Mex>w^{1118}* imaged at 10x with a scale bar of 200 μm**.** A) The fluorescent intensity of *Mex>Pex5*-i PPL1 neurons is reduced in visual comparison to controls, outlined by the red-dotted circles. Corrected total cell fluorescence of *Mex>Pex5*-i PPL1 neurons is significantly reduced in quantitative comparison to controls (*p=0.0280), n=4 brains. B) The fluorescent intensity of *Mex>Pex5*-i PAM neurons is reduced in comparison to controls, outlined by the red-dotted circles. Corrected total cell fluorescence of *Mex>Pex5*-i PAM neurons is significantly reduced compared to controls (*p=0.0274), n=3 brains..

3.3 Summary of chapter 3

To demonstrate that the climbing deficit observed in males was a neurophenotype, I quantified established markers of inflammation and neuronal survival in the brains of *Mex>Pex5*-i and respective control. Expression of AMPs/ICs in the heads were quantified using qPCR. A significantly higher AMP *Att* expression was detected in the heads of 20do *Mex>Pex5*-i males compared to the *Mex>w^{1118}* control, indicating a greater inflammatory status on these gut-KD brains. Other markers of inflammation such as oxidative stress were also measured (DHE for ROS detection and H_2O_2 detection in the brains respectively), and showed to be highly accumulated in the brains of *Mex>Pex5*-i males relative to age-matched controls. Together these experiments confirmed inflammation and redox stress in the brain of *Mex>Pex5-i* males. With redox stress comes mitochondrial damage, and indeed increased mitophagy and mitochondria with abnormal cristae were identified in *Mex>Pex5*-i male brains using TEM, compared to controls with almost no mitophagy, or abnormal mitochondrial cristae. TEM findings were further validated by looking at superoxide accumulation within neuronal mitochondria in the *Mex>Pex5*-i male brains using MitoSOX™ staining. Finally neuronal death in the brain was observed in a TUNEL

stain for apoptosis. An increase of inflammation, oxidative stress, and damage of the mitochondria corresponded to a reduction in brain size of the *Mex>Pex5-i* males in parallel to loss of PPL1 and PAM DA neuron signalling. Altogether allowing me to conclude that dysfunction of peroxisomes in intestinal epithelial cells causes remote inflammation in the brain over aging in males, and causes loss of brain matter and loss of DA neurons. These brain defects ultimately affect the locomotion activity of *Mex>Pex5-i* males.

CHAPTER 4: TRANSCRIPTOMIC SCREENING OF THE *DROSOPHILA MEX>PEX5*-i MIDGUT

4.1 *Mip* expression is elevated in the male *Mex>Pex5*-i midgut on CM, and exacerbated on HFD and AX conditions

Knocking down the essential peroxisomal protein PEX5 exclusively in the midgut of *Drosophila melanogaster,* effected locomotor behaviour in aging animals, distally causing accumulation of oxidative stress and wide spread cellular death in the brain. These phenotypes were exacerbated by feeding a high fat diet (HFD) and/or by antibiotic cocktail/axenic treatment (AX). These findings strongly support the idea that peroxisomes are modulators of the diet-microbiota-gut-brain (DMGB) axis communication network that influences the onset of neurodegenerative diseases (NDs). Therefore a transcriptomic screen was carried out to further dissect the mechanism of action in health and disease.

Each transcriptomic complimentary DNA (cDNA) library consisting of biological duplicates of *Mex>Pex5*-i and *Mex>w*^{1118} (males and females combined) in eight different conditions (cornmeal (CM), 5% sucrose, high and low dose *Pseudomonas entomophila*, antibiotic cocktail or axenic (AX), high fat diet (HFD), and AX or HFD with *P.entomophila*). Results of the RNAseq analyses revealed multiple differences in gene expression profiles between *Mex>Pex5-i* and *Mex>w*^{1118} guts. Gene enrichment analyses revealed that a group of gene strongly dysregulated in *Mex>Pex5-i* midguts compared to *Mex>w*^{1118} was represented by neuropeptides and neuropeptide receptors (NPs/NPRs). Considering the importance of neuropeptides in gut-brain communication, I further focused my study on these gene hits.

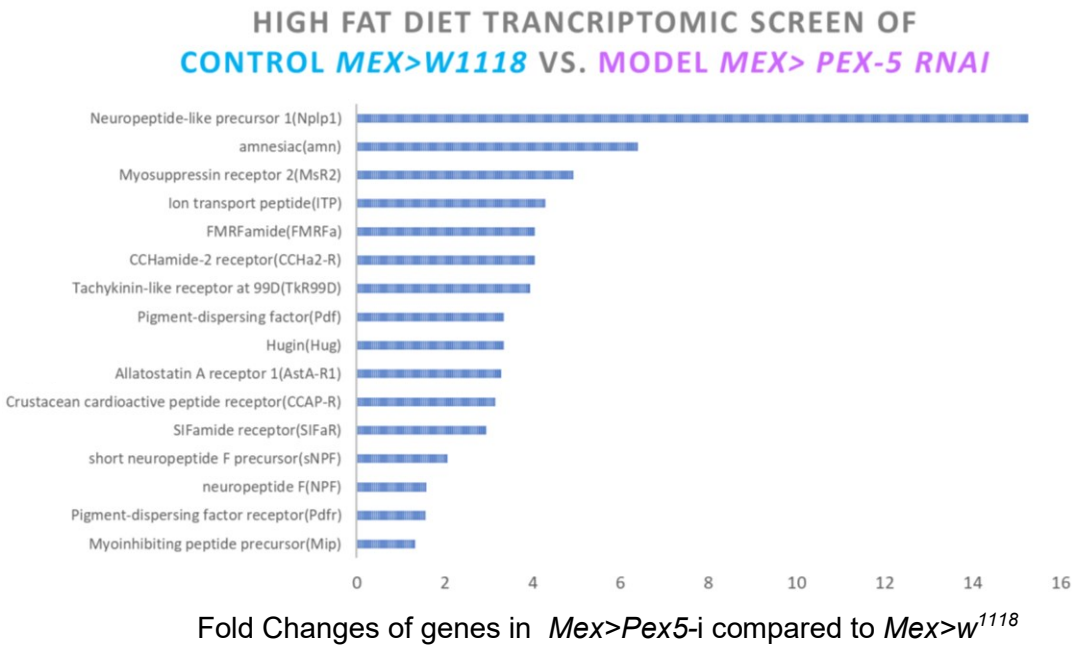

Figure 39. Differential gene expression of NPs/NPRs from the HFD transcriptomic screen enrichment analysis of *Mex>Pex5*-i and *Mex>w^{1118}* of the *Drosophila* midgut.

The identified hits of NPs/NPRs (Figure 39), were then validated in the midguts of mixed male and female samples of *Mex>Pex5*-i and control *Mex>w^{1118}* aged to 7 days old (do) at 29 °C on a CM and HFD diet, (20 guts of 10 males and 10 females per replicate, a minimum of 3 biological replicates per genotype). The following gene hits were tested (using Quantitative Polymerase Chain Reaction, qPCR) according to the results obtained from the transcriptomic screen in HFD condition: Amn (FBgn0086782), AstA (FBgn0015591), AstA-R1 (FBgn0015591), Bursicon (FBgn0038901), CCAP (FBgn0039007), CCAP-R (FBgn0039396), CCHa2 (FBgn0038147), CCHa2-R (FBgn0033058), Dsk (FBgn0000500), FMRFa (FBgn0000715), Ms-R2 (FBgn0264002), NPF (FBgn0027109), PDF-R (FBgn0260753), sNPF (FBgn0032840) , Tk (FBgn0037976) https://flybase.org/ (Supplementary Figure 4).

Gene expression was calculated as reported in Chapter 2 and statistical analyses of the results were carried out using a two-tailed multiple unpaired t-test, assuming equal variance with an $\alpha=0.05$. Comparisons between genotypes were of primary interest (Supplementary Figure 4). The expression of the strongest validated hits, based on results from (Supplementary Figure 4) and the literature (most likely to act within the DMGB axis) included: Amn (Turrel et al., 2020), AstA (Hentze et al., 2015), Bursicon (Scopelliti et al., 2016), CCHa2 (Ren et al., 2015), Dsk (Hentze et al., 2015), and sNPF (S. Lee et al., 2004). These hits were tested in older (30do) flies and in separate sexes reared at 25°C on CM, HFD and AX conditions (Supplementary Figure 5). The reason why the flies were aged to 30do was to test the Negative Geotaxis Climbing Ability (NGCA) of flies at the age where the largest difference between the control and the mutant was observed in the climbing assays. Moreover, since the climbing assays and the brain analyses suggested a stronger effect in *Mex>Pex5*-i males, potential gene hits were tested in separate sexes.

Furthermore, another neuropeptide known as Myo-inhibitory peptide (Mip, FBgn0036713, Hung et al., 2020; Williamson et al., 2001) was chosen for further investigation in accordance with results collected by a former lab member, Julia Kalinowski of the Universität Bonn Germany. Therefore, the initial validation of *Mip* is not present in the supplementary figures. The function of Mip remains unknown, but it has been speculated in *Drosophila* to play roles in sleep circadian in the brain and gut-motility in the gut. Moreover, Mip has been identified as an ortholog of the neuropeptide galanin in mammals that is upregulated in the brain of AD patients (Wraith et al., 2009), therefore it is a strong candidate for the DMGB axis.

Mip was found to be elevated in the midgut whenever there was a locomotor deficit in correspondence, this was observed on a CM diet when comparing expression levels of *Mex>Pex5*-i males (M=0.0061, SD=0.0019), to control *Mex>w*^{1118} male (M=0.00263, SD=0.0005); t=3.0849, *p=0.0368. In 30do *Mex>Pex5*-i males, on a HFD and AX diet, *Mip* was comparably elevated in both genotypes (Figure 40A, Figure 42). This data corresponds to the observed decline of NGCA of the *Mex>w*^{1118} (Figure 14,16, 42A). Interestingly in the females, *Mip* appears to increase within the *Mex>w*^{1118} midgut between CM and HFD and AX conditions, while within the *Mex>Pex5*-i midgut, *Mip* remains the same (Figure 40B), which did not correlate at all with the NGCA of the CM females of *Mex>Pex5*-i (Figure 14, 16).

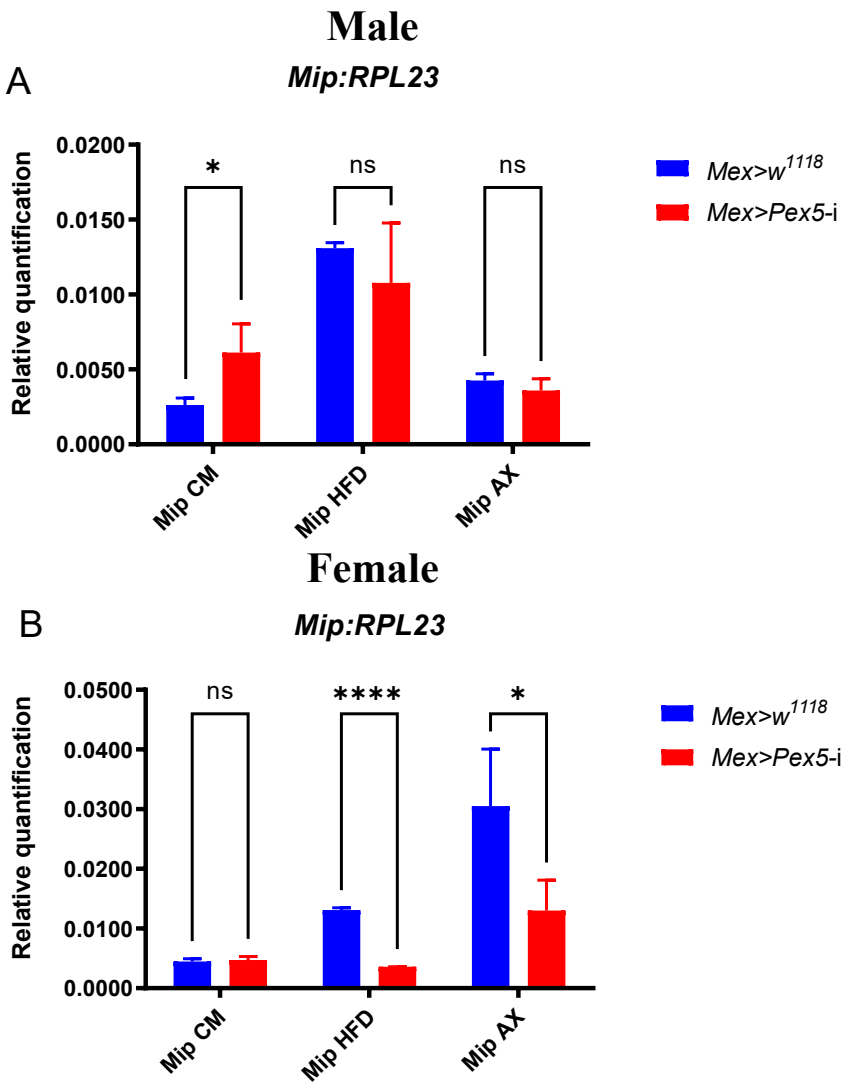

Figure 40. Relative gene expression (quantification) of *Mip* in the midguts of 30do *Drosophila* males and females separaely, using qPCR to validate *Mip* of the HFD transcriptomic screen on CM, HFD and AX conditions. All statistical analyses were carried out using multiple, two-tailed, unpaired t-tests, assuming equal variance with an α=0.05. A) Relative expression of *Mip:RPL23* in males, n=3, between *Mex>Pex5*-i and *Mex>w*^{1118} on CM (t(4)=3.085, *p=0.0368), HFD (t(4)=0.9978, p=0.3750), and AX diets (t(4)=1.287, p=0.2673). B) Relative expression of *Mip:RPL23* in females, n=3, between *Mex>Pex5*-i and *Mex>w*^{1118} on CM (t(4)=0.6655, p=0.5421), HFD (t(4)=44.41, ****p<0.0001), and AX diets (t(4)=2.808, *p=0.048).

When Mip was tested in the midgut of the reference model, male *Mex>SNCA* (M=0.0096, SD= 0.0014) had significantly elevated *Mip* in the midgut compared to control *Mex>GFP* (M=0.00314, SD=0.0009); t(4)=6.785, **p=0.0025) (Figure 41).

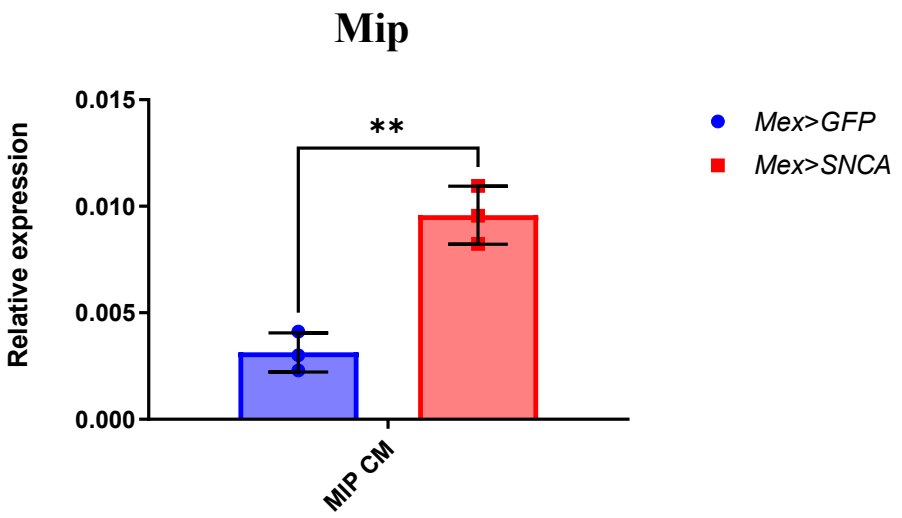

Figure 41: Detection of neuropeptide gene expression in 30do *Mex>SNCA* and control *Mex>GFP Drosophila* from pooled midgut samples extracted from males and females on a CM diet. Statistical tests included an two-tailed unpaired t-test, assuming equal variance with n= 3 replicates of 20 fly guts. Target of interest *Mip* was highly expressed in *Mex>SNCA* compared to control *Mex>GFP* (**p=0.0025).

4.2 *Mip* elevation in the midgut of *Mex>Pex5-i* and *Mex>SNCA* males corresponds to observed pathologies of the brain and behaviour

Mip expression patterns analyzed in flies on CM, HFD and AX correlates with NGCA of male *Mex>Pex5*-i compared to *Mex>w*^{1118} control, where *Mip* expression appears to trend inversely proportional to NGCA of the male flies. For example, at 30do (Figure 40) *Mex>Pex5*-i males on a CM diet expressed a higher expression of *Mip* compared to the controls, corresponding to a drop of NGCA in *Mex>Pex5*-i (~20%) but not controls (~60% climbing success rate) (Figure 42). Likewise, at 30do on a HFD, both the NGCA of *Mex>Pex5*-i and controls were comparable, as well as *Mip* expression,

between the two genotypes. *Mip* expression levels were much higher on HFD than CM, corresponding to the decline of NGCA in both genotypes (Figure 42A). Similarly, at 30do on an AX diet, *Mip* expression was similar between the two genotypes and slightly higher on the AX diet compared to CM, and perfectly correlated to NGCA between both genotypes (~30% climbing success rate) (Figure 42A). When *Mip* expression was tested in *Mex>SNCA,* using midgut RNA samples extracted from males and females, *Mip* was significantly highly expressed at 20do compared to controls, and corresponded to the decline of NGCA in *Mex>SNCA* males at 20do (Figure 42B). The reason why the female *Mex>SNCA* are not compared in (Figure 42B) is because the NGCA of both the males and females on a CM diet were comparable. Therefore, it is assumed that what ever mechanism of action that created a locomotor decline in the males, must be true for the females, until proven otherwise. In subsequent experimentation, separating males and females will be beneficial to rule out an additive effect on the qPCR data, caused by mixing males and females which may express *Mip* in different amounts.

A

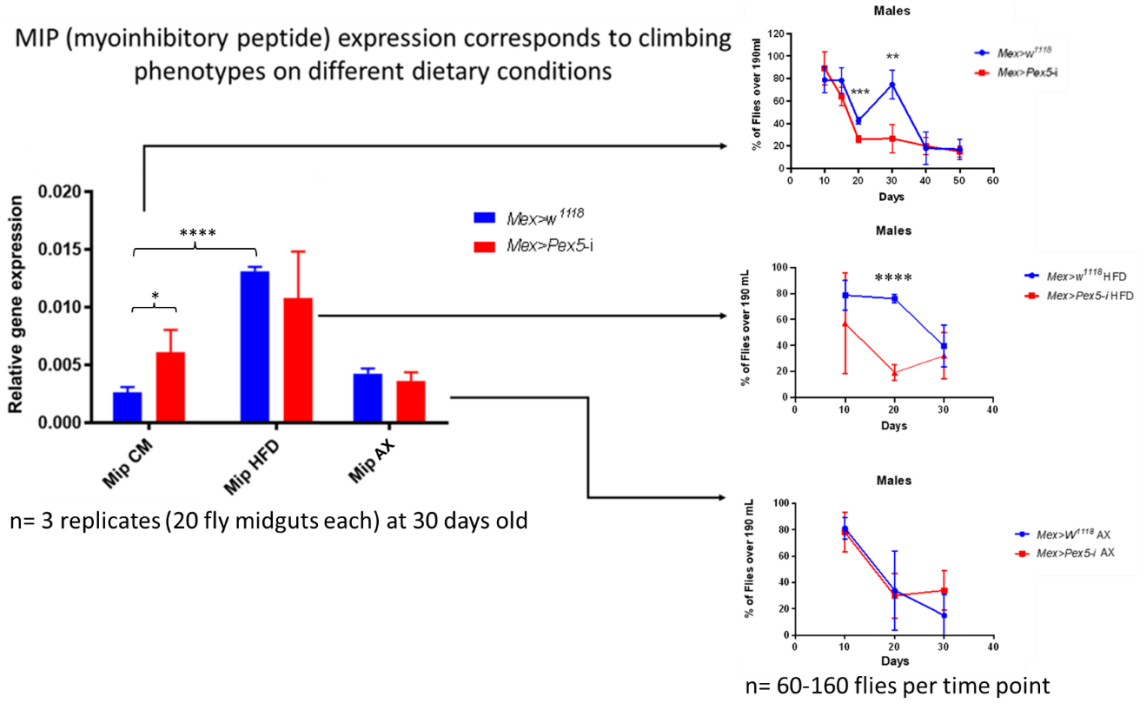

B

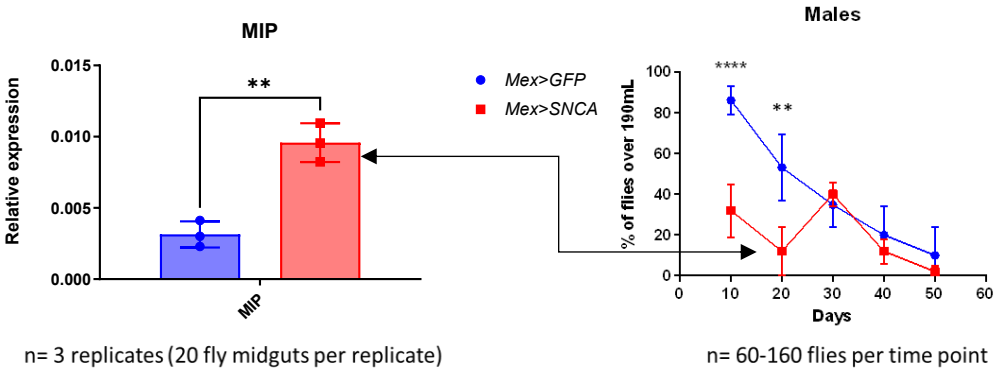

Figure 42: Elevation of Myo-inhibitory peptide gene expression (*Mip*) corresponds to a decreased NGCA. All statistical analyses using two-tailed multiple unpaired t-tests, where based on an α=0.05 and assumed equal variance. A) *Mex>Pex5*-i male midguts at 30do express elevated levels of *Mip* compared to controls *Mex>w*^{1118}, corresponding to the deficit of NGCA seen at 30do in the climbing assays. B). *Mex>SNCA* midguts at 20do express elevated levels of *Mip* compared to controls *Mex>GFP*, corresponding to the deficit of NGCA seen at 20do in the climbing assays.

4.3 Overexpressing *Mip* in the midgut of control *Drosophila* improves male NGCA at an old age

To test whether Mip is neurotoxic, neuroprotective, or a side product of pathological gut-brain communication, I overexpressed *Mip* using a *UAS-Mip* line crossed to the *Mex-GAL4* midgut enterocyte driver, and tested NGCA at 10do, 20do and 30do of age on normal CM conditions; testing both males and females separately (Figure 43). Since *Mex>Mip* is an overexpression model in enterocytes, the respective age and sex matched control were *Mex>GFP.*

At 10do, male *Mex>Mip* (M=75.73%, SD=12.41) NGCA significantly declined by ~17% in comparison to the respective control *Mex>GFP* (M=92.50%, SD=11.62); t(18)=3.121, **p=0.0059 (Figure 43). Between both genotypes there was no difference of NGCA at 20do t(10)=1.018, p=0.3346 however, at 30do there as an improvement of NGCA by *Mex>Mip* (M=57.64%, SD=16.54) in comparison to the respective controls (M=34.48, SD=10.14); t(14)=3.376, **p=0.0045 (Figure 43). At 30do Mip appears to have a neuroprotective effect than the neurotoxic effect seen at 10 days.

On the contrary, the female *Mex>Mip* NGCA was worse than their respective *Mex>GFP* controls at 10, 20, and 30do. At 10do, female NGCA *Mex>Mip* (M=62.65%, SD=10.10) significantly declined by ~15% in comparison to their respective control (M=77.59%, SD=13.20), t(18)=2.844, *p=0.0108 (Figure 43). At 20do NGCA of *Mex>Mip* (M=31.51%, SD=15.59) declined by ~21% compared to the control (M=52.81%, SD=12.57); t(14)=3.008, *p=0.0094 (Figure 43). Finally at 30do, female NGCA *Mex>Mip* (M= 12.52%, SD=15.32) significantly declined by ~15% in comparison to their respective control (M= 34.22%, SD=10.01), t(8)=2.652, *p=0.0210 (Figure 43).

Ultimately, males appeared to improve at 30do with *Mip* overexpression in the enterocytes of the midgut, while females appear to worsen.

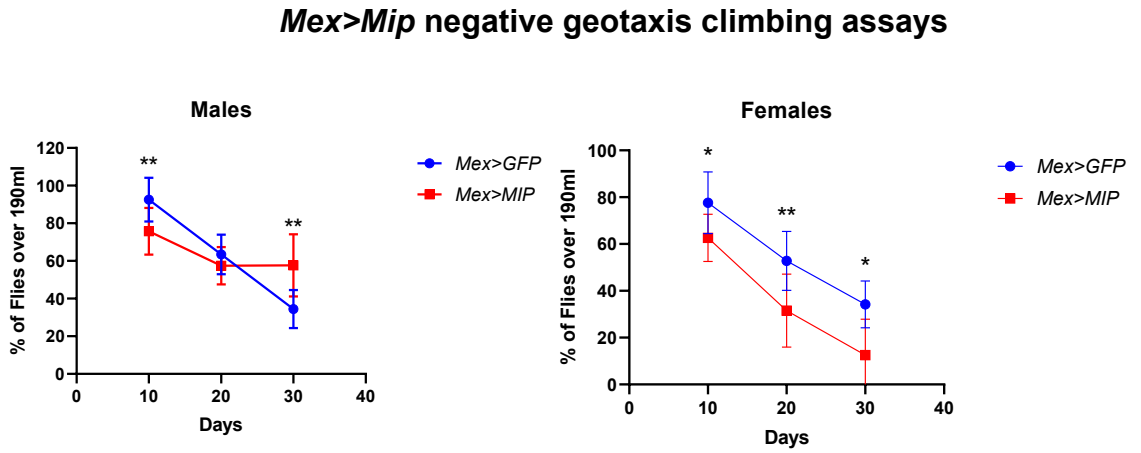

Figure 43. Negative geotaxis climbing assays of *Mex>Mip* in male and female *Drosophila* on CM conditions. A) Male *Mex>Pex5*-i declined of NGCA at 10do (**p=0.0059) compared to the control, while the control at 30do declined of NGCA compared to *Mex>Pex5*-i (**p=0.0045). B) At all three time points, *Mex>Pex5*-i females declined of NGCA compared to controls, 10do (*p=0.0108), 20do (*p=0.0094), and 30do (*p=0.0210).

4.4 Summary of chapter 4

Out of all of the gene hits revealed by our transcriptomic screen of *Mex>Pex5*-i and control *Mex>w*^{1118}, NPs/NPRs emerged as potential peroxisome dependant regulators of the DMGB axis. This is because, gene expression of the identified hits were stronger when the transcriptomic was performed in stressful conditions such as on a HFD. Myo-inhibitory Peptide (Mip) was the neuropeptide that corresponded best with the male climbing assays, and was also upregulated in the same manner on CM conditions in *Mex>SNCA* males compared to *Mex>GFP* controls. When *Mip* was genetically overexpressed in the midgut of control flies, surprisingly the NGCA of the female flies was negatively effected by the overexpression at all time points, while there was no difference of NGCA displayed by the

male until an older age of 30do, where males appeared to climb better than the control. These results conclude that *Mip* in the midgut may be neuroprotective in the males but neurotoxic in the females with dysfunctional midgut peroxisomes. However, subsequent experiments are ongoing to better define the connection between *Mip* expression in the gut of aging *Mex>Pex5*-i and *Mex>SNCA* and the onset of neurodegenerative phenotypes in the brain.

CHAPTER 5: DISCUSSION

5.1 The role of peroxisomes on the gut-brain communication as seen by changes in behaviour, brain pathology, and a transcriptomic screen

Neurodegenerative diseases (NDs) are one of the leading causes of disability and death worldwide that have no cure. These diseases not only impact individual lives, but also heavily affect the health care system, and economy (Aarli et al., 2006; Feigin et al., 2019, 2020; Health, 2022).

Research of NDs has expanded outside of the brain to consider interorgan communications as contributors of pathogenesis and potential aetiologies of NDs. The-Diet-Microbiota-Gut-Brain (DMGB) axis in particular has sparked interest for studying NDs in this light because, the diet, gut-commensals and gut epithelial cells have been identified to interact as a triad; communicating to the brain in a neuroprotective manner (Baxter et al., 2019; Castelli et al., 2021; Custers et al., 2022; Joseph et al., 2017). When protective neurotrophic factors within or secreted by the gut are perturbed, this could affect communication to the brain and lead to the development of NDs. Although this concept has been developed, it has been difficult to identify exactly what is being perturbed in the gut that may drive pathology in the brain, due to the vast metabolic interactome of the triad and to the multiple environmental changes that might affect the triad (Ball et al., 2019; Kim et al., 2021; Kuraishi et al., 2013; Stephens et al., 2018).

Peroxisomes are organelles, which are essential for mediating/modulating complex-lipid and redox metabolism in the intestine and controlling microbiota populations (Di Cara et al., 2018; Klouwer et al., 2015; Smith & Aitchison, 2009, 2013).

Based on this established roles that the peroxisome play in the gut cells, they emerged as major modulators of factors that impact the DMGB axis and, if disturbed, drive NDs. This is a novel and unexplored area of research and during my master degree, I aimed to unravel how peroxisome dysfunctional in gut enterocytes may disrupt neuroprotective communication within the DMGB axis in the context of sporadic NDs.

By using *Drosophila melanogaster* as a highly amenable genetic model for studying human neurological diseases, I knocked-down (KD) peroxisome function in the enterocytes (EC) of the fly's midgut, and then looked at how behaviour changes on different dietary conditions, and when the gut microbiota is eliminated by antibiotic treatments. Additionally, I tested two gut-reference models overexpressing canonical human-mutant-alleles of Alzheimer disease (AD) α-Synuclein (SNCA) and Parkinson disease (PD) β-Secretase (BACE), and assayed these genotypes and under the same dietary conditions. These reference models ultimately aimed to connect previously-studied disease-linked genes of NDs to peroxisome dysfunction in the gut, in light of previous literature implicating the pathogenesis of SNCA and BACE in the gut before the brain in both human and mouse alike (Braak et al., 2003; Brudek, 2019; Q. Chen et al., 2019; Yan et al., 2021). I observed that on normal dietary conditions (cornmeal, CM), the gut-KD alone affected male but not female climbing behaviour (negative geotaxis climbing ability, NGCA). Interestingly, in a study conducted by (Greeve et al., in 2004), male transgenic AD models of *Drosophila* appear to have more amyloid plaque formation in their brains than females. Therefore, males may be more inclined to developing NDs in *Drosophila*, similar to human males being more prone to developing PD. Additionally, considering sexual dimorphisms between male and female *Drosophila,* the behavioural phenotype I

observed may reflect differences between male and female metabolism, especially lipid metabolism in the fly midgut. Implicated from a study looking at the lipid-metabolic sexual dimorphisms of *Drosophila,* male flies appear to metabolize Fatty Acids (FAs) into Triacyl Glycerols (TAGs) more rapidly than females in the midgut (Heier & Kühnlein, 2018), according to the levels of TAGs found in the fly fat-body (adipose tissue equivalent) (De Groef et al., 2021). Peroxisomes are involved in β-oxidation of VLCFAs; when peroxisomes are dysfunctional in the midgut, VLCFAs may accumulate as observed in Peroxisome Biogenesis Disorders (PBDs) (Klouwer et al., 2015; Sellin et al., 2018). Therefore, if male flies are not used to slower metabolism of FAs in the gut like the females, then accumulating VLCFAs from peroxisome dysfunction may be more lipotoxic and overwhelming for male animals; altering gut functions and disrupting the DMGB axis, thus effecting the brain and impacting climbing behaviour. The correlation between accumulation of FAs in the gut and the onset of neurophenotypes, is supported by the fact that there is a decrease in locomotion observed over aging in control flies that are fed a High Fat Diet (HFD).

Specifically the fats that we used to make the HFD were Erucic acid (broccoli oil) which is a monounsaturated VLCFA (22:1ω9) and can only be catabolized by peroxisomes, and coconut oil in high concentrations (made up of Long Chain Fatty Acids, LCFAs) found to reduce *Drosophila* life span and locomotion (Odubanjo et al., 2020). When a HFD was introduced, the male *Mex>Pex5*-i on a HFD and cornmeal (CM) exhibited comparable climbing activity but, HFD females displayed a severe drop of NGCA compared to the CM. This locomotor phenotype in the males suggests that a diet rich in VLCFAs and LCFAs acts in the same way on the DMGB axis as peroxisome

dysfunction in the gut. This hypothesis is also supported by comparing the male control HFD and CM, which show decline in NGCA in old age when gut-metabolism generally begins to wane (Roberts & Rosenberg 2013). This further suggests that with aging, peroxisome function is increasingly important to help prevent mitochondrial dysfunction, and development of NDs.

The dramatic decline of female *Mex>Pex5*-i over aging on a HFD observed at 20 and 30 days, recounts the lipid-metabolic differences identified between males and females on CM conditions, where at 10 days old (do) the females are able to resist the consequences of elevated lipid availability in the gut, but as the fly ages with a *PEX5* gut-KD it cannot. However, unlike males, female controls were severely affected by the HFD from an early age of 10do but, to an even greater extent than the *Mex>Pex5*-i females. This may be due to *Mex>Pex5*-i females having both a slower FAs metabolism and potentially adapting to this metabolism being slowed down further by peroxisomes. Regardless, the females still need further investigation, and the HFD highlights how males and females differ in FAs metabolism in the gut.

Many males also passed-away on the HFD compared to females therefore, males appear to be very sensitive to FAs, and clearance by peroxisomes is essential. Females metabolize general FAs slower and are therefore used to having more FAs in the midgut (Heier & Kühnlein, 2018). So a peroxisome KD will in-turn only effect the females if challenged with excess fat intake (as observed on HFD compared to CM). Ultimately suggesting that peroxisomes in the gut and a high fat diet may impact the DMGB axis in the same metabolic way leading to distal inflammatory signaling that trigger neurodegeneration in the brain. For example, both dysfunctional peroxisomes and high fat

diets are known to induce oxidative stress in the gut and trigger local inflammation which could linked to ND development in the brain from the gut (Di Cara et al., 2018,2019; Reginato et al., 2021; von Frieling et al., 2020). Typically the gut microbiota can help the gut in metabolizing FAs (Custers et al., 2022; Festi et al., 2014), however, a HFD that induces oxidative stress and inflammation in the gut can perturb these important populations, in-turn making the gut more vulnerable to dysplasia, and triggering a shift in DMGB communication which favours neurodegeneration.

By eliminating the gut microbiota, the NGCA of both *Mex>Pex5*-i and *Mex>w*^{1118} males and females declined steeply and acutely beginning at the ages of 10-20 days. The decline of Axenic (AX) *Mex>w*^{1118} males mimic CM *Mex>Pex5*-i males, suggesting that peroxisomal dysfunction can affect the survival of species in the gut microbiota that are positive contributors to the protective signaling of DMGB axis. Moreover, since *Mex>Pex5*-i males on AX versus CM conditions were comparable, this further suggests that the gut commensals are communicating to the brain via peroxisomes. In brief, peroxisomal activity is important to maintain signaling in the DMGB axis that directly impact the gut-brain axis, or that affect the brain via activities of the commensals (Gut-Microbiota-Brain axis) acting upstream of the commensals as demonstrated by the fact that locomotor decline cannot be worsened by eliminating gut-commensals in *Mex>Pex5*-i. Indeed, the peroxisome has been found to modulate commensal populations in *Drosophila* (Di Cara et al., 2018). Particularly, the *PEX5* gut-KD in the CM males impact the *Lactobacilllus* phyla by significantly reducing these species like the AX condition does. *Lactobacilllus* are very important for host behaviour as *Lactobacillus. Brevis* has an identified role in locomotor activity in *Drosophila* (Schretter et al., 2018) Specifically

coordinated behaviour, therefore without *L.Brevis,* according to (Schretter et al., 2018), fly walking speeds are decreased.

However, female CM *Mex>Pex5*-i may have slightly different commensal composition, therefore they do not present the same severe phenotype observed in *Mex>Pex5*-i males. It is possible that they have species that compensates for lost/disturbed populations. The data collected-thus far does not provide the means to make such conclusions therefore, in light of publication, a meta-transcriptomic will be completed in subsequent experiments; allowing us to understand which populations are effected in addition to what metabolites and other factors these microbes may be secreting into the DMGB axis.

Identifying neurotoxic/neuroprotective metabolites such as Short Chain Fatty Acids (SCFAs) in the DMGB axis is one way to begin studying a mechanism of action in neurodegenerative disease development because, both the gut and the gut-commensals secrete a variety of lipid and other metabolites that promote brain health. Niacin (vitamin B3) is one metabolite which has been implicated in both human and *Drosophila* PD studies to improve locomotor behaviour, to maintain gut-epithelial homeostasis and to act as an anti-inflammatory agent in the gut (Jia et al., 2008; Qi et al., 2019; Wakade et al., 2021). In-fact, *Mex>Pex5*-i male guts have extensive dysbiosis which in-turn was correlated to a decline of NGCA, and redox stress in the brain. When the *Mex>Pex5*-i males were treated with niacin (vitamin B3), not only was there an improvement of NGCA, but also a very dramatic decrease of ROS in the brain. These findings suggest that functional peroxisomes may drive the production of important neuroprotective metabolites in the gut, by modulating commensal populations that secrete metabolites such as niacin to prevent

neurodegeneration over aging. Thus, a meta transcriptomic can help us to identify these neuroprotective populations that are effected by peroxisomes. Another method of investigating important peroxisome-linked metabolites and their mechanism of action in the DMGB axis and NDs, is to carry out metabolomic, peptidomic, and lipidomic screens in the midguts, and in *Drosophila* blood (hemolymph) since metabolites in the midgut can be secreted to communicate with the brain, not just via the gut epithelium, but also in an endocrine way via the systemic circulation. These screens were completed in light of publication, but we are still waiting on results. However, hemolymph screens of the reference model *Mex>SNCA* have been completed and we identified that inflammatory ceramides are upregulated in the circulation of the fly, and since *Mex>SNCA* mimics the neurophenotypes observed in aging *Mex>Pex5*-i males, inflammatory ceramides may also be upregulated in the circulation of the *Mex>Pex5*-i males.

Ceramides are known to be pro-inflammatory, and growing evidence suggests that elevation of ceramides in the circulation (metaflammation) of an organism may contribute to NDs like AD in mammalian models (Estes et al., 2021; Jana et al., 2009; Reginato et al., 2021). Likewise, in the *Drosophila*, ceramide accumulation (due to upregulation of ceramide synthase in PEX19 mutant) has been found to impair overall host energy metabolism (over-nutrition/metaflammation) by increasing free fatty acids due to upregulation of ceramide synthase Schlank, in addition to mitochondrial damage in the gut (Sellin et al., 2018). Additionally the severe overexpression of Schlank due to mutating PEX19 globally in the *Drosophila* reduced larval locomotion and caused neurodegeneration. Therefore, considering our findings of gut dysbiosis, neuroinflammation/redox stress/and neuronal death in both *Mex>Pex5*-i and *Mex>SNCA*

males in the gut, *Mex>Pex5*-i and *Mex>SNCA* potentially accumulate inflammatory ceramides leading to metaflammation that drive ND development. A recent study conduced by (Vos et al., 2021), where Schlank was knocked down in a fly PD model for pink1, rescues the flying defects observed in these PD model. Of note, accumulation of ceramides were found by our group also in inflammatory macrophages that have no functional peroxisomes in *Drosophila* (Nath et al., 2022). Moreover, our recent lipidomic analysis on the *Mex>Pex5*-i showed accumulation of various ceramide species in these guts compared to the relative control (data not shown in the thesis).

Considering all of the pathological similarities observed between *Mex>Pex5*-i and *Mex>SNCA* males, we can simply infer that peroxisomes and known disease-linked genes of NDs may share the same mechanism of pathogenesis from the gut; this makes it easier to study a mechanism of action and identify metabolites between the two genotypes to unravel the DMGB axis.

The purpose of the reference models was to compare and connect the effects of peroxisome dysfunction to pathologies of NDs, that may be induced by established human-mutant alleles of NDs in the gut, such as damage to the mitochondria in presence of oligomerizing α-Synuclein mutant proteins. This strategy, could help us to unravel a mechanism or driver of peroxisome-linked DMGB axis neurodegeneration. Since both BACE and SNCA pathological proteins have been identified in the gut to form prion-like fibrils and plaques similar to what is seen in an AD or PD brain, the likelihood that the onset of AD and PD starts in the intestinal tract is a possibility and this study aimed to help to explore this alternative and unexplored mechanism of disease for NDs. We used *Mex>BACE* as a model of AD when *Mex>BACE* males and females on a CM diet were

compared to *Mex>Pex5*-i males and females on a CM diet; both genotypes and sexes show comparable phenotypes in comparison to their respective controls. *Mex>BACE* males exhibit NGCA lower than control and a high mortality rate in the tested population before even reaching 30do. On the other hand, the females did not show a decline of NGCA in respect to control *Mex>GFP,* despite a high mortality in the females at 30do as well. This suggests that peroxisome DMGB axis pathologies correlate with *BACE* DMGB axis pathologies, and share a similar neurodegenerative mechanism of action from the gut; another possibility to explore is whether β-amyloids may be a product of peroxisome dysfunction in the gut.

Both *Mex>GFP* male and female controls, similar to the *Mex>w*^{1118} controls, were effected negatively by the HFD and AX conditions; where both males and females dropped of NGCA. However, the complete opposite occurred in the *Mex>BACE* males on both HFD and AX conditions, where there was a dramatic amelioration of both NGCA at 10do and 20do, comparable to the respective male controls, and survival compared to *Mex>BACE* CM. Only at 30do do the HFD and AX *Mex>BACE* males begin to decline compared to the respective controls. Therefore, I hypothesize that when β-amyloids are abundant in the gut on regular conditions, there is some tertiary factor that males have and females may not have in abundance that is creating plaques and severe dysplasia in the gut of the males. This instability of the gut epithelium is further perturbing commensal populations, to not only eliminate populations that produce neuroprotective lipids (SCFA's) or metabolites but to also promote growth of opportunistic populations that may produce neurotoxic lipids or metabolites. This would explain why eliminating the gut microbiota in *Mex>BACE* males rescues the locomotor phenotype to the same degree as

the respective AX control. With all of this to consider, if *Mex>Pex5*-i was promoting the β-amyloid pathology in the gut, then in theory on HFD or AX conditions, the *PEX5* gut-KD males should have behaved the same as the *BACE* overexpression males. In-fact, the females behaved like *Mex>Pex5*-i females on both CM and HD conditions, however on AX conditions the *Mex>BACE* females were comparable to their respective controls, suggesting that *BACE* may not be effecting the gut microbiota, but lipid metabolism in the gut in the females. In light of all these observation, *Mex>BACE* becomes too convoluted to consider as a reference model, and thus, I decided to focus on the *Mex>SNCA* as means of a positive control for both males and females.

Mex>SNCA males on CM conditions exhibited a NGCA decline similar to the *Mex>Pex5*-i males, but not females; the female *Mex>SNCA* were still used as a positive control. Moreover, the effects of dietary changes on *Mex>SNCA* males and females trended in the same way as observed in *Mex>Pex5*-i males and females. This leaves me with the hypothesis that both genotypes could share the same neuropathological mechanism of action in the DMGB axis. For *SNCA* this mechanism of action is already heavily studied, which may help us to unravel how peroxisome dysfunction may contribute to NDs (PD). This neurodegenerative phenotype was also confirmed in the *Mex>SNCA* males with a second behavioural memory assay, where males on simple CM conditions presented with memory deficits in courtship learning. Although the memory phenotype could not be confirmed in the *Mex>Pex5*-i before the end of the project, there were various other ways I used to confirm the presence of problems in the brains of aging *Mex>Pex5*-i males. I first tested different Anti-Microbial Peptides (AMPs)/ Inflammatory Cytokines (ICs) in the heads of the male and female *Mex>Pex5*-i and respective controls. What I found was that

male *Mex>Pex5*-i flies had more *Attacin* AMP expression in the brain than the respective male controls at 29°C 20do ≈ 30do, and 25°C 20do, but not in the females which is concurrent with the CM locomotor assays. It was very difficult to extract enough RNA from the male heads to test the AMPs, which is why there is a small population tested n=3 biological replicates for each data set and hardly any significance, and why at 25°C 30do no comment can be made because only two of three replicates yielding data for the *Mex>w*^{1118} controls. Therefore, we used other means of assessing inflammation in the brain, such as looking at oxidative stress using Dihydroethidium (DHE), H_2O_2 accumulation, structural abnormalities/cellular death, and increased superoxide accumulation in the mitochondria (using MitoSOX®) of the fly brains of the *Mex>Pex5*-i.

After observing brain-wise tissue apoptosis in both *Mex>Pex5*-i and the reference model *Mex>SNCA* males, I began to look for death and abnormalities of neurons connecting to the mushroom body involved in locomotion (Protocerebral anterior medial (PAM) and Protocerebral posterior lateral 1 neurons (PPL1) dopaminergic (DA) neurons stained with Tyrosine hydroxylase (TH)). What I found was that PAM and PPL1 neurons in the brain of the *Mex>Pex5*-i males are reduced in number, but also fluorescent intensity was reduced, suggesting DA neuron cell death and loss of function. These results were not replicated in the *Mex>SNCA,* however, considering many difficulties while staining for TH particularly with the *Mex>SNCA* males, these experiments will be repeated for further validation.

Overall, the pathologies leading to neurodegeneration in the brain by knocking down *PEX5* in the midgut were akin to those of overexpressing mutant human-ND-linked *SNCA,* further justifying that peroxisomes are important modulators of the DMGB axis and

could even be triggering α-Synuclein peptides to aggregate in the midgut likewise. To begin investigating the mechanism of action, I therefore carried out a transcriptomic screens of the *Mex>Pex5*-i and respective controls' midguts, on different dietary conditions, to better understand which genes in the gut are being dysregulated by peroxisomes and causing a neurodegenerative phenotype in the fly.

5.1.1 The dysregulation of *Mip* in *Mex>Pex5*-i male *Drosophila* midguts corresponds to neurodegenerative phenotypes as seen by the locomotor decline and brain pathology

The most dysregulated genes were observed in the HFD libraries, therefore we chose dysregulated Neuropeptides (NPs) and their Receptors (NPRs) from the enrichment list of differentially expressed genes between the genotypes of interest in HFD condition. Unfortunately, the transcriptomic screens were completed in parallel with the locomotor assays and other experiments to confirm neuroinflammation, oxidative stress, and neuron death in the brains of *Mex>Pex5*-i males. Therefore, the validation of the screens were carried out in samples composed of mixed male and female midguts. The limitation to this was that if one NPs/NPRs was down or upregulated in one sex, that does not necessarily mean that it will be in the other sex, especially considering that we were more interested in the males. With a combination of quantitative PCR validation and information from the literature available for each individual gene hit I selected for validation, I chose five genes to validate in males and female midguts separately on CM, HFD and AX conditions. One neuropeptide stood out above the rest, Myo-inhibitory peptide (Mip).

Mip is known throughout *Drosophila* literature mostly in the brain, effecting satiety, anorexic brain signalling that defines body weight (Min et al., 2016), and is a sleep circadian hormone for both sexes (Oh et al., 2014). In the gut however, not much is known about Mip other than its potential role in gut motility (Williamson et al., 2001), and that it is probably primarily secreted mostly by Enteroendocrine cells (EE) since it is a peptide hormone (Hung et al., 2020). Furthermore, Mips in *Drosophila* have been found to have conservation at the N-terminus to vertebrate neuropeptide galanin (Min et al., 2016), which has been found highly expressed in the frontal lobes of AD patients. Particularly, galanin has been observed to be neuroprotective; for example, eliminating experimental induced autoimmune encephalomyelitis in mouse models (Wraith et al., 2009). Thus, Mip may also be neuroprotective from the gut to the brain in *Drosophila.*

Mip expression patterns at 30do in the males suggested an inversely proportional correlation to NGCA across all three conditions, where elevation of *Mip* meant a decline in climbing ability. Excitingly, the same results were found in 20do CM *Mex>SNCA* midguts (males and females mixed). Therefore, I hypothesized that Mip secreted into the gut, or from the gut into the systemic circulation may be neurotoxic. To confirm this, I overexpressed *Mip* in the midgut of flies, but to my surprise the NGCA of *Mex>Mip* males were slightly, but significantly, worse in climbing than the control at 10do. Interestingly, the NGCA of *Mex>Mip* males at 30do was better than that of the control. Therefore, I hypothesized that perhaps Mip is neuroprotective, like galanin, since *Mex>Mip* males appear to do better as the controls begins to decline at 30do. This hypothesis makes sense, because the more inflammation/oxidative stress occurs in the gut due to perturbing the diet and commensals, the more the fly midgut will try (but fail in our case) to homeostatically

oppose these changes to limit local and collateral damage. If this is true for the males, then future experiments where I will knock down *Mip* in the midgut using RNAi, I may see a decline of NGCA in *Mex>Mip*-i males. Moreover, when *Mip* is upregulated in a *Mex>Pex5*-i fly, a rescue of the negative geotaxis climbing phenotype may occur; in perhaps both males and females *Mip* is KD in the midguts.

If Mip's mechanism of action in the males is similar to the females, then upregulating *Mip* in *Mex>Pex5*-i females may rescue the deficit in negative geotaxis climbing ability observed on HFD and AX conditions. On the other hand, Mip may not be neurotoxic nor neuroprotective, because when the female midguts of *Mex>Pex5*-i were tested for *Mip* on CM, HFD, and AX conditions, only the female *Mex>w*^{1118} controls appeared to have an elevation of this neuropeptide. Therefore, either the females are inhibiting the expression of neuroprotective *Mip*, and that is why we see a decline of NGCA on HFD and AX diets, or Mip may just be a by-product after forming another metabolite which may be neurotoxic. The former hypothesis is the most likely because, when *Mip* expression was tested in the brains of male *Pex5*-i, *Mip* was elevated in comparison to the control (not presented in the thesis).

5.2 Conclusion about *Mip*

Conclusively, it is still unclear how Mip may work in a neuroprotective or neurotoxic manner within or secreted from the fly midgut. Evidence from this study has suggested that Mip does not function alone and is likely highly intertwined with other metabolites that may be sex specific. Moreover, if Mip does not travel to the brain to work on its canonical receptors, then this neuropeptide may work on other receptors which are

yet to be identified in the DMGB axis. To further understand Mip's mechanism of action, the next step is to track Mip as a peptide. Therefore in light of publication and for subsequent experimentation, a GFP fused Mip fly construct was made, whereby expressing *GFP-Mip* under the *Mex-Gal4* midgut driver will allow us to visualize how Mip may be either remaining in the gut to carry out its function from there, or entering systemic circulation to directly target the brain. Additionally, as previously mentioned, the peptidomic screens of the *Mex>Pex5*-i hemolymph can also tell us if Mip is being secreted into the circulation and communicate with the brain in an endocrine fashion. These screens will also help us to unravel other important peptides, along with metabolites from the metabolomic screens, that work alongside Mip, modulated by peroxisomes, to influence DMGB axis communication and NDs.

5.3 Limitations of the study

During the course of my thesis, I encountered several road-blocks which made it difficult to obtain enough data in an efficient manner, having to repeatedly optimize experiments to match the quality of previously published protocols. One of the main issues was the variability within the negative geotaxis climbing assays, where each genotype and sex, despite being assayed together with controls on the same day, still displayed concerning variability. One reason for the high biological variability may have been because not all of the conditions in the room were controlled. The main controls were temperature, apparatus placement, and lighting. One thing I could not control would have been atmospheric pressure, where on rainier and muggier days I anecdotally observed, as also previously published, that both the mutant and control flies performed poorly in

climbing ability compared to a nicer and drier day (Adonyeva et al., 2021). I believe that it is better to see variability and build up statistical power with more replicates than to control the environment too much, and dampen ecological validity. Lab conditions that are too controlled may not yield data representative of a true population/ biological mechanism of action. The variability we see with the flies is simply due to the spectrum of how each individual organism tolerates the induced KD or overexpression of genes in their midguts. The fact in the matter is that, if there is truly an effect of a gut specific *PEX5* KD, and *SNCA* and *BACE* overexpression on the brain, then a difference will be observed between mutants and controls regardless of subtle changes in environment.

Another limitation was considered after countless attempts of trying to optimize TH and TUNEL stains for visualizing DA neurons and neuronal death. I found that mutant brains (such as *Mex>Pex5*-i) stained much better than controls. Therefore, I predicted that the Blood Brain Barrier (BBB)-equivalent of the *Drosophila* may be more permeable in the *Mex>Pex5*-i brains than controls. Indicating that by perturbing gut metabolism via peroxisomes or mitochondria in the gut (via SNCA aggregates), these disturbances somehow are effecting the brains ability to protect itself from external stressors, such as inflammatory mediators, via the BBB. One way to check if the BBB equivalent of the *Drosophila* brain is weaker in the mutants, is by injecting dye into the heads of the flies and live-imaging the penetration of the dye into the brains parenchyma (Pinsonneault et al., 2011). Or, stain the brain with an antibody anti-Repo and TUNEL to observe death of the BBB, where Repo is an excellent antibody that targets glial cells, which the *Drosophila* BBB is primarily composed of. Moreover, what could have helped me to identify death in the brains better would have been a brain-only positive control, unlike the gut-only positive

control of *SNCA* overexpression. This brain-only control would express *BACE* under a tissue specific driver for whole-brain neuropil known as *Elav-Gal4, Elav>BACE,* published as causing atrophy of the *Drosophila* brain (Chakraborty et al., 2011). Additionally, to better visualize and understand DA neuron cellular death patterns, I could have used *DOP2R-Gal4* driver (for dopaminergic neurons in the *Drosophila* brain), to drive the expression of tetanus toxin (*UAS-TNT*) and death of DA neurons as a positive control for the TH immunofluorescence (Min et al., 2016). Therefore, in light of future publication, as a reference model of death in the brain, I will consider using the aforementioned models to help identify and confirm future experiments looking for neuronal death in my *Drosophila* models.

As for what is mediating this potential weakening of the BBB, it could be any of the neuropeptide hits identified during this study, such as *Mip*. Which is why we constructed a GFP-tagged Mip fly line, since there is no antibody for Mip, in order to overexpress Mip in the midgut and then track where it is going and acting. Moreover, the pending results of the other -omic screens, especially the peptidomic of the haemolymph, can tell us whether Mip may be entering the systemic circulation or not. Regardless, knowing the cellular origin of Mip, or any of our genetic, or future metabolic/lipid hits, is essential to begin unraveling a mechanism of action to identify the aetiologies which induce a target cell to produce or stop producing said hit. For example, the *Mex-Gal4* driver is midgut enterocyte specific, and enteroendocrine cells (EE) are known to produce and secrete the hormones and other mediators of communication, potentially our neuropeptide hits more than ECs, in the midgut of the fly (Hung et al., 2020). Therefore, we would have

to shift our gaze to focus on EE cells. Or, how the EC influence juxtacrine signaling of EE, since there is no EE specific driver of the midgut.

5.5 Conclusion and future directions

In conclusion, my three main objectives satisfied my hypothesis, that peroxisomes are important modulators of the DMGB axis in the context of NDs.

1. I found that simply knocking down peroxisome function in the midgut, mimicked the locomotor deficits (neurodegenerative disease-like symptom) of a control fly exposed to an overwhelming amount of dietary lipids (HFD), or total loss of gut commensal bacteria (AX). Recapitulating that peroxisomes play a major role in gut-lipid metabolism and gut microbiota maintenance, and that perturbing these interactions of the peroxisomes reaps detrimental consequences on neuronal survival and behaviour in and of the brain.
2. Next, I found that these behavioural deficits were indeed neuronal, by identifying inflammation, redox and neuronal death of the *Drosophila* brain in correspondence to a decreased climbing ability.
3. Finally, a transcriptomic screen has showed that NPs/NPRs, major communication mediators between the gut and the brain, are also dysregulated. Further confirming that peroxisome dysfunction in the gut hinders gut-brain communication.

The *Drosophila melanogaster* has been an invaluable model for testing my hypothesis. However, I have barely scratched the surface as to how peroxisomes in the gut

modulate development of NDs through the DMGB axis, and therefore for my future directions I will be focusing on unraveling the mechanism of action for Mip, and potentially other identified NPs/NPRs validated throughout my thesis. Including analysis of the completed metabolomic, peptidomic, and lipidomic screens, and a meta transcriptomic on the horizon, I will also manipulate the concentrations of identified hits from these screens (metabolites or commensals), like I did with niacin, to try and rescue the neurophenotypes observed in the *Mex>Pex5*-i males or induce neurodegenerative phenotypes in a wild type fly. Furthermore, since the female flies remain elusive, with meta-analysis between all -omic screens I aim to further understand how a mechanism of action for Mip identified in males might effect females.

The next step after that would be to try and translate what was observed in the *Drosophila* to humans or other mammalian animal models close to humans. All in hopes of unraveling a peroxisome-dependant mechanism of action of the DMGB axis that will help enlighten the future for better detection and treatment options and even manufacturing a cure to NDs.

Bibliography

Adonyeva, N. V., Menshanov, P. N., & Gruntenko, N. (2021). A Link between Atmospheric Pressure and Fertility of *Drosophila* Laboratory Strains Natalya. MDPI, 1–7.

Alberts, B., Johnson, A., Lewis, J., Raff, M., Roberts, K., & Walter, P. (2002). Molecular biology of the cell (4th ed.). Garland Science. Available from: https://www.ncbi.nlm.nih.gov/books/NBK26882/.

Ali, S. A., Begum, T., & Reza, F. (2018). Hormonal Influences on Cognitive Function. The Malaysian journal of medical sciences: MJMS, 25(4), 31–41. https://doi.org/10.21315/mjms2018.25.4.3

Anwal, L. (2021). a Comprehensive Review on Alzheimer's Disease. World Journal of Pharmacy and Pharmaceutical Sciences, 10(7), 1170. https://doi.org/10.20959/wjpps20217-19427

Aarli, J. A., Dua, T., Janca, A., & Muscetta, A. (2006). Neurological Disorders, public health challenges. Archives of Neurology, 54(7), 1–232. https://doi.org/10.1001/archneur.1997.00550190066016

Armutcu, F. (2019). Organ crosstalk: the potent roles of inflammation and fibrotic changes in the course of organ interactions. Inflammation research : official journal of the European Histamine Research Society ... [et al.], 68(10), 825–839. https://doi.org/10.1007/s00011-019-01271-7.

Arora, S., & Ligoxygakis, P. (2020). Beyond Host Defense: Deregulation of *Drosophila* Immunity and Age-Dependent Neurodegeneration. Frontiers in Immunology, 11(July), 1–13. https://doi.org/10.3389/fimmu.2020.01574

Ashraf, G., Greig, N., Khan, T., Hassan, I., Tabrez, S., Shakil, S., Sheikh, I., Zaidi, S., Akram, M., Jabir, N., Firoz, C., Naeem, A., Alhazza, I., Damanhouri, G., & Kamal, M. (2014). Protein Misfolding and Aggregation in Alzheimer's Disease and Type 2 Diabetes Mellitus. CNS & Neurological Disorders - Drug Targets, 13(7), 1280–1293. https://doi.org/10.2174/1871527313666140917095514

Atamna, H., Tenore, A., Lui, F., & Dhahbi, J. M. (2018). Organ reserve, excess metabolic capacity, and aging. Biogerontology, 19(2), 171–184. https://doi.org/10.1007/s10522-018-9746-8.

Badinloo, M., Nguyen, E., Suh, W., Alzahrani, F., Castellanos, J., Klichko, V. I., Orr, W. C., & Radyuk, S. N. (2018). Overexpression of antimicrobial peptides contributes to aging through cytotoxic effects in *Drosophila* tissues. Archives of insect biochemistry and physiology, 98(4), e21464. https://doi.org/10.1002/arch.21464

Bălaşa, A. F., Chircov, C., & Grumezescu, A. M. (2020). Body fluid biomarkers for alzheimer's disease-an up-to-date overview. Biomedicines, 8(10), 1–21. https://doi.org/10.3390/biomedicines8100421

Ball, N., Teo, W. P., Chandra, S., & Chapman, J. (2019). Parkinson's disease and the environment. Frontiers in Neurology, 10(March). https://doi.org/10.3389/fneur.2019.00218

Baron, M. N., Klinger, C. M., Rachubinski, R. A., & Simmonds, A. J. (2016). A Systematic Cell-Based Analysis of Localization of Predicted *Drosophila* Peroxisomal Proteins. Traffic, 17(5), 536–553. https://doi.org/10.1111/tra.12384

Baxter, N. T., Schmidt, A. W., Venkataraman, A., Kim, K. S., Waldron, C., & Schmidt, T. M. (2019). Dynamics of human gut microbiota and short-chain fatty acids in response to dietary interventions with three fermentable fibers. MBio, 10(1), 1–13. https://doi.org/10.1128/mBio.02566-18

Bekris, Kl. M., Yu, C.-E., Bird, T. D., & Tsuang, D. W. (2021). Genetics of Alzheimer's disease. Wiener Medizinische Wochenschrift, 171(11–12), 249–256. https://doi.org/10.1007/s10354-021-00819-9

Bendor, J. T., Logan, T. P., & Edwards, R. H. (2013). The function of α-synuclein. Neuron, 79(6), 1044–1066. https://doi.org/10.1016/j.neuron.2013.09.004

Berding, K., Vlckova, K., Marx, W., Schellekens, H., Stanton, C., Clarke, G., Jacka, F., Dinan, T. G., & Cryan, J. F. (2021). Diet and the Microbiota-Gut-Brain Axis: Sowing the Seeds of Good Mental Health. Advances in Nutrition, 12(4), 1239–1285. https://doi.org/10.1093/advances/nmaa181

Biddinger, J. E., & Fox, E. A. (2014). Reduced intestinal brain-derived neurotrophic factor increases vagal sensory innervation of the intestine and enhances satiation. Journal of Neuroscience, 34(31), 10379–10393. https://doi.org/10.1523/JNEUROSCI.1042-14.2014

Bodine, S. C., Brooks, H. L., Bunnett, N. W., Coller, H. A., Frey, M. R., Joe, B., Kleyman, T. R., Lindsey, M. L., Marette, A., Morty, R. E., Ramírez, J. M., Thomsen, M. B., & Yosten, G. (2021). An American Physiological Society cross-journal Call for Papers on "Inter-Organ Communication in Homeostasis and Disease". American journal of physiology. Lung cellular and molecular physiology, 321(1), L42–L49. https://doi.org/10.1152/ajplung.00209.202.

Botero, V., Stanhope, B. A., Brown, E. B., Grenci, E. C., Boto, T., Park, S. J., King, L. B., Murphy, K. R., Colodner, K. J., Walker, J. A., Keene, A. C., Ja, W. W., & Tomchik, S. M. (2021). Neurofibromin regulates metabolic rate via neuronal mechanisms in *Drosophila*. Nature Communications, 12(1), 1–13. https://doi.org/10.1038/s41467-021-24505-x

Braak, H., Del Tredici, K., Rüb, U., De Vos, R. A. I., Jansen Steur, E. N. H., & Braak, E. (2003). Staging of brain pathology related to sporadic Parkinson's disease. Neurobiology of Aging, 24(2), 197–211. https://doi.org/10.1016/S0197-4580(02)00065-9

Brand, A. H., & Perrimon, N. (1993). Targeted gene expression as a means of altering cell fates and generating dominant phenotypes. Development (Cambridge, England), 118(2), 401–415. https://doi.org/10.1242/dev.118.2.401

Breit, S., Kupferberg, A., Rogler, G., & Hasler, G. (2018). Vagus nerve as modulator of the brain-gut axis in psychiatric and inflammatory disorders. Frontiers in Psychiatry, 9(MAR). https://doi.org/10.3389/fpsyt.2018.00044

Brudek, T. (2019). Inflammatory Bowel Diseases and Parkinson's Disease. Journal of Parkinson's Disease, 9(s2), S331–S344. https://doi.org/10.3233/JPD-191729

Calon, F., Lim, G. P., Yang, F., Morihara, T., Teter, B., Ubeda, O., Rostaing, P., Triller, A., Jr., N. S., Ashe, K. H., Frautschy, S. A., & Cole, G. M. (2004). Docosahexaenoic Acid Protects from Dendritic Pathology in an Alzheimer's Disease Mouse Model. 43(5), 633–645. https://doi.org/DOI: 10.1177/026010600601800307

Campos-Acuña, J., Elgueta, D., & Pacheco, R. (2019). T-cell-driven inflammation as a mediator of the gut-brain axis involved in Parkinson's disease. Frontiers in Immunology, 10(FEB), 1–14. https://doi.org/10.3389/fimmu.2019.00239

Cao, Y., Chtarbanova, S., Petersen, A. J., & Ganetzky, B. (2013). Dnr1 mutations cause neurodegeneration in *Drosophila* by activating the innate immune response in the brain. Proceedings of the National Academy of Sciences of the United States of America, 110(19). https://doi.org/10.1073/pnas.1306220110

Capo, F., Wilson, A., & Di Cara, F. (2019). The intestine of *Drosophila melanogaster:* An emerging versatile model system to study intestinal epithelial homeostasis and host-microbial interactions in humans. Microorganisms, 7(9). https://doi.org/10.3390/microorganisms7090336

Carabotti, M., Scirocco, A., Maselli, M. A., & Severi, C. (2015). The gut-brain axis: Interactions between enteric microbiota, central and enteric nervous systems. Annals of Gastroenterology, 28(2), 203–209.

Cassim, J., Kolkman, F., & Helmer, M. (2018). *Drosophila* models for human diseases. In Advances in Experimental Medicine and Biology (Vol. 1076).

Castelli, V., Angelo, M., & Quintiliani, M. (2021). The emerging role of probiotics in neurodegenerative diseases : new hope for Parkinson ' s disease ? 16(4), 628–634.

Cena, H., & Calder, P. C. (2020). Defining a Healthy Diet : Evidence for the Role of. Nutrients, 12(334), 1–15. https://www.ncbi.nlm.nih.gov/pmc/articles/PMC7071223/pdf/nutrients-12-00334.pdf

Chakraborty, R., Vepuri, V., Mhatre, S. D., Paddock, B. E., Miller, S., Michelson, S. J., Delvadia, R., Desai, A., Vinokur, M., Melicharek, D. J., Utreja, S., Khandelwal, P., Ansaloni, S., Goldstein, L. E., Moir, R. D., Lee, J. C., Tabb, L. P., Saunders, A. J., & Marenda, D. R. (2011). Characterization of a *Drosophila* Alzheimer's disease model: Pharmacological rescue of cognitive defects. PLoS ONE, 6(6). https://doi.org/10.1371/journal.pone.0020799

Chalazonitis, A., & Rao, M. (2018). Enteric nervous system manifestations of neurodegenerative disease. Brain research, 1693(Pt B), 207–213. https://doi.org/10.1016/j.brainres.2018.01.011

Challis, C., Hori, A., Sampson, T. R., Yoo, B. B., Challis, R. C., Hamilton, A. M., Mazmanian, S. K., Volpicelli-Daley, L. A., & Gradinaru, V. (2020). Gut-seeded α-synuclein fibrils promote gut dysfunction and brain pathology specifically in aged mice. Nature Neuroscience, 23(3), 327–336. https://doi.org/10.1038/s41593-020-0589-7

Chen, C., Zhou, Y., Wang, H., Alam, A., Kang, S. S., Ahn, E. H., Liu, X., Jia, J., & Ye, K. (2021). Gut inflammation triggers C/EBPβ/δ-secretase-dependent gut-to-brain propagation of Aβ and Tau fibrils in Alzheimer's disease. The EMBO journal, 40(17), e106320. https://doi.org/10.15252/embj.2020106320.

Chen, H., Meng, L., & Shen, L. (2022). Multiple roles of short-chain fatty acids in Alzheimer disease. Nutrition, 93, 111499. https://doi.org/10.1016/j.nut.2021.111499

Chen, Q. Q., Haikal, C., Li, W., & Li, J. Y. (2019). Gut Inflammation in Association With Pathogenesis of Parkinson's Disease. Frontiers in Molecular Neuroscience, 12(September), 1–13. https://doi.org/10.3389/fnmol.2019.00218

Chen, S. G., Stribinskis, V., Rane, M. J., Demuth, D. R., Gozal, E., Roberts, A. M., Jagadapillai, R., Liu, R., Choe, K., Shivakumar, B., Son, F., Jin, S., Kerber, R., Adame, A., Masliah, E., & Friedland, R. P. (2016). Exposure to the Functional Bacterial Amyloid Protein Curli Enhances Alpha-Synuclein Aggregation in Aged Fischer 344 Rats and Caenorhabditis elegans. Scientific reports, 6, 34477. https://doi.org/10.1038/srep34477

Cipolla, C. M., & Lodhi, I. J. (2017). Peroxisomal Dysfunction in Age-Related Diseases Cynthia. Trends in Endocrinology and Metabolism, 28(4), 297–308. https://doi.org/doi:10.1016/j.tem.2016.12.003

Clancy, B. (2013). 乳鼠心肌提取 HHS Public Access. International Journal of Molecular Sciences, 14(11), 22274–22330. https://doi.org/10.1177/0963721415622634.Developmental

Console, L., Scalise, M., Giangregorio, N., Tonazzi, A., Barile, M., & Indiveri, C. (2020). The Link Between the Mitochondrial Fatty Acid Oxidation Derangement and Kidney Injury. *Frontiers in Physiology*, *11*(July), 1–7. https://doi.org/10.3389/fphys.2020.00794

Costa, V., Giacomello, M., Hudec, R., Lopreiato, R., Ermak, G., Lim, D., Malorni, W., Davies, K. J. A., Carafoli, E., & Scorrano, L. (2010). Mitochondrial fission and cristae disruption increase the response of cell models of Huntington's disease to apoptotic stimuli. EMBO Molecular Medicine, 2(12), 490–503. https://doi.org/10.1002/emmm.201000102

Custers, Emma, E. M., Kiliaan, & Amanda, J. (2022). Dietary lipids from body to brain. Progress in Lipid Research, 85(September 2021), 101144. https://doi.org/10.1016/j.plipres.2021.101144

Da Costa, R. Q. M., de Gobbi Porto, F. H., & Paysano Marrocos, R. (2013). Dissociation of depression from apathy in traumatic brain injury: A case report. Dementia e Neuropsychologia, 7(3), 312–315. https://doi.org/10.1590/s1980-57642013dn70300014

Daubner, S. C., Le, T., & Wang, S. (2011). Tyrosine hydroxylase and regulation of dopamine synthesis. Archives of biochemistry and biophysics, 508(1), 1–12. https://doi.org/10.1016/j.abb.2010.12.017

De Groef, S., Wilms, T., Balmand, S., Calevro, F., & Callaerts, P. (2021). Sexual Dimorphism in Metabolic Responses to Western Diet in *Drosophila* melanogaster. Biomolecules, 12(1), 33. https://doi.org/10.3390/biom12010033.

de Wouters d'Oplinter, A., Rastelli, M., Van Hul, M., Delzenne, N. M., Cani, P. D., & Everard, A. (2021). Gut microbes participate in food preference alterations during obesity. Gut Microbes, 13(1), 1959242. https://doi.org/10.1080/19490976.2021.1959242

Derkinderen, P., Rolli-Derkinderen, M., Chapelet, G., Neunlist, M., & Noble, W. (2021). Tau in the gut, does it really matter?. Journal of neurochemistry, 158(2), 94–104. https://doi.org/10.1111/jnc.15320.

Devos, D., Lebouvier, T., Lardeux, B., Biraud, M., Rouaud, T., Pouclet, H., Coron, E., Bruley des Varannes, S., Naveilhan, P., Nguyen, J. M., Neunlist, M., & Derkinderen, P. (2013). Colonic inflammation in Parkinson's disease. Neurobiology of disease, 50, 42–48. https://doi.org/10.1016/j.nbd.2012.09.007.

Di Cara, F. (2020). Peroxisomes in host defense. PLoS Pathogens, 16(7), 1–10. https://doi.org/10.1371/journal.ppat.1008636

Di Cara, F., Andreoletti, P., Trompier, D., Vejux, A., Bülow, M. H., Sellin, J., Lizard, G., Cherkaoui-Malki, M., & Savary, S. (2019). Peroxisomes in immune response and inflammation. International Journal of Molecular Sciences, 20(16), 1–29. https://doi.org/10.3390/ijms20163877

Di Cara, F., Bülow, M. H., Simmonds, A. J., & Rachubinski, R. A. (2018). Dysfunctional peroxisomes compromise gut structure and host defense by increased cell death and Tor-dependent autophagy. Molecular Biology of the Cell, 29(22), 2766–2783. https://doi.org/10.1091/mbc.E18-07-0434

Di Cara, F., Sheshachalam, A., Braverman, N. E., Rachubinski, R. A., & Simmonds, A. J. (2017). Peroxisome-Mediated Metabolism Is Required for Immune Response to Microbial Infection. Immunity, 47(1), 93–106.e7. https://doi.org/10.1016/j.immuni.2017.06.016

Dinan, T. G., & Cryan, J. F. (2017). Gut instincts: microbiota as a key regulator of brain development, ageing and neurodegeneration. Journal of Physiology, 595(2), 489–503. https://doi.org/10.1113/JP273106

Dinicolantonio, J. J., & Keefe, J. H. O. (2020). The Importance of Marine Omega-3s for Brain. 12, 1–15. https://doi:10.3390/nu12082333

Diop, S. B., Birse, R. T., & Bodmer, R. (2017). High fat diet feeding and high throughput triacylglyceride assay in *Drosophila* Melanogaster. Journal of Visualized Experiments, 2017(127), 1–7. https://doi.org/10.3791/56029

Dorsey, E. R., Sherer, T., Okun, M. S., & Bloemd, B. R. (2018). The emerging evidence of the Parkinson pandemic. Journal of Parkinson's Disease, 8(s1), S3–S8. https://doi.org/10.3233/JPD-181474

Douglas, A. E. (2018). The *Drosophila* model for microbiome research. Physiology & Behavior, 47(6), 157–164. https://doi.org/doi:10.1038/s41684-018-0065-0

Durães, F., Pinto, M., & Sousa, E. (2018). Old drugs as new treatments for neurodegenerative diseases. Pharmaceuticals, 11(2), 1–21. https://doi.org/10.3390/ph11020044

Estes, R. E., Lin, B., Khera, A., & Davis, M. Y. (2021). Lipid Metabolism Influence on Neurodegenerative Disease Progression: Is the Vehicle as Important as the Cargo? Frontiers in Molecular Neuroscience, 14(December), 1–15. https://doi.org/10.3389/fnmol.2021.788695

Family Resource. (2021). How home care helps seniors with neurological disorders: FRHC. Family Resource Home Care. Retrieved from: https://www.familyresourcehomecare.com/how-home-care-helps-seniors-with-neurological-disorders/

Faustini, G., Bono, F., Valerio, A., Pizzi, M., Spano, P., & Bellucci, A. (2017). Mitochondria and α-synuclein: Friends or foes in the pathogenesis of Parkinson's disease? Genes, 8(12), 1–9. https://doi.org/10.3390/genes8120377

Feany, M. B., & Bender, W. W. (2000). A *Drosophila* model of Parkinson's disease. Nature, 404(6776), 394–398. https://doi.org/10.1038/35006074

Feigin, V. L., Nichols, E., Alam, T., Bannick, M. S., Beghi, E., Blake, N., Culpepper, W. J., Dorsey, E. R., Elbaz, A., Ellenbogen, R. G., Fisher, J. L., Fitzmaurice, C., Giussani, G., Glennie, L., James, S. L., Johnson, C. O., Kassebaum, N. J., Logroscino, G., Marin, B., … Vos, T. (2019). Global, regional, and national burden of neurological disorders, 1990–2016: a systematic analysis for the Global Burden of Disease Study 2016. The Lancet Neurology, 18(5), 459–480. https://doi.org/10.1016/S1474-4422(18)30499-X

Feigin, V. L., Vos, T., Nichols, E., Owolabi, M. O., Carroll, W. M., Dichgans, M., Deuschl, G., Parmar, P., Brainin, M., & Murray, C. (2020). The global burden of neurological disorders: translating evidence into policy. The Lancet Neurology, 19(3), 255–265. https://doi.org/10.1016/S1474-4422(19)30411-9

Fink, M., Callol-Massot, C., Chu, A., Ruiz-Lozano, P., Izpisua Belmonte, J. C., Giles, W., Bodmer, R., & Ocorr, K. (2009). A new method for detection and quantification of heartbeat parameters in *Drosophila*, zebrafish, and embryonic mouse hearts. BioTechniques, 46(2), 101–113. https://doi.org/10.2144/000113078

Fernández-Moreno, M. A., Farr, C. L., Kaguni, L. S., & Garesse, R. (2007). *Drosophila melanogaster* as a Model System to Study Mitochondrial Biology. 372, 33–49. https://doi.org/10.1007/978-1-59745-365-3

Friedman, J. R., & Nunnari, J. (2014). Mitochondrial form and function. Nature, 505(7483), 335–343. https://doi.org/10.1038/nature12985

Garden, G. A., & Spada, A. R. La. (2012). HSS Public Access. Neuron, 73(15), 886–901. https://doi.org/10.1016/j.neuron.2012.02.017.Intercellular

Givon, L. E., Lazar, A. A., & Yeh, C. H. (2017). Generating executable models of the *Drosophila* central complex. Frontiers in Behavioral Neuroscience, 11. https://doi.org/10.3389/fnbeh.2017.00102

Greeve, I., Kretzschmar, D., Tschäpe, J. A., Beyn, A., Brellinger, C., Schweizer, M., Nitsch, R. M., & Reifegerste, R. (2004). Age-Dependent Neurodegeneration and Alzheimer-Amyloid Plaque Formation in Transgenic *Drosophila*. Journal of Neuroscience, 24(16), 3899–3906. https://doi.org/10.1523/JNEUROSCI.0283-04.2004

Grochowska, M., Laskus, T., & Radkowski, M. (2019). Gut Microbiota in Neurological Disorders. Archivum Immunologiae et Therapiae Experimentalis, 67(6), 375–383. https://doi.org/10.1007/s00005-019-00561-6

Guest, P. C. (2019). Reviews on Biomarker Studies in Psychiatric and Neurodegenerative Disorders. In Reviews on Biomarker Studies in Psychiatric and Neurodegenerative Disorders (Vol. 1118). http://link.springer.com/10.1007/978-3-030-05542-4

Hakansson, A., & Molin, G. (2011). Gut microbiota and inflammation. Nutrients, 3(6), 637–687. https://doi.org/10.3390/nu3060637

Hampel, H., Hardy, J., Blennow, K., Chen, C., Perry, G., Kim, S. H., Villemagne, V. L., Aisen, P., Vendruscolo, M., Iwatsubo, T., Masters, C. L., Cho, M., Lannfelt, L., Cummings, J. L., & Vergallo, A. (2021). The Amyloid-β Pathway in Alzheimer's Disease. Molecular Psychiatry, 26(10), 5481–5503. https://doi.org/10.1038/s41380-021-01249-0

Hawkes, C. H., Del Tredici, K., & Braak, H. (2010). A timeline for Parkinson's disease. Parkinsonism & related disorders, 16(2), 79–84. https://doi.org/10.1016/j.parkreldis.2009.08.007.

Health, G. (2022). Global, regional, and national burden of diseases and injuries for adults 70 years and older: systematic analysis for the Global Burden of Disease 2019 Study. BMJ (Clinical Research Ed.), 376, e068208. https://doi.org/10.1136/bmj-2021-068208

Hebbar, S., Knust, E., Thibault, G., & Kraut, R. S. (2019). Editorial: Connections to Membrane Trafficking Where You Least Expect Them: Diseases, Dynamics, Diet and Distance. Frontiers in Cell and Developmental Biology, 7(December), 6–8. https://doi.org/10.3389/fcell.2019.00327

Heier, C., & Kühnlein, R. P. (2018). Triacylglycerol Metabolism in *Drosophila melanogaster*. Genetics, 210(4), 1163–1184. https://doi.org/10.1534/genetics.118.301583.

Held. (2017). Deep homology? : uncanny similarities of humans and flies uncovered by evo-devo. Cambridge University Press.

Hentze, J. L., Carlsson, M. A., Kondo, S., Nässel, D. R., & Rewitz, K. F. (2015). The neuropeptide allatostatin a regulates metabolism and feeding decisions in *Drosophila*. *Scientific Reports*, *5*, 1–16. https://doi.org/10.1038/srep11680

Hetz, C., & Saxena, S. (2017). ER stress and the unfolded protein response in neurodegeneration. Nature reviews. Neurology, 13(8), 477–491. https://doi.org/10.1038/nrneurol.2017.99

Hiebler, S., Masuda, T., Hacia, J. G., Moser, A. B., Faust, P. L., Liu, A., Chowdhury, N., Huang, N., Lauer, A., Bennett, J., Watkins, P. A., Zack, D. J., Braverman, N. E., Raymond, G. V., & Steinberg, S. J. (2014). The Pex1-G844D mouse: a model for mild human Zellweger spectrum disorder. Molecular genetics and metabolism, 111(4), 522–532. https://doi.org/10.1016/j.ymgme.2014.01.008.

Hoffmann J. A. (2003). The immune response of *Drosophila*. Nature, 426(6962), 33–38. https://doi.org/10.1038/nature02021

Hoffmann, J. A., & Reichhart, J. M. (2002). *Drosophila* innate immunity: an evolutionary perspective. Nature immunology, 3(2), 121–126. https://doi.org/10.1038/ni0202-121

Huang, K., Miao, T., Chang, K., Kim, J., Kang, P., Jiang, Q., Simmonds, A. J., Di Cara, F., & Bai, H. (2020). Impaired peroxisomal import in *Drosophila* oenocytes causes cardiac dysfunction by inducing upd3 as a peroxikine. Nature Communications, 11(1). https://doi.org/10.1038/s41467-020-16781-w

Huang, Y., Wang, G., Rowe, D., Wang, Y., Kwok, J. B. J., Xiao, Q., Mastaglia, F., Liu, J., Chen, S. Di, & Halliday, G. (2015). SNCA gene, but not MAPT, influences onset age of Parkinson's disease in Chinese and Australians. BioMed Research International, 2015. https://doi.org/10.1155/2015/135674

Hung, R. J., Hu, Y., Kirchner, R., Liu, Y., Xu, C., Comjean, A., Tattikota, S. G., Li, F., Song, W., Sui, S. H., & Perrimon, N. (2020). A cell atlas of the adult *Drosophila* midgut. Proceedings of the National Academy of Sciences of the United States of America, 117(3), 1514–1523. https://doi.org/10.1073/pnas.1916820117

Jahn, R. G. (2019). Introduction. The Role of Consciousness in the Physical World, 1–5. https://doi.org/10.4324/9780429314384-1

Jackson, D. N., & Theiss, A. L. (2020). Gut bacteria signaling to mitochondria in intestinal inflammation and cancer. Gut microbes, 11(3), 285–304. https://doi.org/10.1080/19490976.2019.1592421

Jana, A., Hogan, E. L., & Pahan, K. (2009). Ceramide and neurodegeneration: Susceptibility of neurons and oligodendrocytes to cell damage and death. J Neurol Sci, 15(278(1-2)), 5–15. https://doi.org/doi:10.1016/j.jns.2008.12.010

Jeibmann, A., & Paulus, W. (2009). *Drosophila melanogaster* as a model organism of brain diseases. International Journal of Molecular Sciences, 10(2), 407–440. https://doi.org/10.3390/ijms10020407

Jia, H., Li, X., Gao, H., Feng, Z., Li, X., Zhao, L., Jia, X., Zhang, H., & Liu, J. (2008). High doses of nicotinamide prevent oxidative mitochondrial dysfunction in a cellular model and improve motor deficit in a *Drosophila* model of Parkinson's disease. Journal of neuroscience research, 86(9), 2083–2090. https://doi.org/10.1002/jnr.21650.

Jiang, H., Patel, P. H., Kohlmaier, A., Grenley, M. O., McEwen, D. G., & Edgar, B. A. (2009). Cytokine/Jak/Stat signaling mediates regeneration and homeostasis in the *Drosophila* midgut. Cell, 137(7), 1343–1355. https://doi.org/10.1016/j.cell.2009.05.014

Jin, B., Qu, Y., Zhang, L., & Gao, Z. (2020). Diagnosing Parkinson Disease Through Facial Expression Recognition: Video Analysis. Journal of medical Internet research, 22(7), e18697. https://doi.org/10.2196/18697.

Joseph, J., Cole, G., Head, E., & Ingram, D. (2009). Nutrition, brain aging, and neurodegeneration. Journal of Neuroscience, 29(41), 12795–12801. https://doi.org/10.1523/JNEUROSCI.3520-09.2009

Joseph, J., Depp, C., Shih, P. A. B., Cadenhead, K. S., & Schmid-Schönbein, G. (2017). Modified mediterranean diet for enrichment of short chain fatty acids: Potential adjunctive therapeutic to target immune and metabolic dysfunction in schizophrenia? Frontiers in Neuroscience, 11(MAR), 1–16. https://doi.org/10.3389/fnins.2017.00155

Ju, Y. E. S., McLeland, J. s., Toedebusch, C. D., Xiong, C., Fagan, A. M., Duntley, S. P., Morris, J. C., & Holtzman, D. M. (2013). Sleep quality and preclinical Alzheimer Disease. JAMA Neurology, 70(5), 587–593. https://doi.org/10.1001/jamaneurol.2013.2334.Sleep

Kametani, F., & Hasegawa, M. (2018). Reconsideration of amyloid hypothesis and tau hypothesis in Alzheimer's disease. Frontiers in Neuroscience, 12(JAN). https://doi.org/10.3389/fnins.2018.00025

Kamp, F., Exner, N., Lutz, A. K., Wender, N., Hegermann, J., Brunner, B., Nuscher, B., Bartels, T., Giese, A., Beyer, K., Eimer, S., Winklhofer, K. F., & Haass, C. (2010). Inhibition of mitochondrial fusion by α-synuclein is rescued by PINK1, Parkin and DJ-1. EMBO Journal, 29(20), 3571–3589. https://doi.org/10.1038/emboj.2010.223

Katzenberger, R. J., Loewen, C. A., Wassarman, D. R., Petersen, A. J., Ganetzky, B., & Wassarman, D. A. (2013). A *Drosophila* model of closed head traumatic brain injury. Proceedings of the National Academy of Sciences of the United States of America, 110(44). https://doi.org/10.1073/pnas.1316895110

Kenmoku, H., Hori, A., Kuraishi, T., & Kurata, S. (2017). A novel mode of induction of the humoral innate immune response in *Drosophila* larvae. Disease models & mechanisms, 10(3), 271–281. https://doi.org/10.1242/dmm.027102.

Khan, M., Singh, J., Gilg, A. G., Uto, T., & Singh, I. (2010). Very long-chain fatty acid accumulation causes lipotoxic response via 5-lipoxygenase in cerebral adrenoleukodystrophy. Journal of lipid research, 51(7), 1685–1695. https://doi.org/10.1194/jlr.M002329.

Killinger, B. A., Melki, R., Brundin, P., & Kordower, J. H. (2019). Endogenous alpha-synuclein monomers, oligomers and resulting pathology: let's talk about the lipids in the room. Npj Parkinson's Disease, 5(1), 37–40. https://doi.org/10.1038/s41531-019-0095-3

Kim, H. Y., Huang, B. X., & Spector, A. A. (2014). Phosphatidylserine in the Brain: Metabolism and Function. Progress in Lipid Research, 1–18. https://doi.org/10.1016/j.plipres.2014.06.002.Phosphatidylserine

Kitani-Morii, F., Friedland, R. P., Yoshida, H., & Mizuno, T. (2021). *Drosophila* as a Model for Microbiota Studies of Neurodegeneration. Journal of Alzheimer's Disease, 84(2), 479–490. https://doi.org/10.3233/JAD-215031

Klouwer, F. C. C., Berendse, K., Ferdinandusse, S., Wanders, R. J. A., Engelen, M., & Poll-The, B. T. (2015). Zellweger spectrum disorders: Clinical overview and management approach Inherited metabolic diseases. Orphanet Journal of Rare Diseases, 10(1), 1–11. https://doi.org/10.1186/s13023-015-0368-9

Koemans, T. S., Oppitz, C., Donders, R. A. T., Van Bokhoven, H., Schenck, A., Keleman, K., & Kramer, J. M. (2017). *Drosophila* courtship conditioning as a measure of learning and memory. Journal of Visualized Experiments, 2017(124), 1–11. https://doi.org/10.3791/55808

Komleva, Y., Chernykh, A., Lopatina, O., Gorina, Y., Lokteva, I., Salmina, A., & Gollasch, M. (2021). Inflamm-Aging and Brain Insulin Resistance: New Insights and Role of Life-style Strategies on Cognitive and Social Determinants in Aging and Neurodegeneration. Frontiers in Neuroscience, 14(January), 1–17. https://doi.org/10.3389/fnins.2020.618395

Kou, J., Kovacs, G. G., Höftberger, R., Kulik, W., Brodde, A., Forss-Petter, S., Hönigschnabl, S., Gleiss, A., Brügger, B., Wanders, R., Just, W., Budka, H., Jungwirth, S., Fischer, P., & Berger, J. (2011). Peroxisomal alterations in Alzheimer's disease. Acta Neuropathologica, 122(3), 271–283. https://doi.org/10.1007/s00401-011-0836-9

Kounatidis, I., Chtarbanova, S., Cao, Y., Hayne, M., Jayanth, D., Ganetzky, B., & Ligoxygakis, P. (2017). NF-κB Immunity in the Brain Determines Fly Lifespan in Healthy Aging and Age-Related Neurodegeneration. Cell Reports, 19(4), 836–848. https://doi.org/10.1016/j.celrep.2017.04.007

Kowalski, K., Mulak, A., & Words, K. (2019). Brain-Gut-Microbiota Axis in Alzheimer's Disease. 25(1). https://doi.org/10.5056/jnm18087

Kuczynski, B., & Reo, N. V. (2006). Evidence that plasmalogen is protective against oxidative stress in the rat brain. Neurochemical Research, 31(5), 639–656. https://doi.org/10.1007/s11064-006-9061-7

Kurek, K., Łukaszuk, B., Piotrowska, D. M., Wiesiołek, P., Chabowska, A. M., & Zendzian-Piotrowska, M. (2013). Metabolism, physiological role, and clinical implications of sphingolipids in gastrointestinal tract. BioMed research international, 2013, 908907. https://doi.org/10.1155/2013/908907

Lee, M. J., Park, S. H., Han, J. H., Hong, Y. K., Hwang, S., Lee, S., Kim, D., Han, S. Y., Kim, E. S., & Cho, K. S. (2011). The effects of hempseed meal intake and linoleic acid on *Drosophila* models of neurodegenerative diseases and hypercholesterolemia. Molecules and cells, 31(4), 337–342. https://doi.org/10.1007/s10059-011-0042-6

Lee, K. S., You, K. H., Choo, J. K., Han, Y. M., & Yu, K. (2004). *Drosophila* short neuropeptide F regulates food intake and body size. The Journal of biological chemistry, 279(49), 50781–50789. https://doi.org/10.1074/jbc.M407842200

Letters, S. (2013). Endocrinología y nutrición. 60(1), 37–39.

Levenson, R. W., Sturm, V. E., & Haase, C. M. (2014). Emotional and behavioral symptoms in neurodegenerative disease: a model for studying the neural bases of psychopathology. Annual review of clinical psychology, 10, 581–606. https://doi.org/10.1146/annurev-clinpsy-032813-153653.

Li, N. M., Liu, K. F., Qiu, Y. J., Zhang, H. H., Nakanishi, H., & Qing, H. (2019). Mutations of beta-amyloid precursor protein alter the consequence of Alzheimer's disease pathogenesis. Neural Regeneration Research, 14(4), 658–665. https://doi.org/10.4103/1673-5374.247469

Li, Y., Sun, H., Chen, Z., Xu, H., Bu, G., & Zheng, H. (2016). Implications of GABAergic neurotransmission in Alzheimer's disease. Frontiers in Aging Neuroscience, 8(FEB), 1–12. https://doi.org/10.3389/fnagi.2016.00031

Liu S. (2018). Neurotrophic factors in enteric physiology and pathophysiology. Neurogastroenterology and motility : the official journal of the European Gastrointestinal Motility Society, 30(10), e13446. https://doi.org/10.1111/nmo.13446

Liu, Q., & Zhang, J. (2014). Lipid metabolism in Alzheimer's disease. Neuroscience Bulletin, 30(2), 331–345. https://doi.org/10.1007/s12264-013-1410-3

Loučanová, E., Kalamárová, M., & Parobek, J. (2015). Potencial clusters identification for wood-processing enterprises in Slovakia. Wood Processing and Furniture Manufacturing Challenges on the World Market and Wood-Based Energy Goes Global - Proceedings of Scientific Papers, 121–125. https://doi.org/10.1146/annurev-clinpsy-032813-153653.Emotional

Lu, B., & Vogel, H. (2009). *Drosophila* models of neurodegenerative diseases. Annual Review of Pathology: Mechanisms of Disease, 4, 315–342. https://doi.org/10.1146/annurev.pathol.3.121806.151529

Lye, S. H., & Chtarbanova, S. (2018). *Drosophila* as a model to study brain innate immunity in health and disease. International Journal of Molecular Sciences, 19(12). https://doi.org/10.3390/ijms19123922

Ma, Q., Xing, C., Long, W., Wang, H. Y., Liu, Q., & Wang, R. F. (2019). Impact of microbiota on central nervous system and neurological diseases: The gut-brain axis. Journal of Neuroinflammation, 16(1), 1–14. https://doi.org/10.1186/s12974-019-1434-3

Madabattula, S. T., Strautman, J. C., Bysice, A. M., O'Sullivan, J. A., Androschuk, A., Rosenfelt, C., Doucet, K., Rouleau, G., & Bolduc, F. (2015). Quantitative analysis of climbing defects in a *Drosophila* model of neurodegenerative disorders. Journal of Visualized Experiments, 2015(100), 1–9. https://doi.org/10.3791/52741

Marra, A., Hanson, M. A., Kondo, S., Erkosar, B., & Lemaitre, B. (2021). *Drosophila* Antimicrobial Peptides and Lysozymes Regulate Gut Microbiota Composition and Abundance. MBio, 12(4), 1–16. https://doi.org/10.1128/mBio.00824-21

Martin, C. A., & Krantz, D. E. (2014). *Drosophila* melanogaster as a genetic model system to study neurotransmitter transporters. Neurochem Int, 73, 71–88. https://doi.org/doi:10.1016/j.neuint.2014.03.015

Mast, F. D., Li, J., Virk, M. K., Hughes, S. C., Simmonds, A. J., & Rachubinski, R. A. (2011). A *Drosophila* model for the Zellweger spectrum of peroxisome biogenesis disorders. Disease models & mechanisms, 4(5), 659–672. https://doi.org/10.1242/dmm.007419.

Mattson, M. P. (2005). Dietary modulation of lipid rafts: Implications for disease prevention and treatment. Membrane Microdomain Signaling: Lipid Rafts in Biology and Medicine, 191–201. https://doi.org/10.1385/1-59259-803-X:191

Mayfeild. (2010). Parkinson ' s Disease. 27(1), 1–5. https://doi.org/MayfeildClinic.com

McEvoy, C. T., Guyer, H., Langa, K. M., & Yaffe, K. (2017). Neuroprotective diets are associated with better cognitive function: the Health and Retirement Study. 65(8), 1857–1862. https://doi.org/doi:10.1111/jgs.14922.

McHugh, D., & Gil, J. (2018). Senescence and aging: Causes, consequences, and therapeutic avenues. The Journal of cell biology, 217(1), 65–77. https://doi.org/10.1083/jcb.201708092

Mertsalmi, T. H., Pekkonen, E., & Scheperjans, F. (2020). Antibiotic exposure and risk of Parkinson's disease in Finland: A nationwide case-control study. Movement Disorders, 35(3), 431–442. https://doi.org/10.1002/mds.27924

Mielke, M. M. (2018). Sex and Gender Differences in Alzheimer's Disease Dementia. Sex and Gender Differences in Alzheimer's Disease, 35(11), 14–77. https://doi.org/10.1016/B978-0-12-819344-0.09983-X

Min, S., Chae, H. S., Jang, Y. H., Choi, S., Lee, S., Jeong, Y. T., Jones, W. D., Moon, S. J., Kim, Y. J., & Chung, J. (2016). Identification of a peptidergic pathway critical to satiety responses in *Drosophila*. Current Biology, 26(6), 814–820. https://doi.org/10.1016/j.cub.2016.01.029

Mohandas, E., Rajmohan, V., & Raghunath, B. (2009). Neurobiology of Alzheimer's disease. Indian journal of psychiatry, 51(1), 55–61. https://doi.org/10.4103/0019-5545.44908

Moisan, F., Kab, S., Mohamed, F., Canonico, M., Le Guern, M., Quintin, C., Carcaillon, L., Nicolau, J., Duport, N., Singh-Manoux, A., Boussac-Zarebska, M., & Elbaz, A. (2016). Parkinson disease male-to-female ratios increase with age: French nationwide study and meta-analysis. Journal of Neurology, Neurosurgery and Psychiatry, 87(9), 952–957. https://doi.org/10.1136/jnnp-2015-312283

Moloney, R. D., Johnson, A. C., O'Mahony, S. M., Dinan, T. G., Greenwood-Van Meerveld, B., & Cryan, J. F. (2016). Stress and the Microbiota-Gut-Brain Axis in Visceral PaRelevance to Irritable Bowel Syndrome. CNS Neuroscience and Therapeutics, 22(2), 102–117. https://doi.org/10.1111/cns.12490

Moritz, D. J., Fox, P. J., Luscombe, P. A., & Kraemer, H. C. (2006). Neurological and psychiatric predictors of mortality in patients with Alzheimer disease in California. Archives of Neurology, 54(7), 878–885. https://doi.org/10.1001/archneur.1997.00550190066016

Morowitz, M. J., Carlisle, E. M., & Alverdy, J. C. (2011). Contributions of intestinal bacteria to nutrition and metabolism in the critically ill. The Surgical clinics of North America, 91(4), 771–viii. https://doi.org/10.1016/j.suc.2011.05.001

Morley, J. E., Farr, S. A., & Nguyen, A. D. (2018). Alzheimer Disease. Clinics in Geriatric Medicine, 34(4), 591–601. https://doi.org/10.1016/j.cger.2018.06.006

Muddapu, V. R., Dharshini, S. A. P., Chakravarthy, V. S., & Gromiha, M. M. (2020). Neurodegenerative Diseases – Is Metabolic Deficiency the Root Cause? Frontiers in Neuroscience, 14(March), 1–19. https://doi.org/10.3389/fnins.2020.00213

Myllymäki, H., Valanne, S., & Rämet, M. (2014). The *Drosophila* Imd Signaling Pathway . The Journal of Immunology, 192(8), 3455–3462. https://doi.org/10.4049/jimmunol.1303309

Nath, A. S., Parsons, B. D., Makdissi, S., Chilvers, R. L., Mu, Y., Weaver, C. M., Euodia, I., Fitze, K. A., Long, J., Scur, M., Mackenzie, D. P., Makrigiannis, A. P., Pichaud, N., Boudreau, L. H., Simmonds, A. J., Webber, C. A., Derfalvi, B., Hammon, Y., Rachubinski, R. A., & Di Cara, F. (2022). Modulation of the cell membrane lipid milieu by peroxisomal β-oxidation induces Rho1 signaling to trigger inflammatory responses. Cell reports, 38(9), 110433. https://doi.org/10.1016/j.celrep.2022.110433

Nässel, D. R., & Williams, M. J. (2014). Cholecystokinin-like peptide (DSK) in *Drosophila*, not only for satiety signaling. *Frontiers in Endocrinology*, *5*(DEC), 1–5. https://doi.org/10.3389/fendo.2014.00219

Neophytou, C., & Pitsouli, C. (2022). How Gut Microbes Nurture Intestinal Stem Cells: A *Drosophila* Perspective. Metabolites, 12(2). https://doi.org/10.3390/metabo12020169

Newell, P. D., & Douglas, A. E. (2014). Interspecies Interactions Determine the Impact of the Gut Microbiota on Nutrient Allocation in *Drosophila* melanogaster. Applied and Environmental Microbiology, 80(2), 788–796. https://doi.org/10.1128/AEM.02742-13

Odubanjo, O. V., Oluwarotimi, A. E., Ayeni, C. O., Akingbola, H. O., & Olabisi, P. T. (2020). Fatty acid composition and antioxidant effect of coconut oil in *Drosophila* melanogaster. Comparative Clinical Pathology, 29(6), 1147–1155. https://doi.org/10.1007/s00580-020-03162-4

Oh, Y., Yoon, S. E., Zhang, Q., Chae, H. S., Daubnerová, I., Shafer, O. T., Choe, J., & Kim, Y. J. (2014). A homeostatic sleep-stabilizing pathway in *Drosophila* composed of the sex peptide receptor and its ligand, the myoinhibitory peptide. PLoS biology, 12(10), e1001974. https://doi.org/10.1371/journal.pbio.1001974.

Oldefest, M., Nowinski, J., Hung, C. W., Neelsen, D., Trad, A., Tholey, A., Grötzinger, J., & Lorenzen, I. (2013). Upd3--an ancestor of the four-helix bundle cytokines. Biochemical and biophysical research communications, 436(1), 66–72. https://doi.org/10.1016/j.bbrc.2013.04.107

Onyango, I. G., Jauregui, G. V., Carná, M., Jr., J. P. B., & Stokin, G. B. (2015). Neuroinflammation in Alzheimer's Disease. 243–256.

Ou, Z., Pan, J., Tang, S., Duan, D., Yu, D., Nong, H., & Wang, Z. (2021). Global Trends in the Incidence, Prevalence, and Years Lived With Disability of Parkinson's Disease in 204 Countries/Territories From 1990 to 2019. Frontiers in Public Health, 9(December). https://doi.org/10.3389/fpubh.2021.776847

Pang, S. Y. Y., Teo, K. C., Hsu, J. S., Chang, R. S. K., Li, M., Sham, P. C., & Ho, S. L. (2017). The role of gene variants in the pathogenesis of neurodegenerative disorders as revealed by next generation sequencing studies: A review. Translational Neurodegeneration, 6(1), 1–11. https://doi.org/10.1186/s40035-017-0098-0

Peters, R. (2006). Ageing and the brain. Postgraduate Medical Journal, 82(964), 84–88. https://doi.org/10.1136/pgmj.2005.036665

Petkovic, M., O'Brien, C. E., & Jan, Y. N. (2021). Interorganelle communication, aging, and neurodegeneration. Genes and Development, 35(7), 449–469. https://doi.org/10.1101/gad.346759.120

Pinsonneault, R. L., Mayer, N., Mayer, F., Tegegn, N., & Bainton, R. J. (2011). Novel models for studying the blood-brain and blood-eye barriers in *Drosophila*. Methods in molecular biology (Clifton, N.J.), 686, 357–369. https://doi.org/10.1007/978-1-60761-938-3_17

Podcasy, J. L., & Epperson, C. N. (2016). Considering sex and gender in Alzheimer disease and other dementias. Dialogues in Clinical Neuroscience, 18(4), 437–446. https://doi.org/10.31887/dcns.2016.18.4/cepperson

Prüßing, K., Voigt, A., & Schulz, J. B. (2013). *Drosophila melanogaster* as a model organism for Alzheimer's disease. Molecular Neurodegeneration, 8(1). https://doi.org/10.1186/1750-1326-8-35

Qi, Y., Jo Lohman, Bratlie, K. M., Peroutka-Bigus, Bellaire, N. B., Wannemuehler, M., Yoon, K.-J., Barrett, T. A., & Wang, Q. (2019). Vitamin C and B3 as New Biomaterials to Alter Intestinal Stem Cells. Journal of Biomedical Research, 107(9), 1886–1897. https://doi.org/doi:10.1002/jbm.a.36715

Raghu, P., Joseph, A., Krishnan, H., Singh, P., & Saha, S. (2019). Phosphoinositides: Regulators of Nervous System Function in Health and Disease. Frontiers in Molecular Neuroscience, 12(August). https://doi.org/10.3389/fnmol.2019.00208

Rajan, A., & Perrimon, N. (2012). *Drosophila* cytokine unpaired 2 regulates physiological homeostasis by remotely controlling insulin secretion. Cell, 151(1), 123–137. https://doi.org/10.1016/j.cell.2012.08.019

Raskin, J., Cummings, J., Hardy, J., Schuh, K., & Dean, R. (2015). Neurobiology of Alzheimer's Disease: Integrated Molecular, Physiological, Anatomical, Biomarker, and Cognitive Dimensions. Current Alzheimer Research, 12(8), 712–722. https://doi.org/10.2174/1567205012666150701103107

Rath, E., & Haller, D. (2022). Intestinal epithelial cell metabolism at the interface of microbial dysbiosis and tissue injury. Mucosal Immunology, May. https://doi.org/10.1038/s41385-022-00514-x

Reginato, A., Veras, A. C. C., Baqueiro, M. da N., Panzarin, C., Siqueira, B. P., Milanski, M., Lisboa, P. C., & Torsoni, A. S. (2021). The role of fatty acids in ceramide pathways and their influence on hypothalamic regulation of energy balance: a systematic review. International Journal of Molecular Sciences, 22(10). https://doi.org/10.3390/ijms22105357

Ren, G. R., Hauser, F., Rewitz, K. F., Kondo, S., Engelbrecht, A. F., Didriksen, A. K., Schjøtt, S. R., Sembach, F. E., Li, S., Søgaard, K. C., Søndergaard, L., & Grimmelikhuijzen, C. J. P. (2015). CCHamide-2 is an orexigenic brain-gut peptide in *Drosophila.* PLoS ONE, 10(7), 1–18. https://doi.org/10.1371/journal.pone.0133017

Rinninella, E., Raoul, P., Cintoni, M., Franceschi, F., Miggiano, G. A. D., Gasbarrini, A., & Mele, M. C. (2019). What is the healthy gut microbiota composition? A changing ecosystem across age, environment, diet, and diseases. Microorganisms, 7(1). https://doi.org/10.3390/microorganisms7010014

Risiglione, P., Zinghirino, F., Di Rosa, M. C., Magrì, A., & Messina, A. (2021). Alpha-synuclein and mitochondrial dysfunction in parkinson's disease: The emerging role of vdac. Biomolecules, 11(5). https://doi.org/10.3390/biom11050718

Roberts, S. B., & Rosenberg, I. (2006). Nutrition and aging: changes in the regulation of energy metabolism with aging. Physiological reviews, 86(2), 651–667. https://doi.org/10.1152/physrev.00019.2005

Roh, J. H., Huang, Y., Bero, A. W., Kasten, T., Stewart, F. R., Bateman, R. J., & Holtzman, D. M. (2012). Disruption of the sleep-wake cycle and diurnal fluctuation of β-amyloid in mice with Alzheimer's disease pathology. Science translational medicine, 4(150), 150ra122. https://doi.org/10.1126/scitranslmed.3004291.

Ruiz-Riquelme, A., Lau, H. H. C., Stuart, E., Goczi, A. N., Wang, Z., Schmitt-Ulms, G., & Watts, J. C. (2018). Prion-like propagation of β-amyloid aggregates in the absence of APP overexpression. Acta Neuropathologica Communications, 6(1), 26. https://doi.org/10.1186/s40478-018-0529-x

Rydbom, J., Kohl, H., Hyde, V. R., & Lohr, K. M. (2021). Altered Gut Microbial Load and Immune Activation in a *Drosophila* Model of Human Tauopathy. 15(731602), 2–9. https://doi.org/10.3389/fnins.2021.731602

Sadiq, N.M., & Tadi. P. (2022). Physiology, Pituitary Hormones. In: StatPearls. Treasure Island (FL): StatPearls Publishing; 2022 Jan-. Available from: https://www.ncbi.nlm.nih.gov/books/NBK557556/

Sampson, Timothy R, and Sarkis K Mazmanian. "Control of brain development, function, and behavior by the microbiome." Cell host & microbe vol. 17,5 (2015): 565-76. doi:10.1016/j.chom.2015.04.011.

Sarantseva, S., Timoshenko, S., Bolshakova, O., Karaseva, E., Rodin, D., Schwarzman, A. L., & Vitek, M. P. (2009). Apolipoprotein E-mimetics inhibit neurodegeneration and restore cognitive functions in a transgenic *Drosophila* model of Alzheimer's disease. PLoS ONE, 4(12). https://doi.org/10.1371/journal.pone.0008191

Sassa, T., & Kihara, A. (2014). Metabolism of very long-chain Fatty acids: genes and pathophysiology. Biomolecules & therapeutics, 22(2), 83–92. https://doi.org/10.4062/biomolther.2014.017.

Schrader, M., Costello, J., Godinho, L. F., & Islinger, M. (2015). Peroxisome-mitochondria interplay and disease. Journal of Inherited Metabolic Disease, 38(4), 681–702. https://doi.org/10.1007/s10545-015-9819-7

Schretter, C. E. (2020). Links between the gut microbiota, metabolism, and host behavior. Gut Microbes, 11(2), 245–248. https://doi.org/10.1080/19490976.2019.1643674

Schretter, C. E., Vielmetter, J., Bartos, I., Marka, Z., Marka, S., Argade, S., & Mazmanian, S. K. (2018). A gut microbial factor modulates locomotor behavior in *Drosophila.* 563(7731), 402–406. https://doi.org/doi:10.1038/s41586-018-0634-9

Sciambra, N., & Chtarbanova, S. (2021). The Impact of Age on Response to Infection in *Drosophila. Microorganisms*, *9*(5), 958. https://doi.org/10.3390/microorganisms9050958

Scopelliti, A., Bauer, C., Cordero, J. B., & Vidal, M. (2016). Bursicon-α subunit modulates dLGR2 activity in the adult *Drosophila* melanogaster midgut independently to Bursicon-β. *Cell Cycle*, *15*(12), 1538–1544. https://doi.org/10.1080/15384101.2015.1121334

Sellin, J., Wingen, C., Gosejacob, D., Senyilmaz, D., Hänschke, L., Büttner, S., Meyer, K., Bano, D., Nicotera, P., Teleman, A. A., & Bülow, M. H. (2018). Dietary rescue of lipotoxicity-induced mitochondrial damage in Peroxin19 mutants. PLoS Biology, 16(6), 1–24. https://doi.org/10.1371/journal.pbio.2004893

Senanayake, V., & Goodenowe, D. B. (2019). Plasmalogen deficiency and neuropathology in Alzheimer's disease: Causation or coincidence? Alzheimer's and Dementia: Translational Research and Clinical Interventions, 5, 524–532. https://doi.org/10.1016/j.trci.2019.08.003

Shadfar, S., Hwang, C. J., Lim, M. S., Choi, D. Y., & Hong, J. T. (2015). Involvement of inflammation in Alzheimer's disease pathogenesis and therapeutic potential of anti-inflammatory agents. Archives of Pharmacal Research, 38(12), 2106–2119. https://doi.org/10.1007/s12272-015-0648-x

Shahmoradian, S.H, Lewis, A. J., Genoud, C., Hench, J. rgen, Moors, T. E., Navarro, P. P., Castaño-Díez, D., Schweighauser, G., Graff-Meyer, A., Goldie, K. N., Sütterlin, R., Huisman, E., Ingrassia, A., Gier, Y. de, Rozemuller, A. J. M., Wang, J., Paepe, A. D., Erny, J., Staempfli, A., … Lauer, M. E. (2019). Lewy pathology in Parkinson's disease consists of crowded organelles and lipid membranes. Nature Neuroscience, 22(7), 1099–1109.

Siju, K. P., De Backer, J. F., & Grunwald Kadow, I. C. (2021). Dopamine modulation of sensory processing and adaptive behavior in flies. Cell and Tissue Research, 383(1), 207–225. https://doi.org/10.1007/s00441-020-03371-x

Silva, Y. P., Bernardi, A., & Frozza, R. L. (2020). The Role of Short-Chain Fatty Acids From Gut Microbiota in Gut-Brain Communication. 11(January), 1–14. https://doi.org/10.3389/fendo.2020.00025

Simon, M. (2018). The amyloid hypothesis on trial. Nature, 559, 4–7. https://personal.utdallas.edu/~tres/aging_seminar2019/Makin.2018.pdf

Smith, J. J., & Aitchison, J. D. (2013). Peroxisomes take shape. Nature Reviews Molecular Cell Biology, 14(12), 803–817. https://doi.org/10.1038/nrm3700

Sonne J, Reddy V, Beato MR. Neuroanatomy, Substantia Nigra. [Updated 2021 Oct 30]. In: StatPearls [Internet]. Treasure Island (FL): StatPearls Publishing; 2022 Jan-. Available from: https://www.ncbi.nlm.nih.gov/books/NBK536995/?report=classic.

St Laurent, R., O'Brien, L. M., & Ahmad, S. T. (2013). Sodium butyrate improves locomotor impairment and early mortality in a rotenone-induced *Drosophila* model of Parkinson's disease. Neuroscience, 246, 382–390. https://doi.org/10.1016/j.neuroscience.2013.04.037.

Staff, N. P., & Windebank, A. J. (2014). Peripheral neuropathy due to vitamin deficiency, toxins, and medications. CONTINUUM Lifelong Learning in Neurology, 20(5), 1293–1306. https://doi.org/10.1212/01.CON.0000455880.06675.5a

Stark, I., Bates, A. S., Pleijzier, M. W., & Schlegel, P. (2020). The connectome of the adult. 1–192.

Steinkamp, M., Schulte, N., Spaniol, U., Pflüger, C., Hartmann, C., Kirsch, J., & von Boyen, G. (2012). Brain derived neurotrophic factor inhibits apoptosis in enteric glia during gut inflammation. Medical Science Monitor, 18(4), 117–122. https://doi.org/10.12659/msm.882612

Storelli, G., Defaye, A., Erkosar, B., Hols, P., & Royet, J. (2011). Article Lactobacillus plantarum Promotes *Drosophila* Systemic Growth by Modulating Hormonal Signals through TOR-Dependent Nutrient Sensing. 403–414. https://doi.org/10.1016/j.cmet.2011.07.012

Su, X. Q., Wang, J., & Sinclair, A. J. (2019). Plasmalogens and Alzheimer ' s disease : a review. 1–10.

Swanson, D., Block, R., & Mousa, S. A. (2012). Omega-3 fatty acids EPA and DHA: Health benefits throughout life. Advances in Nutrition, 3(1), 1–7. https://doi.org/10.3945/an.111.000893

Tanaka, H., Okazaki, T., Aoyama, S., Yokota, M., Koike, M., Okada, Y., Fujiki, Y., & Gotoh, Y. (2019). Peroxisomes control mitochondrial dynamics and the mitochondrion-dependent apoptosis pathway. Journal of Cell Science, 132(11). https://doi.org/10.1242/jcs.224766

Thau, L., Reddy, V., & Singh, P. (2022). Anatomy , Central Nervous System. StatPearls Publishing NCBI Bookshelf. 1–8.

Tracy, T. E., Madero-Pérez, J., Swaney, D. L., Chang, T. S., Moritz, M., Konrad, C., Ward, M. E., Stevenson, E., Hüttenhain, R., Kauwe, G., Mercedes, M., Sweetland-Martin, L., Chen, X., Mok, S. A., Wong, M. Y., Telpoukhovskaia, M., Min, S. W., Wang, C., Sohn, P. D., … Gan, L. (2022). Tau interactome maps synaptic and mitochondrial processes associated with neurodegeneration. Cell, 185(4), 712-728.e14. https://doi.org/10.1016/j.cell.2021.12.041

Trinder, M., Daisley, B. A., Dube, J. S., & Reid, G. (2017). *Drosophila* melanogaster as a high-throughput model for host-microbiota interactions. Frontiers in Microbiology, 8(APR), 1–8. https://doi.org/10.3389/fmicb.2017.00751

Turrel, O., Rabah, Y., Plaçais, P. Y., Goguel, V., & Preat, T. (2020). *Drosophila* middle-term memory: Amnesiac is required for pKA activation in the mushroom bodies, a function modulated by neprilysin 1. *Journal of Neuroscience*, *40*(21), 4219–4229. https://doi.org/10.1523/JNEUROSCI.2311-19.2020

Van Veldhoven, P. P., & Baes, M. (2013). Peroxisome deficient invertebrate and vertebrate animal models. Frontiers in physiology, 4, 335. https://doi.org/10.3389/fphys.2013.00335

Venkat, P., Chopp, M., & Chen, J. (2015). Models and mechanisms of vascular dementia. Experimental neurology, 272, 97–108. https://doi.org/10.1016/j.expneurol.2015.05.006

Vidal-Martínez, G., Vargas-Medrano, J., Gil-Tommee, C., Medina, D., Garza, N. T., Yang, B., Segura-Ulate, I., Dominguez, S. J., & Perez, R. G. (2016). FTY720/Fingolimod Reduces Synucleinopathy and Improves Gut Motility in A53T Mice: CONTRIBUTIONS OF PRO-BRAIN-DERIVED NEUROTROPHIC FACTOR (PRO-BDNF) AND MATURE BDNF. The Journal of biological chemistry, 291(39), 20811–20821. https://doi.org/10.1074/jbc.M116.744029.

Virmani, A., Pinto, L., Binienda, Z., & Ali, S. (2013). Food, nutrigenomics, and neurodegeneration - Neuroprotection by what you eat! Molecular Neurobiology, 48(2), 353–362. https://doi.org/10.1007/s12035-013-8498-3

Vossius, J. P., Janvin, C., & Aarsland, D. (2011). The economic impact of cognitive impairment in Parkinson's disease. Movement Disorders, 26(8), 1541–1544. https://doi.org/10.1002/mds.23661

Wakade, C., Chong, R., Seamon, M., Purohit, S., Giri, B., & Morgan, J. C. (2021). Low-Dose Niacin Supplementation Improves Motor Function in US Veterans with Parkinson's Disease: A Single-Center, Randomized, Placebo-Controlled Trial. Biomedicines, 9(12), 1881. https://doi.org/10.3390/biomedicines9121881.

Wang, G., Huang, Y., Wei Chen, Chen, S., Wang, Y., Xiao, Q., Liu, J., Fung, V. S. C., Halliday, G., & Chen, S. (2016). Variants in the SNCA gene associate with motor progression while variants in the MAPT gene associate with the severity of Parkinson's disease. Parkinsonism and Related Disorders, 24, 89–94. https://doi.org/10.1016/j.parkreldis.2015.12.018

Wang, Y., Pan, Y., & Li, H. (2020). What is brain health and why is it important? The BMJ, 371, 1–7. https://doi.org/10.1136/bmj.m3683

Weintraub, Comella, C. L., & Horn, S. (2008). Parkinson's disease--Part 1: Pathophysiology, symptoms, burden, diagnosis, and assessment. The American Journal of Managed Care, 14(2 Suppl), S40–S48.

World Health Organization. (2022). Dementia. Retrieved form: https://www.who.int/news-room/fact-sheets/detail/dementia

Williamson, M., Lenz, C., Winther, A. M., Nässel, D. R., & Grimmelikhuijzen, C. J. (2001). Molecular cloning, genomic organization, and expression of a B-type (cricket-type) allatostatin preprohormone from *Drosophila* melanogaster. Biochemical and biophysical research communications, 281(2), 544–550. https://doi.org/10.1006/bbrc.2001.4402.

Winiarska-Mieczan, A., Baranowska-Wójcik, E., Kwiecień, M., Grela, E. R., Szwajgier, D., Kwiatkowska, K., & Kiczorowska, B. (2020). The role of dietary antioxidants in the pathogenesis of neurodegenerative diseases and their impact on cerebral oxidoreductive balance. Nutrients, 12(2). https://doi.org/10.3390/nu12020435

Wong, W. (2020). Economic burden of Alzheimer disease and managed care considerations. The American journal of managed care, 26(8 Suppl), S177–S183. https://doi.org/10.37765/ajmc.2020.88482.

Wraith, D. C., Pope, R., Butzkueven, H., Holder, H., Vanderplank, P., Lowrey, P., Day, M. J., Gundlach, A. L., Kilpatrick, T. J., Scolding, N., & Wynick, D. (2009). A role for galanin in human and experimental inflammatory demyelination. Proceedings of the National Academy of Sciences of the United States of America, 106(36), 15466–15471. https://doi.org/10.1073/pnas.0903360106

Xie, A., Gao, J., Xu, L., & Meng, D. (2014). Shared mechanisms of neurodegeneration in alzheimer's disease and parkinson's disease. *BioMed Research International*, *2014*. https://doi.org/10.1155/2014/648740

Yadav, R. S., & Tiwari, N. K. (2014). Lipid integration in neurodegeneration: an overview of Alzheimer's disease. Molecular neurobiology, 50(1), 168–176. https://doi.org/10.1007/s12035-014-8661-5.

Yakunin, E., Moser, A., Loeb, V., Saada, A., Faust, P., Crane, D. I., Baes, M., & Sharon, R. (2010). A-Synuclein Abnormalities in Mouse Models of Peroxisome Biogenesis Disorders. Journal of Neuroscience Research, 88(4), 866–876. https://doi.org/10.1002/jnr.22246

Yan, Y., Ren, S., Duan, Y., Lu, C., Niu, Y., Wang, Z., Inglis, B., Ji, W., Zheng, Y., & Si, W. (2021). Gut microbiota and metabolites of α-synuclein transgenic monkey models with early stage of Parkinson's disease. Npj Biofilms and Microbiomes, 7(1), 1–9. https://doi.org/10.1038/s41522-021-00242-3

Yang, J., Pu, J., Lu, S., Bai, X., Wu, Y., Jin, D., Cheng, Y., Zhang, G., Zhu, W., Luo, X., Rosselló-Móra, R., & Xu, J. (2020). Species-Level Analysis of Human Gut Microbiota With Metataxonomics. Frontiers in Microbiology, 11(August). https://doi.org/10.3389/fmicb.2020.02029

Yang, W., Hamilton, J. L., Kopil, C., Beck, J. C., Tanner, C. M., Albin, R. L., Ray Dorsey, E., Dahodwala, N., Cintina, I., Hogan, P., & Thompson, T. (2020). Current and projected future economic burden of Parkinson's disease in the U.S. Npj Parkinson's Disease, 6(1), 1–9. https://doi.org/10.1038/s41531-020-0117-1

Yaqoob, P., & Shaikh, S. R. (2010). The nutritional and clinical significance of lipid rafts. Current opinion in clinical nutrition and metabolic care, 13(2), 156–166. https://doi.org/10.1097/MCO.0b013e328335725b.

Zeng, M., Inohara, N., & Nuñez, G. (2017). Mechanisms of inflammation-driven bacterial dysbiosis in the gut. Physiology & Behavior, 10(1), 18–26. https://doi.org/doi:10.1038/mi.2016.75

APPENDIX

Supplementary Table 1: Materials

	Materials	Identification # or recipe	Manufacturer/strain
***Drosophila* husbandry**	Polypropylene narrow	AS507	ThermoFischer Scientific™
	Narrow vial tray	59-207BLU	Genesee Scientific™
	CO_2	NA	Linde Canada
	Anesthetizing Flypad	59-114	Genesee Scientific™
***Drosophila* stocks**	**Fly line**	**Bloomington *Drosophila* Stock Center, Vienna, or Korean *Drosophila* Resource Center**	
	Mex Gal4	BDSC:91367	*P{w[+mC]=mex1-GAL4.2.1}9-1, y[1] w[1118]*
	w^{1118}	BDSC:5905	*w[1118]*
	UAS Pex5 RNA-i	VDRC:42332	*w1118; P{GD14972}v42332*
	UAS GFP	BDSC:5137	*y[1] w[*]; P{w[+mC]=UAS-mCD8::GFP.L}LL5, P{UAS-mCD8::GFP.L}2*
	UAS SNCA	BDSC:51375	*w[1118]; P{w[+mC]=UAS-SNCA.J}1/CyO*
	UAS BACE	BDSC:29877	*w[1118]; P{w[+mC]=UAS-BACE1.L}2*
	UAS Mip	KDRC:10027	*w[1118](I); P(UAS-Mip) vie72a (II)*
	UAS CAS9	BDSC:54595	*w[1118]; P{y[+t7.7] w[+mC]=UAS-Cas9.C}attP2*
	U6-sgRNA PEX3/Cyo ; UAS GFP/Tm6b	NA	*y[1] v[1]; P{y[+t7.7] v[+t1.8]=Lab made fly-line}attP40*
	$Myo1A^{ts}$-Gal4/Cyo;Tubulin-$Gal80^{ts}$,UAS GFP	NA	A kind gift from Dr. Edan Foley, University of Alberta
	Elav Gal4	BDSC:458	*P{w[+mW.hs]=GawB}elav[C155]*
***Drosophila* food**	Ampicillin D-(-)	A1593	Sigma-Aldrich™
	Coconut oil	C1758	Sigma-Aldrich™

	Materials	Identification # or recipe	Manufacturer/strain
	Erucic acid	E3385	Sigma-Aldrich™
	Methyl benzoate	JRD0440	Sigma-Aldrich™
	Metronidazole	M3761	Sigma-Aldrich™
	Narrow DrosoFiller™	59-168	Genesee Scientific™
	Neomycin trisulfate salt hydrate	N1876	Sigma-Aldrich™
	Nicotinic acid	N4126	Sigma-Aldrich™
	Nutrifly®	66-116	Genesee Scientific™
	Phosphoric acid	P5811	Sigma-Aldrich™
	Propionic acid	402907	Sigma-Aldrich™
	Tetracycline	08168	Sigma-Aldrich™
	Vancomycin hydrochloride	1709007	Sigma-Aldrich™
Climbing Assays	Desk Lamp (Bendable)		
	Foam Mat		
	iPhone XR camera	A1984	Apple Inc.
	Pyrex™ 250mL graduated cylinder	3066	Corning® by Sigma-Aldrich™
Courtship Assays	9-well assay plates		Dr. Jamie Kramers Lab
	Arena Camera		Dr. Jamie Kramers Lab
	Arena Incubator		Dr. Jamie Kramers Lab
	Housing plates	Custom	Dr. Jamie Kramers Lab
	Timer		Apple iPhone
	Wide mouth *Drosophila* stock vials	Kindly gifted by	Dr. Jamie Kramers Lab
Brain Pathology /Transcriptomic screens	0.05% PBST	1x PBS + 0.05% Triton-X	
	0.3% PBST	1x PBS + 0.3% Triton-X	
	0.2%,0.3%,0.5% PBSTw	1x PBS + (-%) Tween-20	

	Materials	Identification # or recipe	Manufacturer/strain
	1.5 mL microcentrifuge tube	022363204	Eppendorf™
	1x PBS (Phosphate buffer saline) (1L)	Sodium Chloride (8g, 0.137M), Potassium chloride (0.2g, 0.0027M), Sodium Phosphate Dibasic (1.44g, 0.01M), Potassium Phosphate Monobasic (0.245g, 0.0018M) 1L distilled water, PH~7.4	
	2.5% glutaraldehyde fixative diluted in 0.1M sodium cacodylate buffer	Kindly prepared by	Mary Anne Trevors, EM Facility
	4% Formaldehyde	J19943.K2 (16% diluted 1:4 in 1x PBS)	ThermoFischer Scientific™
	Alexa Fluor™ 488 & Propidium Iodide (PI)	A10788	ThermoFischer Scientific™
	Amplex™ Red Hydrogen Peroxide/Peroxidase Assay Kit	A22188	ThermoFischer Scientific™
	Capacity RNA-to-cDNA™ Kit	4387406	ThermoFischer Scientific™ Applied Biosystems™
	Cordless pestle motor	47747-370	VWR®
	DAPI	ab228549	abcam™ Sigma-Aldrich™
	Dihydroethidium assay kit	30980035MG	ThermoFischer Scientific™
	DNase 1	18047019	ThermoFischer Scientific™
	Dumont #5 micro-dissection forceps	11251-10	Fine Science Tools™

	Materials	Identification # or recipe	Manufacturer/strain
	Dumont straight micro-dissection scissors	15040-11	Fine Science Tools™
	Eppendorf 6331 Nexus Gradient Flexlid Thermal Cycler		Eppendorf™
	In Situ Cell Death Detection Kit, TMR red	12156792910	Roche™ Sigma-Aldrich™
	MicroAmp™ Optical 96-Well Reaction Plate	4306737	ThermoFischer Scientific™ Applied Biosystems™
	MitoSOX™ Red Mitochondrial Superoxide Indicator	M36008	ThermoFischer Scientific™
	Nanodrop™ spectrophotometer	ND-ONEC-W	ThermoFischer Scientific™
	Normal Goat Serum (NGS)	31872	ThermoFischer Scientific™
	Plastic pestles	47747-358	VWR®
	PowerTrack SYBR™ Green PCR Master Mix	A46109	ThermoFischer Scientific™ Applied Biosystems™
	ProLong™ Gold Antifade mounting media	P10144	ThermoFischer Scientific™
	QIAseq UPX 3’ Transcriptome Kits	333088	QIAGEN
	QIAseq UPX 3' Trans. 12-index (48)	333074	QIAGEN
	Qubit Fluorometer	Q33238	ThermoFischer Scientific™
	Qubit RNA BR/HS kit	Q32852	ThermoFischer Scientific™

	Materials	Identification # or recipe	Manufacturer/strain
	Qubit RNA IQ kit	Q33221	ThermoFischer Scientific™
	QUBIT™ fluorometer	Q33238	ThermoFischer Scientific™
	Qubit™ Protein BR Assay Kit	A50669	ThermoFischer Scientific™
	Rneasy Mini Kit (50)	74004	QIAGEN
	SFM4 (*Drosophila* culture medium)	89130-770	VWR™
	The QuantStudio™ 6 Flex Real-Time PCR (qPCR) System		ThermoFischer Scientific™ Applied Biosystems™
	Triton-X	9036-19-	Sigma-Aldrich™
	TRIzol™ reagent	15596026	ThermoFischer Scientific™
	Tween-20		Sigma-Aldrich™
	ZYMO™ Research, Direct-zol® RNA Microprep kit	R2061	ZYMO™
Programs/Machines	FIJI ImageJ		FIJI ImageJ
	GraphPad PRISM (v 9.4.0)		GraphPad PRISM®
	Zeiss AXIO-Observer fluorescence microscope		Zeiss
	Zeiss LSM 880 confocal microscope		Zeiss
	Zeiss Zen-Black		Zeiss
	Zeiss Zen-Blue		Zeiss
	Zeiss Zen-Blue lite		Zeiss
Antibodies	Primary antibody Armadillo β-catenin	N2 7A1	Developmental Studies Hybridoma Bank™

	Materials	Identification # or recipe	Manufacturer/strain
	Rabbit anti-TH	T8700-1VL	abcam™ Sigma-Aldrich™,
	Secondary antibody donkey-α mouse Alexa fluorophore A555 (Red)	A-31570	ThermoFischer Scientific ™
	Secondary antibody donkey-α mouse Alexa fluorophore A488 (Green)	A-21202	ThermoFischer Scientific ™
	Secondary antibody donkey-α rabbit Alexa fluorophore A555 (Red)	A-31573	ThermoFischer Scientific ™
	Secondary antibody donkey-α rabbit Alexa fluorophore A488 (Green)	A-21206	ThermoFischer Scientific ™

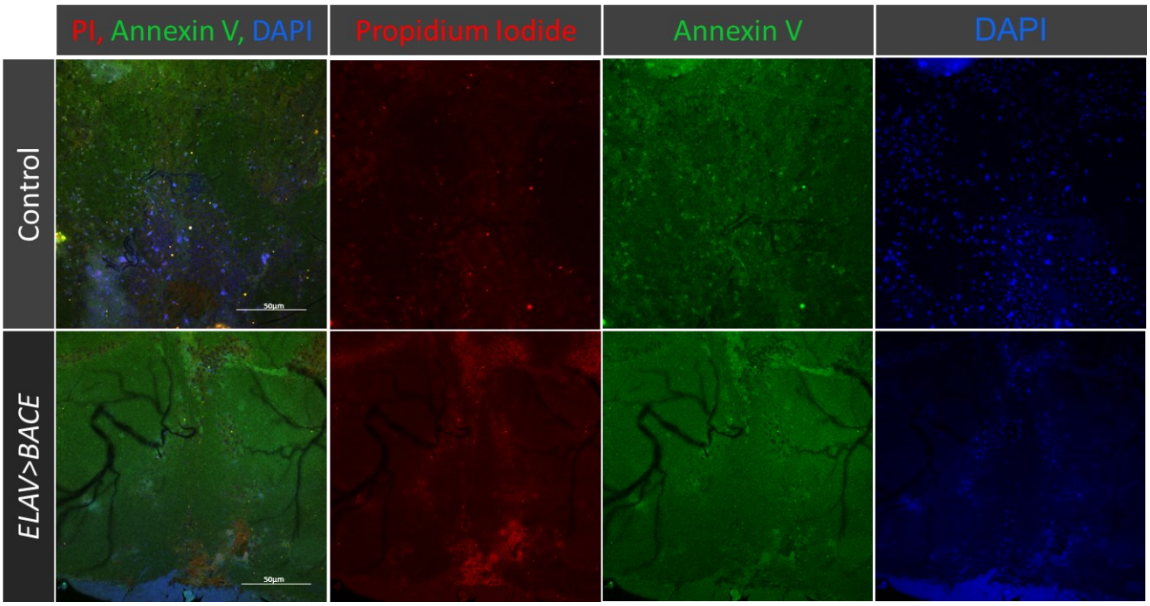

Supplementary Figure 1. Efforts to optimize annexin and propidium iodide staining for cellular apoptosis and necrosis respectively were unsuccessful. Immunofluorescence imaging of CM *Elav>BACE* positive control for cellular death in the brain and control CM *Elav>w*^{1118} age matched at 20do, stained with propidium iodide (Red), Annexin V (Green), and DAPI (Blue). Images were captured using a Zeiss LSM 880 confocal microscope at 40x magnification, scale bar reading 50 μm.

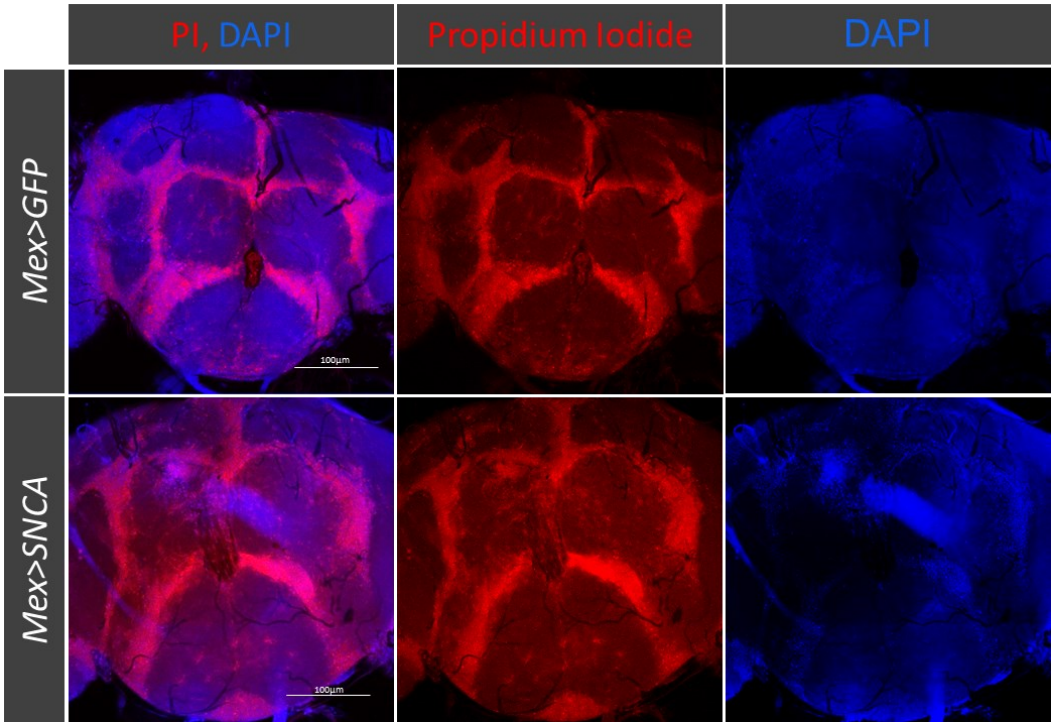

Supplementary Figure 2. Efforts to optimize propidium iodide staining for cellular necrosis were unsuccessful. Immunofluorescence imaging of CM *Mex>SNCA* males for cellular death in the brain and control CM *Mex>GFP* age matched at 20do, stained with propidium iodide (Red) and DAPI (Blue). Images were captured using a Zeiss LSM 880 confocal microscope at 20x magnification, scale bar reading 100 µm.

Agilent Bioanalyzer results for 8 libraries

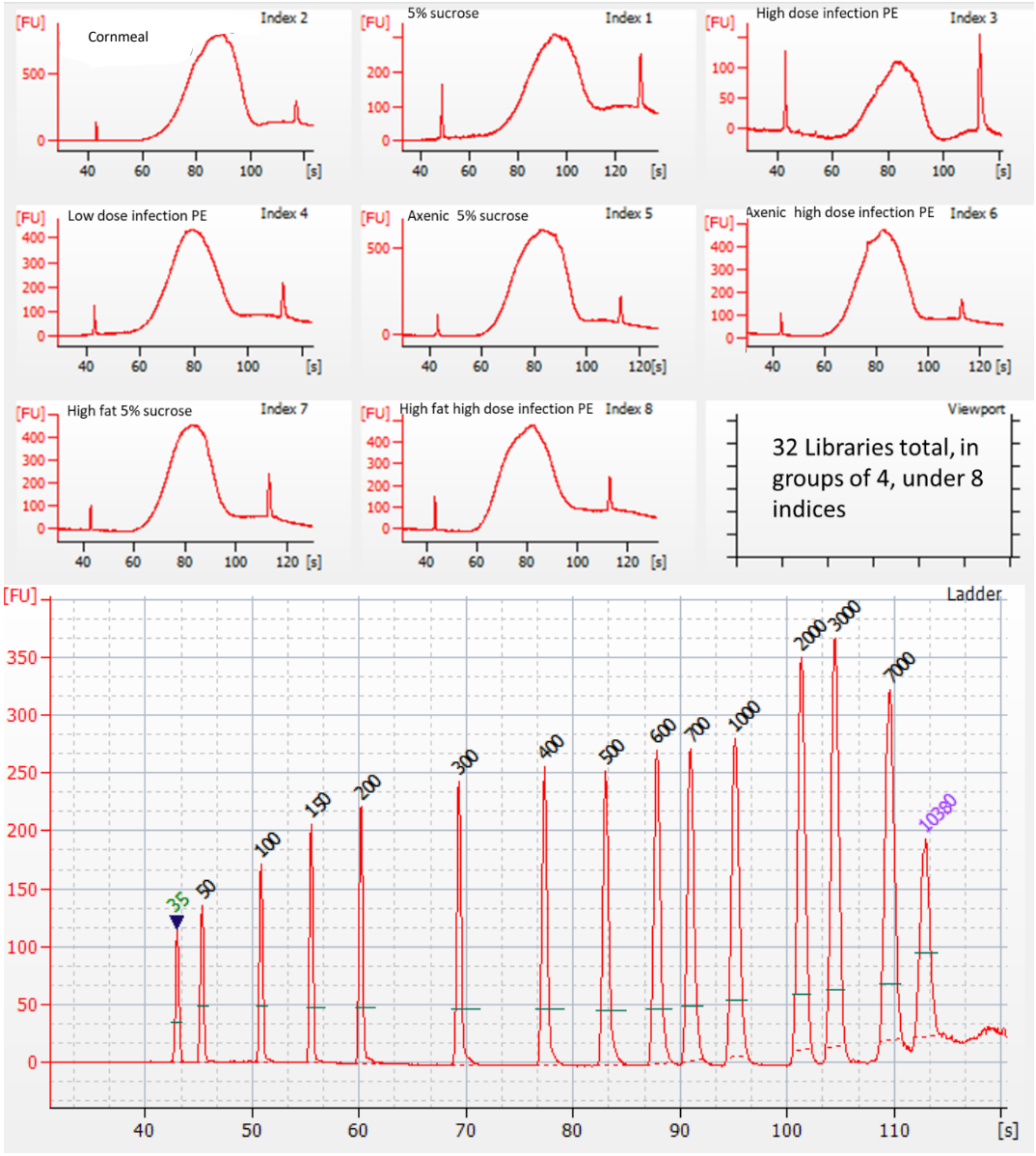

Supplementary Figure 3. Agilent Bioanalyzer transcriptomic screen results of genotypes *Mex>Pex5*-i and *Mex>w^{1118}* on eight different conditions. The numbers above each peak of the reference ladder electropherogram represent cDNA library size in bp. FU: Fluorescent units, s: sec taken to migrate on Bioanalyzer chip microchannel.

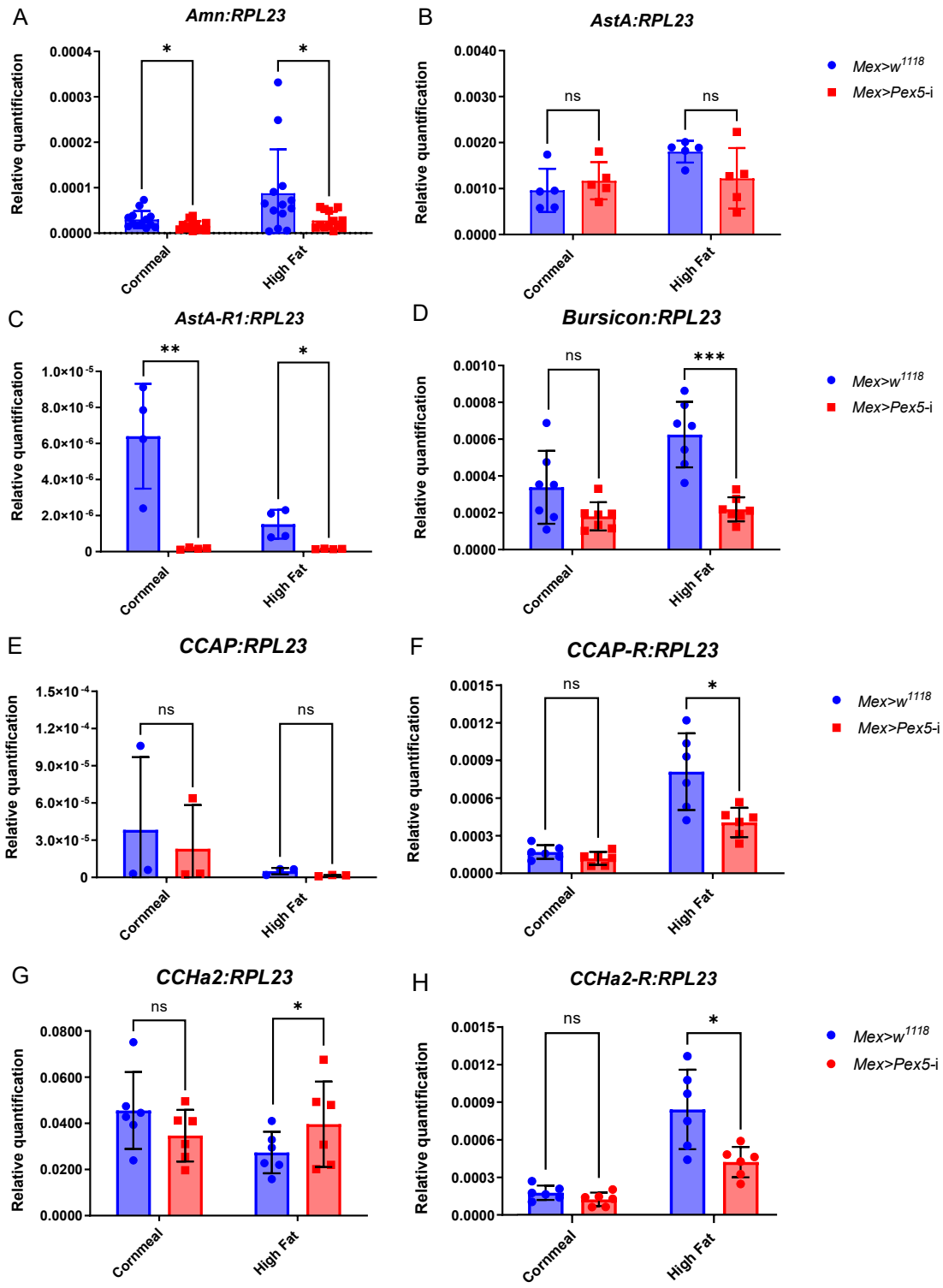
A
Amn:RPL23
Relative quantification
0.0004
0.0003
0.0002
0.0001
0.0000
*
*
Cornmeal
High Fat
B
AstA:RPL23
Relative quantification
0.0040
0.0030
0.0020
0.0010
0.0000
ns
ns
Cornmeal
High Fat
Mex>w1118
Mex>Pex5-i
C
AstA-R1:RPL23
Relative quantification
1.0×10-5
8.0×10-6
6.0×10-6
4.0×10-6
2.0×10-6
0
**
*
Cornmeal
High Fat
D
Bursicon:RPL23
Relative quantification
0.0010
0.0008
0.0006
0.0004
0.0002
0.0000
ns
***
Cornmeal
High Fat
Mex>w1118
Mex>Pex5-i
E
CCAP:RPL23
Relative quantification
1.5×10-4
1.2×10-4
9.0×10-5
6.0×10-5
3.0×10-5
0
ns
ns
Cornmeal
High Fat
F
CCAP-R:RPL23
Relative quantification
0.0015
0.0012
0.0009
0.0006
0.0003
0.0000
ns
*
Cornmeal
High Fat
Mex>w1118
Mex>Pex5-i
G
CCHa2:RPL23
Relative quantification
0.0800
0.0600
0.0400
0.0200
0.0000
ns
*
Cornmeal
High Fat
H
CCHa2-R:RPL23
Relative quantification
0.0015
0.0012
0.0009
0.0006
0.0003
0.0000
ns
*
Cornmeal
High Fat
Mex>w1118
Mex>Pex5-i

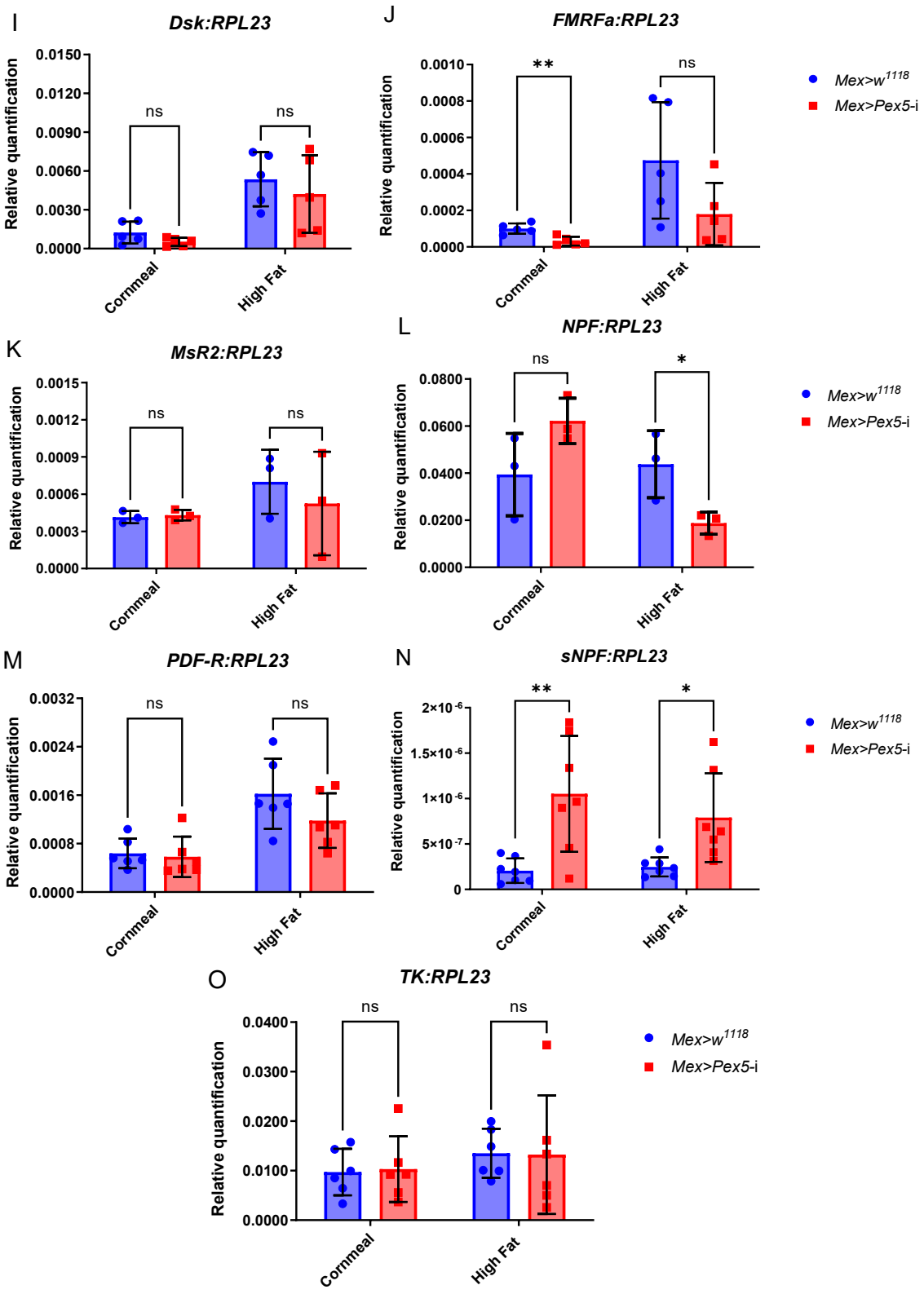
I
Dsk:RPL23
Relative quantification
0.0150
0.0120
0.0090
0.0060
0.0030
0.0000
ns
ns
Cornmeal
High Fat
J
FMRFa:RPL23
Relative quantification
0.0010
0.0008
0.0006
0.0004
0.0002
0.0000
**
ns
Cornmeal
High Fat
Mex>w1118
Mex>Pex5-i
K
MsR2:RPL23
Relative quantification
0.0015
0.0012
0.0009
0.0006
0.0003
0.0000
ns
ns
Cornmeal
High Fat
L
NPF:RPL23
Relative quantification
0.0800
0.0600
0.0400
0.0200
0.0000
ns
*
Cornmeal
High Fat
Mex>w1118
Mex>Pex5-i
M
PDF-R:RPL23
Relative quantification
0.0032
0.0024
0.0016
0.0008
0.0000
ns
ns
Cornmeal
High Fat
N
sNPF:RPL23
Relative quantification
2×10-6
1.5×10-6
1×10-6
5×10-7
0
**
*
Cornmeal
High Fat
Mex>w1118
Mex>Pex5-i
O
TK:RPL23
Relative quantification
0.0400
0.0300
0.0200
0.0100
0.0000
ns
ns
Cornmeal
High Fat
Mex>w1118
Mex>Pex5-i

Supplementary Figure 4. Relative gene expression (quantification) in the midguts of 7do *Drosophila* males and females mixed, using qPCR to validate hits identified from the HFD transcriptomic screen. All statistical analyses were carried out using multiple, two-tailed, unpaired t-tests, assuming equal variance with an α=0.05. A) Relative expression of *Amn:RPL23*, n=13, between *Mex>Pex5*-i and *Mex>w^{1118}* on CM (t(24)=2.352, *p=0.0272) and HFD (t(24)=2.199, *p=0.0377). B) Relative expression of *AstA:RPL23*, n=5, between *Mex>Pex5*-i and *Mex>w^{1118}* on CM (t(8)=0.7536, p=0.4727) and HFD (t(8)=1.849, p=0.1017). C) Relative expression of *AstA-R1:RPL23,* n=4, between *Mex>Pex5*-i and *Mex>w^{1118}* on CM (t(6)=4.279, **p=0.0052) and HFD (t(6)=3.431,*p=0.0140). D) Relative expression of *Bursicon:RPL23,* n=7, between *Mex>Pex5*-i and *Mex>w^{1118}* on CM (t(12)=1.962, p=0.0733) and HFD (t(12)=5.670, ***p>0.0001). E) Relative expression of *CCAP:RPL23,* n=3, between *Mex>Pex5*-i and *Mex>w^{1118}* on CM (t(4)=0.3865, p=0.7188) and HFD (t(4)=2.240, p=0.0886). F) Relative expression of *CCAP-R:RPL23,* n=6, between *Mex>Pex5*-i and *Mex>w^{1118}* on CM (t(10)=1.639, p=0.1322) and HFD (t(10)=3.027, *p=0.0127). G) Relative expression of *CCHa2:RPL23,* n=6, between *Mex>Pex5*-i and *Mex>w^{1118}* on CM (t(10)=1.329, p=0.2134) and HFD (t(10)=1.461, *p=0.0274). H) Relative expression of *CCHa2-R:RPL23,* n=6, between *Mex>Pex5*-i and *Mex>w^{1118}* on CM (t(10)=1.639, p=0.1322) and HFD (t(10)=3.027, *p=0.0127). I) Relative expression of *Dsk:RPL23,* n=5, between *Mex>Pex5*-i and *Mex>w^{1118}* on CM (t(8)=1.807, p=0.1085) and HFD (t(8)=0.6962, p=0.5054). J) Relative expression of *FMRFa:RPL23,* n=5, between *Mex>Pex5*-i and *Mex>w^{1118}* on CM (t(8)=4.074, **p=0.0036) and HFD (t(8)=1.819, p=0.1065). K) Relative expression of *MsR2:RPL23,* n=3, between *Mex>Pex5*-i and *Mex>w^{1118}* on CM (t(4)=0.4475, p=0.6777) and HFD (t(4)=0.6211, p=0.5682). L) Relative expression of *NPF:RPL23,* n=3, between *Mex>Pex5*-i and *Mex>w^{1118}* on CM (t(4)=1.977, p=0.1192) and HFD (t(4)=2.894, *p=0.0438). M) Relative expression of *PDF-R:RPL23,* n=6, between *Mex>Pex5*-i and *Mex>w^{1118}* on CM (t(10)=0.3357, p=0.7440) and HFD (t(4)=1.476, p=0.0.1707). M) Relative expression of *PDF-R:RPL23,* n=6, between *Mex>Pex5*-i and *Mex>w^{1118}* on CM (t(10)=0.3357, p=0.7440) and HFD (t(10)=1.476, p=0.1707). N) Relative expression of *sNPF:RPL23,* n=7, between *Mex>Pex5*-i and *Mex>w^{1118}* on CM (t(12)=3.432,**p=0.0050) and HFD (t(12)=2.874, *p=0.0139). O) Relative expression of *TK:RPL23,* n=6, between *Mex>Pex5*-i and *Mex>w^{1118}* on CM (t(10)=0.1819, p=0.8593) and HFD (t(10)=0.0522, p=0.9593).

Males

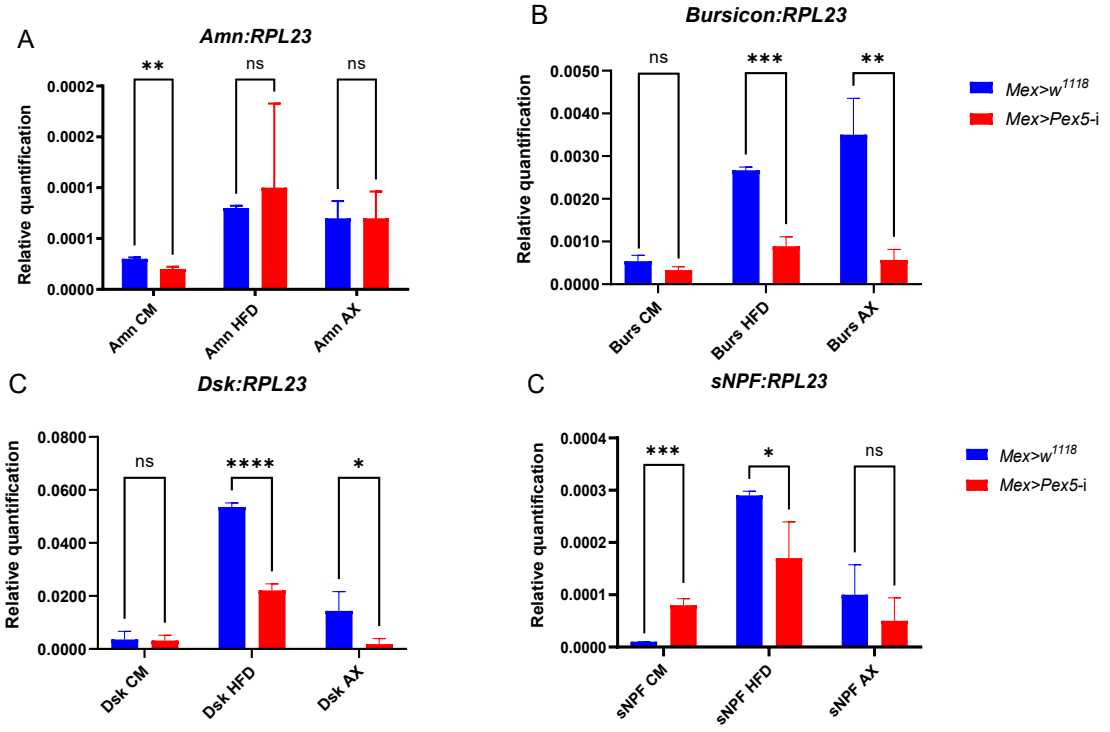

Females

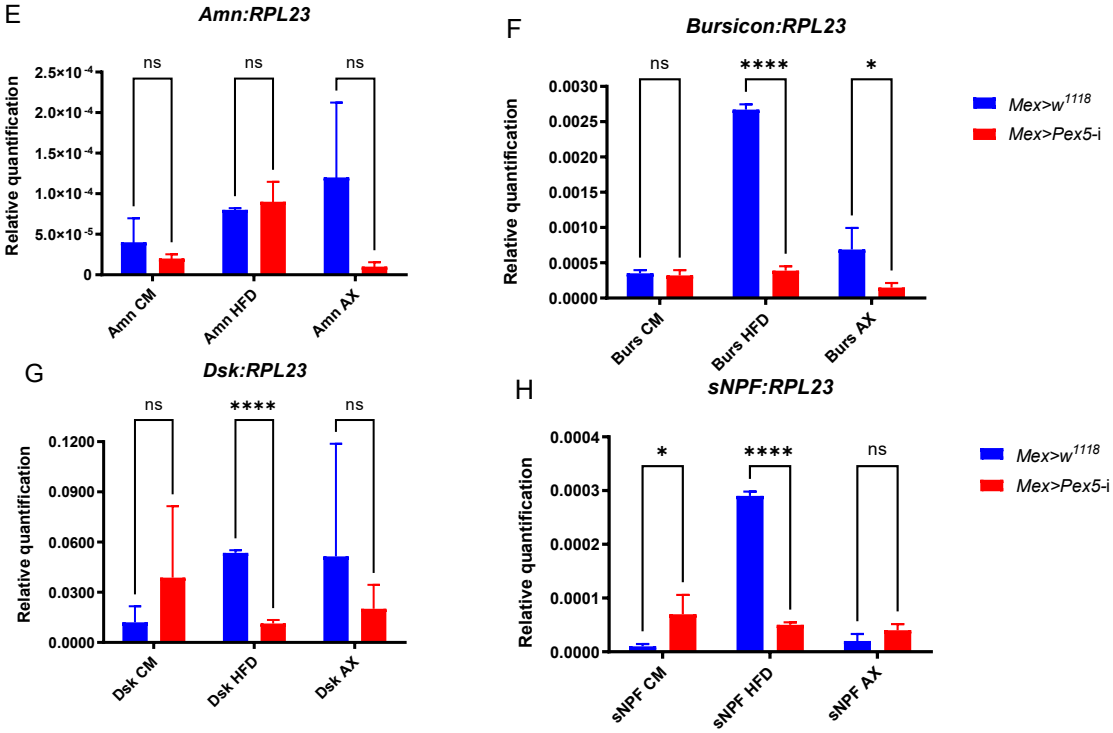

Supplementary Figure 5. Relative gene expression (quantification) in the midguts of 30do *Drosophila* males and females separaely, using qPCR to validate gene-hits of the HFD transcriptomic screen on CM, HFD and AX conditions. All statistical analyses were carried out using multiple, two-tailed, unpaired t-tests, assuming equal variance with an α=0.05. A) Relative expression of *Amn:RPL23* in males, n=3, between *Mex>Pex5*-i and *Mex>w*^{1118} on CM (t(4)=6.482, **p=0.0029), HFD (t(4)=0.4187, p=0.6969), and AX diets (t(4)=1.805e-5, p>0.9999). B) Relative expression of *Bursicon:RPL23* in males, n=3, between *Mex>Pex5*-i and *Mex>w*^{1118} on CM (t(4)=2.291, p=0.0837), HFD (t(4)=13.31, ***p=0.0002), and AX diets (t(4)=5.718, **p=0.0046). C) Relative expression of *Dsk:RPL23* in males, n=3, between *Mex>Pex5*-i and *Mex>w*^{1118} on CM (t(4)=0.1657, p=0.8764), HFD (t(4)=18.88, ****p<0.0001), and AX diets (t(4)=2.878, *p=0.0451). D) Relative expression of *Bursicon:RPL23* in males, n=3, between *Mex>Pex5*-i and *Mex>w*^{1118} on CM (t(4)=6.482, **p=0.0029), HFD (t(4)=0.4187, p=0.6969), and AX diets (t(4)=1.805e-5, p>0.9999). E) Relative expression of *Amn:RPL23* in females, n=3, between *Mex>Pex5*-i and *Mex>w*^{1118} on CM (t(4)=1.152, p=0.3134), HFD (t(4)=0.6984, p=0.5234), and AX diets (t(4)=2.061, p=0.1084). F) Relative expression of *Bursicon:RPL23* in females, n=3, between *Mex>Pex5*-i and *Mex>w*^{1118} on CM (t(4)=0.5869, p=0.5888), HFD (t(4)=40.93, ****p<0.0001), and AX diets (t(4)=3.013, *p=0.039). G) Relative expression of *Dsk:RPL23* in females, n=3, between *Mex>Pex5*-i and *Mex>w*^{1118} on CM (t(4)=1.057, p=0.3502), HFD (t(4)=28.18, ****p<0.0001), and AX diets (t(4)=0.7880, p=0.4748). H) Relative expression of *sNPF:RPL23* in females, n=3, between *Mex>Pex5*-i and *Mex>w*^{1118} on CM (t(4)=2.887, *p=0.0447), HFD (t(4)=42.98, ****p<0.0001), and AX diets (t(4)=1.970, p=0.1201).